U.PORTO
FACULDADE DE CIÊNCIAS
UNIVERSIDADE DO PORTO

PhD

Cosmic Paleontology: Searching for Superstrings

Ivan Rybak

Doutoramento em Astronomia
Departamento de Física e Astronomia
Faculdade de Ciências da Universidade do Porto
2014/2018

Orientadores:
Carlos José Amaro Parente Martins
Investigador Coordenador
Centro de Astrofísica da Universidade do Porto
Anastasios Avgoustidis
Assistant Professor, Faculty of Science
Centre for Astronomy & Particle, University of Nottingham

Cosmic Paleontology: Searching for Superstrings

Ivan Rybak

DOCTORAL PROGRAM IN ASTRONOMY

Centro de Astrofísica (CAUP)

Faculty of Sciences of the University of Porto

PhD Thesis

June 2018

Acknowledgements

The result obtained in this thesis is done under the supervision of Carlos Martins and Anastasios Avgoustidis. I am grateful to them for the guidance, constant support, astute advices, work flexibility and freedom to explore new ideas. It was a pleasure to work with them, collect knowledge and insight from our discussions. I also would like to thank them for reading my thesis and providing suggestions to improve it.

I would like to thank all members of CAUP and IA for creating friendly atmosphere to work, as well as I would like to thank for the hospitality the School of Physics & Astronomy of the University of Nottingham. Special thankfulness I would like to address to Paul Shellard, Pedro Avelino, Lara Sousa, José Pedro Vieira, Tom Charnock and José Ricardo Correia for collaboration, fruitful discussions and help in the thesis development.

I am grateful to number of people that made my life easier during the PhD period. Especially I want to express my gratitude to João P. Faria for programming skill support, to Juliane F. de Oliveira for advices about mathematical tricks, Portuguese language assistance and of course I would like to thank my family for endless support during this excited time of studying.

I acknowledge financial support from the FCT fellowship (SFRH/BD/52699/2014), under the FCT PD Program PhD::SPACE (PD/00040/2012), which made it possible for this thesis to be done.

Abstract

Cosmic strings as hypothetical objects passed through ups and downs of scientific community attention. They were predicted in the 1970s and reborn in the 2000s due to the implementation of superstring theory to the description of the early universe. The connection with superstring theory led to the new properties and a new name – cosmic superstrings, which remains the subject of theoretical and observational researchers.

This thesis is aimed at clarifying questions of the cosmic (super)string network evolution and subsequent observational predictions. The **first** chapter reviews the main principles and motivations to study cosmic (super)strings.

The **second** chapter is dedicated to the description of a semi-analytic velocity-dependent one scale (VOS) model in order to study the evolution of topological defect networks. This chapter provides a thorough comparison between numerical simulations and the semi-analytic approaches. We investigate a broad range of regimes, conditions and possible errors to test the VOS model validity.

In the **third** chapter we develop our approach to go beyond the standard cosmic strings and include possible extensions to the strings dynamics. The developed general treatment applies to wiggly strings and strings with chiral currents. The latter is generalized for an arbitrary Lagrangian, and the exact solution in Mikowski space for such strings is found. Also we generalize the study of the scaling regimes for string networks evolution in the framework of the VOS model.

The properties of cosmic superstrings are discussed in the **fourth** chapter. We consider dynamics and conditions for the production of string junctions both for superstrings in an expanding universe and for superstrings with currents. In addition, we suggest an approach for integrating junction dynamics in the VOS model. For this case we revisit the averaged treatment of strings collisions and averaged correlation function evolution. This leads to the formulation of the generalized VOS model with dynamical junctions.

The possible observational outcomes of this work are studied in chapter **five**. We review the main observational opportunities to confirm/restrict the existence of cosmic (super)strings. In particular, we revisit the cosmic microwave background anisotropies produced by cosmic strings. We generalize this study for the case of strings with non-trivial internal structure, i.e. with presence of currents. Specifically we study anisotropies caused by wiggly and superconducting (chiral) cosmic strings. In addition, we explore the stochastic gravitational background from cosmic strings and highlight the main adjustments that should be implemented in order to extend the study for non-conventional cosmic strings.

The outlook and conclusions end the thesis in chapter **six**.

Resumo

Cordas cósmicas são objetos físicos hipotéticos, para os quais atenção da comunidade científica passou por altos e baixos. Previstas na década de 1970, o estudo das cordas cósmicas renasce em 2000 devido à implementação da teoria das supercordas à descrição do universo, no seu momento inicial. A conexão com a teoria das supercordas originou, além de um novo nome – supercordas cósmicas – novas propriedades que permanecem o tema de investigadores teóricos e observacionais.

Esta tese tem como objetivo esclarecer algumas questões sobre a evolução das redes de (super)cordas cósmicas e as suas previsões observacionais. Em particular, o **primeiro** capítulo revê os principais princípios e motivações para estudar as supercordas cósmicas.

Para estudar a evolução de redes de defeitos topológicos, o **segundo** capítulo dedica-se à descrição do modelo semi-analítico de uma escala dependente da velocidade (VOS). Este capítulo fornece uma comparação completa de simulações numéricas, e também uma abordagem semi-analítica. Investiga-se uma ampla gama de regimes, condições e possíveis erros para testar a validade do modelo VOS.

No **terceiro** capítulo apresenta-se uma abordagem para ir além da corda cósmica padrão e incluir extensões possíveis da dinâmica de cordas. O tratamento geral desenvolvido aplica-se às cordas com estrutura de pequena escala e cordas com correntes quirais. Este último é generalizado para um Lagrangeano arbitrário, sendo a solução exata no espaço de Minkowski para tais redes encontrada. Generaliza-se também o estudo dos regimes de escalonamento para evolução de redes de cordas no contexto do modelo VOS.

As propriedades das supercordas cósmicas são apresentadas no **quarto** capítulo. Consideramos a dinâmica e as condições para a produção de junções tanto para supercordas nu universo em expansão como para supercordas com correntes. Sugerimos um cenário de como a dinâmica das junções pode ser integrada no modelo VOS. Para este caso, revisitamos o tratamento médio das colisões de cordas e a evolução da função de correlação média. Isto leva à formulação do modelo VOS generalizado com junções dinâmicas.

Possíveis consequências observacionais foram estudadas no **quinto** capítulo. Revemos as principais oportunidades de observação para confirmar/restringir a existência de (super)cordas cósmicas. Em particular, revisitamos as anisotropias da radiação cósmica de fundo de micro-ondas produzidas por (super)cordas cósmicas. Generalizamos este estudo para o caso de cordas com estrutura interna não trivial, ou seja, com presença de correntes. Especificamente, estudamos anisotropias causadas por redes de cordas com estrutura de pequena escala e supercondutoras (quirais). Finalmente, exploramos o fundo gravitacional estocástico devido

às cordas cósmicas e enfatizamos as principais alterações que devem ser implementados para estender o estudo para cordas cósmicas não convencionais.

As perspectivas e conclusões terminam a tese pelo **sexto** capítulo.

Glossary of Symbols and Acronyms

Throughout this thesis the natural units are used: speed of light, reduced Planck constant and Boltzmann constant are unity $c_l = \hbar = k_B = 1$. The metric signature is chosen -2. Greek indices $\mu, \nu, ...$ run over 4 space-time dimensions $(0, 1, 2, 3)$, Latin indices in the middle of alphabet $i, k, ...$ run over spatial coordinates $(1, 2, 3)$, while first letters a, b run over two dimensional worldsheet coordinates $(0, 1)$. The Einstein notations are used unless otherwise specified. Bold letters as $\mathbf{x}$ define a 3d vector. Partial derivatives are defined as $\frac{\partial}{\partial x^\mu} = \partial_\mu$, gauge covariant derivatives as $\mathcal{D}_\mu$.

Symbol	**Reference**	**Definition**
a	Eq.(1.1)	Scale factor
t	Eq.(1.1)	Physical time
τ	Eq.(1.2)	Conformal time
$T_{\mu\nu}$	Eq.(1.3)	Energy-momentum tensor
$g_{\mu\nu}$	Eq.(1.3)	Metric tensor
G	Eq.(1.3)	Gravitational constant
ρ	Eq.(1.4)	Energy density
P	Eq.(1.4)	Pressure
H	Eq.(1.5)	Hubble parameter
$\rho_{\rm crit}$	Eq.(1.7)	Critical energy density
Ω	Eq.(1.10)	Density parameters
z	Eq.(1.14)	Redshift
$F_{\mu\nu}$	Eq.(1.20)	Electromagnetic tensor
μ_0	Eq.(1.36)	String tension
γ_{ab}	Eq.(1.35)	Worldsheet metric
ε_V, η_V	Eq.(1.48), (1.49)	Slow-roll parameters
M_{pl}	Eq.(1.63)	Planck mass
δ_{ab}	Eq.(2.2)	Kronecker symbol
ε	Eq.(2.4)	Coordinate energy per unit length
$\delta(...)$	Eq.(2.5)	Dirac delta function
υ	Eq.(2.7)	Root-mean-square speed
k	Eq.(2.9)	Momentum parameter
L	Eq.(2.10)	Correlation length

Symbol	Reference	Definition
c	Eq.(2.10)	Chopping parameter
γ_v	Eq.(2.17)	Lorentz factor
ε_{ab}	Eq.(3.5)	Levi-Civita symbol
E_{ab}	Eq.(3.6)	Levi-Civita tensor
T	Eq.(3.7)	Tension
U	Eq.(3.7)	Mass per unit length
η_{ab}	Eq.(3.41)	Metric of Minkowski space
T_E	Eq.(4.1)	Imaginary time
κ_G	Eq.(4.6)	Gravitational coupling
$\Gamma(...)$	Eq.(4.7)	Gamma function
${}_2F_1$	Eq.(4.42)	Hypergeometric function
ℓ	Eq.(4.71)	Physical length of the string
T_K	Eq.(5.1)	Absolute temperature
Y_l^m	Eq.(5.14)	Spherical harmonics
C_l	Eq.(5.15)	Angular power spectrum

Acronym	Reference	Name
ΛCDM	1.1	Lambda cold dark matter - standard cosmological model
GUT	1.1	Grand Unified Theory
GR	1.2	General Theory of Relativity
FLRW	1.2	Friedmann–Lemaître–Robertson–Walker
CMB	1.5	Cosmic Microwave Background
BPS	1.7	Bogomol'nyi–Prasad–Sommerfield
VOS	2	Velocity-depend one scale
PRS	2	Press-Ryden-Spergel
ACK	2.1	Austin-Copeland-Kibble
rms	2.1	Root-mean-square
DBI	3.2	Dirac-Born-Infeld
COBE	5.1.2	Cosmic Background Explorer
WMAP	5.1.2	Wilkinson Microwave Anisotropy Probe
LISA	5.3.2	Laser Interferometer Space Antenna
PTA	Fig.5.8	Pulsar timing array
SMBBH	Fig.5.8	Supermassive binary black hole
aLIGO	Fig.5.8	Advanced Laser Interferometer Gravitational-Wave Observatory
BBO	Fig.5.8	Big Bang Observer

Table of contents

Chapter 1

Introduction

> String theory cosmologists have discovered cosmic strings lurking everywhere in the undergrowth [1]
>
> *Tom Kibble*

1.1 Prelude

Today's standard description of the universe evolution is the ΛCDM model. It is consistent with observational evidence spanning a wide range of scales [2]. However, it still leaves some unsolved tensions/problems, such as the lithium problem [3] (although this may be connected with nuclear physics [4]), the value of Hubble constant [5] and some other questions [6] that can eventually extend the current ΛCDM concept. At the same time, there is also one essential supplementation for the ΛCDM model that is considered to be unavoidable - a theory of inflation. It is responsible for the description of very early time in the history of the universe and intended to resolve some basic puzzles of the ΛCDM model, including the "flatness" and "horizon" problems (for details see [7]).

The reason that causes inflation is still unclear. But since the period when inflation happened is characterised by extremely high energy ($\sim 10^{15}$ GeV), it looks reasonable to search for the answer in fundamental theories. There are different approaches to how inflation can be established [8, 9]. Depending on the model we can anticipate finding observational evidence that confirm or rule out some of these models. One possible remnant of inflation that can survive till the current day is a network of topological defects. The possible mechanism of topological defects production was fully described at first by Tom Kibble [10]. Meanwhile, it was noticed that two types of defects formed at high energy scales, domain walls and monopoles, lead to cosmological disasters: disagreement with observation due to their domination in the universe [11, 12]. In turn, cosmic strings with tension comparable to the *Grand Unified Theory* (GUT) energy scale ($G\mu_0 \sim 10^{-6}$) are not in agreement with measurements of cosmological microwave background anisotropies [13]. As a result, the original idea to consider topological defects as a main seed of fluctuations for large scale structure growth [14], was disapproved and this duty was successfully imposed on inflation

models. Nevertheless, topological defects didn't stay aside for long time and were noticed as an outcome of a wide range of inflation models and some high energy particle physics scenarios: brane inflation (where they obtained name of cosmic superstrings) [15–20], supersymmetric grand unified theory [21–26], some other types of inflation [27–30] and particle physics [31–34].

As a result, we can think about topological defects as an additional observational signal, which can tell us about high energy physics in the early period of the universe. In order to have an accurate prediction for the observational signal from cosmic strings, the evolution of their networks should be studied properly. The current PhD thesis "Cosmic Paleontology: Searching for Superstrings" is aimed to make some progress in this direction.

In the current chapter 1 we will make a groundwork for further chapters of the thesis.

1.2 ΛCDM Cosmology

Nowadays, the universe on a large scale seems very isotropic and homogeneous. The main interaction, which plays the key role in the evolution of the universe is gravity. The Einstein's *General Theory of Relativity* (GR) is the best candidate for the description of this type of interaction. The space-time in this theory can be represented as a 4-dimensional manifold $\mathfrak{M}$, which can be foliated into a spatial 3-dimensional Riemannian hypersurface and time $\Sigma_3 \times R$ respectively. The homogeneity and isotropy imply that the spatial part Σ_3 is maximally symmetric: it possesses the maximal number of Killing vectors, $\frac{n(n+1)}{2}$, where n is the dimension of the considered space. For this case one finds the general form of the metric to be the *Friedmann–Lemaître–Robertson–Walker* (FLRW) metric, which has maximally symmetric spatial part with the space-time interval

$$ds^2 = dt^2 - a(t)^2 \left(\frac{dr^2}{1 - kr^2} + r^2 \left(d\theta^2 + \sin^2 \theta d\phi^2 \right) \right), \tag{1.1}$$

where $a(t)$ is a scale factor, speed of light is set to be one $c_l = 1$, (t, r, θ, ϕ) - space-time coordinates and k is responsible for a curvature of the hypersurface Σ_3. For $k = -1$ the spatial part will have hyperbolic geometry, for $k = 1$ - elliptic and Euclidean for $k = 0$.

Sometimes, for the convenience, we will use the FLRW metric (1.1) expressed in terms of conformal time τ instead of physical one t. They are related by the following expression

$$dt^2 = a^2 d\tau^2. \tag{1.2}$$

The FLRW metric is a result of the cosmological principle's application: homogeneity and isotropy. The dynamics in GR is described by Einstein equations

$$R_{\mu\nu} - \frac{1}{2} R g_{\mu\nu} = 8\pi G T_{\mu\nu}, \tag{1.3}$$

where $R_{\mu\nu}$ and R are the Ricci tensor and scalar respectively, G is the gravitational constant, $T_{\mu\nu}$ is an energy-momentum tensor, $g_{\mu\nu}$ is a metric of a space-time, Greek indices (μ, ν) run from 0 to 3 and represent space-time coordinates.

In order to obtain equations of the universe evolution, the energy-momentum tensor must be defined. By using the assumption that the substance of the universe on a large scale can be described by a perfect isotropic fluid, the energy-momentum tensor takes the form

$$T_{\mu\nu} = (P + \rho)\, U_\mu U_\nu - P g_{\mu\nu}, \tag{1.4}$$

where P is a pressure, ρ is a density and U_μ is a fluid's four-velocity.

Let us return to Einstein equations (1.3) to calculate its "00" component and the trace. By doing this, one can obtain two Friedmann equations

$$H^2 = \frac{8\pi G}{3}\rho - \frac{k}{a^2}, \tag{1.5}$$

$$\dot{H} + H^2 = -\frac{4\pi G}{3}\left(\rho + 3P\right), \tag{1.6}$$

where $H = \frac{1}{a}\frac{da}{dt}$ is the Hubble parameter.

It is useful to define the critical density: the case when the curvature k equals zero. By setting $k = 0$ in equation (1.5), the critical density has the form

$$\rho_{crit} = \frac{3H^2}{8\pi G}. \tag{1.7}$$

By differentiating the equation (1.5) and using (1.6), the equation of continuity for the FLRW metric can be obtained as

$$\frac{d\rho}{dt} + 3H\left(\rho + P\right) = 0. \tag{1.8}$$

It is possible, by using the form of equation of state as $P = w\rho$ (assuming that w is a constant), to obtain the general solution of equation (1.8)

$$\rho \propto a^{-3(1+w)}, \tag{1.9}$$

where the equation of state is $w = 0$ for matter, $w = \frac{1}{3}$ for radiation and $w = -1$ for a cosmological constant.

The Friedmann equation (1.5), by using the definition of today's critical density (1.7) and the general solution (1.9), can be rewritten in a more common form

$$H^2 = H_0^2\left(\Omega_r a^{-4} + \Omega_m a^{-3} + \Omega_k a^{-2} + \Omega_\Lambda\right), \tag{1.10}$$

where $\Omega_i = \frac{\rho_i}{\rho_{crit}}$ and index i is r for radiation, m for matter, k for curvature, Λ for dark energy, H_0 is the Hubble parameter at present epoch (when $a_0 = 1$).

The equation (1.10) defines the dynamics of the universe. It is useful to obtain the scale factor as a function of time for radiation, matter and dark energy domination periods. For this purpose we consider the domination of correspondingly terms Ω_i in the (1.10).

In this way, for the radiation epoch

$$a \propto t^{1/2} \propto \tau, \tag{1.11}$$

for the matter domination period

$$a \propto t^{2/3} \propto \tau^2 \tag{1.12}$$

and for dark energy domination

$$a \propto \exp(t) \propto -1/\tau. \tag{1.13}$$

An additional parameter that is useful to define here is a redshift z. Due to expansion of the universe, the wavelength of an electromagnetic wave λ is stretching. We can define the redshift through the ratio between observed λ_o and emitted λ_e wavelengths, which also connected with the scale factor as

$$1 + z = \frac{\lambda_o}{\lambda_e} = \frac{a_o}{a}, \tag{1.14}$$

where a_o corresponds to the scale factor value in the moment of observation.

1.3 The Kibble Mechanism

It is believed that at the very beginning of the universe's evolution, when the energy density was extremely high, the *Grand Unification* happened: the moment when weak, electromagnetic and strong interactions were unified in one type of interaction. The idea of *Grand Unification* was inspired by the success of electroweak theory, which unifies weak and electromagnetic interactions by the gauge group $SU(2) \times U(1)$. As a result, it is believed that at high energy the strong interaction is unified with the electroweak one. When the energy density of the universe dropped down due to expansion, different types of interactions became separated as a result of symmetry breaking processes. Because of the finite correlation distance between different patches in the universe, these processes can produce topological defects. This mechanism was called after Tom Kibble [10], who gave the first comprehensive description of such phenomena (more details can be found in [35, 36]).

For the sake of clarity, let us us consider the Kibble mechanism [10] that causes cosmic strings production. The potential, which is responsible for cosmic strings appearance during a phase transition is illustrated in figure 1.1. When the energy in the universe decreases, due to expansion, the field (in that case it is a scalar complex field φ) will have to chose one of the true vacuum minima (one of the minima of the potential shown in figure 1.1). The choice is mainly determined by random fluctuations. Moreover, the choices of different patches of

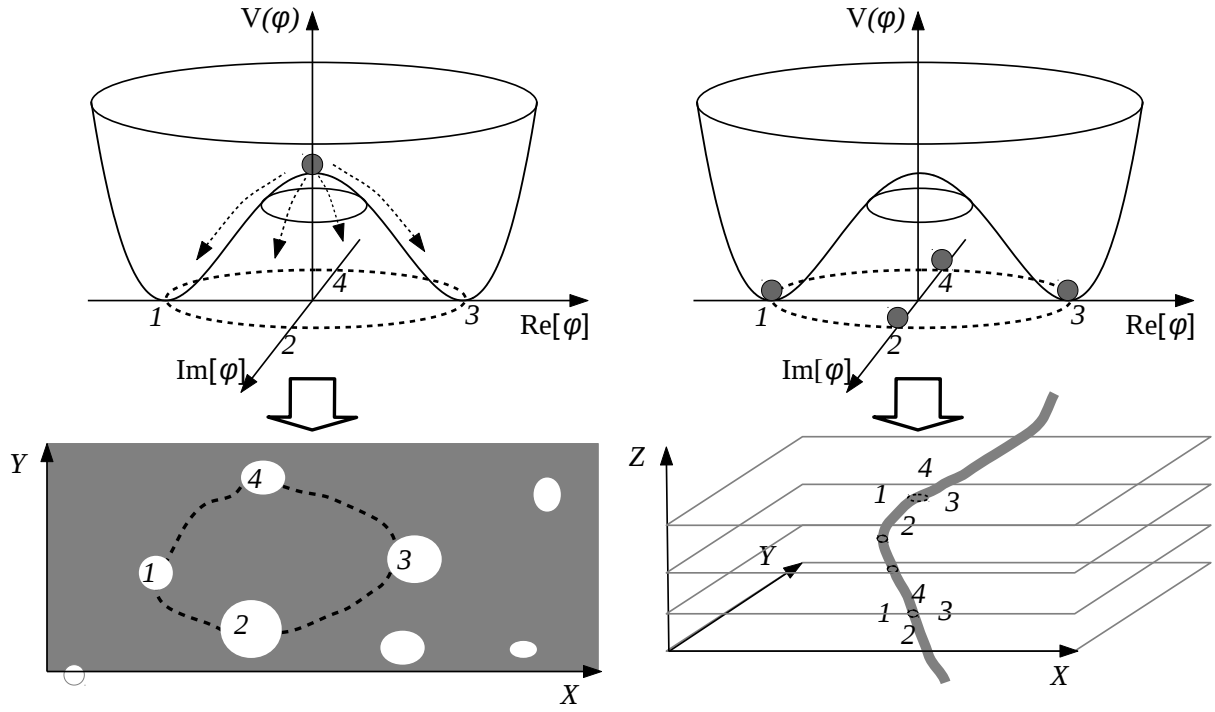

Fig. 1.1 Kibble mechanism: symmetry breaking by a complex scalar field that produces cosmic strings [36]. On the left panel patches with true vacua (white regions) start growing as the symmetry is broken. On the right picture patches with true vacua merge and a false vacuum region (grey region) is squeezed and forms a topological defect.

the field are correlated only on a distance of the particle horizon

$$R_H = a(t) \int_0^t \frac{dt'}{a(t')}, \tag{1.15}$$

namely, the signal can cross the distance R_H for the time t.

That is why different segments, separated by a distance bigger than R_H (1.15), in the time period of symmetry breaking, can choose different vacua. This process is illustrated in the figure 1.1 (left panel). Eventually, patches start to grow and become causally connected. Points surrounded by different vacua and whose phases are different by 2π (right panel of figure 1.1), will give rise to a cosmic string. It happens due to requirement that the field φ must be a continuous function of space-time coordinates (X, Y, Z coordinates for the case in figure 1.1).

Depending on a symmetry breaking scenario, there are different types of defects that can be produced. Let us provide a classification of all possible topological defects. It can be accomplished by studying the corresponding homotopy groups. Let's suppose that the considered field obeys a symmetry, which is defined by a group G (universal covering group), and this group is broken to a subgroup K: $G \to K$. In such case, topological defects can be classified by considering the n-th homotopy group π_n of quotient space G/K. In particular, when the first homotopy group of this quotient space is non-trivial: $\pi_1(G/K) \neq I$, the

string-like topological defects can be produced by symmetry breaking: $G \to K$. Non-triviality for the first homotopy group means that there is a loop in quotient space G/K that cannot be shrunk into a point.

In the same manner we can do it for other topological defects and classify them in the following way:

$\pi_0(G/K) \neq I$ - walls;
$\pi_1(G/K) \neq I$ - strings;
$\pi_2(G/K) \neq I$ - monopoles;
$\pi_3(G/K) \neq I$ - textures.

1.4 The zoo of cosmic strings

In the previous section we already saw how cosmic strings can be produced. Let's consider in more detail their existence in some models of field theory.

1.4.1 Global U(1) strings

For the first and simplest case, global strings [37], we can consider a complex scalar field φ with the potential illustrated in the figure 1.1. In this case the Lagrangian has a $U(1)$ symmetry and can be written in the form (the metric signature is chosen -2)

$$\mathcal{L} = (\partial_\mu \varphi)^* \partial^\mu \varphi - \frac{\lambda}{4}\left(|\varphi|^2 - \eta^2\right)^2, \tag{1.16}$$

where η is a constant.

Varying the Lagrangian (1.16) with respect to the scalar field φ, the equation of motion can be obtained as

$$\partial_\mu \partial^\mu \varphi + \frac{\lambda}{2}\varphi\left(|\varphi|^2 - \eta^2\right) = 0. \tag{1.17}$$

To see the presence of a string, as a solution of (1.17), we can use the corresponded static ansatz in Minkowski space

$$\varphi = \eta f_s(m_s r)\mathrm{e}^{i n_s \theta}, \tag{1.18}$$

where we defined the constants as $m_s^2 = \lambda\eta^2$ and free parameter n_s. The orientation of the string is chosen along z in the cylinder coordinates $(r,\ \theta,\ z)$.

As a result, the equation (1.17) can be rewritten as

$$\frac{\partial^2 f_s}{\partial R^2} + \frac{1}{R}\frac{\partial f_s}{\partial R} - \frac{n_s^2}{R^2} f_s - \frac{f_s}{2}\left(f_s^2 - 1\right) = 0, \tag{1.19}$$

where $R = m_s r$.

We need to impose the following boundary condition: $f \xrightarrow[r\to 0]{} 0$ - to preserve the continuity of the field φ at the origin of the string; $f \xrightarrow[r\to\infty]{} 1$ - to recover the ground state far away from the string. As a result, we can solve the differential equation (1.19) numerically by using relaxation techniques for the boundary value problem. An example of the string profile from the equation (1.19) is shown on the left panel of figure 1.2. It is seen how the field f_s forms

the string profile: it tends to zero (and restores the $U(1)$ symmetry), when the distance is small $R \to 0$, and increases to unity (breaks the $U(1)$ symmetry), when we are far away from the core $R \to \infty$. As a result, there is a global string[1] solution for the system defined by the Lagrangian (1.16).

1.4.2 Abelian Higgs strings

Another type of strings, which can be thought as a generalization of global strings is the Abelian Higgs model of strings [38]. In this case the $U(1)$ symmetry of the field φ is local and the system can be described by the charged complex scalar field φ and by a gauge abelian field A_μ with the Lagrangian

$$\mathcal{L} = (\mathcal{D}_\mu\varphi)^* \mathcal{D}^\mu\varphi - \frac{1}{4}F_{\mu\nu}F^{\mu\nu} - \frac{\lambda}{4}\left(|\varphi|^2 - \eta^2\right)^2. \tag{1.20}$$

where the constant e is a charge, $F_{\mu\nu} = \partial_\mu A_\nu - \partial_\nu A_\mu$ and the gauge-covariant derivative $\mathcal{D}_\mu = \partial_\mu - ieA_\mu$.

Equations of motion obtained from the Lagrangian (1.20) are

$$\begin{gathered} \mathcal{D}_\mu\mathcal{D}^\mu\varphi + \frac{\lambda}{2}\varphi\left(|\varphi|^2 - \eta^2\right) = 0, \\ \partial_\mu F^{\mu\nu} = j^\nu, \end{gathered} \tag{1.21}$$

where the current is given as $j^\nu = 2\,e\,\mathrm{Im}\,[\varphi^*\mathcal{D}^\nu\varphi]$.

It is seen that the Abelian Higgs string is different from a global one by the presence of a gauge field A_μ. It can be reduced to the previous case when $e = 0$. The gauge field A_μ doesn't change the approach to study string solution of equations of motion (1.21). As before, to see the presence of the string we need to search for the field φ solution in the form (1.18) together with the gauge field A_μ ansatz

$$A_\theta = -n_s\frac{\alpha_s(r)}{er}, \tag{1.22}$$

where the index θ defines the non-zero component of the gauge field A_μ in the cylinder coordinates frame, when the string is placed along the z axis (the same coordinates frame as for global strings in 1.4.1).

Using ansatz (1.22), from (1.21) we obtain equations

$$\begin{gathered} \frac{\partial^2 f_s}{\partial R^2} + \frac{1}{R}\frac{\partial f_s}{\partial R} - \frac{n_s^2}{R^2}f_s\left(\alpha_s - 1\right)^2 - \frac{f_s}{2}\left(f_s^2 - 1\right) = 0, \\ \frac{\partial^2\alpha_s}{\partial R^2} - \frac{\partial\alpha_s}{\partial R} - \beta_s^2 f_s^2\left(\alpha_s - 1\right) = 0, \end{gathered} \tag{1.23}$$

where $\beta_s = 2e^2/\lambda$.

[1]The name global means that the symmetry $U(1)$ is a global symmetry, without a gauge field.

As it was done for global strings, we need to establish boundary conditions as: $f_s, \alpha_s \xrightarrow[r\to 0]{} 0$ and $f_s, \alpha_s \xrightarrow[r\to\infty]{} 1$. Using these boundary conditions, numerically we can find the profile of Abelian Higgs string (right panel of the figure 1.2).

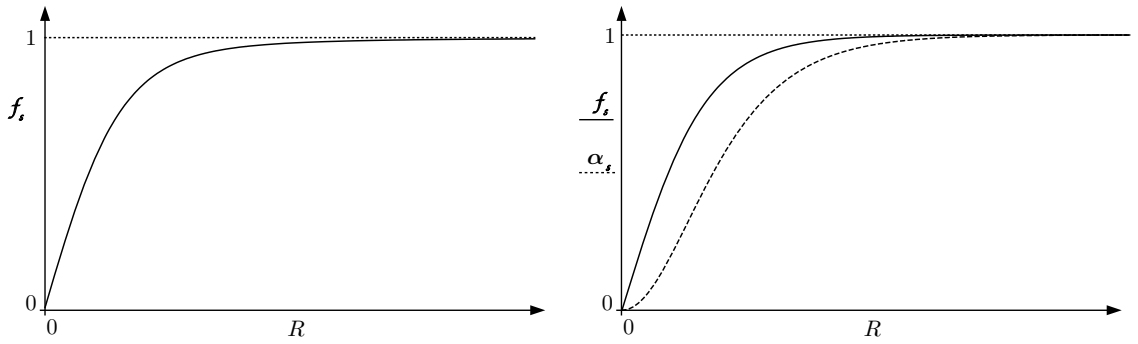

Fig. 1.2 Left panel shows string profile for the global string (described by equations (1.19)) when $n_s = 1$. Right panel shows string profile for the Abelian Higgs string (described by equations (1.23) when $n_s = \beta = 1$.

1.4.3 Non-Abelian strings

A more general situation can appear if the group G is broken to the non-Abelian subgroup K (according to notations in the section 1.3) [39, 40]. Let's consider the N-component field

$$\Phi = \begin{pmatrix} \varphi_1 \\ ... \\ \varphi_N \end{pmatrix} \tag{1.24}$$

that transforms locally according to some simple compact Lie group G. In this case the gauge field can be put together in the form

$$A_\mu = t_a A^a_\mu, \tag{1.25}$$

where t_a are generators of the group G.

Eventually, we can build the Lagrangian as

$$\mathcal{L} = (\mathcal{D}_\mu \Phi)^\dagger \mathcal{D}^\mu \Phi - \frac{1}{4}\mathrm{Tr} F_{\mu\nu} F^{\mu\nu} - V(\Phi, \Phi^\dagger), \tag{1.26}$$

where $F_{\mu\nu} = \partial_\mu A_\nu - \partial_\nu A_\mu + e\,[A_\mu,\, A_\nu]$, $[\dots, \dots]$ denotes commutator and † is responsible for the conjugate transposition.

The equation of motion for the field Φ formally can be written as

$$\mathcal{D}_\mu \mathcal{D}^\mu \Phi = \frac{\partial V}{\partial \Phi}. \tag{1.27}$$

By introducing the corresponding ansatz with cylindrical symmetry, one can study solutions for non-Abelian string profiles with the same method as was done in the previous

sections [41]. For the vacuum solution, far away from the string, the potential V should reach the minimum. Hence, $\frac{\partial V}{\partial \Phi} = 0$ and, using the left hand side of (1.27), one can obtain that far away from the string the field satisfies

$$\partial_\mu \Phi - ieA_\mu \Phi = 0. \tag{1.28}$$

Considering a small field displacement $\Phi(x + dx)$ and using (1.28), it is seen that

$$\Phi(x + dx) = \mathrm{e}^{idx^\mu A_\mu} + O(dx)^2. \tag{1.29}$$

One can integrate (1.28) along the curve using relation (1.29). We chose the curve of integration in cylindrical coordinates that begins at angle 0 and ends at angle θ. This integration is called the path-order exponent, which transforms the field Φ: rotate it by $U(\theta)$ for the angle θ

$$\Phi(\theta) = U(\theta)\Phi(0) = P \exp\left(ie \int_0^\theta dx^\mu A_\mu\right) \Phi(0), \tag{1.30}$$

where P defines path-ordering.

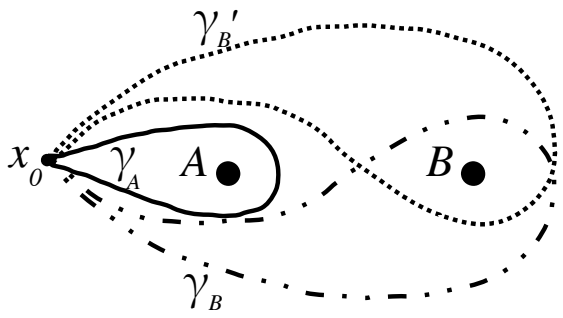

Fig. 1.3 Homotopically inequivalent loops γ_A, γ_B and γ_B' on a surface with holes A and B. The difference between loops γ_B and γ_B' demonstrates the case of non-Abelian strings.

The path-order exponent in (1.30) can probe fields for the presence of string-like defects. When the integral in (1.30) makes a complete winding $U(2\pi)$, it forms a closed curve. Depending on a loop choice, they can be associated with elements $k \in K$ of the unbroken subgroup K as $U(2\pi) = D(k)$, where $D(k)$ is some representation of group elements. It can be visualized by considering loops on a two dimensional surface, where the set of N possible different strings is represented by N holes (for example A and B in the figure 1.3). The location of each string is defined by the set $\mathcal{M} = \mathcal{M}(x_1, x_2, .., x_N)$. Choosing the fixed base at the point x_0, we can build the fundamental group $\pi_1(\mathcal{M}, x_0)$ on this surface. Each closed curve $\gamma \in \pi_1(\mathcal{M}.x_0)$ around holes can be mapped on some non-trivial elements of the group K: $\pi_1(\mathcal{M}, x_0) \to K$. In figure 1.3 we see an example of this realization, the surface with two holes, which presents strings A, B, and different possible loops γ. It is seen that two curves γ_B' and γ_B are homotopically inequivalent. This ambiguity of the different paths corresponds to the fact that K is a non-Abelian group: $\gamma_B' \neq \gamma_A \circ \gamma_B \circ \gamma_A^{-1}$. For the case

of an Abelian group K, curves γ_B and γ'_B are mapped to the same element of K, which excludes the ambiguity of the path choice.

The non-Abelian structure of the group K brings additional properties to such strings. There should be a "holonomy interaction" between these strings [40]. Moreover, whereas previously studied strings could reconnect or pass through each other if they collide, non-Abelian strings can form only entanglements when the collision happens. These properties are dictated by the flux conservation [42, 43].

The cosmic string network with non-Abelian strings was studied in [44] and will be discussed briefly in the chapter 4.

1.4.4 Superconducting strings

As we saw above, the main features of cosmic strings are defined by properties of a broken symmetry group $G \to K$. There were shown examples for global, Abelian-Higgs and non-Abelian string models. All these analyses were done for the simple group G. If we consider an example of direct group product $U(1) \times \tilde{U}(1)$, we can find new interesting features for defects [45]. The Lagrangian for this case can be written as

$$\mathcal{L} = \frac{1}{2}\left(\mathcal{D}_\mu\varphi\right)^* \mathcal{D}^\mu\varphi + \frac{1}{2}\left(\tilde{\mathcal{D}}_\mu\sigma\right)^* \tilde{\mathcal{D}}^\mu\sigma - \frac{1}{4}F_{\mu\nu}F^{\mu\nu} - \frac{1}{4}\tilde{F}_{\mu\nu}\tilde{F}^{\mu\nu} - V(\sigma,\varphi), \tag{1.31}$$

where the potential is chosen as $V(\sigma,\varphi) = \frac{\lambda}{4}\left(|\varphi|^2 - \eta^2\right)^2 + \frac{\tilde{\lambda}}{4}\left(|\sigma|^2 - \tilde{\eta}^2\right)|\sigma|^2 + g|\sigma|^2|\varphi|^2$, the gauge-covariant derivative is $\tilde{\mathcal{D}}_\mu = \partial_\mu - i\tilde{e}\tilde{A}_\mu$, $\tilde{F}_{\mu\nu} = \partial_\mu\tilde{A}_\nu - \partial_\nu\tilde{A}_\mu$ and constants must obey the relation $\lambda\eta^4 > \tilde{\lambda}\tilde{\eta}^4$, $g\eta^2 \geq \frac{1}{4}\tilde{\lambda}\tilde{\eta}^2$.

The relation for constants provides the situation that for the vacuum state it is energetically more favourable to have a broken symmetry $U(1)$ ($|\varphi| = \eta$, $\sigma = 0$), rather than $\tilde{U}(1)$. At the same time, in the core of the string, when the field $\varphi = 0$, the other field is not necessary zero $\sigma \neq 0$ [46, 47].

The string-like solution can be found by using the ansatz (1.18) and

$$\begin{gathered} \sigma = \eta h_s(R_s)\mathrm{e}^{i(\omega t - kz)}, \\ \tilde{A}_t = \frac{1 - b_s(R_s)}{\tilde{e}}\omega, \quad \tilde{A}_z = \frac{b_s(R_s) - 1}{q}k, \\ A_\theta = \frac{1}{e}\left(n_s - P_s(r)\right), \end{gathered} \tag{1.32}$$

with the convenient substitution of constants as $q = \frac{\tilde{\eta}}{\eta}$, $a^2 = \frac{e^2}{\lambda}$, $\tilde{a}^2 = \frac{\tilde{e}^2}{\lambda}$, $\gamma = \frac{\tilde{\lambda}}{\lambda}$, $\tilde{\gamma} = \frac{g}{\lambda}$ and initial conditions $P_s(0) = n_s$, $b_s(0) = 1$, $h_s(0) = \frac{\partial f_s(R_s)}{\partial R_s}|_{R_s\to 0} = \frac{\partial b_s(R_s)}{\partial R_s}|_{R_s\to 0} = 0$, $P_s(\infty) = f_s(\infty) = 0$ and $h_s(\infty) = 1$ [48].

Using the ansatz, one can obtain a final system of differential equations for the simple case when the vector field $\tilde{A}_\mu = 0$ (which means $b_s(R_s) = 1$) [48]

$$\begin{aligned} \frac{\partial}{\partial R_s}\left(\frac{1}{R_s}\frac{\partial P_s}{\partial R_s}\right) &= a^2\frac{P_s h_s^2}{R_s}, \\ \frac{1}{R_s}\frac{\partial}{\partial R_s}\left(R_s\frac{\partial h_s}{\partial R_s}\right) &= h_s\left(\frac{P_s^2}{R_s^2} + \left(h_s^2 - 1\right) + \tilde{\gamma} f_s^2 h_s\right), \\ \frac{1}{R_s}\frac{\partial}{\partial R_s}\left(R_s\frac{\partial f_s}{\partial R_s}\right) &= w f_s b_s^2 + \gamma f_s\left(f_s^2 - q^2\right) + \tilde{\gamma} h_s^2 f_s. \end{aligned} \tag{1.33}$$

The simple example of solution without the vector field $\tilde{A}_\mu = 0$ is represented in figure 1.4. There are many different possible interesting solutions that exhibit non-trivial field presence inside the string core [49–51]. These fields do influence string properties (such as its equation of state) and their network evolution correspondingly. The possible effective description of such strings and their network evolution will be discussed in the chapter 3.

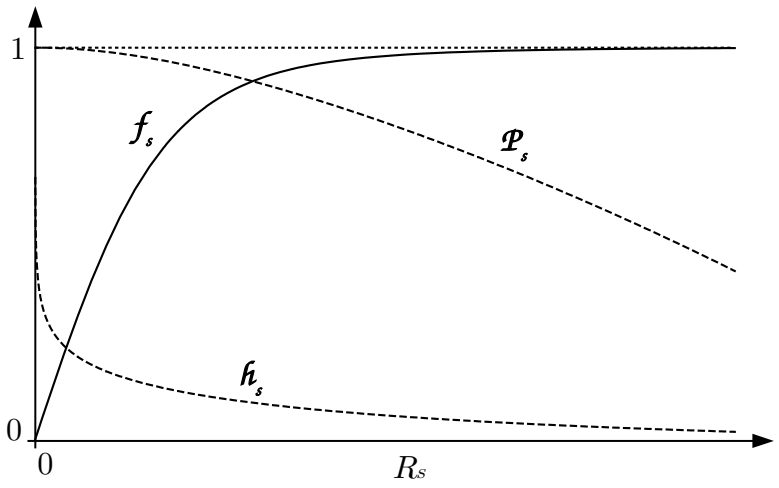

Fig. 1.4 String-like solution for f_s and h_s of equations (1.33) for the superconducting string, described by the model (1.31) with the following choice of constants: $a = 0.01$, $\gamma = 10^{-6}$, $\tilde{\gamma} = 0.01$, $q = 0.1$, $w = 0$, $\tilde{a} = 0$, $b(R_s) = 1$.

1.4.5 Nambu-Goto strings

String-like solutions in the context of a field theory allow us to gain insight into the core structure properties, interactions, stability and some energy loss characteristics of these defects. Meanwhile, these solutions do not provide us a convenient way to study the evolution of string networks analytically. Through the field theory description we can study string networks only by numerical simulations. Taking into account the possible complexity of some networks, simulations can be very time-consuming and do not let us achieve the goal. In order to make some progress in the network evolution study, one can use an approximated description - the Nambu-Goto Lagrangian. This approximation is dictated by the fact that we do not anticipate to have any big contribution to string dynamics from field excitations at

the string core. Hence, this approach should give us a macroscopic picture, even though it is not valid at microscopic level. In particular when the string curvature is high (small-scale structure) and at the point of string intersection.

Let us consider the Abelian Higgs Lagrangian (1.20) and build the effective model from it. We chose the space-time coordinate as functions of two-dimensional world sheet coordinates $x^\mu(\sigma^a)$, where $a = 0, 1$. Coordinates σ^0 and σ^1 describe the space-time area that is swept by the string motion. Let's chose σ^0 as timelike and σ^1 as spacelike vectors. Hence, there will be two vectors tangent to the world-sheet surface $x^\mu_{,a} = \partial x^\mu / \partial \sigma^a$. We also can build vectors orthogonal to the world-sheet surface $n^{\mu\, A}$, where $A = 2, 3$ and therefore $x^\mu_{,a} n^A_\mu = 0$. Requiring that vectors $n^{\mu\, A}$ are normalized for unity, one can describe any point on the string-like defect as (see figure 1.5) [52]

$$X^\mu(\xi^\nu) = x^\mu(\sigma^a) + r^A n^\mu_A(\sigma^a), \tag{1.34}$$

where $\xi^\nu = \left(\sigma^a, r^A\right)$.

Making the coordinate transformation $X^\mu \to \xi^\mu$ and using (1.34) we can evaluate the Jacobian determinant as

$$\det\left[J_{ab}\right] = \det\left(g_{\mu\nu}\frac{\partial X^\mu}{\partial \xi^{\mu'}}\frac{\partial X^\nu}{\partial \xi^{\nu'}}\right) = \det\begin{bmatrix}\gamma_{ab} & \mathbf{0}_{2x2} \\ \mathbf{0}_{2x2} & -\delta_{AB}\end{bmatrix} + O\left(\frac{|r^A|}{R_k}\right) \approx \det\left(\gamma_{ab}\right), \tag{1.35}$$

where we used the fact that the function $X^\mu(\xi^\nu)$ (1.34) is well-defined only when $R > |r^A|$.

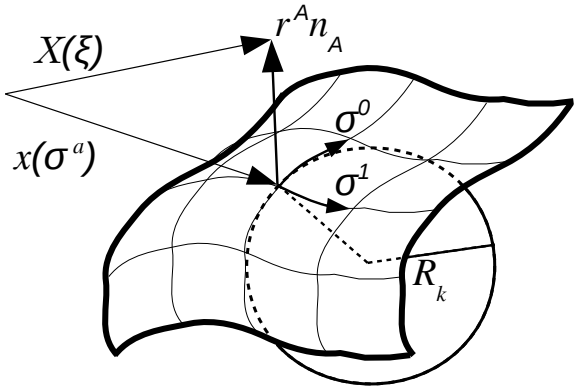

Fig. 1.5 Parametrization of the surface swept by the string-like object.

We need to apply the change of coordinates with the Jacobian (1.35) and leave only terms with accuracy $O\left(\frac{|r^A|}{R_k}\right)$. Normal coordinates r^A can be integrated out and from the Lagrangian (1.20) we obtain the lower order effective Nambu-Goto action

$$S = -\mu_0 \int \sqrt{-\gamma} d^2\sigma, \tag{1.36}$$

where $\gamma = \det\left(\gamma_{ab}\right)$, $d^2\sigma = d\sigma^0 d\sigma^1$ and the part from the r^A integration is included in the string tension μ_0.

The action (1.36) is the first term of the original model expansion around $O\left(\frac{\delta_s}{R_k}\right)$, where the parameter $|r^A|$ was changed for the string width δ_s, which is defined by the string profile. Additional terms to the action (1.36) can be included [53], however for the case of cosmic strings we do not anticipate big corrections from them.

Other modifications that can appear in the Nambu-Goto action (1.36) can come from the presence of non-trivial internal structure, as for superconducting strings 1.4.4. Further discussion and developments in this direction will be in the chapter 3.

1.5 Inflation

As it was already mentioned above (section 1.1), the inflation scenario is an essential structure of today's cosmology. It was developed to find an explanation to problems that emerged in the "hot big bang" model. Let's consider these problems with a solution that the inflation scenario proposes.

The horizon problem. This issue comes from the observational evidence that the "surface of the last scattering", which we observe today as the *Cosmic Microwave Background* (CMB), is highly homogeneous. This means that all regions on the CMB sky (even separated by a big distance) are statistically the same. It makes us to assume that these separated patches were somehow causally connected in the early period. In order to see it properly, we can introduce the cosmological horizon R_c [54]: [2]

$$R_c = r_c a = \frac{1}{H}, \tag{1.37}$$

where r_c is the comoving cosmological horizon, which would be more convenient to use.

If we assume that due to some conditions, r_c decreases when the scale factor a increases, we can resolve the horizon problem: all the presently visible universe could be causally connected at some earlier period (see figure 1.6).

Flatness problem. Substituting the critical density (1.7) in the Friedmann equation (1.5) we can obtain that

$$|1 - \Omega| = \frac{|k|}{H^2 a^2}, \tag{1.38}$$

where $\Omega = \sum_i \Omega_i$.

Since the factor H^2a^2 is decreasing when $a \propto t^\lambda$ grows for all $0 < \lambda < 1$ ($\lambda = 1/2$ radiation, $\lambda = 2/3$ matter domination eras, section 1.2), the relation (1.38) tells us that an initial small deviation from the *flat* universe will increase with time. Thereby, if we have a small curvature deviation for the Planck era, this discrepancy will grow by 10^{60} times. This result requires fine-tuning or corresponding mechanism that can lead to an increase of H^2a^2, when a^2 is increasing. It is the same condition that we needed for the horizon problem and which can be accomplished by the inflation model.

[2] It should be noticed the difference between R_H (1.15) and R_c (1.37). If two points are separated by the distance bigger than particle horizon, R_H, they were never causally connected; if by the cosmological horizon, R_c, they are causally disconnected now. It follows that we can have $R_H > R_c$, which is sufficient for solution of the horizon problem [55].

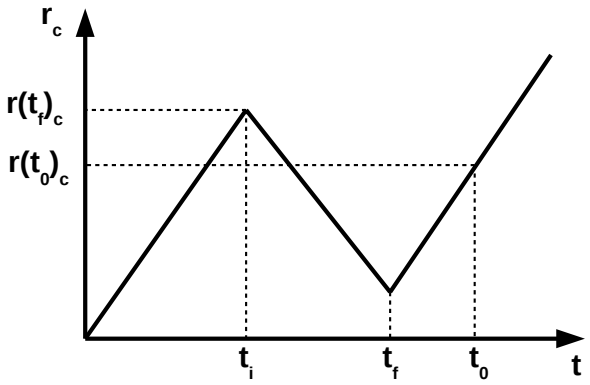

Fig. 1.6 Schematic picture of the evolution of comoving cosmological horizon r_c (1.37). The inflation period starts at t_i, finishes at t_f. Current time t_0 corresponds to smaller value of comoving cosmological horizon than at the beginning of inflation: $r_c(t_i) > r_c(t_0)$. In this way, all observable universe was causally connected during some earlier period.

Monopole problem. We know that the gauge symmetry of electromagnetic interaction is described by the group $U(1)$. Let's assume that there is a GUT, whose gauge symmetry is described by a compact covering group G. And let's then assume that this group G includes an unbroken subgroup $U(1)$ (which just means that GUT includes electromagnetism). In this case, the symmetry breaking process of the group G inevitably gives rise to magnetic monopoles [56], [57]. The mass of this particle should be very high and it is not limited by any theoretical constraints: $M_M \approx 500 - 10^{16} GeV$ [58]. It is much bigger than the proton mass $M_p \approx 1 GeV$. Therefore, a GUT with a compact covering group predicts the existence of very heavy particles, which should be separated by the particle horizon distance R_H (1.15) at the moment of their production. As it was shown in the paper [59], monopole annihilation proceeds very slowly, which is why the density parameter of monopoles $\rho_M \propto \frac{M_p}{R_H^3}$ will exceed the critical density ρ_{crit} (1.7) by many orders of magnitude. Possessing this density the universe would have collapsed a long time ago. This disagreement, as it is going to be shown below, can be resolved by the inflation scenario, as well as the two previous issues.

Inflation dynamics. Now we can consider the solution of all mentioned problems. As it was already emphasised, we need to achieve the condition when the comoving cosmological horizon r_c (1.37) is shrinking:

$$\frac{d}{dt}(r_c) = \frac{d}{dt}\left(\frac{1}{Ha}\right) < 0 \rightarrow \frac{d^2a}{dt^2} > 0. \tag{1.39}$$

It means that we need to have an accelerated expansion of the universe. Substituting the condition (1.39) in the equation (1.6), we see that we need to satisfy the following relation between density and pressure

$$\rho + 3P < 0. \tag{1.40}$$

The last condition can be realized by a scalar field φ. We can write the general Lagrangian for this scalar field as

$$\mathcal{L} = \frac{1}{2}\partial_\mu\varphi\partial^\mu\varphi - V(\varphi), \tag{1.41}$$

where $V(\varphi)$ is a potential of this field.

Using the definition of the energy-momentum tensor

$$T^{\mu\nu} = -\frac{2}{\sqrt{g}}\frac{\delta S}{\delta g^{\mu\nu}} \tag{1.42}$$

and the expression for a perfect isotropic fluid (1.4), we can conclude that

$$\rho_\varphi = \frac{1}{2}\left(\frac{d\varphi}{dt}\right)^2 + V(\varphi), \tag{1.43}$$

$$P_\varphi = \frac{1}{2}\left(\frac{d\varphi}{dt}\right)^2 - V(\varphi). \tag{1.44}$$

Let's substitute (1.43), (1.44) in (1.5), (1.8) and obtain equations of motion for scalar field in the FLRW metric

$$H^2 = \frac{1}{3M_{pl}^2}\left[V(\varphi) + \frac{1}{2}\left(\frac{d\varphi}{dt}\right)^2\right], \tag{1.45}$$

$$\frac{d^2\varphi}{dt^2} + 3H\frac{d\varphi}{dt} = -V', \tag{1.46}$$

where $M_{pl} = 1/\sqrt{8\pi G}$ and $V' = \frac{dV}{d\varphi}$.

From these relations it is seen that the inflation takes place when

$$V(\varphi) >> \left(\frac{d\varphi}{dt}\right)^2. \tag{1.47}$$

Making an assumption that the scalar field dominates and satisfies (1.47), one can obtain the following conditions for the form of the field potential (so called slow-roll conditions)

$$\varepsilon_V = \frac{M_{pl}^2}{2}\left(V'/V\right)^2 << 1, \tag{1.48}$$

$$|\eta_V| = M_{pl}^2\left|V''/V\right| << 1. \tag{1.49}$$

In order to solve the flatness, horizon and monopole problems, the inflation should persist for a sufficient period. We can express this demand by the e-fold parameter [60]

$$N = \int_{\varphi_{end}}^{\varphi}\frac{d\varphi}{\sqrt{2\varepsilon_V}} \gtrsim 60. \tag{1.50}$$

Thus scalar field, which causes the inflation period, we will call inflaton.

In order to stop the inflation period of the universe, one can use the symmetry breaking mechanism, as is done in the hybrid inflation mechanism [61]. Another scalar field ψ should be introduced for this purpose. Let's say that we have an inflaton field φ, which satisfies the slow-roll conditions (1.48)-(1.49), and another field ψ, whose mass depends on inflaton field. The system in this situation can be described by the potential

$$V(\varphi, \psi) = a(\varphi^2 - \varphi_0^2)\psi^2 + b\psi^4 + c, \tag{1.51}$$

where φ_0^2, a, b and c are positive constants.

It is seen from the (1.51) that when the inflaton is big $\varphi^2 > \varphi_0^2$, the additional field ψ is massive. When the inflaton reaches the relation $\varphi^2 = \varphi_0^2$, the field ψ becomes massless. And when $\varphi^2 < \varphi_0^2$, the field ψ has negative mass (tachyonic field). As a result, for the case $\psi = 0$, the potential (1.51) is flat in the inflaton φ direction and satisfies the slow roll conditions (1.48)-(1.49). It corresponds to the 1-point in the figure 1.7, and provides the inflation period. When the inflaton reaches the value $\varphi^2 = \varphi_0^2$ the field ψ starts to be unstable and this point is illustrated by the number 2 in the figure 1.7. Further decrease of φ^2 induces symmetry breaking of the field ψ and leads to the end of inflation period. Points 3 and 4 correspond to possible values of the field $\psi_0^2 = \frac{a\varphi_0^2}{2b}$.

Because of symmetry breaking at the end of the inflation period, we anticipate that topological defects should be common for these scenarios. The potential described above appears in a range of supersymmetric models [21, 23–26] (details in the section 1.6). Additionally, a similar form of potential (1.51) appears in the brane type of inflation (details in the sections 1.7).

1.6 Cosmic strings from D- and F-term inflation

1.6.1 F-term inflation and cosmic strings

In the context of supersymmetry, there are different scenarios that can be used for inflation. One possible way to implement inflation in supersymmetric theory is to use the dominant contribution from the so-called F-term (for details see [62, 63]). It can be realized by the renormalisable superpotential

$$W_{\text{inf}}^F = d\Phi_0 \left(\Phi_+\Phi_- - \eta^2\right), \tag{1.52}$$

where $\Phi_\pm$ are charged ($q_\pm = \pm 1$) and the Φ_0 are neutral superfields with real constants η, d.

The F-term part of the scalar potential from (1.52) is

$$\begin{aligned} V_F(\phi_+, \phi_-, \varphi) &= |F_{\Phi_+}|^2 + |F_{\Phi_-}|^2 + |F_{\Phi_0}|^2 = \\ &= d^2|\phi_+\phi_- - \eta^2|^2 + d^2|\varphi|^2\left(|\phi_-|^2 + |\phi_+|^2\right), \end{aligned} \tag{1.53}$$

where $|F_{\Phi_i}| = |\frac{\partial W}{\partial \Phi_i}|_{\theta=0}$ ($i = +, -, 0$) means that after differentiation only the scalar component of the superfields is taken into account: ϕ_+, ϕ_- and φ correspondingly.

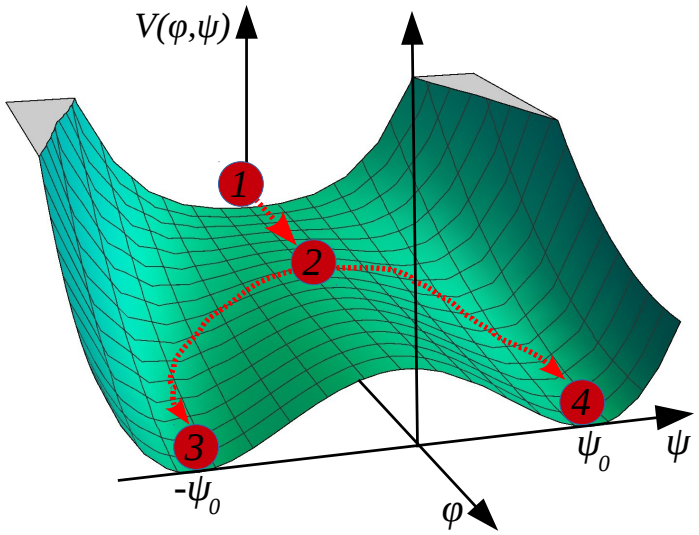

Fig. 1.7 The form of the potential for hybrid type of inflation (1.51). When the field $\psi^2 = 0$, the potential provides conditions for inflation, being flat in the φ field direction. The inflation starts from the point 1, with positive mass of the field ψ. With decrease of the value φ^2, at the point 2 the field ψ becomes massless. When the inflaton field reaches $\varphi = 0$, the inflation period ends and the field ψ experiences symmetry breaking. Possible values of the field ψ are denoted by points 3 and 4, where $\psi_0 = \frac{a\varphi_0^2}{2b}$.

From (1.52) it is seen that until $\varphi^2 > \eta^2$ the potential has a valley of local minima $V_F = d^2\eta^4$, this valley corresponds to the line 1-2 in figure 1.7. The period when the potential is constant is responsible for the inflation period and can satisfy slow-roll conditions (1.48)-(1.49). When the field reaches $\varphi = 0$, the potential becomes $V_F = 0$ with $\phi_+ = \phi_- = \eta$, which is responsible for the end of inflation. As a result, we see that a supersymmetric model with dominant F-term leads to the hybrid inflation scenario. However, the generalization of this approach to supergravity leads to the η-problem: the condition $|\eta_V| << 1$ (1.49) cannot be satisfied. Only some specific terms can help to tackle this problem [64–66].

The relevant issue for us is that this inflation ends with the phase transition and consequently can produce cosmic strings. By establishing the full Lagrangian one can find equations of motion that possess string-like solutions [67]. In particular, for the bosonic part of the Lagrangian, the ansatz (1.18) together with (1.22) gives an equation of motion identical to (1.23) (the string profile is illustrated on the right panel in figure 1.2) [63]. At the same time, if the Yukawa coupling is present, as it is anticipated for the supersymmetric model [67], in the core of the string there should exist a fermionic contribution.

The fermion field trapped on the string core propagates along the string. In order to study this effect, one can consider the following ansatz in the cylinder coordinates [45]

$$\Psi(r, \theta, z, t) = \beta(z, t)\Psi_0(r, \theta), \tag{1.54}$$

where Ψ_0 is the zero mode, while $\beta(z, t)$ is responsible for the field propagation.

The Dirac operator for this fermion field can be split into components transverse $\not{D}_T = \gamma^1\partial_x + \gamma^2\partial_y$ and longitudinal to the string $\not{D} = \gamma^0\partial_t + \gamma^3\partial_z + \not{D}_T$, where γ^μ are Dirac matrices. Since in the core of the string all scalars are equal to zero, one can write the equation for the longitudinal components as

$$\left(\frac{\partial}{\partial t} \pm \frac{\partial}{\partial z}\right)\beta(t,z) = 0, \tag{1.55}$$

where we used the property that $i\gamma^0\gamma^1\gamma^2\gamma^3\Psi = -\Psi \;\Rightarrow\; \gamma^0\gamma^3\beta(t,z) = \pm\beta(t,z)$.

The general solution of the equation (1.55) is given by

$$\beta(t,z) = F_f(z \pm t), \tag{1.56}$$

where F_f is an arbitrary function.

We see that the fermion can travel along the string with a speed of light in one string direction $\pm z$. As a result, we end up with a superconducting string, described in [45]. The presence of the internal structure can influence cosmic string dynamics and consequently observational predictions. The effect of the current on the string network evolution will be presented in the chapter 3.

1.6.2 D-term inflation and cosmic strings

Another type of inflation that can be implemented in the context of supersymmetry is D-term inflation. We can start the consideration of this model with the same superfields as for F-term inflation: Φ_0, Φ_+, $\Phi-$. But this time, these fields form the superpotential in the following way

$$W^D_{\text{inf}} = d\,\Phi_0\Phi_+\Phi_-. \tag{1.57}$$

As a result, from the equation (1.57) one can obtain the full scalar potential for global supersymmetry as[3]

$$V = \underbrace{d^2|\varphi|^2\left(|\phi_-|^2 + |\phi_+|^2\right) + d^2|\phi_-\phi_+|^2}_{F-\text{term}} + \underbrace{\frac{g^2}{2}\left(|\phi_+|^2 - |\phi_-|^2 - \xi\right)^2}_{D-\text{term}}, \tag{1.58}$$

where constants are: g - gauge coupling, ξ - Fayet-Iliopoulos term, which is non zero only if the gauge symmetry is $U(1)$.

It is seen from the expression (1.58) that when the $|\varphi| > g\sqrt{\xi}/d$, the minimum of the potential is reached when $\phi_+ = \phi_- = 0$. Hence, the F-term is vanishing and only the D-term stays important. This situation provides the valley of the constant potential $V = g^2\xi^2/2$ in the φ direction. As a result, satisfying conditions (1.48) and (1.49), we can obtain an inflation scenario from the D-term as well. It is worth to note that the generalization of this idea to supergravity does not lead to a η-problem, as it was for the F-term inflation [68, 69].

As the field $\varphi \to 0$ the D-term inflation ends with symmetry breaking. Let's consider just the dominant D-term contribution of the potential (1.58), to see how cosmic strings can

[3]For details of the full expression for the scalar potential in global supersymmetry see [62, 63]

arise from this type of inflation

$$V_D = \frac{g^2}{2}\left(|\phi|^2 - \eta^2\right)^2, \tag{1.59}$$

where we introduced the field ϕ instead of ϕ_- and ϕ_+ and redefined, for convenience, $\xi = \eta^2$, since ξ is a positive constant.

Applying the ansatz (1.18) and (1.22) in the cylinder coordinates, one can show that from the equations of motion the following equations can be obtained [67]

$$\begin{aligned} f' &= n\frac{1-\alpha}{r}f, \\ n\frac{\alpha'}{r} &= g^2\eta^2(1-f^2). \end{aligned} \tag{1.60}$$

Equations (1.60) describe the profile of cosmic strings, which can be formed from the D-term inflation. Using these equations, one can study the internal structure of cosmic strings. It was shown that the supersymmetry in that case is only half broken and hence, the zero mode can propagate along the string only in one direction. By comparison, for strings from F-term, the supersymmetry is completely broken and zero modes can propagate in both directions [67].

The presence of cosmic strings from inflation scenarios allows us to put additional constraints on these models. In particular, it was shown that using observational predictions from cosmic strings, it is possible to restrict F and D-term inflations [70, 71][4]. Moreover, supersymmetric GUT due to spontaneously broken symmetry also can lead to cosmic string formation. It was shown that for all supersymmetric GUT models that do not produce monopoles, contain proper baryogenesis description and stay in agreement with proton life time measurements, lead to creation of cosmic strings [21].

It should be noted that models which were used for cosmic string network description to obtain restrictions for D, F-term inflations, are not sufficiently accurate. They do not take into account some important features of these strings. Improvements in this direction will be presented here in the chapter 3.

1.7 Brane Inflation and Cosmic Superstrings

Let us consider a schematic picture of brane inflation and how cosmic strings can be produced at the end of it [73, 74]. It can be done by considering a Type IIB string model. The ground state in this theory can be represented as a direct product of two Dirac spinors (left and right moving modes), whose dimension is $2^{n/2}$ for n-dimensional space. Since the dimension of strings of Type IIB is 10, the ground state is $32 \otimes 32$. This 32-dimensional representation is reducible: Dirac spinors can be written in terms of two 16-dimensional Weyl spinors with opposite chiralities. By imposing a physical state condition (mass-shell condition

[4]It should be noted that for the superstring-inspired D-term inflation in principle it is possible to avoid cosmic string production [72]

and $L_m|\phi\rangle = 0$, where L_m - Virasoro operators), nonphysical states can be decoupled and $16 \to 8$. In order to produce a chiral theory, two spinors with the same chirality must be taken. As a result, the ground state for strings of type IIB is $8 \otimes 8$. This spinor product can be decomposed into a sum of tensor representations

$$8 \otimes 8 = [0] \oplus [2] \oplus [4]_+ . \tag{1.61}$$

This means that Type IIB theory possesses a scalar, two form and self-dual four form gauge fields. By contraction with the totally antisymmetric symbol $\epsilon_{\alpha_1\alpha_2\ldots\alpha_n}$, the six, eight and ten forms of gauge field can be built from four, two and zero forms correspondingly. Each $p+1$ gauge field determines the stability of the p-brane. That is why for Type IIB theory there are $D9$, $D7$, $D5$, $D3$ and $D1$[5] stable branes [74].

These stable p-branes inspired the original idea for brane inflation. The inflation potential comes from brane interactions [75]. Later this idea got development for more realistic case, where the potential is represented by a brane-antibrane system[6] [76]. In this scenario the brane and antibrane configuration is embedded into a highly warped geometrical throat [77], which has a Klebanov-Strassler solution [78].

The potential between 3-dimensional brane and antibrane separated by a long distance in terms of scalar field φ can be written as

$$V(\varphi) = 2T_3 \left(1 - \frac{1}{2\pi^3} \frac{T_3^3}{M_{pl10}^8 \varphi^4}\right), \tag{1.62}$$

with slow-roll parameters as

$$\varepsilon_V \approx \frac{M_{pl}^2}{N^2} \frac{\varphi_0^2}{\varphi^{10}}, \tag{1.63}$$

$$\eta_V \approx -\frac{M_{pl}^2}{N} \frac{\varphi_0^4}{\varphi^6}, \tag{1.64}$$

where $M_{pl10} = \frac{M_{pl}^2}{L^6}$ is a 10-dimensional Planck mass, T_3 is a tension of 3 brane/antibrane, L is a volume of compactifaction manifold and φ_0 is a parameter defined by a tension of branes, string coupling and integrals that specify fluxes (for details see [76]).

Moreover, since the brane and antibrane attract each other, they eventually collide. The approximation, which was used above, does not work for a short distance between branes. As a result, the potential (1.62) is not valid anymore. To describe the system when brane and antibrane come close to each, we should introduce an additional scalar field ψ. This field plays the same role as in the hybrid inflation scenario. Specifically, for a large distance the field ψ is massive. When the distance reaches characteristic length, the field ψ becomes massless. Eventually, the field ψ is tachyonic, when brane and antibrane annihilate. This model gives a natural mechanism for the end of inflation period. The form of potential in

[5]The letter D means that these branes ensure the Dirichlet boundary conditions for fundamental strings.
[6]An antibrane is a charge conjugate brane with the same tension as the corresponding brane.

this case we can represent as

$$V(\varphi,\psi) = a\left(\varphi^2 - \varphi_0^2\right)\psi^2 + b\psi^4 + 2T_3\left(1 - \frac{1}{2\pi^3}\frac{T_3^3}{M_{pl10}^8\varphi^4}\right), \tag{1.65}$$

where a, b and φ_0^2, as it was in (1.51), are positive constants.

Eventually we end up with a potential in the form (1.65). As we already mentioned before, such form of potential can lead to formation of topological defects at the end of inflation. It happens due to symmetry breaking by the field ψ, when it becomes tachyonic. The table 1.1 shows possible brane inflation models and the corresponding string productions. The term *thermal* cosmic strings defines such string that are produced by reheating, which eventually should appear after the inflation [79], [20].

Table 1.1 Types of viable inflation scenarios, and strings that can be produced at the end of each scenario. More details can be found in [20].

Types of branes:	Inflation	Cosmic string types	
		Kibble	Thermal
$D(9-\bar{9})$	×		
$D(7-\bar{7})_{1,2}$	✓	$5_{1,2}$	-
$D(7-\bar{7})_{1,3}$	✓	$5_{1,3}$	-
$D(5-\bar{5})_1$	✓	3_1	1_0
$D(5-\bar{5})_3$	✓	3_3	-
$D(3-\bar{3})_0$	✓	1_0	-
$D(1-\bar{1})$	×		

Additionally, it is worth to note one important feature that restricts the variety of topological defects in the brane inflation scenario. In order to obtain the usual 4-dimensional space-time, the initial 10-dimensional space-time should be compactified as $(T^2\times T^2\times T^2)/Z_N$. In this case, stable branes can warp different dimensions. Since there are only odd-dimensional stable branes, after the compactification only string-like objects (or $\mathbb{R}^{3,1}$ branes that cover all space), can be produced as a topological defect. It happens due to the fact that the Kibble mechanism doesn't work for compactified dimensions: they are not big enough to provide patches separated by particle horizon distances R_H (see figure 1.8). The table 1.2 demonstrates how it should be for $D5$ branes.

We saw that the model of brane inflation has an outcome in the form of cosmic strings. In addition, D-strings (1-dimensional branes), described above, can be bounded with fundamental strings, F-strings [80]. Let us suppose that the F-string is charged by an antisymmetric field $B_{\mu\nu}$ and D-strings are charged by the field $A_{\mu\nu}$. Then, $SL(2,\mathbb{Z})$ transformations interchange their potentials

$$\begin{pmatrix} B_{\mu\nu} \\ A_{\mu\nu} \end{pmatrix} \to \begin{pmatrix} 0 & 1 \\ -1 & 0 \end{pmatrix}\begin{pmatrix} B_{\mu\nu} \\ A_{\mu\nu} \end{pmatrix} = \begin{pmatrix} -A_{\mu\nu} \\ B_{\mu\nu} \end{pmatrix}. \tag{1.66}$$

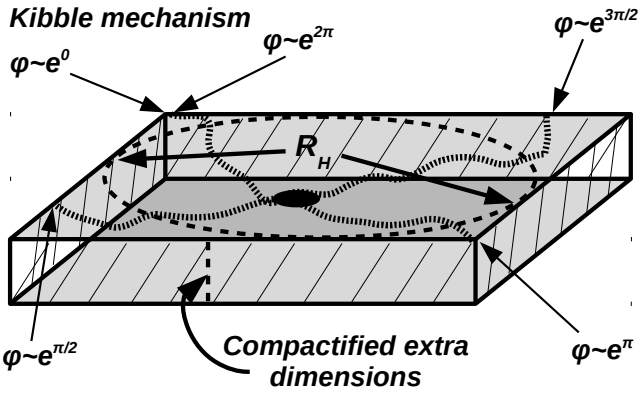

Fig. 1.8 Kibble mechanism for compactified extra dimensions. Topological defects can be produced only for extended dimensions. The Kibble mechanism is not applicable for compactified dimensions, since their size is smaller than particle horizon size (1.15).

Table 1.2 Possible combinations of wrapping for the stable branes D5. The labels on the branes indicate which of the 2-cycles they wrap in the compactified dimensions. The empty spots indicate unwrapped dimensions, and check marks indicate dimensions that are wrapped by branes [20].

	Dimensions					
Stable branes	01	23	45	67	89	
$D5_1$	✓	✓	✓			$\mathbb{R}^{3,1}$ branes
$D5_2$	✓	✓		✓		
$D5_3$	✓	✓			✓	
$D5_{1,2}$	✓		✓	✓		strings
$D5_{1,3}$	✓		✓		✓	
$D5_{2,3}$	✓			✓	✓	

Additionally, we should anticipate existence of a complex scalar doublet[7]

$$\tau = C_0 + \frac{i}{g_s}, \tag{1.67}$$

where C_0 is a scalar field [81]. The scalar doublet τ transforms under the $SL(2,\mathbb{Z})$ in the following way

$$\tau \to -\frac{1}{\tau}. \tag{1.68}$$

As a result, we can conclude that F-strings are connected with D-strings by these transformations. It means that when the coupling constant is small, $g_s << 1$, F-strings behave as fundamental strings, when $g_s >> 1$, D-strings behave as fundamental strings. This is called S-duality (the description can be found in [81] and [82]). From this duality it follows that F and D-strings can form a bound state. If we assume that supersymmetry is not

[7]Sometimes τ is referred as *axion-dilaton* field. The coupling constant g_s is connected with the vacuum expectation value of dilation field Φ as $g_s =< \mathrm{e}^{\Phi} >$ and the scalar field C_0 possess a shift symmetry: $C_0 \to C_0 + \mathrm{const}$

broken, then the *Bogomol'nyi–Prasad–Sommerfield* (BPS) condition should saturate. In this case, the tension of a new (p, q)string can be determined as [17, 83, 84]

$$\mu_{p,q} = \mu_F \sqrt{(p - q\, C_0)^2 + q^2/g_s^2}. \tag{1.69}$$

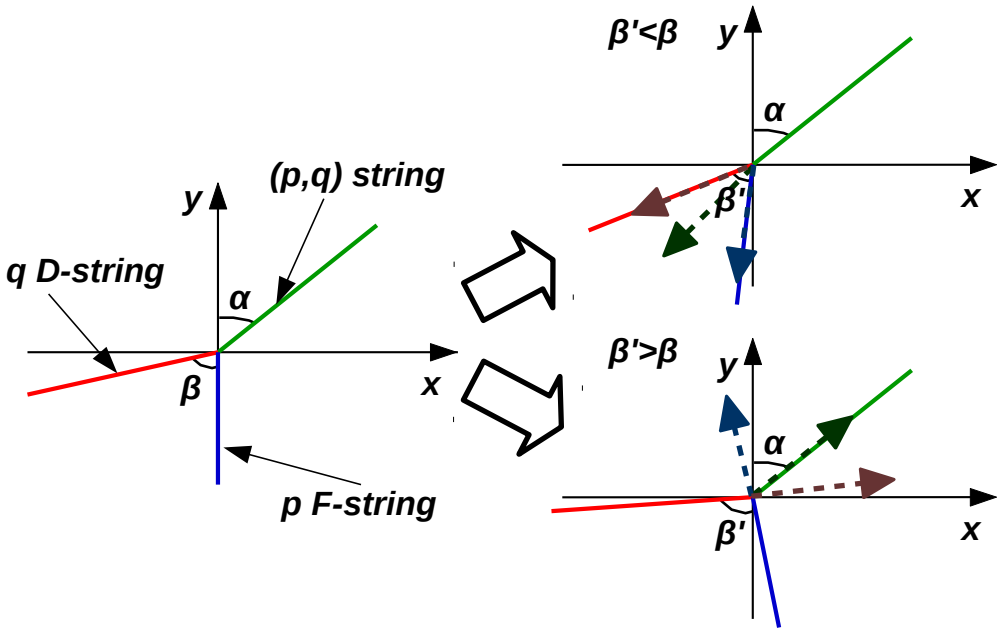

Fig. 1.9 Collision of p F-string with q D-string gives rise to (p, q)string. The balance between strings is provided not only by string tensions, but also by the junction dynamics. The left part of the figure illustrates the configuration of strings in the rest frame defined by angles α and β. When the angle β' (angle between straight D and F-strings) is bigger than the angle β, the green string is shrinking. When the angle β' is smaller than the angle β the green string is growing.

When the BPS condition is saturated, it corresponds to the string tension balance, figure 1.9 and these strings are called cosmic superstrings. However, we should remember that in this situation strings can be shrinking or enlarging during the evolution. The dynamics of this phenomena leads to other possible configurations of strings (other α and β angles in the figure 1.9) with dynamical change of the length [85]. More details about junction dynamics and their influence on string networks will be given in chapter 4.

Production of cosmic superstrings at the end of brane inflation should lead to observational consequences. Absence of cosmic superstrings detection with particular tensions leads to restrictions on brane inflation [86, 87]. In that sense, cosmic superstrings play the role of the probe of early period of the universe.

It should be noted that the valid brane inflation scenario imposes bounds on F-string tension [18, 20]

$$10^{-12} < G\mu_F < 10^{-6}, \tag{1.70}$$

while D-string tension is related as

$$\mu_D = \frac{\mu_F}{g_s}. \tag{1.71}$$

This condition comes from the inflation requirements for the brane inflation.

In order to obtain some possible predictions from the presence of cosmic superstrings, the evolution of its network should be studied in detail. Until now, most progress was achieved in the description of ordinary cosmic string network evolution. Due to a number of numerical simulations and analytical models there were obtained some observational predictions of cosmic strings presence. However, some debatable questions on cosmic string networks are still open. The current thesis is aimed to clarify some of them.

1.8 Summary

In this chapter we gave a brief introduction to the standard ΛCDM model and inflation period at the early stage of the universe's evolution. There were presented only aspects relevant to the current work, which will be used further. In this context we reviewed the condition under which topological defects can appear on the cosmological scale. In particular, we reviewed the Kibble mechanism and gave a short overview of possible cosmic strings. Specifically we revisited global, Abelian Higgs, non-Abelian, superconducting strings and provided a connection between field theory strings and their infinitely thin limit analogue - Nambu-Goto string action.

Special attention was dedicated to the possible scenarios under which cosmic strings can appear. We gave some details of hybrid type of inflation and have shown how strings can be produced at the end of it. With some details we revisited possible situations when supersymmetric models give rise to cosmic strings. Especially we described situations with F and D terms inflation from supersymmetric models, where cosmic strings can be produced. We underlined the importance of cosmic strings in possible additional restrictions for these types of inflations.

Another scenario, which is relevant to cosmic strings production, brane type of inflation, was recalled in the last section. It was shown how cosmic (super)strings can be produced at the end of the brane inflation. We presented details about specific properties for these kind of cosmic strings and pointed out important differences that can influence the scaling of the cosmic superstring network.

In the same way as it is applied to some supersymmetric models of the early universe, a proper understanding of the behaviour of junctions (example of junction is illustrated in the figure 1.9) for superstring networks will give a more accurate way to put restrictions on brane inflation. The analytic approach, the base of which is going to be described in the next chapter 2, opens the opportunity to study specifics of cosmic superstrings, which are not reachable by numerical simulations.

Chapter 2

The standard VOS model and simulations of defect networks

As was already mentioned in section 1.4, a network of defects can be readily studied using numerical techniques. To make a realistic simulation of strings with all possible properties is an impracticable task today, due to the necessity of huge computing power. Meanwhile, simulations of simple defect networks can reveal important features and play the role of a testbed for more complicated examples. Moreover, these simulations are necessary to calibrate analytic approaches.

In this chapter we are going to introduce the semi-analytic *velocity-depend one scale* (VOS) model for topological defect networks evolution. It is based on the assumption that defects are infinitely thin (section 1.4.5). Developing the equations of motion for these defects, we apply an averaging procedure to obtain macroscopic variables. Since there is no firm approach to include dissipation mechanisms at the level of the Lagrangian, we need to include mechanisms of energy loss phenomenologically. Eventually, applying all these steps, it is possible to build a final system of differential equations, called VOS model. It is aimed to describe the defect network's evolution at a macroscopic level [88, 89]. This approach is applicable for discussing defect networks of arbitrary dimensions, evolving in arbitrary dimensional space [90–94].

At the step when energy loss terms are introduced into the VOS model, new undefined constants appear. These constants cannot be determined from first principles. As a result, numerical simulations are required to determine them phenomenologically. In this chapter we are going to test the VOS model against data from domain wall network simulations. Specifically, we are going to build upon the work done in [95, 96] and study an extensive set of high-resolution field theory simulations of domain wall networks, which use the *Press, Ryden and Spergel* PRS algorithm [97]. Compared to earlier works, these simulations are both larger (4096^3 boxes, the largest currently available) and span a more diverse set of conditions, including simulations with fixed expansion rates as well as, for the first time for domain walls, a series of simulations that accurately span the radiation-matter transition. This extended high-resolution dataset enables us to calibrate and significantly improve the analytic model, as was previously done for strings [98, 99].

Additionally, we revisit the issue of the role of damping mechanisms on the evolution of defect networks. In particular, we show that a sufficiently large Hubble damping (specifically, a power-law dependence of the scale factor $a \propto t^{\lambda}$ with λ below, but close to, unity) leads to a linear scaling regime where the network is non-relativistic. This is therefore another realization of a Kibble scaling regime, allowing us to interpret the linear scaling solution as the Kibble regime for Hubble-damped networks [36, 100]. Moreover, there is also a stretching regime counterpart for Hubble-damped networks, whose behaviour we first derive analytically in a VOS model context and then confirm numerically (for a description and definitions of scaling regimes see sections 2.2.2 and 2.2.5).

The wider range of expansion rates simulated yields an additional benefit. The low velocities and high densities of these fast expansion networks imply that the averages of sets of simulations with the same expansion rate but different initial conditions will have smaller statistical uncertainties than those for slower expanding boxes of the same size. Additionally, we study numerical tests allowing us to estimate the systematic uncertainties in the measurements of the numerical quantities relevant for the calibration of the model. Both of these allow us to make additional improvements in the VOS model calibration for domain walls.

At the same time, the simulations confirm that the VOS model approach is very successful in describing defect networks. This gives us the opportunity for better insight and contemplation of the network dynamics.

2.1 The Standard VOS Model

To give the analytic description of defect network evolution, one should concentrate on macroscopic (thermodynamic) parameters. The first attempt in this direction was done in reference [101], where the one-scale model was presented. In this original model the string network was described by a single macroscopic variable: a characteristic length, which was playing the role of correlation length, radius of string curvature and string separation distance. Later this description was extended in [102, 103], where a detailed study of loop production and their fragmentation was given. Notable progress on the network description, using arguments of statistical mechanics was achieved in [104]. A more sophisticated model was presented by Austin, Copeland and Kibble (ACK) [105], where already three distinct length scales are taken into account. The original analytic VOS model was developed in [88]. This model gave a firm description of the so-called scaling behaviour of the network and was refined in [89].

The VOS model does not include as many details as the ACK model [105], but it is sufficient to give the main properties of the defect network evolution, implementing a dynamical equation for the network's *root-mean-square* (rms) velocity. Moreover, in contrast to the ACK model, the VOS model avoids the introduction of many undefined parameters. Another important feature of the VOS model is that it can be relatively easily extended to string models with more complex properties [44, 106–109]

Let us revisit the main steps in the derivation of the original VOS model for strings. The description starts from the effective Nambu-Goto action introduced in section 1.4.5. To obtain equations of motion we need to vary the action (1.36) with respect to x^μ. Using the following useful property

$$d\sqrt{\gamma} = \frac{1}{2}\sqrt{\gamma}\gamma^{ab}d\gamma_{ab}\,, \tag{2.1}$$

one can obtain

$$\frac{1}{2}\sqrt{\gamma}\gamma^{ab}g_{\mu\nu,\eta}x^\mu_{,a}x^\nu_{,b} = \partial_c\left(\sqrt{\gamma}\gamma^{ab}g_{\mu\eta}x^\mu_{,a}\delta^c_b\right), \tag{2.2}$$

where δ^c_b is a Kronecker symbol.

To simplify equations (2.2) we can chose a convenient parametrization. As it is shown on figure 1.5 we can chose the following form of the worldsheet parametrization

$$\begin{gathered}\sigma^0 = \tau, \quad \sigma^1 = \sigma,\\ g_{\mu\nu}\,\dot{x}^\nu x'^\mu = 0,\end{gathered} \tag{2.3}$$

where $x^\mu_{,0} = \dot{x}^\mu$, $x^\mu_{,1} = x'^\mu$ and the second equation means that tangent vectors for (τ,σ) parametrization are orthogonal.

The parametrization (2.3) can be always established for any background $g_{\mu\nu}$ metric. At the same time, for the case when the metric $g_{\mu\nu}$ is a Minkowski space, there is an additional degree of freedom that allows us to simplify equations even more. This additional degree of freedom comes from the presence of time translation invariance, i.e. the presence of timelike Killing vector fields. In general it is not the case for the FLRW metric.

Using the parametrization (2.3), let us rewrite the equation (2.2) in a handy form for the flat ($k = 0$) FLRW metric (1.1) with conformal time τ

$$\begin{gathered}\dot{\varepsilon} + 2\varepsilon\frac{\dot{a}}{a}\dot{\mathbf{x}}^2 = 0,\\ \ddot{\mathbf{x}} + 2\frac{\dot{a}}{a}\dot{\mathbf{x}}(1-\dot{\mathbf{x}}^2) = \frac{1}{\varepsilon}\left(\frac{\mathbf{x}'}{\varepsilon}\right)',\end{gathered} \tag{2.4}$$

where $\varepsilon^2 = \frac{\mathbf{x}'^2}{1-\dot{\mathbf{x}}^2}$ and $\mathbf{x}$ defines three-dimensional spatial vector.

From the first equation (2.4) it is seen that for the Minkowski space ($\dot{a} = 0$), the value ε is preserved during the evolution. In order to infer the physical meaning of the variable ε we can calculate the energy-momentum tensor for the Nambu-Goto action (1.36)

$$T^{\mu\nu}\sqrt{-g} \equiv -2\frac{\delta S}{\delta g_{\mu\nu}} = \mu_0\int\sqrt{\gamma}\gamma^{ab}x^\mu_{,a}x^\nu_{,b}\delta^4(x^\rho - x^\rho(\sigma^c))d\sigma^0 d\sigma^1, \tag{2.5}$$

where $\delta^4(...)$ is a Dirac delta function for the four-dimensional argument.

To study the evolution of the string network, we need to apply the averaging procedure from [88]. To achieve this goal and to find a large-scale description, we need to integrate equations (2.4) over the parameter σ. The integration over σ has rather symbolic meaning, which implies that we integrate over all strings and obtain macroscopic parameters for the whole network. In this way, using the parametrization (2.3), the macroscopic energy of the

string network can be written as

$$E_0 = \mu_0 a(\tau) \int \sqrt{\gamma}\gamma^{00} d\sigma = \mu_0 a(\tau) \int \varepsilon d\sigma \,. \tag{2.6}$$

From the expression (2.6) we see that ε plays the role of energy density of the string. Hence, the first equation (2.4) corresponds to evolution of the microscopic energy density ε, which is conserved for Minkowski space.

Let's introduce another macroscopic variable, the rms velocity:

$$\upsilon^2 = \frac{\int \dot{x}^2 \varepsilon d^2\sigma}{\int \varepsilon d^2\sigma}. \tag{2.7}$$

Using the definitions of macroscopic variables (2.6) and (2.7), one can average equations (2.4) and obtain evolution equations for macroscopic variables [88]

$$\begin{aligned} \frac{d\rho}{dt} &= -2H\rho\left(1+\upsilon^2\right), \\ \frac{d\upsilon}{dt} &= \left(1-\upsilon^2\right)\left(\frac{k(\upsilon)}{R} - 2H\upsilon\right), \end{aligned} \tag{2.8}$$

where $\rho = E_0/a^3$ is an energy density, R is an average curvature of strings in the network, $k(\upsilon)$ is a momentum parameter, which was analytically estimated as [88]

$$k(\upsilon) = \frac{2\sqrt{2}}{\pi}(1-\upsilon^2)(1+2\sqrt{2}\upsilon^3)\frac{1-8\upsilon^6}{1+8\upsilon^6}. \tag{2.9}$$

The system of equations, as it was mentioned in the beginning of this chapter, does not include an energy loss part, while the real string network during the evolution can dissipate its energy. There are several mechanisms that can be responsible for loss of energy in the string network. The most significant should be the loop production and radiation[1]. The loop production can be caused by self-intersection of the curved string or by exchange of strings ends (figure 2.1 top and bottom panels correspondingly). To include the energy loss term caused by the loop production, we can add an appropriate term in the system (2.8) (for more details see [88, 102, 103])

$$\frac{d\rho}{dt}\Big|_{loops} = c\upsilon\frac{\rho}{L}, \tag{2.10}$$

where the new variable L - corresponds to average distance between strings.

[1]This mechanism will be considered for domain wall networks in the section 2.3.2

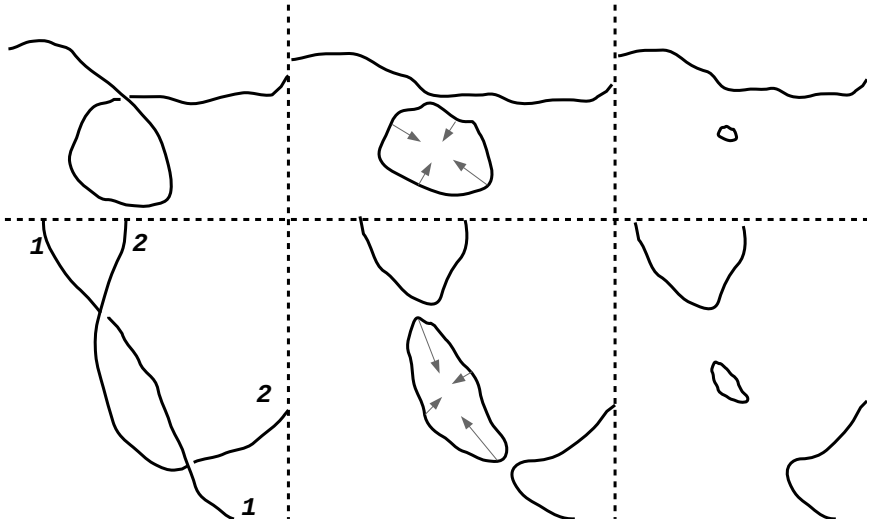

Fig. 2.1 Collisions of string/strings that can produce loops. On top panel there is an example of self-intersection and loop production. On the bottom panel the example of two strings intersection and loop production is shown. All loops eventually collapse due to their tension, reducing the amount of energy in the string network.

Making an assumption that the correlation length, average distance between strings and average radius of curvature for string network are equal to each other, we can obtain final VOS model for cosmic strings

$$\begin{aligned} 2\frac{dL}{dt} &= 2HL\left(1+v^2\right)+cv, \\ \frac{dv}{dt} &= \left(1-v^2\right)\left(\frac{k(v)}{L}-2Hv\right), \end{aligned} \tag{2.11}$$

where the Brownian assumption about strings distribution was used: $\rho = \frac{\mu_0}{L^2}$.

The VOS model (2.11) can be generalized to $p+1$-dimensional defects evolving in $N+1$-dimensional space-time [90, 94]. To do so the parameter σ with indices $a, b, ..$ should be enlarged to $p+1$-dimensions and space-time indices $\mu, \nu, ...$ to $N+1$-dimensions in equations (2.2), (2.5). At the same time the Brownian assumption is needed to be extended in the following way [94].

$$\rho = \frac{\mu_{0\,p}}{L^{N-p}}. \tag{2.12}$$

Taking into account all changes, one can obtain the generalization of the VOS model [94]

$$\begin{aligned} \frac{dL}{dt} &= HL\left(1+\frac{p+1}{N-p}v^2\right)+\frac{c}{N-p}v, \\ \frac{dv}{dt} &= \left(1-v^2\right)\left(\frac{k(v)}{L}-(p+1)Hv\right). \end{aligned} \tag{2.13}$$

In spite of the fact that there is an analogue of the VOS model for more dimensions, such functions as the momentum parameter (2.9) and the phenomenological energy loss function

(2.10) can be different for other dimensional topological defects. We will come back to this question for domain walls ($p = 2$) in details 2.3.

2.2 Simulations of domain wall network evolution

2.2.1 Simulations set up

As was already discussed, simulations are important for the test and calibration of semi-analytic VOS models. The more precise a simulation is, the more accurately we can calibrate the VOS model. At the same time, the bigger range of parameters we can probe, the more confident we can say if the VOS model describes the defect network evolution properly. We want to make such set of simulations that allows us to make a proper calibration of VOS model and at the same time tells us if the VOS model describes the network evolution correctly. The easiest model of defects to fulfil our desire is a domain wall network. It is the easiest example of defects to simulate, which allows us to make very accurate simulations and to cover a big range of possible parameters.

Numerical simulations follow in the footsteps of those reported in [95, 96]. We assume a domain wall producing field theory model with a single scalar field φ. The Lagrangian for this case has the form

$$\mathcal{L} = \frac{1}{2}\partial_\mu\varphi\partial^\mu\varphi - V(\varphi). \tag{2.14}$$

We are going to study the field φ in FLRW universes with power law expansion rates, $a \propto t^\lambda$. After using the PRS procedure [97] the equation of motion in conformal time τ has the form

$$\frac{\partial^2\varphi}{\partial\tau^2} + 3\frac{\mathrm{d}\ln a}{\mathrm{d}\ln\tau}\frac{\partial\varphi}{\partial\tau} - \frac{\partial^2\varphi}{\partial x^i\partial x_i} = -\frac{\partial V}{\partial\varphi}\,, \tag{2.15}$$

where the potential is

$$V = V_0\left(\frac{\varphi^2}{\varphi_0^2} - 1\right)^2. \tag{2.16}$$

Relevant numerical parameters are $\varphi_0 = \pm 1$ for the minima of the potential, while the maximum of the potential is $V_0 = \pi^2/2W_0^2$ (where $W_0 = 10$ is the initial wall thickness in grid units). All these are similar to the ones used in earlier simulations [95–97]. Current simulations have following key points

- We used a faster and more memory-efficient version of the earlier WALLS code [95, 96], optimized for the Intel Xeon Phi architecture.

- This optimization allows us to increase the box size (and therefore the spatial resolution and dynamic range). Specifically, we ran several series of 4096^3 simulations on the COSMOS supercomputer, thus gaining a factor of 8 in volume and a factor of 2 in dynamic range as compared to [96]. Each simulation starts with $\tau_i = 1$ and is stopped when the horizon becomes half the box size ($\tau_f = 2048$), ensuring that the periodic boundary conditions of the simulation boxes do not affect the results. Each such

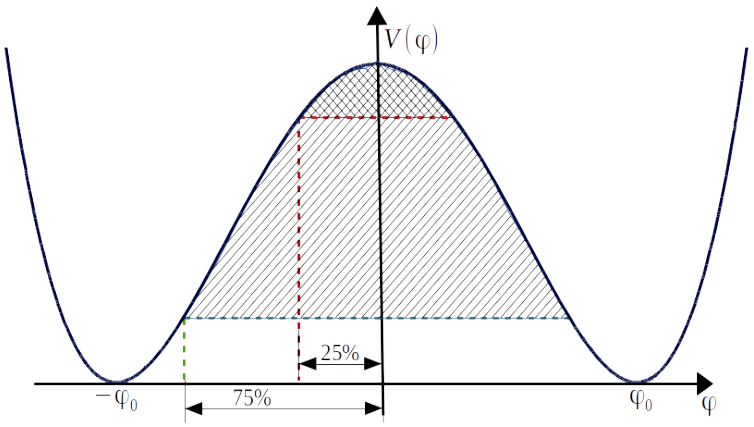

Fig. 2.2 In order to make measurements for the field φ in the simulation box, we need to define where wall boundaries are. Since for the wall the field φ should be around $\varphi = 0$, we can put bounds to define for which φ we measure the wall edge. In this way, the green and red dashed lines represent different thresholds that are aimed to define if we indeed measure the wall in simulations or just a field φ oscillations. Specifically the red one is for the 25% threshold and the green one is for 75% threshold, providing an estimate of systematic uncertainties.

simulation requires 1 Tb of memory and takes about 3.7 hours of wall clock time to run on 512 CPUs.

- We explore a large range of fixed expansion rates, including radiation era ($\lambda = 1/2$), matter era ($\lambda = 2/3$) and other expansion rates, ranging from $\lambda = 1/10$ to $1 - \lambda = 10^{-7}$. Additionally we simulated universes during the transition from radiation to matter domination epochs.

- For each choice of expansion rate we have carried out 10 simulations with different (random) initial conditions: although each of the 10 choices was made randomly, the same 10 choices were used for each of the simulated expansion rates. This ensures that any differences can be solely ascribed to the different expansion rates. Unless otherwise stated, the results presented in what follows correspond to the average of each set of 10 runs.

- We estimated systematic errors by making simulations for different choice of thresholds for velocity measurements. The threshold is changing from 25% to 75% of the value φ_0 to define if we have a wall on the measured grid or it is just a field fluctuation. Schematically differences in the threshold can be seen on the figure 2.2.

Simulations describe the evolution of the field φ in the box with periodic boundary conditions obeying the equation (2.15). Let us recall how parameters of domain wall networks are going to be measured by these simulations. The static solution of the equation (2.15) is [11, 91]

$$\varphi = \varphi_0 \tanh\left[\sqrt{2V_0}\frac{\gamma_v}{\varphi_0}\left(z - z_0 - v\tau\right)\right]. \tag{2.17}$$

The solution (2.17) represents a planar wall moving along the coordinate z with the velocity v (where $\gamma_v = 1/\sqrt{1-v^2}$ is a Lorentz factor). Using the solution (2.17) we can consequently define the relevant parameters[2]

$$\begin{aligned} v^2\gamma_v^2 &= \left\langle \frac{\dot{\varphi}^2}{2V(\varphi)} \right\rangle, \\ \rho &= \left\langle \frac{\dot{\varphi}^2}{2} + \frac{\nabla\varphi^2}{2} + V(\varphi) \right\rangle, \end{aligned} \tag{2.18}$$

where $\nabla = \frac{\partial^2}{\partial x^i \partial x_i}$, brackets $\langle ... \rangle$ represent the averaging over all network, ρ defines the density of the wall network, while v without index s defines rms velocity for the wall network.

Making measurements for velocity and for the density parameter, as in the (2.18), one can study the evolution of these values for domain walls. Results of simulations for the range of $1/10 \leq \lambda \leq 19/20$ are presented in figure 2.3.

Note that our choice of initial conditions lead to large energy gradients in the early timesteps of the simulation, and the network needs some time (which is proportional to the wall thickness) to wash away these initial conditions. This implies that in many grid points the field will go over the top of the potential to get into the other minimum, transiently leading to a relatively small average velocity (the more so the faster the expansion rate), which is clearly visible in the early timesteps in the bottom panel of figure 2.3—note that $\tau = 10$ is the light-crossing time for walls of the average thickness being simulated. This erasing of initial conditions is done in a quasi-coherent way at the various points in the box, leading to the damped oscillations in the average velocity that are also visible in the left panel of the figure 2.3 (though in this case they are clearer for the slower expansion rates, corresponding to weaker damping).

A similar result, but for faster expansion rates $0.03 \leq 1 - \lambda \leq 10^{-7}$ is presented in the figure 2.7. We split expansion rates formally for two ranges, which are on figures 2.3 and 2.7. It is seen that in figure 2.7 that the rms velocity and the density have some kind of transition between two scaling regimes. These results will be clarified below. For now let's study the Kibble scaling regime, which appears after the relaxation timesteps in figure 2.3.

2.2.2 The Kibble scaling regime

Since simulations are evolved in conformal time, the quantity we measure is the conformal correlation length divided by conformal time, which can be straightforwardly related to the physical time quantities

$$\frac{\xi_c}{\tau} = (1-\lambda)\frac{L}{t} = (1-\lambda)\epsilon\,, \tag{2.19}$$

where ϵ is a constant in the linear scaling regime.

Similarly for the velocity we measure $\gamma_v v$ (or, more precisely, $(\gamma_v v)^2$) [95]. In order to identify accurate asymptotic values, we should find the simulation dynamic range when

[2]The equation for the density ρ in equation (2.18) can be obtained from the canonical energy-momentum tensor $T^{\mu\nu} = \frac{\partial \mathcal{L}}{\partial(\partial_\mu \varphi)}\partial^\nu \varphi - g^{\mu\nu}\mathcal{L}$

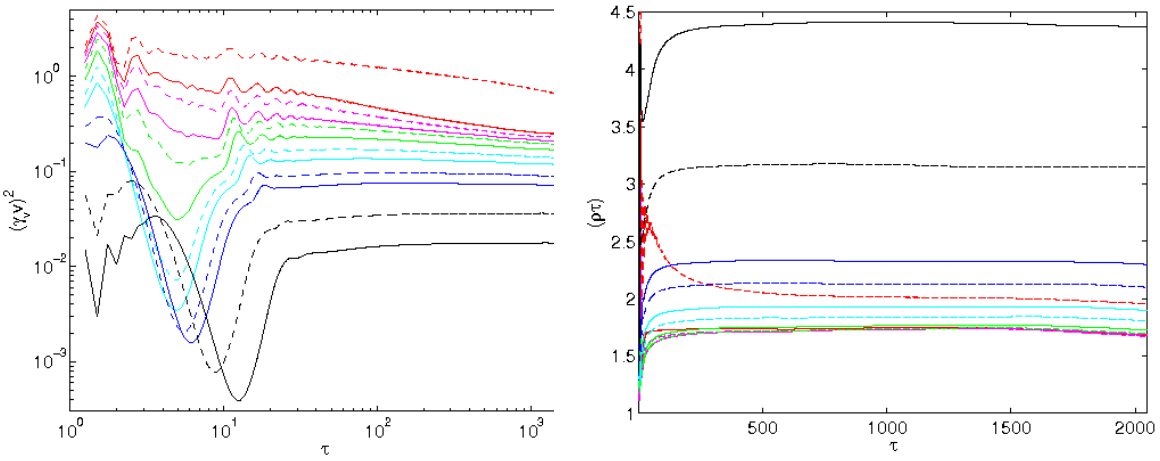

Fig. 2.3 The evolution of the dimensionless density $\rho\tau$ and the rms speed $(\gamma_v v)^2$ in 4096^3 domain wall simulations with different expansion rates, from $\lambda = 1/10$ (red dashed, corresponding to the highest velocity and lowest density) to $\lambda = 19/20$ (black solid, corresponding to the highest density and lowest velocity).

ξ_c/τ and $\gamma_v v$ have already reached the asymptotic behaviour and the simulation box still has enough walls for robust statistics (towards the end of each simulation only a few long walls remain, resulting in comparatively poor statistics). After some tests, we conservatively defined the region $\tau = 500 - 1500$ in which our simulations are generally well behaved for expansion rates $1/10 \leq \lambda \leq 19/20$ (specifically, they are in scaling solutions without significant fluctuations).

Once this region is specified, the averaged values of ξ_c/τ and $\gamma_v v$ can be obtained. These results are presented in table 2.1. Together with values of ξ_c/τ and $\gamma_v v$ we also list the scaling exponents ν and μ, quantifying convergence to the attractor scaling solution. These are defined as

$$\begin{aligned} \frac{1}{\xi_c} &\propto \tau^{\mu}, \\ \gamma_v v &\propto \tau^{\nu}, \end{aligned} \tag{2.20}$$

so for a scaling network these exponents should be numerically consistent with $\mu = -1$ and $\nu = 0$. As expected, one finds that the convergence to the scaling solution is faster for faster expansion rates (corresponding to a larger damping term in the wall equations of motion). Indeed, the ν diagnostic shows that for the slowest expansion rate we have simulated ($\lambda = 1/10$) the network has not converged to the scaling behaviour and, as a result, it cannot be used for further analysis. In fact this is also qualitatively clear from a simple visual inspection of figure 2.3.

Let's test the standard VOS model for domain wall network description, which was used in previous works [95, 96]: the parameters c and k in equations (2.13) are constants ($p = 2$, $N = 3$ should be chosen for equations (2.13) to describe a domain wall network evolution in

Table 2.1 Scaling properties of numerical simulations for domain wall networks with expansion rates $1/10 \leq \lambda \leq 19/20$ in the range $\tau = (500 - 1500)$. See the main text for the definition of the various parameters.

λ	μ	ν	ξ_c/τ	$\gamma_v v$	k_w	c_w
1/10	-1.020 ± 0.005	-0.147 ± 0.001	0.496 ± 0.016	0.867 ± 0.040	0.108 ± 0.004	0.65 ± 0.03
1/5	-0.992 ± 0.005	-0.085 ± 0.003	0.575 ± 0.020	0.514 ± 0.017	0.20 ± 0.01	1.06 ± 0.04
1/4	-0.984 ± 0.005	-0.066 ± 0.003	0.578 ± 0.020	0.489 ± 0.015	0.25 ± 0.01	1.06 ± 0.04
1/3	-0.984 ± 0.005	-0.057 ± 0.003	0.580 ± 0.021	0.467 ± 0.013	0.37 ± 0.02	1.00 ± 0.04
2/5	-0.983 ± 0.005	-0.054 ± 0.004	0.577 ± 0.021	0.449 ± 0.014	0.47 ± 0.03	0.94 ± 0.04
1/2	-0.989 ± 0.005	-0.046 ± 0.004	0.568 ± 0.019	0.418 ± 0.012	0.66 ± 0.04	0.81 ± 0.04
3/5	-0.996 ± 0.004	-0.039 ± 0.004	0.545 ± 0.018	0.379 ± 0.012	0.87 ± 0.05	0.67 ± 0.05
2/3	-1.000 ± 0.004	-0.032 ± 0.004	0.519 ± 0.015	0.348 ± 0.011	1.02 ± 0.05	0.56 ± 0.06
3/4	-1.003 ± 0.003	-0.026 ± 0.004	0.470 ± 0.012	0.302 ± 0.008	1.22 ± 0.06	0.41 ± 0.07
4/5	-1.006 ± 0.003	-0.021 ± 0.003	0.430 ± 0.009	0.269 ± 0.007	1.34 ± 0.05	0.31 ± 0.06
9/10	-1.006 ± 0.002	0.003 ± 0.003	0.316 ± 0.004	0.190 ± 0.004	1.59 ± 0.05	0.11 ± 0.06
19/20	-0.997 ± 0.001	0.008 ± 0.002	0.227 ± 0.002	0.133 ± 0.002	1.70 ± 0.03	0.03 ± 0.04

$3+1$ dimensions). For clarity, further we will use c_w and k_w (instead of c and k) for domain wall networks. Eventually, using the function for the scale factor as in simulations $a \propto t^{\lambda}$, one can obtain from (2.13) the following relations

$$\begin{aligned} k_w &= 3\lambda\epsilon v_0 \,, \\ c_w v_0 &= \epsilon \left[1 - \lambda\left(1 + 3v_0^2\right)\right] \,, \end{aligned} \tag{2.21}$$

where we used the asymptotic scaling solution

$$\begin{aligned} L &= \epsilon t, \\ v &= v_0, \end{aligned} \tag{2.22}$$

with λ, ϵ and v_0 as constants [91].

Using the asymptotic values, one can obtain $\epsilon = \frac{\xi_c}{\tau(1-\lambda)}$ and the velocity v_0 for each expansion rate. By inserting ϵ and v_0 in (2.21) one numerically obtains the momentum and chopping parameters. The values thus obtained for each expansion rate are also listed in Table 2.1. It is noteworthy that, with the exception of the $\lambda = 1/10$ case, k_w increases monotonically with λ, while c_w correspondingly decreases.

For comparison with previous work [95, 96], it is interesting to carry out a joint analysis of the data (except the $\lambda = 1/10$ case, which hasn't reached scaling), and determine the best-fit values for these phenomenological parameters if one imposes that they should have the same constant value for all epochs. The results of this analysis are shown in the right panel of the figure 2.4, and the following best-fit parameters and uncertainties were found $c_w = 0.63 \pm 0.36$, $k_w = 0.88 \pm 0.51$. It should be noted that in this analysis only the statistical errors were taken into account.

We studied the standard VOS model with constant c_w and k_w. The important conclusion that we can make after the calibration is that the model with constant chopping parameter

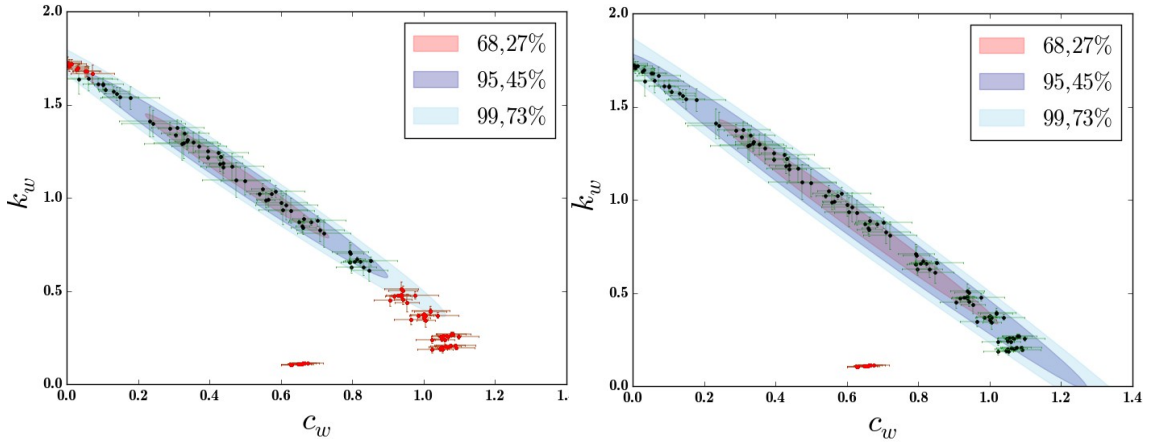

Fig. 2.4 The likelihood contours for the VOS model with constant parameters c_w and k_w, for all scaling expansion rates $0.2 \leq \lambda \leq 0.95$ (right panel) and for the restricted range $0.5 \leq \lambda \leq 0.9$ (left panel). Each point with error bars in the plot presents asymptotic values from one simulation. The black dots denote the simulations used in the fit, and the red dots the simulations not used. The slowest expansion rate data was not used in either case: it has a manifestly different behaviour because the simulations did not reach the asymptotic scaling behaviour.

c_w and momentum parameter k_w does not describe properly all possible expansion rates. This means that the model requires extension, which is going to be done later in section 2.3.

For now, let's finish the exploration of the Kibble scaling regime for the wall network simulations. In the figure 2.7 we see that in spite of the grow of velocity v and conservation of energy density ρ in first steps of simulations, eventually we obtain the Kibble scaling regime at the end of some simulations. Conducting similar analyses for ν and μ (defined in equations (2.20)), as it was done above, we have chosen sets of 10 simulations, for which we still can study asymptotic the Kibble scaling regime, which we will further discuss below. Obtained results for these 10 simulations are listed in the table 2.2.

2.2.3 Systematic and statistical errors

We already mentioned the fact that for all our simulations we have calculated statistical errors, but systematic ones have not been considered so far. From table 2.1 it is noteworthy that the statistical error bars, which come from averages of ten simulations with different (random) initial conditions, decrease significantly as the expansion rate increases. Therefore, we can anticipate that systematic errors intrinsic to the simulations (having to do with the discretization, the PRS algorithm, the identification of the domain walls in the box and the estimation of their velocities) will eventually dominate the error budget for sufficiently large expansion rates. It is therefore important to obtain estimates of these systematic uncertainties.

In order to do this, we performed additional sets of simulations for different choices of threshold for velocity measurements. In the previously described simulations, the velocity is

Table 2.2 Scaling properties of numerical simulations for domain wall networks with different expansion rates λ in the linear scaling regime. In addition to the slope parameters μ and ν we also list the asymptotic values of the dimensionless density and the wall energy, as well as the range of conformal times used in each set of simulations. One-sigma statistical uncertainties are quoted throughout.

λ	μ	ν	ξ_c/τ	$\gamma_v v$	Fit range (τ)
0.97	-0.993 ± 0.001	0.006 ± 0.001	0.177 ± 0.001	0.102 ± 0.001	$500 - 1500$
0.98	-0.992 ± 0.001	0.005 ± 0.001	0.145 ± 0.001	0.083 ± 0.001	$500 - 1500$
0.99	-0.990 ± 0.0003	0.004 ± 0.001	0.103 ± 0.0004	0.059 ± 0.0002	$500 - 1500$
0.995	-0.992 ± 0.0003	0.001 ± 0.001	0.073 ± 0.0002	0.041 ± 0.0002	$900 - 2046$
0.997	-0.991 ± 0.0002	0.006 ± 0.0004	0.057 ± 0.0001	0.032 ± 0.0001	$1050 - 2046$
0.998	-0.989 ± 0.0002	0.013 ± 0.0002	0.046 ± 0.0001	0.026 ± 0.0001	$1200 - 2046$
0.999	-0.982 ± 0.0001	0.018 ± 0.0002	0.033 ± 0.0001	0.018 ± 0.0001	$1350 - 2046$
0.9995	-0.971 ± 0.0001	0.031 ± 0.0001	0.023 ± 0.0001	$0.013 \pm 4 \cdot 10^{-5}$	$1500 - 2046$
0.9997	-0.960 ± 0.0001	0.044 ± 0.0001	0.018 ± 0.0001	$0.010 \pm 3 \cdot 10^{-5}$	$1650 - 2046$
0.9998	-0.949 ± 0.00003	0.055 ± 0.0001	$0.015 \pm 3 \cdot 10^{-5}$	$0.008 \pm 2 \cdot 10^{-5}$	$1800 - 2046$

estimated as an average over all points in the box in which the field obeys $|\phi| < 0.5$ (recall that the minima of the potential are at $\phi = \pm 1$). This has been previously shown to be an optimal choice. As a test, we have carried out further simulations for expansion rates $\lambda = 0.4$ and $\lambda = 0.999$ with exactly the same initial conditions (in other words, a fixed seed) but with thresholds for the velocity calculation spanning the range from 0.25 to 0.75; this is illustrated in figure 2.2, and the results of these simulations are shown on the left and right panels in figure 2.5.

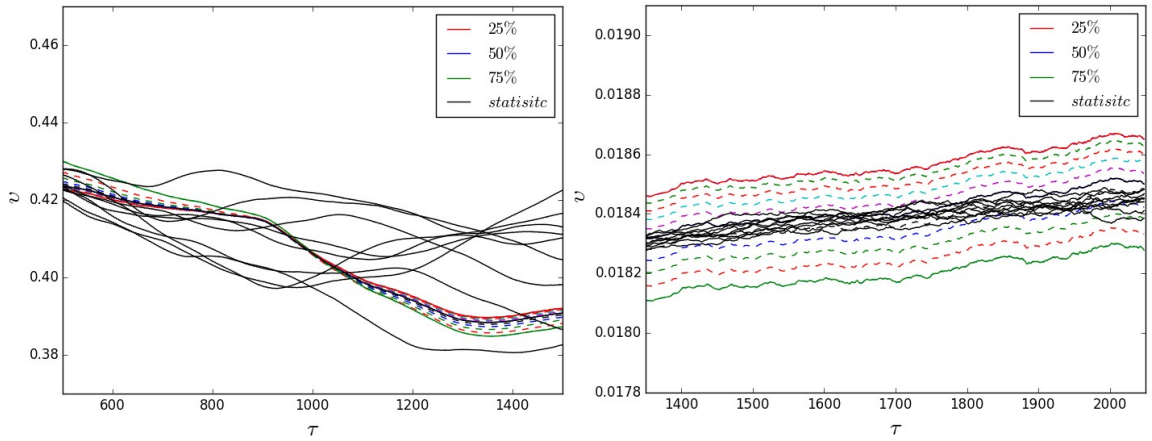

Fig. 2.5 Results from velocity measurements for different choices of thresholds, illustrated in figure 2.2. The left panel presents the result for expansion rate $\lambda = 0.4$ and the right one for $\lambda = 0.999$. Black lines represent the velocities in the ten individual simulations with different initial conditions, measured with a canonical 50% threshold, and provide the statistical errors. Colored lines represent the velocity in one of the ten simulations, measured using different thresholds (specifically the solid red one is for the 25% threshold and the solid green one is for 75% threshold), providing an estimate of systematic uncertainties.

Making the plausible assumption that the effect of the choice of thresholds on the velocity measurements is a reliable proxy for the systematic numerical uncertainties, this test confirms our intuition that as the expansion rate is increased the statistical uncertainties decrease much faster than the systematic ones, and therefore the latter will dominate for sufficiently large expansion rates λ. Specifically, we find that the systematic error for $\lambda = 0.4$ is

$$\delta v_{syst,\lambda=0.4} = \pm 12.3 \times 10^{-4}\,, \tag{2.23}$$

while for $\lambda = 0.999$ it is

$$\delta v_{syst,\lambda=0.999} = \pm 4.7 \times 10^{-4}\,. \tag{2.24}$$

Since the difference between systematic errors for different λ is comparatively small, in what follows we will make a linear interpolation in order to estimate the systematic uncertainty for other expansion rates.

2.2.4 The radiation-matter transition

As an additional test, and the most important one from the point of view of cosmological application, we have carried out analogous field theory simulations of the radiation-matter transition. In this case the scale factor has the following exact analytic expression

$$\frac{a(\tau)}{a_{eq}} = \left(\frac{\tau}{\tau_*}\right)^2 + 2\left(\frac{\tau}{\tau_*}\right)\,, \tag{2.25}$$

where $\tau_* = \tau_{eq}/(\sqrt{2}-1)$ and the parameters a_{eq} and τ_{eq} are constants denoting the scale factor and conformal time at the epoch of equal radiation and matter densities. For illustration purposes we can also calculate an 'effective' expansion rate during the transition

$$\lambda_{eff} = \frac{2 + 2\frac{\tau}{\tau_*}}{4 + 3\frac{\tau}{\tau_*}}\,; \tag{2.26}$$

as expected this interpolates between the radiation and matter era values.

In this case we ran various sets of simulations with the same parameters and (random) initial conditions that were described in the section 2.2.1, except that the scale factor obeys the equation (2.25). The requirement of sufficient resolution implies that there is not enough memory available for a single simulation to span the entire transition epoch; instead, various sets of runs were carried out starting at various different conformal times relative to the transition epoch, equally spaced in the logarithm of τ_i/τ_{eq}.

Figure 2.6 (to be compared to figure 2.3) summarizes the results of these simulations. Note that the two black solid lines correspond to the radiation ($\lambda = 1/2$) and matter ($\lambda = 2/3$) simulations already discussed in the section 2.2.2. This is an important test of our code: it shows that simulations evolving sufficiently early and sufficiently late in the transition behave exactly like radiation and matter era simulations—as they must. This figure also makes it visually clear that although the 'early' and 'late' simulations reach scaling (since they are effectively evolving with a constant or quasi-constant expansion rate) this is not case for

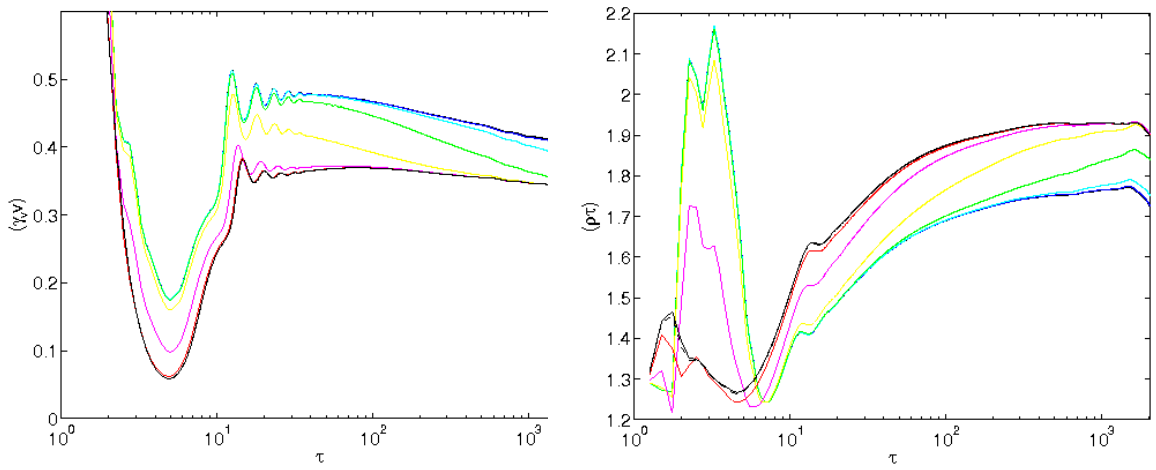

Fig. 2.6 The evolution of the dimensionless density ($\rho\tau$, right panel) and ($\gamma_v v$) (left panel) in 4096^3 domain wall simulations around the radiation-matter transition. Note that the two black solid lines correspond to the radiation ($\lambda = 1/2$) and matter ($\lambda = 2/3$) simulations already discussed in the section 2.2.2.

the ones evolving during the transition itself: in that case the effective expansion rate is changing and the network is constantly trying to adapt (as fast as allowed by causality) to these changing conditions. This is clear in the cyan, green and yellow lines in the plots. Later in this chapter we will compare the VOS model behaviour for the non-scaling regime and compare it with the radiation-matter transition simulated here.

2.2.5 The conformal stretching regime

As was already mentioned in section 2.2.2, the early timesteps of evolution show another kind of scaling behaviour. It is clearly seen directly from the result of the $\gamma_v v$ and ρ evolution for very fast expansion rates in the figure 2.7. The simulation with highest λ (purple line in the figure 2.7) does not even reach the Kibble scaling regime, all evolution in the simulated time interval is in the stretching regime.

To figure out why this regime appears and what is going on there, we must consider extra term in the VOS model (2.13): ℓ_f - friction length. The friction length can appear due to particles scattering on strings, which eventually influences on the network evolution [110]. This kind of friction force is anticipated to be present in the radiation domination epoch. And effectively wee can put it as [88, 111, 112]

$$\ell_f \propto a^{2+p}\,, \tag{2.27}$$

to equations (2.13) in the following way

$$\frac{dL}{dt} = HL + v^2\frac{L}{\ell_d} + cv\,, \tag{2.28}$$

where for convenience we introduced the damping length as

$$\frac{1}{\ell_d} = (p+1)H + \frac{1}{\ell_f}. \tag{2.29}$$

Now, following Kibble [36, 100] we note that in damped regimes the velocity is expected to change slowly. Then from the velocity equation it follows that

$$v \sim k\frac{\ell_d}{L} \tag{2.30}$$

and substituting this in the evolution equation for the correlation length we find

$$\frac{dL}{dt} = HL + k(c+k)\frac{\ell_d}{L}\,. \tag{2.31}$$

We now have four possible scenarios, depending on whether the damping is provided by friction or by the expansion of the universe, and on whether or not the velocities are negligible.

Starting with the case where the damping length is due to friction, $\ell_d = \ell_f$, as discussed in [88, 91] there is a transient scaling solution

$$L \propto a\,, \quad v \propto \frac{\ell_f}{a} \propto a^{p+1} \tag{2.32}$$

this is known as the stretching regime, and corresponds to the case where the network's average velocity and density are sufficiently small to make the probability of self-intersections negligible. In this case the network is conformally stretched by the expansion. However, velocities are increasing so this regime must be a transient, at least in an expanding universe. If friction domination persists, eventually these assumptions will no longer hold, and the network will switch to the canonical Kibble regime [36, 100]

$$L \propto (\ell_f t)^{1/2}\,, \quad v \propto \left(\frac{\ell_f}{t}\right)^{1/2}; \tag{2.33}$$

here the energy losses are significant, and therefore the correlation length grows faster than in the stretching regime while the velocity grows more slowly.

Now let us repeat this analysis if the damping is simply provided by the expansion of the universe; as we will confirm numerically in what follows, a sufficiently fast expansion rate is enough to make the defects move with non-relativistic speeds. In this case the damping length is $\ell_d^{-1} = (p+1)H$ and we will consider generic expansion rates $a \propto t^\lambda \propto \tau^{\lambda/(1-\lambda)}$, where t and τ are, respectively, physical and conformal time. In this case the correlation length equation becomes

$$(3-p)\frac{dL}{dt} = (3-p)HL + k\frac{c+k}{(p+1)HL}\,, \tag{2.34}$$

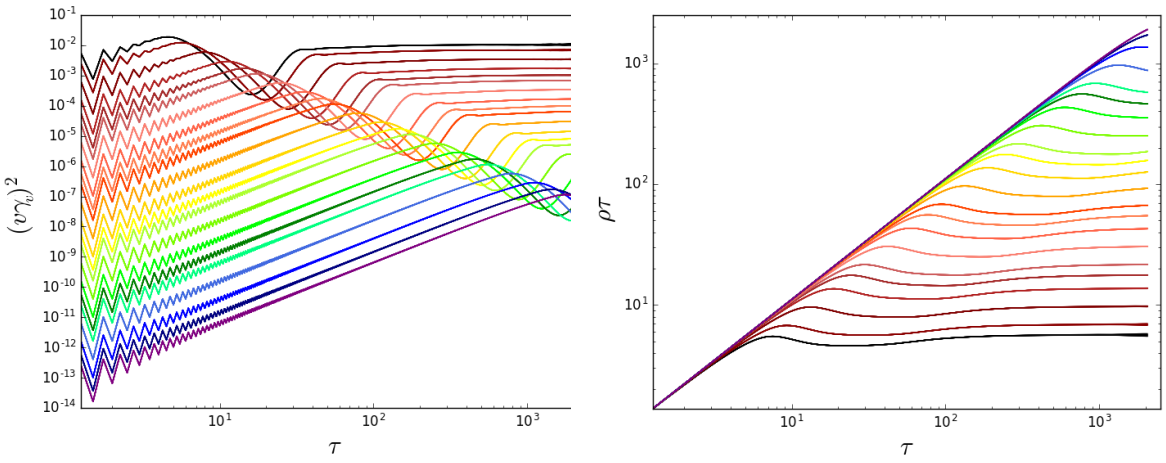

Fig. 2.7 The evolution of the dimensionless density $\rho\tau$ and the rms speed $(\gamma_v v)^2$ in 4096^3 domain wall simulations with different expansion rates, from $(1-\lambda) = 0.03$ to $(1-\lambda) = 10^{-7}$ (from black-red to blue-purple). Each line is the average of the 10 simulations, with random initial conditions.

and just like in the previous case we find two scaling regimes. The transient scaling regime also corresponds to conformal stretching

$$L \propto a\,, \quad v \propto \frac{1}{(p+1)\lambda}\frac{t}{a} \propto \frac{1-\lambda}{(p+1)\lambda}\,\tau\,. \tag{2.35}$$

On the other hand, the analogue of the Kibble regime is precisely the standard linear scaling regime,

$$L = \sqrt{\frac{k(c+k)}{(3-p)(p+1)\lambda(1-\lambda)}}\,t\,, \quad v = \sqrt{\frac{3-p}{p+1}\frac{1-\lambda}{\lambda}\frac{k}{k+c}}\,. \tag{2.36}$$

The two friction-dominated regimes and the linear scaling regime are all well known, but in what follows we will use a high-resolution field-theory simulations to study the Hubble-damped stretching regime, as well as to confirm that it is a transient which eventually switches to the linear regime.

The analysis leads us to expect a conformal stretching regime which translated into the numerically measured quantities should correspond to

$$\rho_w \propto \text{const.}\,, \quad v \propto \frac{1-\lambda}{\lambda}\,\tau\,; \tag{2.37}$$

naturally the Lorentz factor is irrelevant for non-relativistic speeds.

Relations (2.37) show us exactly what is happening at the beginning of simulations. In the figure 2.7 first timesteps correspond to relation described by (2.37). Below in this chapter we will use the stretching scaling regime as an additional method to calibrate/probe the VOS model.

2.3 Extending the VOS model

As we already mentioned in section 2.2.2, the standard VOS model (2.13) for walls is not able to reproduce results from simulations, if one wants to keep c_w and k_w as constants. If we compare the likelihood contours in the left panel of the figure 2.4 with the same plot from the work [96] (which only had data from three expansion rates, $\lambda = 1/2, 2/3, 4/5$), it is seen that they are statistically consistent, but in our case the error bars are significantly larger (as is the reduced chi-squared for the fit). As a comparison, if we repeat the analysis using only the simulations in the range $0.5 \leq \lambda \leq 0.9$ we find $c_w = 0.48 \pm 0.24$, $k_w = 1.12 \pm 0.31$; the results of this analysis are shown in the right panel of the figure 2.4. The error bars become smaller and the agreement with [96] is even better. This implies that assuming c_w and k_w to be constants is not accurate enough.

More explicitly this can be shown by plotting the right-hand sides of relations (2.21) in terms of the velocity—cf. figure 2.8. For the first of these (left panel), the right-hand side describes the behaviour of the momentum parameter $k(v)$ for different expansion rates, while for the second one (right panel) it describes an energy loss function which we will denote $F(v)$. For constant k_w and c_w, equations (2.21) would imply a constant value for the first plot and a linear function for the second one. Data from our simulations show that this is not the case. As a final, more straightforward check, table 2.1 also lists the numerically inferred c_w and k_w for each expansion rate. Hence, the momentum parameter should depend on velocity, and the chopping parameter is not sufficient for describing the energy losses.

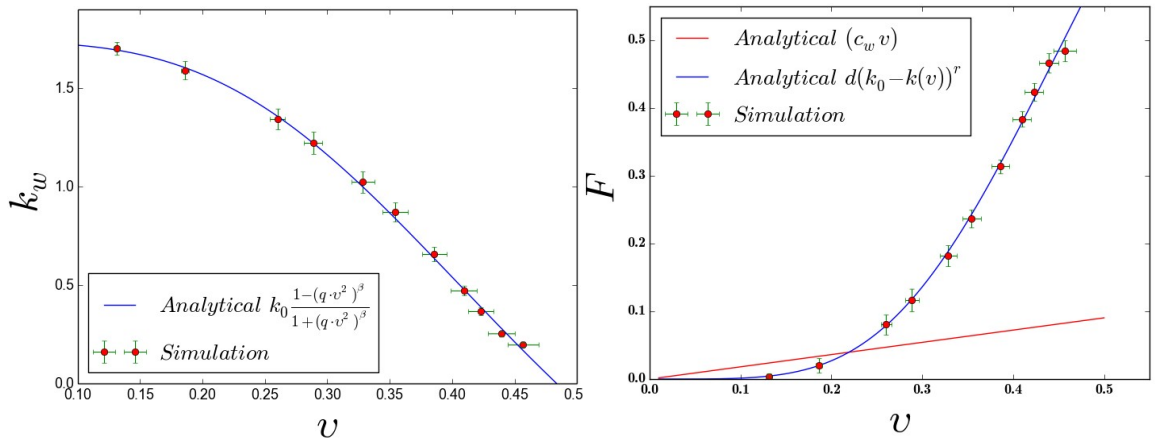

Fig. 2.8 Momentum parameter $k_w(v)$ (left panel) and energy loss function $F(v)$ (right panel), as numerically determined from the right-hand side of equations (2.21). The red line in the energy loss plot is a linear function of the rms velocity $c_w v$ fitted for high λ (hence low velocity). The blue lines are from the extended analytic model, using phenomenological forms of the momentum parameter (2.45) and energy loss due to scalar radiation (2.47) with the following best-fit parameters $d = 0.28$, $r = 1.30$, $\beta = 1.69$, $k_0 = 1.73$ and $q = 4.27$, discussed in the text.

Moreover, analytical treatment of VOS equations also suggests that at least k_w cannot be a constant, when λ is varying. This result can be seen from the ratio (2.21): if the expansion

rate tends to zero $\lambda \to 0$, it follows that k_w should inevitably tend to zero, which is not the case when k_w is a constant.

As a result, being motivated by the simulations data, we are going to improve the standard VOS model for domain wall networks. Below we will give a description of the extended analytic VOS model, with more accurately modelled the momentum parameter and the energy loss term.

Before going to detailed description of the extension, let's revisit general microscopic equations (2.2). Let us redefine the coordinates σ_1 and σ_2 there to s_1 and s_2 in such way that $|\frac{\partial x^i}{\partial s_\alpha}|^2 = 1$ $(\alpha = 1, 2)$. This means that derivatives will be changed in the following way

$$\frac{\partial x^i}{\partial \sigma_\alpha} = |x^i_{,\alpha}| \frac{\partial x^i}{\partial s_\alpha}, \tag{2.38}$$

(no summation over α). In these new coordinates, it is possible to introduce an orthonormal basis (refer to figure 2.9): $\xi^i_\alpha = \frac{\partial x^i}{\partial s_\alpha}$, and $\mathrm{n}^i = \frac{\dot{x}^i}{|\dot{x}^i|}$. Consequently, the zeroth component of equation (2.2) (index $\eta = 0$) can be written as

$$\dot{\varepsilon} + 3\frac{\dot{a}}{a}\varepsilon \dot{x}^i \dot{x}_i = 0\,. \tag{2.39}$$

The spatial part (index $\eta = i$) of equation (2.2) contracted with the vector n_i has the form

$$\ddot{x}^i \mathrm{n}_i + 3\frac{\dot{a}}{a}\dot{x}^i \mathrm{n}_i \left(1 - \dot{x}^i \dot{x}_i\right) = \left(1 - \dot{x}^i \dot{x}_i\right) k^i_1 \mathrm{n}_i + \left(1 - \dot{x}^i \dot{x}_i\right) k^i_2 \mathrm{n}_i\,, \tag{2.40}$$

where $k^i_\alpha = \frac{\partial \xi^i_\alpha}{\partial s_\alpha}$.

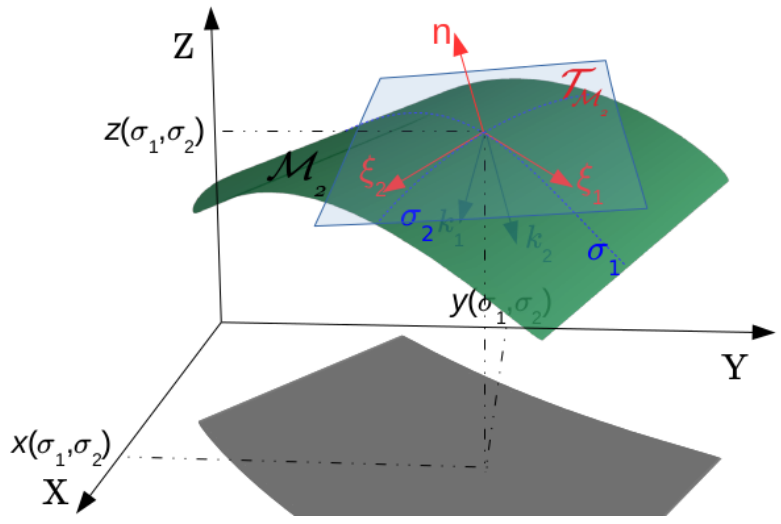

Fig. 2.9 The wall surface $\mathcal{M}_2$ parametrized by two parameters, σ_1 and σ_2.

The scalar products $k^i_\alpha \mathrm{n}_i$ project the curvatures corresponding to σ_1 and σ_2 along the normal vector n^i. It should be noted that $k^i_\alpha = \frac{a}{R_\alpha} u^i_\alpha$, where u^i_α are unit vectors and R_α are the radii of curvature for σ_1 and σ_2, respectively.

Now it is possible to obtain averaged equations, using the same strategy that was described in the section 2.1. One introduces two macroscopic (averaged) quantities, the energy density for domain walls[3]

$$\rho = \frac{\sigma_w a^2}{V} \int \varepsilon d^2\sigma \tag{2.41}$$

and the rms velocity as (2.7).

Thus, the microscopic equations (2.39) and (2.40) can be averaged

$$\begin{aligned} \frac{d\rho}{dt} &= -H\rho\left(1+3\upsilon^2\right), \\ \frac{d\upsilon}{dt} &= \left(1-\upsilon^2\right)\left(\frac{K_1+K_2}{L} - 3H\upsilon\right), \end{aligned} \tag{2.42}$$

where we made the assumption that curvature radii have the same averaged value and are equal to the correlation length: $R_1 = R_2 = L$. The K_1 and K_2 parameters are curvature/momentum parameters. The component K_1 can be written as

$$K_1 = u_1^i n_i\,, \tag{2.43}$$

suitably averaged over the network, with an analogous definition for K_2. In the next section 2.3.1 we will work out how they may depend on the velocity υ.

2.3.1 The momentum parameter

The momentum parameter can be estimated in an analogous way to what was done for cosmic strings in [89]. As we saw, the momentum parameter in our VOS wall model is given by $k_w = K_1 + K_2$ (2.42). The component K_1 was defined in (2.43). We now need to estimate this scalar product in terms of the velocity υ. As can be seen in the figure 2.9, there is an orthonormal basis $\{\xi_1^i, \xi_2^i, n^i\}$, and therefore we can decompose the vector

$$u_1^i = An^i + B\xi_2^i\,; \tag{2.44}$$

note that vector ξ_1^i is orthogonal to u_1^i. Therefore $u_1^i n_i = A$ and $u_1^i u_{1i} = A^2 + B^2 = 1$.

When the expansion rate is slow, the velocity squared tends to some maximal value $1/q$ and perturbations on the wall surface increase. Since the wall surface is highly perturbed in that regime, the averaged value of $u_1^i n_i$ goes to zero ($A \to 0$). In the opposite limit when the rate of expansion is fast, the velocity squared tends to zero, and perturbations on the wall surface are very small. As a result, the scalar product $u_1^i n_i$ goes to some value $k_0/2$. The same considerations apply for K_2.

Hence, $k_w(v)$ should reach some value k_0 when the velocity is zero and tend to zero when the velocity squared is $1/q$. In that case $k_w(v)$ can be written similarly to the momentum

[3]It should be noticed that the energy density compared to expression for strings (2.6) has an additional scale factor multiplier. It comes from the extended induced metric determinant $\sqrt{\gamma}$ in (2.6).

parameter of the string network [89]

$$k_w(v) = k_0 \frac{1 - (q v^2)^\beta}{1 + (q v^2)^\beta}, \tag{2.45}$$

where β, k_0 and q are unknown parameters.

At this point there is one difference between the string and wall cases: there are no non-trivial analytic solutions for walls (like the helicoidal solution for strings) that can be used to infer exact values of q, k_0 and β, as it was done for strings. Consequently, it is only possible to impose physical restrictions on these parameters. The constant k_0 characterizes the maximum value of the momentum parameter: it is positive, but cannot be bigger than 2. The parameter $1/q$ is an averaged maximal velocity for the wall network. Similarly to what was done for strings in [101], using the general expression for the n-dimensional topological defect dynamics (2.2) [93], it can be shown that the maximal possible velocity is $v^2_{max} = \frac{n}{n+1}$. For walls this is $v^2_w = 2/3$, as expected, but this result requires a set of assumptions that need not be satisfied. In that case the maximal averaged velocity of the network can be smaller (but not larger). We therefore have

$$0 < \frac{1}{q} \leq v^2_w \,. \tag{2.46}$$

Other than these general physical constraints, these parameters must be calibrated numerically. Fortunately, the resolution of our simulations is high enough to enable this calibration, as we will show below.

2.3.2 Energy loss mechanisms

The modification of the momentum parameter described above is not sufficient to account for the mismatch between the simulation data and the analytic prediction for the energy losses. We should also improve the modeling of the latter for a better description of the wall network evolution. In addition to the chopping mechanism, another significant contribution to energy losses is expected to be from scalar radiation. Moreover, one may expect it to be proportionally more important (compared to the chopping mechanism) for slower expansion rates.

Energy loss due to scalar radiation was considered in [113]. It was shown that the uniformly moving wall does not radiate. Only perturbations on the wall surface produce scalar radiation. We have already estimated the level of perturbations in the momentum parameter expression $k_w(v)$. The maximal value k_0 corresponds to the minimal rms velocity and hence to minimal perturbations on the wall surface. Conversely the case when the momentum parameter is zero corresponds to a maximal rms velocity and a maximally perturbed surface. It looks reasonable to anticipate that the amount of radiation is proportional to the surface perturbations. As a result, we can introduce a modified analytic description of energy losses

$$F(v) = c_w v + d[k_0 - k(v)]^r \,, \tag{2.47}$$

where d and r are constants. In the maximally perturbed (slow expansion) limit $v^2 \to 1/q$ this behaves as

$$F(v) = \frac{c_w}{\sqrt{q}} + dk_0^r\,, \tag{2.48}$$

and we expect the scalar radiation term to be the dominant one. Conversely in the uniform surface (fast expansion) limit we have

$$F(v) \sim c_w v + d(2k_0)^r q^{\beta r} v^{2\beta r}\,, \tag{2.49}$$

and in this case we expect the chopping term to be more important, and possibly dominate (depending on the values of the free parameters to be calibrated numerically).

2.4 Calibration of the extended VOS model

Putting together the extensions mentioned above, the VOS model equations (2.42) for a domain wall network together with relation (2.12) can finally be rewritten as

$$\begin{aligned} \frac{dL}{dt} &= (1+3v^2)HL + c_w v + d[k_0 - k_w(v)]^r, \\ \frac{dv}{dt} &= (1-v^2)\left(\frac{k_w(v)}{L} - 3Hv\right), \end{aligned} \tag{2.50}$$

where $k_w(v)$ is defined by (2.45).

Equations (2.50) contain undefined parameters that should be calibrated by numerical simulations. As it was already discussed in the section 2.2.2 we can use the asymptotic values of simulations to find values for the phenomenological constants in (2.50).

One can easily confirm that the extended VOS model given by equations (2.50) possess the same scaling behaviour as the original one (2.22) (but of course with other values of constants ϵ and v_0). In this way, the Kibble scaling regime for equations (2.50) can be written in algebraic form

$$\begin{gathered} F(v_0) = c_w v_0 + d[k_0 - k_w(v_0)]^r = \epsilon\left(1 - \lambda\left(1 + 3v_0^2\right)\right), \\ k_w(v_0) = 3\lambda\epsilon v_0. \end{gathered} \tag{2.51}$$

We see that right-hand sides of equations (2.51) contain only parameters that can be measured by the simulations set for the Kibble scaling regime. At the same time left-hand sides of (2.51) represent phenomenological parameters as functions of velocity. Hence, from simulations we can directly define velocity-depend functions: the energy loss function F and momentum parameter k_w. In figure 2.8 one can see data from simulations for F and k_w.

Let us perform the fitting of the extended VOS model to asymptotic values of simulations in the Kibble scale regime, presented in the table 2.1 and shown in the figure 2.3: $1/5 \leq \lambda \leq 19/20$. We excluded the simulation $\lambda = 1/10$, since the simulation doesn't reach required scaling regime.

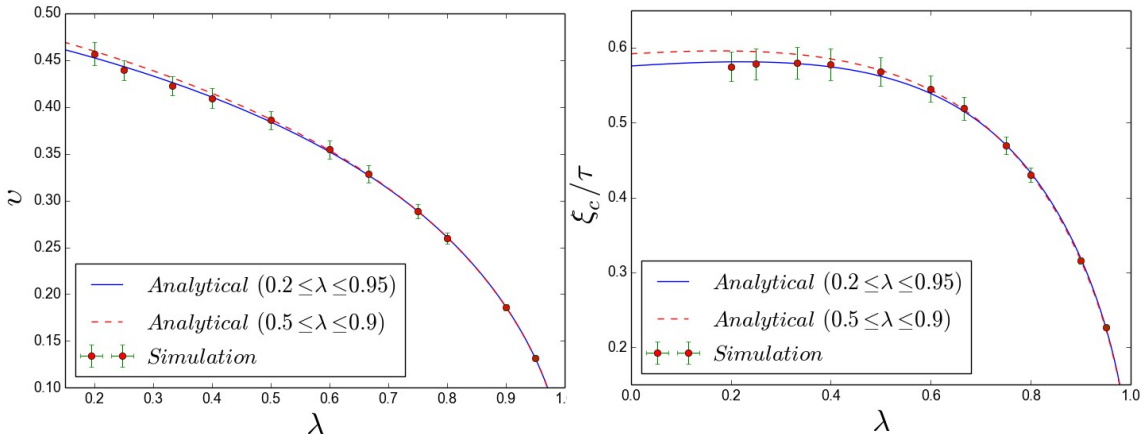

Fig. 2.10 Velocity v and conformal correlation length divided by conformal time ξ_c/τ obtained from the model using equations (2.50) with the best-fit parameters described in the text, compared to the data (with statistical error bars) from the numerical simulations for different expansion rates. The solid blue line corresponds to the best-fit parameters for the full range of expansion rates considered while the red dashed one corresponds to the best-fit parameters for the restricted range.

In the extended model we have in principle 6 undefined parameters that should be determined from numerical simulation data. By using bootstrapping techniques one finds that the chopping parameter c_w is negligibly small in comparison with the contribution from scalar radiation and may be neglected as a first approximation (specifically, we find $c_w = 0.00 \pm 0.01$), while the other five parameters are presented in the table 2.3 (for comparison, we have also repeated this analysis for the restricted range $0.5 \leq \lambda \leq 0.9$)

Table 2.3 The best-fit values for the free parameters of the extended VOS model; for comparison, we also show the values obtained for the fit with other ranges of expansion rates. One-sigma statistical uncertainties are quoted throughout.

λ	Systematics	c_w	d	r
$0.5 \leq \lambda \leq 0.9$	No	0.00 ± 0.03	0.29 ± 0.01	1.30 ± 0.06
$0.2 \leq \lambda \leq 0.95$	No	0.00 ± 0.01	0.28 ± 0.01	1.30 ± 0.02
$0.97 \leq \lambda \leq 0.9998$	Yes	0.01 ± 0.01	0.10 ± 0.09	1.34 ± 0.25
$0.2 \leq \lambda \leq 0.9998$	Yes	0.00 ± 0.08	0.26 ± 0.02	1.42 ± 0.04
		k_0	q	β
$0.5 \leq \lambda \leq 0.9$	No	1.72 ± 0.03	4.10 ± 0.17	1.65 ± 0.12
$0.2 \leq \lambda \leq 0.95$	No	1.73 ± 0.01	4.27 ± 0.10	1.69 ± 0.08
$0.97 \leq \lambda \leq 0.9998$	Yes	1.82 ± 0.02	1.20 ± 0.72	0.94 ± 0.38
$0.2 \leq \lambda \leq 0.9998$	Yes	1.77 ± 0.03	3.35 ± 0.32	1.08 ± 0.07

The scaling solution of equations (2.50) with the best-fit parameters is shown in figure 2.8 (for explicit demonstration of energy loss F function and momentum parameter k_w) and in figure 2.10 (to compare the final result of velocity v and correlation length ξ_c). As can be seen, this now provides an excellent agreement with the entire range of numerical simulations.

A smaller fit range ($0.5 \leq \lambda \leq 0.9$) leads to parameters that are fully consistent with the ones obtained for the $1/5 \leq \lambda \leq 19/20$ range of expansion rates. While this is not entirely surprising (since the fit is dominated by the high expansion rates, for which the statistical uncertainties of the parameters measured in the simulations are smaller) it is supporting evidence for the fact that the model can accurately describe all expansion rates. We note that in this restricted range the chopping parameter is still negligible ($c_w = 0.00 \pm 0.03$).

To make the full analyses of undefined parameters, we need to make the analyses of ν, μ in tables 2.1, 2.2, to identify which simulations we can use for calibration of the VOS model by the Kibble regime. Eventually, the maximal range is $0.2 \leq \lambda \leq 0.9998$. We can now improve upon the calibration of the VOS model. Combining all data and adding the statistical and (estimated) systematic uncertainties (for details see section 2.2.3) in quadrature for each expansion rate, we obtain the best-fit values for each of these model parameters indicated in the table 2.3. For comparison, this table contains different ranges of expansion rates for the fit, as well as for the case where only the fast expansion rates are used (with the caveat that this will be the case where the results of our fit will be most vulnerable to our estimates of the systematic uncertainties).

It is worthy of note that the loop chopping efficiency is still statistically consistent with zero, with the exception of the case where only expansion rates $\lambda \geq 0.97$ are used in the fit in which case a non-zero value is preferred at one sigma. This is in agreement with our expectations, already discussed above, and confirms the expectation that the production of 'wall blobs' is a subdominant energy loss mechanism, unlike the analogous production of loops in cosmic string networks. As for the other fitted parameters, we find general agreement with our previous analysis: the only parameter that is significantly changed is β, which leads to a corresponding shift (and an increased error bar) for q, with which it is clearly correlated. Shifts in the remaining parameters are within about one standard deviation.

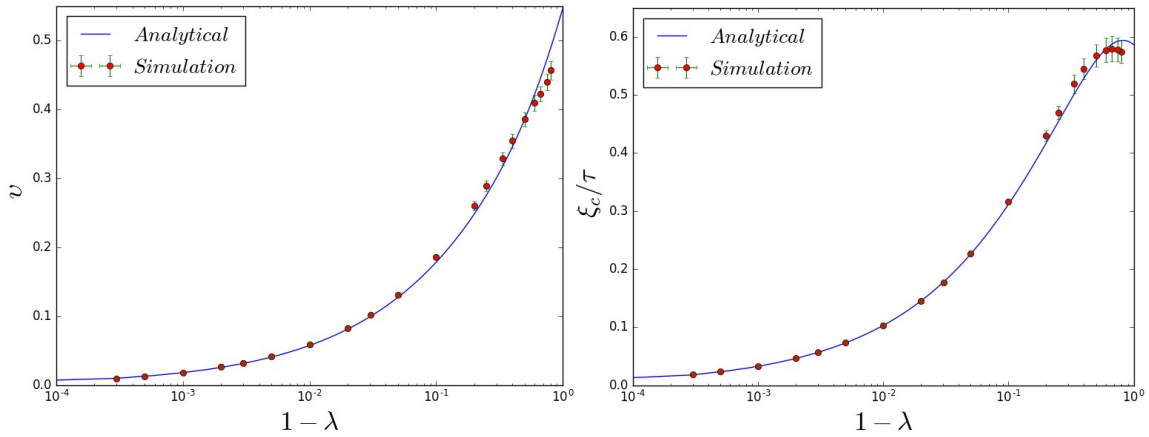

Fig. 2.11 Velocity v and conformal correlation length divided by conformal time ξ_c/τ obtained from the extended VOS model with the best-fit parameters indicated in the last line of table 2.3, compared to the data from the numerical simulations for different expansion rates.

It is particularly suggestive that a value of $\beta = 1$ provides a good fit to the simulations. In this case the momentum parameter has the simpler form

$$k_w(v) = k_0 \frac{1 - qv^2}{1 + qv^2}\,, \tag{2.52}$$

to be contrasted with the analogous parameter for cosmic strings

$$k(v) \propto k_{0,s} \frac{1 - 8v^6}{1 + 8v^6}\,. \tag{2.53}$$

It is tempting to speculate that the velocity dependence in the former would be associated with energy losses due to scalar radiation [113], which are indeed dominant in our simulations from which this calibration has emerged. Similarly, the velocity dependence in the latter could be associated with quadrupole radiation—which is implicitly assumed as an energy loss mechanism in the phenomenological modeling which, together with a comparison with Goto-Nambu string simulations, led to the analogous expression for strings [89]. Exploring this hypothesis is certainly worthy of future study.

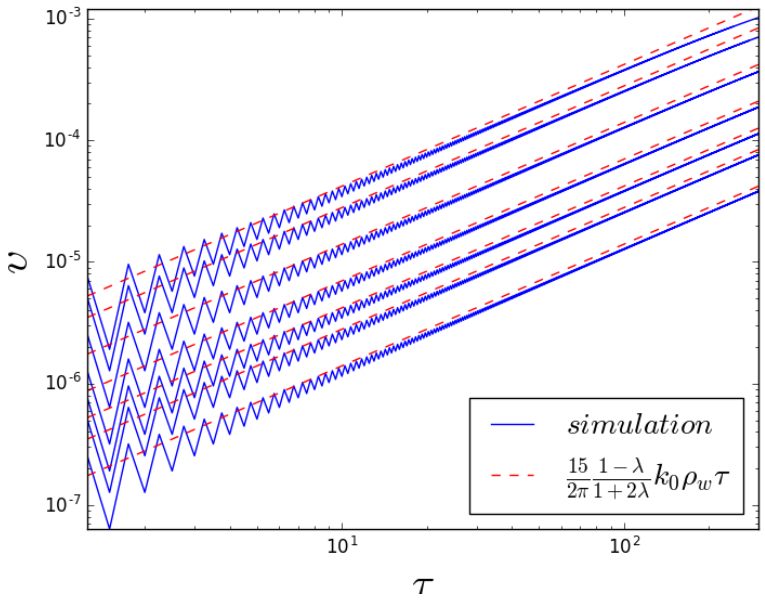

Fig. 2.12 Comparing the analytic solution of the VOS model, with the free parameters fixed at their best-fit values, for domain walls in the stretching regime (red dashed lines) with the result of our field theory numerical simulations for high values of λ (blue solid lines).

Now we can use another scaling regime, the conformal stretching regime, to make an alternative calibration of some parameters in the extended VOS model. For this purpose we need to quantify the proportionality factor that appears in the equation (2.37). To do so, we

need to use equations (2.50) with the asymptotic solution (2.37)

$$v = \frac{15}{2\pi}\frac{1-\lambda}{1+2\lambda}\, k_0 \rho_w \tau\,, \tag{2.54}$$

where we have used our definition of $k(v)$ (2.45)—which in the non-relativistic limit is simply k_0—and again the numerical factor stems from our choices of parameters for the potential and the thickness of the domain walls[4].

In order to further quantify this behaviour we will again use the scaling diagnostic parameters μ and ν defined in (2.20). For the conformal stretching regime we expect $\mu = 0$ and $\nu = 1$. Table 2.4 shows the results of this analysis and fully confirms the presence of this regime, for the faster expansion rates for which it persists longer.

Table 2.4 Scaling properties of numerical simulations for domain wall networks with different expansion rates λ in the conformal stretching regime. In addition to the slope parameters μ and ν we also list the asymptotic values of the (constant) comoving correlation length and the slope of the wall energy, as well as the range of conformal times used for the fits in each set of simulations. One-sigma statistical uncertainties are quoted throughout.

$1-\lambda$	μ	ν	ξ_c	$\gamma_v v/\tau(10^{-6})$	Fit range (τ)
$3\cdot10^{-6}$	-0.001 ± 0.001	0.997 ± 0.217	0.900 ± 0.001	3.792 ± 0.357	$1-76$
$2\cdot10^{-6}$	-0.005 ± 0.003	0.967 ± 0.125	0.905 ± 0.006	2.502 ± 0.142	$1-226$
$1\cdot10^{-6}$	-0.007 ± 0.004	0.955 ± 0.099	0.908 ± 0.008	1.245 ± 0.058	$1-376$
$5\cdot10^{-7}$	-0.007 ± 0.003	0.956 ± 0.085	0.908 ± 0.008	0.623 ± 0.025	$1-526$
$3\cdot10^{-7}$	-0.007 ± 0.003	0.956 ± 0.075	0.908 ± 0.008	0.374 ± 0.014	$1-676$
$2\cdot10^{-7}$	-0.006 ± 0.003	0.956 ± 0.068	0.907 ± 0.008	0.249 ± 0.009	$1-826$
$1\cdot10^{-7}$	-0.004 ± 0.002	0.968 ± 0.061	0.905 ± 0.005	0.125 ± 0.004	$1-976$

As a result, the equation (2.54) allows us to carry out a further test of the VOS model calibration, since we can use it to numerically measure the value of the parameter k_0. This is a useful consistency test, since in the analysis in the previous section k_0 as well as the other model parameters were determined using data from the linear scaling regime. Here we find that

$$k_0 = 1.76 \pm 0.11\,, \tag{2.55}$$

which is fully consistent with the results of table 2.3. Figure 2.12[5] shows the conformal stretching part of the evolution of our simulations, plotted together with the predictions of the VOS model with its best-fit parameters.

The last probe that is left for the VOS model in our treatment is a set of radiation-matter transition simulations, already described in section 2.2.4. For this purpose we insert the scale factor expression (2.25) with the corresponding constants a_{eq} and τ in the system of equations (2.50). We can now compare the dynamics of the extended analytic model and the simulations. This comparison is summarized in the figure 2.13, where the results of simulations (solid color

[4]The multiplier for equation (2.54) can be obtained from the expression for the wall tension $\sigma_w = \int \varphi'(z)dz$ [35], where $\varphi(z)$ is given by (2.17) with parameters for the potential (2.16)

[5]It should be noted that in the paper [114] the legend in the similar to 2.12 figure contains an error, which is corrected here.

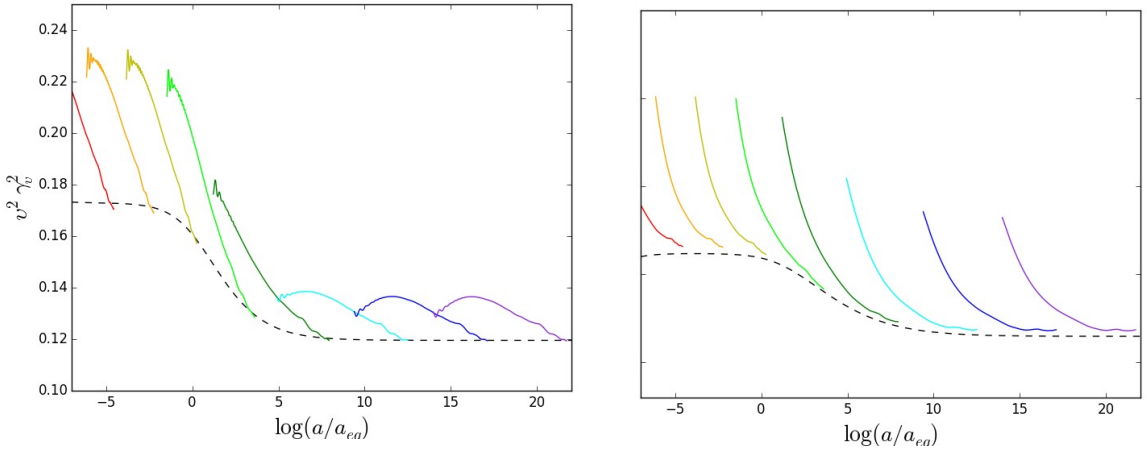

Fig. 2.13 Evolution of the conformal correlation length divided by conformal time ξ_c/τ (right panel) and of $(\gamma_v v)^2$ (left panel) during the radiation-matter transition, plotted as a function of the natural logarithm of the scale factor (relative to a_{eq}). The simulations are denoted by solid color lines (each line being an average of 10 simulations with random initial conditions) while the prediction of the extended analytic model with the best-fit parameters discussed in the text is shown by the black dashed lines. The plot only includes the dynamic range $20 \leq \tau \leq 1500$ of each set of simulations; the earlier part (which is dominated by the initial conditions in the box rather than converging to the attractor solution) and the latter part (due to lack of statistics) have been omitted for clarity.

lines) and the extended analytic model (dashed black line) are compared. It is seen that the analytic model provides an excellent description of the radiation-matter transition. It should be emphasized that this is an independent test of the VOS model calibration, since it does not rely on scaling regime.

2.5 Summary

In this chapter we revisited the standard description of the VOS model [88, 89], and reviewed a possible generalization for $p+1$-dimensional defects evolving in the $N+1$ FLRW space-time manifold [90, 94]. This description provided the base to study the evolution of domain wall networks in expanding FLRW universes in more detail.

We took advantage of recent progress in computing power and hardware to scrutinize the largest and most extensive set of field theory simulations of domain walls, using the PRS algorithm. Domain wall networks were simulated in FLRW expanding universes for a wide range of expansion rates λ. These simulations allowed us to significantly improve the analytic description of wall network evolution, based on the quantitative VOS model. We have explicitly shown that a constant momentum parameter k_w and chopping parameter c_w cannot fully reproduce the simulations for different expansion rates. Motivated by this mismatch, we used phenomenological arguments to introduce an extended model, given by equations (2.50). In this model the momentum parameter is described by a velocity-dependent function

$k_w(v)$ (2.45), and there is a generalized energy loss function $F(v)$ (2.47), which in addition to chopping losses also includes scalar radiation of the walls. We did not address the issue of possible losses to gravitational radiation, which is left for subsequent work. Fitting the phenomenological parameters to the simulations, we found that energy losses due to creation of sphere-like objects are typically subdominant in comparison with scalar radiation.

Also we revisited the role of damping mechanisms in the cosmological evolution of topological defect networks, comparing and contrasting friction due to particle scattering and the expansion of the universe as damping mechanisms capable of making the evolution of the networks non-relativistic. In both cases the network can either be conformally stretched or evolve in a Kibble scaling regime [36, 100]. In particular we have explicitly demonstrated that a sufficiently large Hubble damping (that is a sufficiently fast expansion rate) eventually leads to a linear scaling regime where the network is non-relativistic, but this is typically preceded by a stretching regime counterpart which we characterize for the first time.

We have for the first time simulated domain wall networks in universes with very fast expansion rates (from $1-\lambda = 0.03$ to $1-\lambda = 10^{-7}$, for $a \propto t^{\lambda}$). In addition to confirming to high accuracy the two scaling regimes, we have also used these simulations to improve the calibration of the VOS model for the case of domain walls. This improvement stems both from the wider range of expansion rates now available and from the inclusion of an estimated systematic uncertainty in our error budget.

Additionally we have confirmed that the extended analytic model can describe both the fixed expansion rate cases and the transition from the radiation to the matter-dominated era. The latter one is an important test of the model, since the network is not scaling during the transition (while the model parameters were calibrated from fixed expansion rate data in the scaling regime).

Chapter 3

Strings with non-trivial internal structure

As it was already demonstrated in sections 1.4 and 1.6, there are many different types of possible strings. If we want to obtain accurate observational constraints on models that produce strings, we need to be able to describe a variety of strings properties. Hence, in order to achieve reliable observational constraints on the underlying early universe models from cosmic string network phenomenology, one needs to develop an accurate description of cosmic string network evolution, taking into account the distinctive features of different types of cosmic strings. One way to accomplish this task is to conduct numerical simulations [115, 116]. This approach provides reliable results, but it is currently limited by computer capabilities, especially for the case of cosmic strings with non-trivial internal structure (section 1.4.4).

The alternative – and largely complementary – semi-analytic approach for the description of cosmic string network evolution is based on the VOS model (already presented in section 2.1). In this treatment it is much easier to add non-trivial features for cosmic strings (some examples can be found in [44, 92, 106, 107, 109, 117–119]) allowing evolution over large dynamical ranges that cannot be achieved by numerical simulations. However, as it was emphasised in section 2.1, semi-analytic descriptions involve free parameters, which can only be reliably calibrated by comparison to simulations. As a result, a combination of such analytic descriptions and numerical simulations is at present the best approach for studying the evolution of cosmic string networks with non-trivial properties.

One of such extensions is aimed to study superconducting cosmic strings. These strings were described for the first time in [45] and can be found as an outcome of a wide range of grand unified scenarios [26, 67, 120, 121]. These strings are characterized by the presence of a worldsheet current. This can be caused by a coupling between the field forming the cosmic string and other fields, by trapped charged fermion modes along the string [45] (which as we saw is common in supersymmetric models [67, 122]), by trapped vector fluxes on non-Abelian strings [123], and other specific mechanisms (for example symmetry breaking of an accidental symmetry in SU(2) strings [124]).

In addition, it should be mentioned that the presence of a current enables the inclusion of effective macroscopic properties. For example, it was shown that the small-scale structure

(wiggles) is described by the elastic type of string and can be successfully mimicked by a specific type of current [110, 125, 126].

In what follows, we will show quantitatively how the presence of currents on the string worldsheet can affect the string network evolution. In particular, we obtain the general microscopic description of strings with any type of current in the section 3.2. Then we move on to study the effective macroscopic description of wiggly cosmic strings in the section 3.5. In the section 3.6 the description of superconducting string network evolution will be presented, specifically for the chiral type of current.

3.1 Modifications of the Nambu-Goto action

3.1.1 The effective action for superconducting strings

In section 1.4.5 we already demonstrated how the approximation in the form of the Nambu-Goto action can be obtained from the original $3+1$-dimensional field theory description. Let's review the approach that leads to extension of the Nambu-Goto action caused by the current inside the string core (the field theory description is given in sections 1.4.4, 1.6) [45]. To do so, we need to recall the string-like solution from section 1.4.4. Instead of studying the numerical solution of the equations, as it was done above, we consider small fluctuations of the field σ around the φ background. For this purpose we write the equations of motion for the σ field from the Lagrangian (1.31) keeping only terms linear in σ terms and putting $\tilde{A}_\mu = 0$

$$\partial^\mu \partial_\mu \sigma + \sigma \left(4g|\varphi|^2 - \tilde{\lambda}\tilde{\eta}^2 \right) = 0. \tag{3.1}$$

Let's use the ansatz $\sigma = \mathrm{e}^{i\omega t}\sigma_0(r)$ to equation (3.1) in cylinder coordinates. This allows us to obtain the following equation [45]

$$\left(\partial_r^2 + \frac{1}{r}\partial_r \right) \sigma_0 = \left(U(r) - \omega^2 \right), \tag{3.2}$$

where $U(r)$ is defined by the string profile, and hence has following boundary values $U(0) = -\tilde{\lambda}\tilde{\eta}^2$, $U(\infty) = 4\eta^2 g - \tilde{\lambda}\tilde{\eta}^2$.

Equation (3.2) is similar to the Schrödinger equation for the motion of a particle in the potential $U(r)$. Therefore, to have a bound state for the system (3.2), the following relation should be satisfied $4\eta^2 g > \tilde{\lambda}\tilde{\eta}^2$, which is exactly the condition to have superconducting strings (see section 1.4.4). The presence of the bound state for the field σ means that the string is stable when $\sigma \neq 0$, which guarantees the non-trivial structure inside the string core [45].

Considering small fluctuations of the field σ, we can obtain an effective action for the infinitely thin string, in a similar way as it was done in section 1.4.5 for the Nambu-Goto action. We can write small excitations of the σ field in the form

$$\sigma = \mathrm{e}^{i\theta(z,t)}\sigma_0(r), \tag{3.3}$$

where θ is an arbitrary slowly varying function [45].

Similarly, the vector field $\tilde{A}_\mu(z,t)$ can be chosen to be a slowly varying function of coordinates t, z. Recalling that in the string core we anticipate $\varphi = 0$ and $A_\mu = 0$, we can rewrite the Lagrangian (1.31) in the form of the action

$$S_{\mathrm{W}} = -\frac{1}{4}\int \tilde{F}_{\mu\nu}\tilde{F}^{\mu\nu}d^4x + K\int \left(\partial_a\theta + \tilde{e}\tilde{A}_a\right)^2 dzdt, \tag{3.4}$$

where $a = 0, 1$ runs over t, z coordinates and K is a constant which appeared from the integration over x, y coordinates.

Thus, the current on the string worldsheet for the action (3.4) can be written as

$$J_a = -2K\tilde{e}\left(\partial_a\theta + \tilde{e}A_a\right) = q\varepsilon_{ab}\gamma^{bc}\partial_a\phi, \tag{3.5}$$

where $q = \tilde{e}\sqrt{2K}$, ε_{ab} is the Levi-Civita symbol and the last identity was obtained from the fact that any two dimensional conserved current can be represented as a derivative of a scalar field ϕ.

As a result, we can substitute the field ϕ in the action (3.4) and apply the same method as in the section 1.4.5, i.e. change coordinates X^μ to ξ^μ and take the limit of infinitely thin strings. Carrying out all steps listed above, one can obtain the effective action for the infinitely thin string, which takes into account the presence of non-trivial internal structure (for more details see [35])

$$S_{\mathrm{W}} = \int \sqrt{-\gamma}\left(-\mu_0 + \frac{1}{2}\gamma^{ab}\phi_{,a}\phi_{,b} - q\tilde{A}_\mu x^\mu_{,a}E^{ab}\phi_{,b}\right)d\sigma_0 d\sigma_1, \tag{3.6}$$

where $E^{ab} = \frac{\varepsilon^{ab}}{\sqrt{-\gamma}}$ is the covariant Levi-Civita tensor.

We see from the action (3.6) that the Nambu-Goto action should be modified for stings with non-trivial internal structure. Let's introduce relevant parameters, which are needed to investigate the string properties. At first, using the definition in (2.5), we can obtain the *tension* T and the *mass per unit length* U from $3+1$-dimensional field theory with following relations [127, 128]

$$\begin{aligned} T^\mu_\nu u^\nu &= U\delta^\mu_\nu u^\nu, \\ T^\mu_\nu v^\nu &= T\delta^\mu_\nu v^\nu, \end{aligned} \tag{3.7}$$

where u^ν, v^ν are orthonormal time-like and space-like eigenvectors of the energy-momentum tensor $T^{\mu\nu}$ with corresponding eigenvalues U, T respectively.

The energy-momentum tensor on the string worldsheet T^{ab} is related to the space-time energy-momentum tensor $T^{\mu\nu}$ (3.7) by the coordinate transformation

$$T^{\mu\nu} = T^{ab}x^\mu_{,a}x^\nu_{,b}. \tag{3.8}$$

Having the definition of the mass per unit length U and the tension T, we can define the speed v_{E} of transverse perturbations (which are called *wiggles*) and the speed v_{L} of

longitudinal perturbations (which are called *jiggles* or *woggles*) (details can be found in [128])

$$\begin{aligned} \upsilon_{\mathrm{T}}^2 &= \frac{T}{U}, \\ \upsilon_{\mathrm{L}}^2 &= -\frac{dT}{dU}. \end{aligned} \tag{3.9}$$

The quantities introduced above are important for the string properties description. In this way, the action developed by Witten (3.6) is supposed to be able to mimic the main features of the original four dimensional field theory model of the superconducting string (1.31). However, further study of the effective action (3.6) revealed that this action requires generalization [129]. Moreover, and what is more important, the original model of the superconducting string, described by the Lagrangian (1.31), is supersonic, i.e. $\upsilon_{\mathrm{T}} > \upsilon_{\mathrm{L}}$. This means that wiggles on this string propagate faster than jiggles. On the other hand, the effective action (3.6) describes the subsonic type of strings [130], i.e. $\upsilon_{\mathrm{T}} < \upsilon_{\mathrm{L}}$. This, in turn, means that wiggles propagate on the string slower than jiggles. As a result, the alternative phenomenological action was suggested to settle down this inconsistency [131, 132]

$$\begin{aligned} S_{\mathrm{m}} &= \int \sqrt{-\gamma}\left(-\mu_0 - \frac{\kappa}{2}\left(1+\frac{\kappa}{\mu_*}\right)^{-1}\right) d\sigma_0 d\sigma_1 \\ &\qquad \text{magnetic regime: } \kappa > 0, \\ S_{\mathrm{e}} &= \int \sqrt{-\gamma}\left(-\mu_0 - \mu_* \ln\left(1+\frac{\kappa}{\mu_*}\right)\right) d\sigma_0 d\sigma_1 \\ &\qquad \text{electric regime: } \kappa < 0, \end{aligned} \tag{3.10}$$

while in the weak current limit

$$S_{\mathrm{weak}} = \int \sqrt{-\gamma}\left(-\mu_0 - \frac{\kappa}{2}\left(1+\frac{\kappa}{\mu_*}\right)\right) d\sigma_0 d\sigma_1, \tag{3.11}$$

where $\kappa = \kappa_0 \gamma^{ab}\phi_{;a}\phi_{;b}$ with the gauge-covariant derivative and μ_*, κ_0 are positive constants.

3.1.2 The effective action for wiggly strings

It was shown above that some models with non-trivial structure on the string worldsheet lead to modifications of the Nambu-Goto action. However, these extensions can be caused not only by the presence of additional fields on the string worldsheet. There are situations in which the effective current on the worldsheet plays the role of the effective description of string macroscopic properties. This is the important case of wiggly strings[1] (see figure 3.1). Wiggles unavoidably appear on small scales during string evolution. Their presence on a microscopic scale affects macroscopic properties of the string. In particular, it was shown that microscopic string excitations can be effectively taken into account at a macroscopic level, independently of the noise details [125]. Later on, it was argued that the *transonic* elastic string model can effectively describe wiggles [126]. Here transonic means that transverse

[1] Wiggles here has the same meaning as in the previous section, scilicet, transverse perturbations on a string.

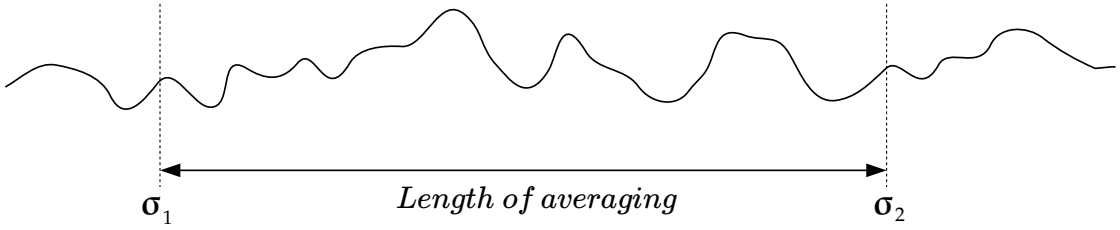

Fig. 3.1 The averaging over wiggly strings. The typical size of wiggles is smaller than the averaging length and can be taken into account effectively by introducing the Lagrangian (3.12). Parameter ω takes into account the presence of small-scale structure, as less ω, as more wiggles inside the averaging length.

and longitudinal perturbations propagate with the same speed $v_{\mathrm{T}} = v_{\mathrm{L}}$. Elasticity implies presence of a specific form of the current on the string worldsheet, which leads to the action

$$S_{\mathrm{wiggly}} = -\mu_0 \int \sqrt{-\gamma\,(1-\kappa)}. \tag{3.12}$$

Having the effective action (3.12) and using definitions (2.5) and (3.7), one can show that the tension and the mass per unit length obey the equation of state

$$\begin{aligned} UT =& \mu_0^2, \\ U = \mu_0/\omega,&\ T = \mu_0\omega, \end{aligned} \tag{3.13}$$

where $\omega = \sqrt{1-\kappa}$.

It was shown that the exact form of the equation of state (3.13) appears on a macroscopic scale for wiggly strings [133]. It should be noted that from equation (3.13) it follows that the transverse and longitudinal speeds are equal, as it is supposed to be for the transonic model

$$v_{\mathrm{T}}^2 = \frac{T}{U} = v_{\mathrm{L}}^2 = -\frac{dT}{dU} = \omega^2. \tag{3.14}$$

The ratio (3.14) implies that $\omega \leq 1$, the usual Nambu-Goto action (1.36) is recovered when $\omega = 1$. We anticipate to recover the Nambu-Goto action when the averaging length has similar size compared to the size of wiggles. At the same time we depart from the Nambu-Goto action as the size of averaging becomes bigger than the typical size of wiggles (see figure 3.1).

The effective action (3.12) allows us to study the wiggly string network. In particular, by using the VOS model approach, described in the section 2.1, it is possible to obtain evolution equations for the wiggly string network. We do this below.

3.2 General microscopic equations for strings with current

As we already saw in the section 3.1, strings with non-trivial structure require an extension of the Nambu-Goto action. As was shown before, to obtain an effective two-dimensional action

of a string-like object from a $3+1$-dimensional field theory, one can follow the procedure of [45]. This coarse-graining approach leads to loss of some string features compared to the original description. As a result, there is only a phenomenological approach to reproduce properties of the original model correctly (details in section 3.1.1). On the other hand, one is often interested in averaged equations of motion and these can be the same for different Lagrangians (for an explicit example see [106]). Thus, focusing on deriving the exact form of the Lagrangian is not necessarily the most productive route to obtaining accurate string network evolution.

Bearing in mind the subtleties described above, we consider the general form of a two-dimensional Lagrangian involving an arbitrary function of a string current. First, as it was already mentioned in section 3.1.1, let's note that a current on a two-dimensional space can be represented as a derivative of a scalar field φ,

$$J_a = \varphi_{,a}. \tag{3.15}$$

We can thus build three possible terms "living" on the worldsheet, out of which the Lagrangian will be constructed

$$\begin{aligned} &[1]: \quad \varphi^{,a}\varphi^{,b}\gamma_{ab} = \kappa, \\ &[2]: \quad \varepsilon^{ac}\varepsilon^{bd}\gamma_{ab}\gamma_{cd} = \gamma, \\ &[3]: \quad \varepsilon^{ac}\varepsilon^{bd}\gamma_{ab}\varphi_{,c}\varphi_{,d} = \Delta. \end{aligned} \tag{3.16}$$

The term Δ is motivated by the Dirac-Born-Infeld (DBI) action for cosmic strings (relevant studies can be found in [134], [135] and [109]).

Taking into account the three possible terms in (3.16) we can write down the general form of the action generalising the Nambu-Goto action to the case of a string with current

$$S = -\mu_0 \int f(\kappa, \gamma, \Delta)\sqrt{-\gamma}d^2\sigma. \tag{3.17}$$

The arbitrary choice of the function $f(\kappa, \gamma, \Delta)$ can break reparametrisation invariance of the generalized action (3.17). In order to preserve invariance of the action under reparametrizations, the last two terms of (3.16) should be connected in the following way $f(\kappa, \Delta/\gamma)$. Hereinafter, for the sake of simplicity, the function $f(\kappa, \Delta/\gamma)$ in equations will be denoted as f.

Assuming that cosmic strings are moving in a flat FLRW background metric (1.1), we can build the energy-momentum tensor from the action (3.17)

$$\begin{aligned} T^{\mu\nu}(y) = \frac{\mu_0}{\sqrt{-g}} \int d^2\sigma\sqrt{-\gamma}\delta^{(4)}(y - x(\sigma)) \\ \left(\tilde{U}\tilde{u}^\mu\tilde{u}^\nu - \tilde{T}\tilde{v}^\mu\tilde{v}^\nu - \Phi(\tilde{u}^\mu\tilde{v}^\nu + \tilde{v}^\mu\tilde{u}^\nu)\right), \end{aligned} \tag{3.18}$$

where $\tilde{u}^\mu = \frac{\sqrt{\varepsilon}\dot{x}^\mu}{(-\gamma)^{1/4}}$ and $\tilde{v}^\mu = \frac{x'^\mu}{\sqrt{\varepsilon}(-\gamma)^{1/4}}$ are orthonormal timelike and spacelike vectors respectively ($\tilde{u}^\mu\tilde{u}_\mu = 1$, $\tilde{v}^\mu\tilde{v}_\mu = -1$) and

$$\tilde{U} = f - 2\frac{\partial f}{\partial\gamma}\frac{\Delta}{\gamma} + 2\gamma^{00}\frac{\partial f}{\partial\kappa}\dot{\varphi}^2 + 2\gamma^{11}\frac{\partial f}{\partial\Delta}\varphi'^2, \tag{3.19}$$

$$\tilde{T} = f - 2\frac{\partial f}{\partial\gamma}\frac{\Delta}{\gamma} + 2\gamma^{11}\frac{\partial f}{\partial\kappa}\varphi'^2 + 2\gamma^{00}\frac{\partial f}{\partial\Delta}\dot{\varphi}^2, \tag{3.20}$$

$$\Phi = \frac{2}{\sqrt{-\gamma}}\left(\frac{\partial f}{\partial\kappa} - \frac{\partial f}{\partial\Delta}\right)\varphi'\dot{\varphi}\,. \tag{3.21}$$

It is important to note that for this modification of the Lagrangian, the energy-momentum tensor (3.18) has non-diagonal terms induced by the presence of the current. Let us obtain the equations of motion for the action (3.17) using the definitions of $\tilde{U}$ in (3.19), $\tilde{T}$ in (3.20) and Φ in (3.21). Variation of the action (3.17) with respect to x^μ and φ gives

$$\partial_\tau(\varepsilon\tilde{U}) + \frac{\dot{a}}{a}\varepsilon\left(\dot{\mathbf{x}}^2(\tilde{U}+\tilde{T}) + \tilde{U} - \tilde{T}\right) = \partial_\sigma\Phi, \tag{3.22}$$

$$\ddot{\mathbf{x}}\varepsilon\tilde{U} + \dot{\mathbf{x}}\varepsilon\frac{\dot{a}}{a}\left(1-\dot{\mathbf{x}}^2\right)\left(\tilde{U}+\tilde{T}\right) = \partial_\sigma\left(\frac{\tilde{T}}{\varepsilon}\mathbf{x}'\right) + \mathbf{x}'\left(2\frac{\dot{a}}{a}\Phi + \dot{\Phi}\right) + 2\Phi\dot{\mathbf{x}}', \tag{3.23}$$

$$\partial_\tau\left(\left(\frac{\partial f}{\partial\kappa} + \frac{\partial f}{\partial\Delta}\right)\varepsilon\dot{\varphi}\right) = \partial_\sigma\left(\left(\frac{\partial f}{\partial\kappa} + \frac{\partial f}{\partial\Delta}\right)\frac{\varphi'}{\varepsilon}\right). \tag{3.24}$$

As can be seen from the equations of motion (3.22) and (3.23), string dynamics does not depend explicitly on the form of the current contribution $f(\kappa, \Delta/\gamma)$. The dynamics of the string is defined completely by $\tilde{U}$, $\tilde{T}$ and Φ, which can be associated to mass per unit length and string tension. Indeed, it is only the dynamics of φ itself – equation (3.24) – that explicitly depends on $\partial f/\partial\kappa$ and $\partial f/\partial\Delta$. This provides us an alternative approach to studying string dynamics effectively, without an explicit connection between an effective Nambu-Goto-like action and the original field theory model. One can instead study the behaviour of $\tilde{U}$, $\tilde{T}$ and Φ in the original four-dimensional model in the framework of field theory (as it was done for example in [49, 50, 136–138]) and then insert the dynamics of $\tilde{U}$, $\tilde{T}$ and Φ in the equations of motion (3.22) and (3.23).

Additionally, we note that one can easily generalize the equations of motion (3.22)-(3.24) to include any number of uncoupled scalar fields, associated to corresponding currents. In this case, we can simply rewrite the variables κ and Δ as

$$\kappa_i = \gamma_{ab}\varphi_i^{,a}\varphi_i^{,b}, \quad \Delta_i = \varepsilon^{ac}\varepsilon^{bd}\gamma_{ab}\varphi_{i,c}\varphi_{i,d}\,, \tag{3.25}$$

where the index i runs over the number of fields. There is no summation over i; if a sum over this index is to be taken it will be written explicitly.

Definitions (3.19), (3.20) and (3.21) in the case of multiple currents generalise to

$$\tilde{U} = f + 2\sum_i \left(\gamma^{00} \frac{\partial f}{\partial \kappa_i} \dot{\varphi}_i{}^2 + \gamma^{11} \frac{\partial f}{\partial \Delta_i} \varphi_i'{}^2 - \frac{\partial f}{\partial \gamma} \frac{\Delta_i}{\gamma} \right), \tag{3.26}$$

$$\tilde{T} = f + 2\sum_i \left(\gamma^{11} \frac{\partial f}{\partial \kappa_i} \varphi_i'{}^2 + \gamma^{00} \frac{\partial f}{\partial \Delta_i} \dot{\varphi}_i{}^2 - \frac{\partial f}{\partial \gamma} \frac{\Delta_i}{\gamma} \right), \tag{3.27}$$

$$\Phi = \frac{2}{\sqrt{-\gamma}} \sum_i \left(\frac{\partial f}{\partial \kappa_i} - \frac{\partial f}{\partial \Delta_i} \right) \varphi_i' \dot{\varphi}_i. \tag{3.28}$$

With definitions (3.26)-(3.28) the form of the energy-momentum tensor (3.18) and the equations of motion (3.22)-(3.23) stay unchanged. On the other hand, the equation of motion for the scalar field (3.24) is substituted by the set of equations

$$\partial_\tau \left(\left(\frac{\partial f}{\partial \kappa_i} + \frac{\partial f}{\partial \Delta_i} \right) \varepsilon \dot{\varphi}_i \right) = \partial_\sigma \left(\left(\frac{\partial f}{\partial \kappa_i} + \frac{\partial f}{\partial \Delta_i} \right) \frac{\varphi_i'}{\varepsilon} \right). \tag{3.29}$$

We see, therefore, that if we extend the action (3.17) to include additional scalar fields φ_i, the structure of the equations of motion together with the form of the general energy-momentum tensor remains unchanged; we only need to add a new index i to κ and Δ. This fact will be useful in our considerations below. For now, let us diagonalise the energy-momentum tensor (3.18) and use the definition of the mass per unit length and tension (3.7). The eigenvalues U, T are related to the original $\tilde{U}$, $\tilde{T}$ and Φ in (3.19)-(3.21) by

$$\begin{aligned} U &= \mu_0/2 \left(\tilde{U} + \tilde{T} + \Delta_\Phi \right), \\ T &= \mu_0/2 \left(\tilde{U} + \tilde{T} - \Delta_\Phi \right), \end{aligned} \tag{3.30}$$

while the eigenvectors can be expressed in terms of the original $\tilde{u}^\mu$ and $\tilde{v}^\mu$ as

$$\begin{aligned} u^\mu &= a\tilde{u}^\mu + \sqrt{a^2 - 1}\tilde{v}^\mu, \\ v^\mu &= \sqrt{a^2 - 1}\tilde{u}^\mu + a\tilde{v}^\mu, \end{aligned} \tag{3.31}$$

with

$$a = \frac{1}{2} \left[1 + \frac{\tilde{U} - \tilde{T}}{\Delta_\Phi} \right]$$

and

$$\Delta_\Phi = \sqrt{(\tilde{U} - \tilde{T})^2 - 4\Phi^2}\,.$$

The passage from the equations of motion of a single string segment to an effective description of a whole network of strings is done through an averaging procedure [88] leading to the VOS model for cosmic strings. Following this approach, we begin by dotting equation (3.23) with vectors $\dot{\mathbf{x}}$ and $\mathbf{x}'$ and using the property of our parametrization $\dot{\mathbf{x}} \cdot \mathbf{x}' = 0$

to obtain

$$\dot{\mathbf{x}}\cdot\ddot{\mathbf{x}}\varepsilon\tilde{U}+\dot{\mathbf{x}}^2\varepsilon\frac{\dot{a}}{a}\left(1-\dot{\mathbf{x}}^2\right)\left(\tilde{U}+\tilde{T}\right)=\frac{\tilde{T}}{\varepsilon}\dot{\mathbf{x}}\cdot\mathbf{x}''-2\Phi\ddot{\mathbf{x}}\cdot\mathbf{x}', \tag{3.32}$$

$$\mathbf{x}'\cdot\ddot{\mathbf{x}}\varepsilon\tilde{U}-\mathbf{x}'\cdot\mathbf{x}''\frac{\tilde{T}}{\varepsilon}+2\Phi\mathbf{x}''\cdot\dot{\mathbf{x}}=\mathbf{x}'^2\left(2\frac{\dot{a}}{a}\Phi+\dot{\Phi}+\frac{\tilde{T}'}{\varepsilon}-\frac{\tilde{T}}{\varepsilon^2}\varepsilon'\right). \tag{3.33}$$

Using the expression $\frac{\varepsilon'}{\varepsilon}=\frac{\mathbf{x}'\cdot\mathbf{x}''}{\mathbf{x}'^2}-\frac{\mathbf{x}'\cdot\ddot{\mathbf{x}}}{1-\dot{\mathbf{x}}^2}$ we can eliminate the terms proportional to ε' and $\mathbf{x}'\cdot\ddot{\mathbf{x}}$ obtaining the equation

$$\begin{aligned}&\dot{\mathbf{x}}\cdot\ddot{\mathbf{x}}\varepsilon\tilde{U}+\dot{\mathbf{x}}^2\varepsilon\frac{\dot{a}}{a}\left(1-\dot{\mathbf{x}}^2\right)\left(\tilde{U}+\tilde{T}\right)-\frac{\tilde{T}}{\varepsilon}\dot{\mathbf{x}}\cdot\mathbf{x}''=\\&=2\Phi\frac{1-\dot{\mathbf{x}}^2}{\tilde{U}-\tilde{T}}\left(\tilde{T}'+\varepsilon\left(2\frac{\dot{a}}{a}\Phi+\dot{\Phi}-2\Phi\frac{\mathbf{x}''\cdot\dot{\mathbf{x}}}{\mathbf{x}'^2}\right)\right).\end{aligned} \tag{3.34}$$

As a result, we obtained the system of equations (3.22) and (3.34), for any kind of currents. These equations are determined only by $\tilde{U}$, $\tilde{T}$ and Φ parameters, which in principle can be studied numerically from the field theory approach. The general connection between $\tilde{U}$, $\tilde{T}$ and Φ with worldsheet current is defined by the equations (3.26)-(3.28). Later we will consider how we can average these equations and apply them to the string network.

3.3 Exact solution in Minkowski space for chiral current

In this section we consider the most general action (3.17) in Minkowski space for the string with a "chiral" current[2]

$$\Delta,\ \kappa\to 0 \tag{3.35}$$

described by an arbitrary function $f(\kappa,\Delta/\gamma)$.

To consider this situation, at first we need to obtain the equations of motion, and then we need to take the limit (3.35). The equations of motion for the action (3.17) can be written in the form

$$\partial_a\left(\mathcal{T}^{ab}x^{\mu}_{,b}\right)=0, \tag{3.36}$$

$$\partial_a\left(\mathcal{S}^{ab}\varphi_{,b}\right)=0, \tag{3.37}$$

with

$$\mathcal{T}^{ab}=\sqrt{-\gamma}\left(\gamma^{ab}f+\theta^{ab}\right), \tag{3.38}$$

[2]Chiral type of current doesn't mean that the current disappears, it just means that the current is described by a null (light-like) vector.

with $\theta^{ab} = 2\left(\frac{\partial f}{\partial \kappa}\gamma^{ac}\gamma^{bd} + \frac{1}{\gamma}\frac{\partial f}{\partial \Delta}\varepsilon^{ac}\varepsilon^{bd}\right)\varphi_{,c}\varphi_{,d}$ and

$$\mathcal{S}^{ab} = \sqrt{-\gamma}\left(\gamma^{ab}\frac{\partial f}{\partial \kappa} + \frac{1}{\gamma}\frac{\partial f}{\partial \Delta}\varepsilon^{ac}\varepsilon^{bd}\gamma_{cd}\right), \tag{3.39}$$

where the limit (3.35) has been taken.

We try to find a parametrisation of the worldsheet such that the usual (without current) equations of motion for the string are valid

$$\partial_a\left(\eta^{ab}x^{\mu}_{,b}\right) = 0, \tag{3.40}$$

which requires that

$$\mathcal{T}^{ab} = \eta^{ab}, \tag{3.41}$$

where η^{ab} is a 2x2 Minkowski metric.

In order to show that it is possible to chose such a parametrization, to satisfy relations (3.40) and (3.41), we will follow the method elaborated in [139], i.e. we will study the $\mathcal{T}^{ab}$ determinant[3]

$$\det \mathcal{T}^c_a = -\det\left(f\delta^c_a + \theta^c_a\right) = -f^2 - f\mathrm{Tr}\theta^c_a - \det\theta^c_a. \tag{3.42}$$

If the expression (3.42) is equal to $\det\eta^c_a = -1$, there should exist the parametrization that allows to satisfy conditions (3.40), (3.41). Let's consider the terms in the expression (3.42) separately. At first we can calculate the determinant of the θ^c_a

$$\begin{aligned}\det\theta^c_a = \varepsilon_{cd}\varepsilon^{ab}\theta^c_a\theta^d_b \sim \underbrace{\varepsilon_{cd}\varepsilon^{ab}(\varphi_{,a}\varphi^{,c})(\varphi_{,b}\varphi^{,d})}_{=0 \text{ (since } \varphi_{,a}\varphi_{,b} = \varphi_{,b}\varphi_{,a})} + \\ + \varepsilon_{cd}\varepsilon^{ab}(\varepsilon_{am}\varphi^{,m}\varepsilon^{ck}\varphi_{,k})(\varepsilon^{dp}\varphi_{,p}\varepsilon_{bn}\varphi^{,n}) + \varepsilon_{cd}\varepsilon^{ab}(\varepsilon_{am}\varphi^{,m}\varepsilon^{ck}\varphi_{,k})(\varphi^{,d}\varphi_{,b}) = \\ = \delta^k_d\delta^b_m(\varphi^{,m}\varphi_{,k})(\varepsilon^{dp}\varphi_{,p}\varepsilon_{bn}\varphi^{,n}) + \delta^k_d\delta^b_m(\varphi^{,m}\varphi_{,k})(\varphi^{,d}\varphi_{,b}) = 0.\end{aligned} \tag{3.43}$$

We demonstrated that the third term in the expression (3.42) is zero. Let's consider the second one

$$\mathrm{Tr}\theta^c_a = \theta^a_a \sim \underbrace{(\varphi_{,a}\varphi^{,a})}_{=0 \text{ (chirality)}} + \varepsilon_{ab}\varphi^{,b}\varepsilon^{ad}\varphi_{,d} = \delta^d_b\varphi^{,b}\varphi_{,d} = \underbrace{\varphi^{,b}\varphi_{,b}}_{=0 \text{ (chirality)}} = 0. \tag{3.44}$$

We didn't include f derivatives in equations (3.43), (3.44), because each term in these expressions is equal to zero separately. To see that (3.42) is equal to -1 we need to recall that $f \to 1$ for the chiral current. As a result, for chiral currents it is possible to choose a parametrization that leads to equations of motion (3.40). The general solution of equations (3.40) is

$$\mathbf{x} = \frac{1}{2}\left(\mathbf{a}(\sigma+\tau) + \mathbf{b}(\sigma-\tau)\right). \tag{3.45}$$

[3]Note the absence of μ_0 comparing with [139]. This happens due to the fact that we can take out the constant μ_0 for the action (3.17).

where $\mathbf{a}(\sigma+\tau)$ and $\mathbf{b}(\sigma-\tau)$ are arbitrary vector-valued functions.

We still need to consider the equation for the field φ (3.37). Using the identity (3.39), we rewrite the equation (3.37) explicitly

$$\begin{aligned}
&\partial_a\left(\sqrt{-\gamma}\left(\gamma^{ab}\frac{\partial f}{\partial\kappa}+\frac{1}{\gamma}\frac{\partial f}{\partial\Delta}\varepsilon^{ac}\varepsilon^{bd}\gamma_{cd}\right)\varphi_{,b}\right)=\\
&=\partial_a\left(\sqrt{-\gamma}\left(\varphi^{,a}\frac{\partial f}{\partial\kappa}-\frac{\partial f}{\partial\Delta}\underbrace{E^{ac}E^{bd}\gamma_{cd}\gamma_{bk}}_{=\delta^a_k}\varphi^{,k}\right)\right)=\\
&=\partial_a\left(\sqrt{-\gamma}\gamma^{ab}\left(\frac{\partial f}{\partial\kappa}-\frac{\partial f}{\partial\Delta}\right)\varphi_{,b}\right)=0,
\end{aligned}\tag{3.46}$$

where we used the tensor $E^{ab}=\frac{1}{\sqrt{-\gamma}}\varepsilon^{ab}$ instead of the Levi-Civita symbol. This was done to allow the manipulation of E^{ab} indices by the metric γ_{ab}.

At the same time, it is seen that from equations (3.41) and (3.38) we can obtain the following relations

$$\begin{aligned}
\sqrt{-\gamma}\gamma^{ab}&=\mathfrak{T}^{ab}-\sqrt{-\gamma}\theta^{ab},\\
\sqrt{-\gamma}\varepsilon^{ac}\varepsilon^{bd}\gamma_{cd}&=\varepsilon^{ac}\varepsilon^{bd}\left(\mathfrak{T}_{cd}-\sqrt{-\gamma}\theta_{cd}\right).
\end{aligned}\tag{3.47}$$

Let's use the calculated expressions (3.47) in equation (3.46). Recalling the proven identity (3.41), we obtain the following construction

$$\partial_a\left[\left(\eta^{ab}-\sqrt{-\gamma}\theta^{ab}\right)\left(\frac{\partial f}{\partial\kappa}-\frac{\partial f}{\partial\Delta}\right)\varphi_{,b}\right]=0,\tag{3.48}$$

where the multiplier inside brackets can be simplified as

$$\begin{aligned}
\left(\eta^{ab}-\sqrt{-\gamma}\theta^{ab}\right)\varphi_{,b}&=\eta^{ab}\varphi_{,b}-2\sqrt{-\gamma}\left(\frac{\partial f}{\partial\kappa}\gamma^{ac}\gamma^{bd}+\frac{1}{\gamma}\frac{\partial f}{\partial\Delta}\varepsilon^{ac}\varepsilon^{bd}\right)\varphi_{,c}\varphi_{,d}\varphi_{,b}=\\
&=\eta^{ab}\varphi_{,b}-2\sqrt{-\gamma}\left(\frac{\partial f}{\partial\kappa}\gamma^{ac}\varphi_{,c}\underbrace{\varphi^{,b}\varphi_{,b}}_{=0}+\frac{1}{\gamma}\frac{\partial f}{\partial\Delta}\varepsilon^{ac}\varphi_{,c}\underbrace{\varepsilon^{bd}\varphi_{,d}\varphi_{,b}}_{=0}\right)=\eta^{ab}\varphi_{,b}.
\end{aligned}\tag{3.49}$$

Combining all results together, the final equation for the field φ can be expressed as

$$\partial_a\left[\left(\frac{\partial f}{\partial\kappa}-\frac{\partial f}{\partial\Delta}\right)\eta^{ab}\varphi_{,b}\right]=0,\tag{3.50}$$

Using the condition $\theta^{ab}\varphi_{,a}\varphi_{,b}=0$ together with (3.38) and (3.41), one can conclude that

$$\eta^{ab}\varphi_{,a}\varphi_{,b}=0.\tag{3.51}$$

Let's recall that $\frac{\partial f}{\partial\kappa}$ and $\frac{\partial f}{\partial\Delta}$ are constants for the chiral current. As a result, assuming that $\frac{\partial f}{\partial\kappa}-\frac{\partial f}{\partial\Delta}\neq 0$, the general solution of equations (3.50), (3.51) is

$$\varphi=F(\sigma\pm\tau),\tag{3.52}$$

where for the later discussion we will chose the + sign, which does not reduce the generality of the consideration.

We found the general solution for the string with a chiral current. However, there are some additional constraints that should be imposed. These conditions can be obtained by considering the metric γ^{ab}. The equation for the metric components comes from the chiral condition

$$\gamma^{00} + \gamma^{11} + 2\gamma^{01} = 0 \quad \text{or} \quad \gamma_{00} + \gamma_{11} - 2\gamma_{01} = 0. \tag{3.53}$$

Using the definition $\gamma_{ab} = x^{\mu}_{,a} x_{\mu,b}$ for (3.53), we obtain the equation

$$\dot{x}^{\mu}\dot{x}_{\mu} + x^{\mu\prime}x^{\prime}_{\mu} - 2\dot{x}^{\mu}x^{\prime}_{\mu} = \left(\dot{x}^{\mu} - x^{\mu\prime}\right)\left(\dot{x}_{\mu} - x^{\prime}_{\mu}\right) = 0, \tag{3.54}$$

which allows us to conclude that

$$|\mathbf{b}'| = 1. \tag{3.55}$$

Using the identity $\theta^{ab}\theta_{bc} = 0$ and (3.41) together with the fact that θ^{ab}, γ^{ab} are symmetric, we can conclude that

$$\frac{1}{\sqrt{-\gamma}}\left(\gamma_{ab} - \theta_{ab}\right) = \eta_{ab}. \tag{3.56}$$

Calculating the *"01"* components in the equation (3.56), we conclude that

$$\gamma_{01} = \frac{1}{4}\left(1 - |\mathbf{a}'|^2\right). \tag{3.57}$$

and with the condition (3.56), one can obtain the final connection between the solution (3.45) and (3.52)

$$1 - |\mathbf{a}'|^2 = 8\left(\frac{\partial f}{\partial \kappa} - \frac{\partial f}{\partial \Delta}\right)F'^2. \tag{3.58}$$

One can show that components *"00"* and *"11"* for the equation (3.56) coincide with equation (3.58). As a result, we obtained the general solution for the superconducting string (3.45, 3.52) together with condition (3.58) for any type of the chiral current. The difference between the obtained solutions and the previously studied particular cases [140], [141], [139] appears only in the multiplier $\left(\frac{\partial f}{\partial \kappa} - \frac{\partial f}{\partial \Delta}\right)$ in the equation (3.58).

3.4 General macroscopic equations for strings with current

In the previous section 3.2 we developed the microscopic description for strings with any type of currents, which is defined by an arbitrary function $f(\kappa, \Delta/\gamma)$. In this section we will average microscopic equations and subsequently apply them to the string network description.

To do so, let's introduce the additional macroscopic parameter

$$E = \mu_0 a \int \tilde{U} \varepsilon d\sigma \,. \tag{3.59}$$

We will call the macroscopic quantities (3.59), (2.6), (2.7) as the total energy, the 'bare' energy (without the contribution from the current) and rms velocity respectively. Using these definitions we proceed to average equations (3.22) and (3.34) finding

$$\dot{E} + \frac{\dot{a}}{a} E \left(v^2 \left(1 + W\right) - W \right) = \left\langle \Phi' / \varepsilon \right\rangle E_0, \tag{3.60}$$

$$\begin{aligned} &\dot{v} + v \frac{\dot{a}}{a} \left(1 - v^2\right) \left(1 + W\right) - \left(1 - v^2\right) \frac{k(v)}{R_c} = \\ &= \left\langle 2 \frac{\Phi}{\tilde{U}} \frac{1 - \dot{\mathbf{x}}^2}{1 - \tilde{T}/\tilde{U}} \left(\frac{\tilde{T}'}{\varepsilon} + 2 \frac{\dot{a}}{a} \Phi + \dot{\Phi} - 2 \Phi \frac{\mathbf{x}'' \cdot \dot{\mathbf{x}}}{\mathbf{x}'^2} \right) \right\rangle , \end{aligned} \tag{3.61}$$

where $\langle ... \rangle = \frac{\int ... \varepsilon d\sigma}{\int \varepsilon d\sigma}$ denotes the (energy-weighted) averaging operation, the same as it was used in section 2.7.

Here, we have defined $W = \left\langle \tilde{T}/\tilde{U} \right\rangle$ and introduced the average comoving radius of curvature of strings in the network, R_c, and the curvature parameter, $k(v)$, satisfying $\left\langle \frac{\dot{\mathbf{x}}}{\varepsilon} \cdot \left(\frac{\mathbf{x}'}{\varepsilon} \right)' \right\rangle = \frac{k(v)}{R_c} v(1 - v^2)$. For ordinary cosmic strings, an accurate ansatz for the curvature parameter as a function of velocity has the form (2.9) [89]. We assume that this function stays valid for strings with currents as well.

Following the procedure of [88, 89], we rewrite the averaged equations of motion (3.60-3.61) in terms of more convenient macroscopic variables: the comoving characteristic length L_c and the comoving correlation length ξ_c, which are related to the energies in (2.6), (3.59) by the following expressions

$$E = \frac{\mu_0 V}{a^2 L_c^2}$$

and

$$E_0 = \frac{\mu_0 V}{a^2 \xi_c^2} \,,$$

where V is the volume over which the averaging has been performed. In addition, we employ the VOS model approximation that the average radius of curvature of cosmic strings in the network is equal to the correlation length, i.e. $R_c \approx \xi_c$. Assuming further that the averaged macroscopic quantities can be split as $\left\langle \Phi \tilde{U} \tilde{T} \right\rangle = \langle \Phi \rangle \left\langle \tilde{U} \right\rangle \left\langle \tilde{T} \right\rangle$ we obtain the following system of equations

$$2 \dot{L}_c = \frac{\dot{a}}{a} L_c \left(v^2 \left(1 + W\right) - W + 1 \right) - \frac{\sqrt{1 - v^2} Q_{,s}}{\hat{U}}, \tag{3.62}$$

$$\begin{aligned}\dot{\upsilon}+\upsilon\frac{\dot{a}}{a}\left(1-\upsilon^2\right)(1+W)-(1-\upsilon^2)\frac{k(\upsilon)}{\xi_c}=\\ =2\frac{Q}{\hat{U}}\frac{1-\upsilon^2}{1-W}\left(\sqrt{1-\upsilon^2}\,\hat{T}_{,s}+\dot{Q}+2Q\left(\frac{\dot{a}}{a}-\frac{k(\upsilon)\upsilon}{\xi_c}\right)\right),\end{aligned} \tag{3.63}$$

where $\langle\Phi\rangle = Q$, $\left\langle\dot{\Phi}\right\rangle = \dot{Q}$, $\hat{U} = \left\langle\tilde{U}\right\rangle$, $\hat{T} = \left\langle\tilde{T}\right\rangle$, the correlation and characteristic lengths are related by $\xi_c = L_c\sqrt{\hat{U}}$ and a new derivative variable ${}_{,s} = \frac{\partial}{\partial s}$ has been introduced, corresponding to the parametrization $ds = \sqrt{\mathbf{x}'^2}d\sigma$.

Equations (3.62-3.63) are the averaged macroscopic equations describing a network of cosmic strings with a current. It is apparent that scaling solutions ($L_c = \epsilon_c\tau,\ \upsilon = \text{const}$ when $a \propto \tau^n$ with ϵ_c and n constants [88, 89]) exist if the averaged quantities $\hat{U}$, $\hat{T}$ and Q are appropriately restricted. In particular we see from (3.62)-(3.63) that scaling behaviour – typical for ordinary string networks – can arise when $\hat{U}, \hat{T}, Q = \text{const}$, while $T_{,s}$ and $Q_{,s} \sim 1/\tau$. Additionally, the requirement of a well-defined ϵ_c implies the condition

$$\upsilon^2 < \frac{2+n(W-1)}{n(W+1)}. \tag{3.64}$$

Equation (3.64) relates the rms string velocity υ to the ratio $W = \left\langle\tilde{T}/\tilde{U}\right\rangle$ for a given expansion rate (characterisd by n) for a cosmic string network with currents. These general relations will be useful when we consider the special case of a wiggly string network.

3.5 Wiggly model

In this section we consider in detail the particular form of the current for the case of wiggly cosmic strings. This model was developed as an effective description of small-scale structure on cosmic strings [110, 125, 126]. By applying a suitable phenomenological Lagrangian, the evolution of wiggly string networks was studied in [107, 142]. However, a great deal about the dynamics and scaling behaviour of the network can be understood by focusing on the equation of state for wiggly strings, without specifying the precise form of the Lagrangian.

The equation of state for wiggly strings is (3.13). We will use more convenient averaged variables that were defined above and form the following equation of state

$$\begin{aligned}\hat{U}\hat{T} &= 1\,,\\ \hat{U} = \mu,\ \ \hat{T} &= 1/\mu,\ \ Q = 0\,,\end{aligned} \tag{3.65}$$

where μ is a dimensionless parameter quantifying the amount of wiggles on the string, and $\mu = 1$ corresponds to the usual Nambu-Goto string.

Applying the equation of state (3.13) to the averaged equations of motion (3.62) and (3.63) we obtain

$$2\frac{dL_c}{d\tau} = \frac{\dot{a}}{a}L_c\left[1+\upsilon^2-\frac{1-\upsilon^2}{\mu^2}\right], \tag{3.66}$$

$$\frac{dv}{d\tau} = \left(1 - v^2\right)\left[\frac{k(v)}{L_c\mu^{5/2}} - \frac{\dot{a}}{a}v\left(1 + \frac{1}{\mu^2}\right)\right]. \tag{3.67}$$

Note that the comoving correlation length is connected to comoving characteristic length by the following relation $\xi_c = \sqrt{\mu}L_c$.

We can now include an energy loss term $F(v, \mu)$ on the right-hand side of equation (3.66) and assume scaling behaviour of the network $L_c = \epsilon\tau$ (while $\xi_c = \xi_0\tau$). Note that in this case the previously obtained constraint (3.64) has the form

$$v^2 < \frac{2/n - 1 + 1/\mu^2}{1 + 1/\mu^2}, \tag{3.68}$$

where, in the scaling regime, μ is a constant.

The expression (3.68) means that the rms string velocity has an upper limit, determined by the expansion rate n and amount of wiggles μ on the string; this is illustrated in figure 3.2.

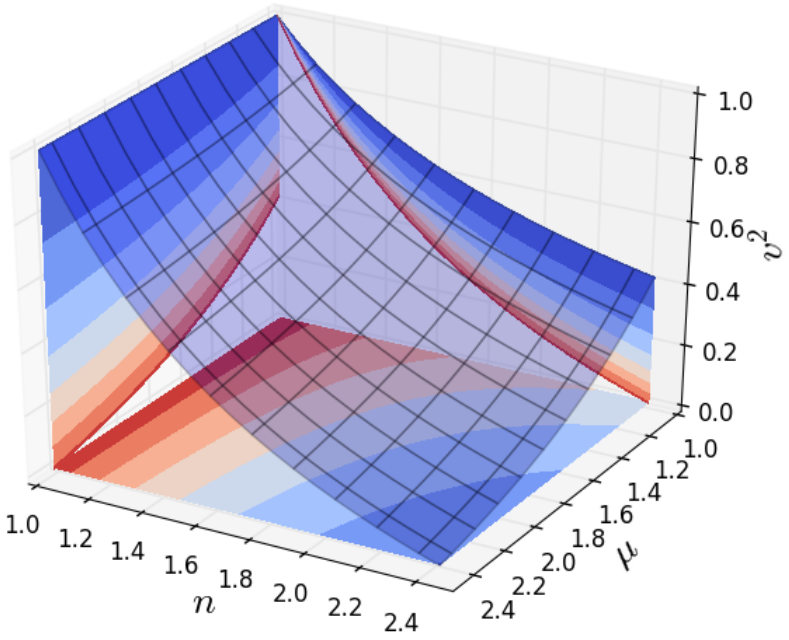

Fig. 3.2 The constraint (3.68) on the square of the rms velocity, v^2, depending on the expansion rate n and the amount of wiggles μ.

It is important to note that this restriction was obtained just by using the equation of state for wiggly cosmic strings (3.13) in our general equation (3.62). This means that any Lagrangian suitable for wiggly string description (i.e. any choice of $f(\kappa, \Delta/\gamma)$ satisfying (3.13) for the equation of state) cannot change this relation. Moreover, it is valid for any energy loss function $F(v, \mu)$. Thus, any wiggly cosmic string network with any energy loss function of the form $F(v, \mu)$ must satisfy the constraint (3.68).

To get a feeling for the size of the maximum network velocity in (3.68) we consider two limiting cases: strings without wiggles ($\mu = 1$) and highly wiggly strings ($\mu \to \infty$):

$$v^2 < 1/n \qquad (\mu = 1), \tag{3.69}$$

$$v^2 < 2/n - 1 \qquad (\mu \to \infty). \tag{3.70}$$

As seen from (3.69), for strings without wiggles only very fast expansion rates n can cause a significant restriction to the string network velocity, while for highly wiggled strings the limit (3.70) provides a severe constraint even when $n = 2$ (matter domination era). For wiggly strings with $\mu = 1.5$ in the matter domination era ($n = 2$) the velocity is limited as $v^2 < 0.3$, which is close to the values of rms velocities from field theory simulations [116] in the matter domination era.

Let us now study the full description of the wiggly cosmic string network model [107, 142] described by the action (3.12). The derivation of the averaged equations of motion for this model can be found in [107, 142]. We will use the final system of equations in the following form (where we have omitted the term responsible for scale dependence)

$$2\frac{dL_c}{d\tau} = \frac{\dot{a}}{a}L_c\left[1 + v^2 - \frac{1-v^2}{\mu^2}\right] + \frac{cf_a v}{\sqrt{\mu}}, \tag{3.71}$$

$$\frac{dv}{d\tau} = \left(1 - v^2\right)\left[\frac{k}{L_c\mu^{5/2}} - \frac{\dot{a}}{a}v\left(1 + \frac{1}{\mu^2}\right)\right], \tag{3.72}$$

$$\begin{aligned}\frac{1}{\mu}\frac{d\mu}{d\tau} = \frac{v}{L\sqrt{\mu}}\left[k\left(1 - \frac{1}{\mu^2}\right) - c(f_a - f_o - S)\right] - \\ - \frac{\dot{a}}{a}\left(1 - \frac{1}{\mu^2}\right),\end{aligned} \tag{3.73}$$

where the three functions $f_a(\mu)$, $f_0(\mu)$ and $S(\mu)$ quantify energy loss/transfer:

$$2\left(\frac{d\xi}{dt}\right)_{\text{only big loops}} = cf_0(\mu)v, \tag{3.74}$$

$$2\left(\frac{dL}{dt}\right)_{\text{all loops}} = cf_a(\mu)\frac{vL}{\xi}, \tag{3.75}$$

$$2\left(\frac{d\xi}{dt}\right)_{\text{energy transfer}} = cS(\mu)v\,. \tag{3.76}$$

Let's notice that in (3.74-3.76) $\xi = \xi_c a$, $L = L_c a$ are the physical (rather than comoving) lengthscales corresponding to ξ_c and L_c.

The term $f_0(\mu)$ accounts for the energy loss due to the formation of big loops. Here, "big" means that they are formed by intersections of strings separated by distances of order the correlation length ξ or by self-intersections at the scale of the radius of curvature $R \approx \xi$.

The function $f_a(\mu)$ describes the energy loss caused by all types of loops, and the difference $f_a(\mu) - f_0(\mu)$ corresponds to the energy loss by small loops only, which is driven by the presence of wiggles.

In order to reproduce correctly the original model without wiggles, we can use the energy loss/transfer functions as discussed in [142]

$$f_0(\mu) = 1, \tag{3.77}$$

$$f_a(\mu) = 1 + \eta\left(1 - \frac{1}{\sqrt{\mu}}\right), \tag{3.78}$$

$$S(\mu) = D(1 - \frac{1}{\mu^2}), \tag{3.79}$$

where D and η are constants.

Thus, the evolution of a wiggly string network is described by the system of ordinary differential equations (3.71)-(3.73), which, in view of equations (3.77)-(3.79) includes three free constant parameters c, D and η [142]:

• c is the “loop chopping efficiency" parameter quantifying how much energy the network loses due to the production of ordinary loops;

• η is a parameter describing the energy loss enhancement due to the creation of small loops caused by the presence of wiggles;

• D is a parameter quantifying the amount of energy transferred from large to small scales.

By making different choices of parameters c, η and D we can explore the effects of the energy loss/transfer mechanisms described above on the evolution of the string network. Note that c has been measured in Abelian-Higgs and Goto-Nambu simulations to be $c = 0.23 \pm 0.04$ [98, 144], but there are no such measurements for the other two parameters. We have chosen to vary parameter D, keeping η fixed, which allows us to cover a wide range of μ values. Fixing D and increasing η is equivalent to decreasing the amount of wiggles and an effective change of c, which is already covered from our variation of D with fixed η. Let us solve equations for the network evolution numerically and see how these phenomenological quantities change the evolution of the string network. In the figure 3.3 we present the solution of differential equations (3.71-3.73) for the "real" universe, whose evolution is defined by equation (1.10). Equations are numerically solved in the modified CMBact code [143], since we will use these results to study the CMB anisotropies in the section 5.2.

It is important to note that in order to have an attractor scaling solution when $a \propto \tau^n$ the following condition must be satisfied

$$\eta > \frac{D\left(1 - 1/\mu^2\right)}{1 - 1/\sqrt{\mu}}. \tag{3.80}$$

Physically, this means that in order to achieve a scaling solution, small scale structure should be able to lose energy (controlled by parameter η) faster than it receives the energy

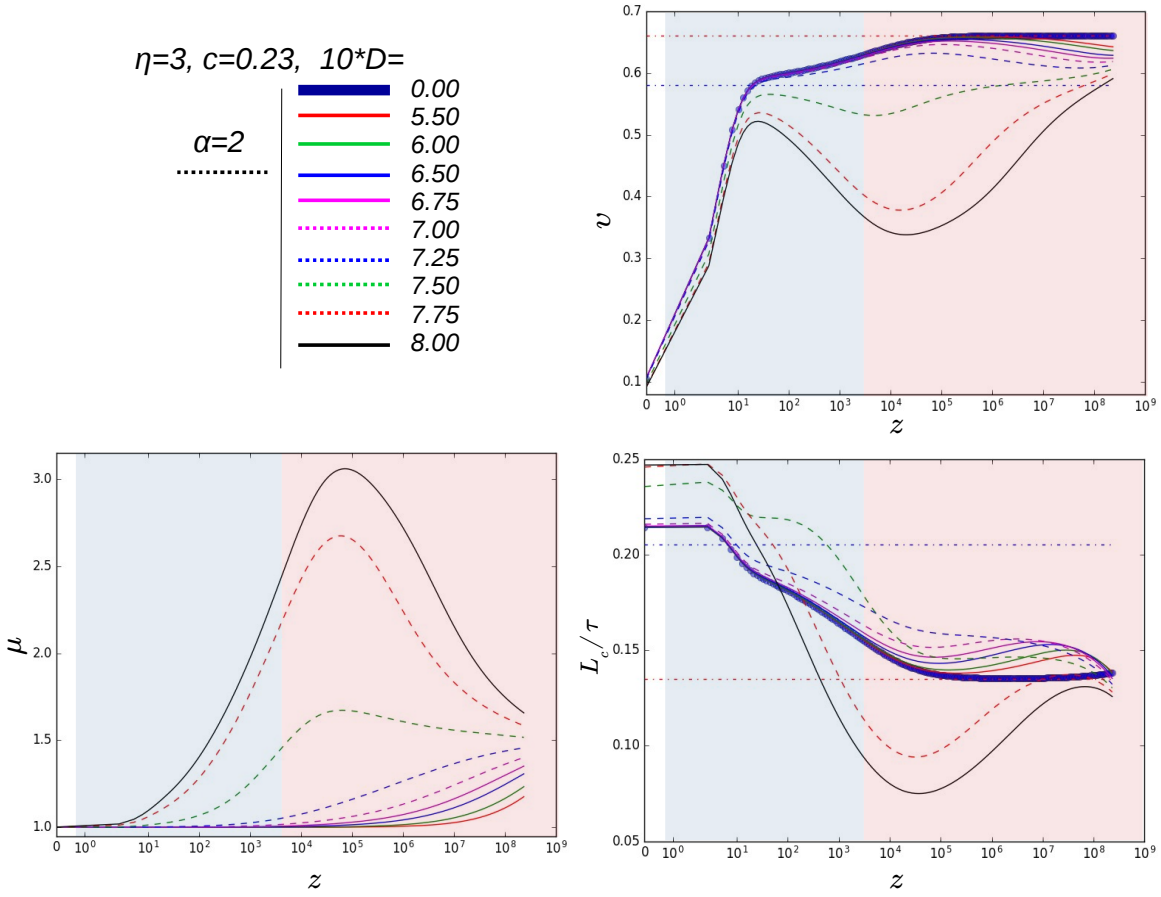

Fig. 3.3 Evolution of the rms velocity υ, comoving characteristic length L_c and amount of wiggles μ as a function of redshift z for wiggly cosmic string networks with different values of the parameter D, obtained by a modified version of the CMBact code [143]. The horizontal dashed red and blue lines correspond to the usual (without wiggles; $\mu = 1$) scaling regimes for radiation (red shaded area) and matter domination (blue shaded area) epochs respectively. Note that the horizontal (redshift) axis is depicted in a linear scale in the redshift range $0 < z < 1$ and in a logarithmic scale for $z > 1$.

from large scales (controlled by parameter D). When the condition (3.80) is violated, energy accumulates at small scales and there is no stable scaling regime for these wiggly cosmic strings. In practice, the condition (3.80) is used as a guide for estimating the range of variation of D. The situation when the scaling solution is not an attractor implies limitations to possible values of υ, μ and ϵ (details in the next section 3.5.1).

3.5.1 Scaling solutions and their stability for wiggly string networks

As we discussed above, the system of differential equations (3.71-3.73) has a scaling solution in the form: $L = \epsilon\tau$, υ, μ, $\epsilon = \text{const}$. The presence of this solution doesn't mean that it is an attractor (a similar question was raised and studied in the paper [142]). Let's show that it is the case for some combinations of υ, μ, ϵ. It means that these asymptotic values cannot be reached by the wiggly string network, described by equations (3.71-3.73), at all.

Let's define some additional functions for convenience $f_2(\mu) = c(f_0(\mu) + s(\mu))$, $f_1(\mu) = f_a(\mu)$. Thus, we can rewrite the system of differential equations for the scaling variables

$$\begin{aligned}
\dot{\epsilon}\tau &= \frac{1}{2}\left(n\epsilon\left[1+\upsilon^2-\frac{1-\upsilon^2}{\mu^2}\right]+\frac{\upsilon c f_1(\mu)}{\sqrt{\mu}}\right)-\epsilon = F_1(\upsilon,\epsilon,\mu),\\
\dot{\upsilon}\tau &= \left(1-\upsilon^2\right)\left[\frac{k}{\epsilon\mu^{5/2}}-n\upsilon\left(1+\frac{1}{\mu^2}\right)\right] = F_2(\upsilon,\epsilon,\mu),\\
\dot{\mu}\tau &= \mu\left[\left(\frac{\upsilon k}{\epsilon\sqrt{\mu}}-n\right)\left(1-\frac{1}{\mu^2}\right)-\frac{\upsilon}{\epsilon\sqrt{\mu}}\left(cf_1(\mu)-sf_2(\mu)\right)\right] = F_3(\upsilon,\epsilon,\mu),
\end{aligned} \tag{3.81}$$

where we introduced the functions $F_1(\upsilon,\epsilon,\mu)$, $F_2(\upsilon,\epsilon,\mu)$, $F_3(\upsilon,\epsilon,\mu)$.

The system of equations (3.81) has scaling solutions when the phenomenological parameters are related to the asymptotic scaling values by the following expressions

$$\begin{aligned}
c &= f_1(\mu)^{-1}\sqrt{\mu}\frac{\epsilon}{\upsilon}\left(2-n\left[1+\upsilon^2-\frac{1-\upsilon^2}{\mu^2}\right]\right),\\
k &= \epsilon\mu^{5/2}n\upsilon\left(1+\frac{1}{\mu^2}\right),\\
s &= \left(cf_1(\mu)+\left(\frac{n\epsilon\sqrt{\mu}}{\upsilon}-k\right)\left(1-\frac{1}{\mu^2}\right)\right)f_2(\mu)^{-1}.
\end{aligned} \tag{3.82}$$

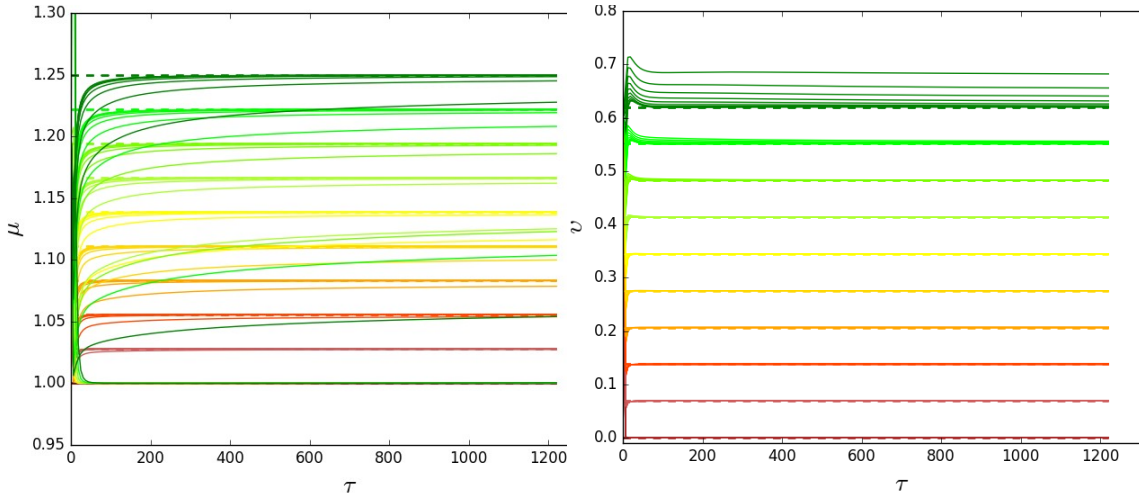

Fig. 3.4 Scaling solutions for wiggly string networks with different values of υ and μ, when $n = 2$. The same color corresponds to the same value of υ^* (left panel) and ten different values of μ^* are chosen to fix c, s and k. Similarly for the right panel: different colors correspond to different values of μ^* and the same color for ten different values of υ^*. Dashed lines correspond to υ^*, μ^* and solid lines represent solutions of differential equations (3.81). The value of ϵ^* is the same everywhere, since it almost doesn't affect convergence to the scaling regime.

We have scaling solutions for the system of differential equations (3.81), but we do not know if the system tends to them. Let's study the stability of these solutions. We chose some

values (physically allowed) of velocity (υ^*), correlation length over time (ϵ^*) and amount of wiggles (μ^*). This choice fixes constants c, s and k, as functions of υ^*, ϵ^* and μ^* by relations (3.82).

Let's test straightforwardly if it is always possible to reach the scaling solution. To do so, we can evolve the differential equations (3.81) for the set of initial conditions, which are meaningful (we avoid trivial and unphysical initial conditions, as an example when the velocity $\upsilon_0 = 1$). The numerical result of wiggly string network evolution is presented in the figure 3.4. This shows whether the system approaches the scaling solution for range of υ^*, ϵ^* and μ^* values. In particular, for big μ^* and big υ^* the system stops approaching the scaling solution and eventually deviates from it. It is a clear signal that the scaling solution is not an attractor for such μ^* and υ^*. It means that the system of differential equations (3.81) cannot reproduce such values of velocity and wiggles.

It is possible to check the stability of scaling solutions in more details. For that we consider linear perturbations around an exact scaling solution. Let's define $\mathbf{Y} = (\epsilon, \upsilon, \mu)$ and $\mathbf{F} = (F_1(\upsilon, \epsilon, \mu), F_2(\upsilon, \epsilon, \mu), F_3(\upsilon, \epsilon, \mu))$. In this way, the equations (3.81) can be rewritten as

$$\dot{\mathbf{Y}}\tau = \mathbf{F(Y)}. \tag{3.83}$$

Considering perturbations around the scaling solution we obtain

$$\dot{\mathbf{Y}}\tau = \mathbf{F}(\mathbf{Y}^*) + \left.\frac{\partial F(\mathbf{Y})}{\partial \mathbf{Y}}\right|_{\mathbf{Y}=\mathbf{Y}^*} (\mathbf{Y} - \mathbf{Y}^*) + O\left((\mathbf{Y} - \mathbf{Y}^*)^2\right), \tag{3.84}$$

where $\mathbf{Y}^* = (\upsilon^*, \epsilon^*, \mu^*)$ - scaling solutions and $O\left((\mathbf{Y} - \mathbf{Y}^*)^2\right)$ defines higher order terms.

We can denote $(\mathbf{Y} - \mathbf{Y}^*) = \delta\mathbf{Y}$ in that case $\delta\dot{\mathbf{Y}} = \dot{\mathbf{Y}}$ and

$$\delta\dot{\mathbf{Y}}\tau = J^*\delta\mathbf{Y}, \tag{3.85}$$

where J^* is a Jacobian matrix evaluated at the point $\mathbf{Y} = \mathbf{Y}^*$.

The solution of equations (3.85) can be written as $\mathbf{Y} \propto t^{\lambda_i}$, where λ_i are eigenvalues of the J^*. In order to achieve the convergence to scaling solutions, the real part of λ_i should be negative. In this case perturbations around the scaling solution decays as a power function.

Let's study eigenvalues of the Jacobian matrix J^* at the point of exact solution. We can do it by searching for the smallest eigenvalue, which is plotted in figure 3.5.

As a result, in order to have the system of differential equations that can reproduce values of the string network with some specific velocity, wiggliness and correlation length over time, we need to require "good" behaviour. This means that the scaling solution should be an attractor. As it is seen in figure 3.5, a different choice of loss/transfer functions leads to different properties of the scaling solution stability. This additional condition can be useful for phenomenological choice of energy loss/transfer functions (3.77 - 3.79).

To end this section, let us return to the wiggly model but this time without referring to the specific Lagrangian, only to equation of state (3.13). We wish to study the scaling regime for wiggly strings but leaving the amount of wiggles μ as a free parameter that we can tune. Instead of varying parameter D, we can vary μ. This approach does not require an

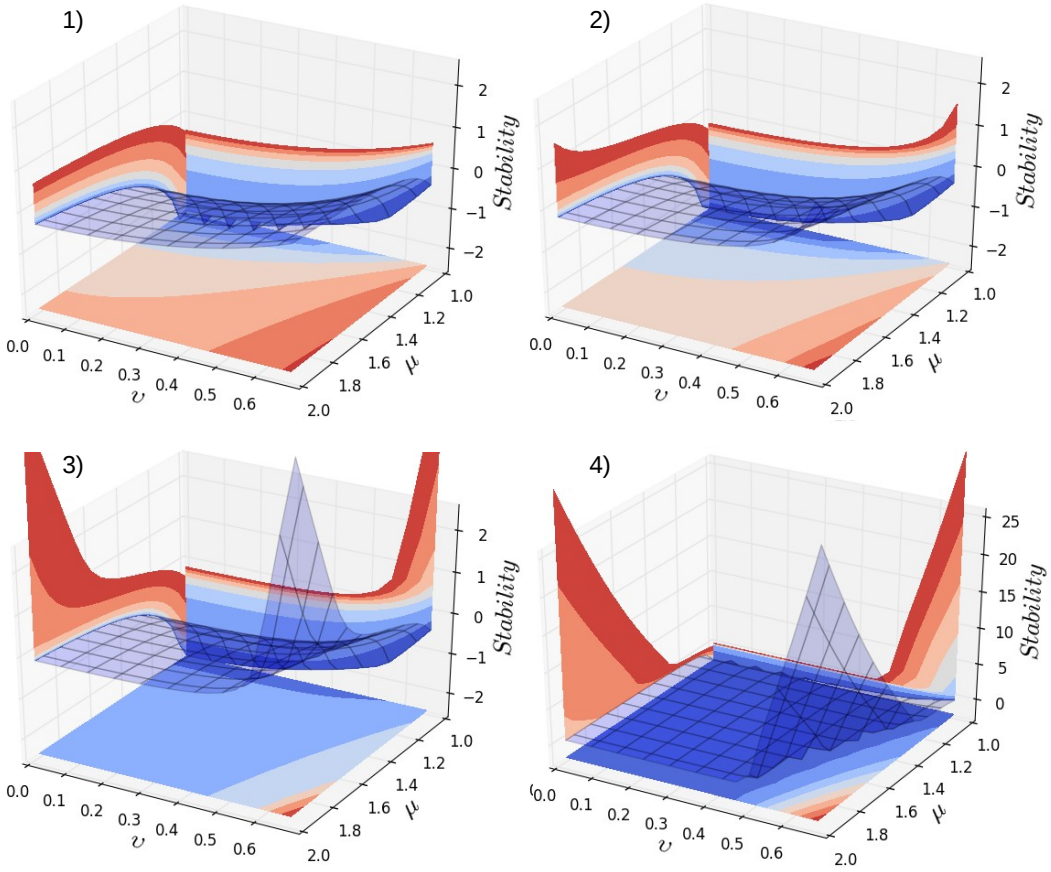

Fig. 3.5 In the plot you can see how the smallest eigenvalue (called "Stability" axis) depends on velocity v and wiggles μ, when $n = 2$. As long as the "stability" value is negative (blue color), the scaling solution is an attractor. The first plot represents result for functions $f_1(\mu) = f_2(\mu) = 1$, the second: $f_1(\mu) = f_2(\mu) = \frac{1}{1+\mu^2}$, the third: $f_1(\mu) = f_2(\mu) = \frac{1}{1+\mu^4}$, the forth: $f_1(\mu) = f_2(\mu) = \frac{1}{1+\mu^{20}}$.

assumption on the energy transfer function (3.79); we only need to define how energy loss depends on the amount of wiggles (3.78). Let us now estimate how the rms velocity v and comoving characteristic length over time ϵ are related to the parameters c, η and μ in the scaling regime. We insert the scaling solution $L_c = \epsilon\tau$, v =const to equations (3.71), (3.72) to obtain algebraic equations

$$\begin{aligned} \epsilon\left(2 - n\left[1 + v^2 - \frac{1-v^2}{\mu^2}\right]\right) &= \frac{c f_a(\mu) v}{\sqrt{\mu}}, \\ \frac{k(v)}{\epsilon\mu^{5/2}} &= nv\left(1 + \frac{1}{\mu^2}\right), \end{aligned} \tag{3.86}$$

where we have included energy loss function $f_a(\mu)$ defined by (3.78).

Despite the reduction of the equations of motion to algebraic equations (3.86) in the scaling regime, it is still not possible to solve them analytically, mainly due to the complicated form of the momentum parameter (2.9). To study how the amount of wiggles affects the

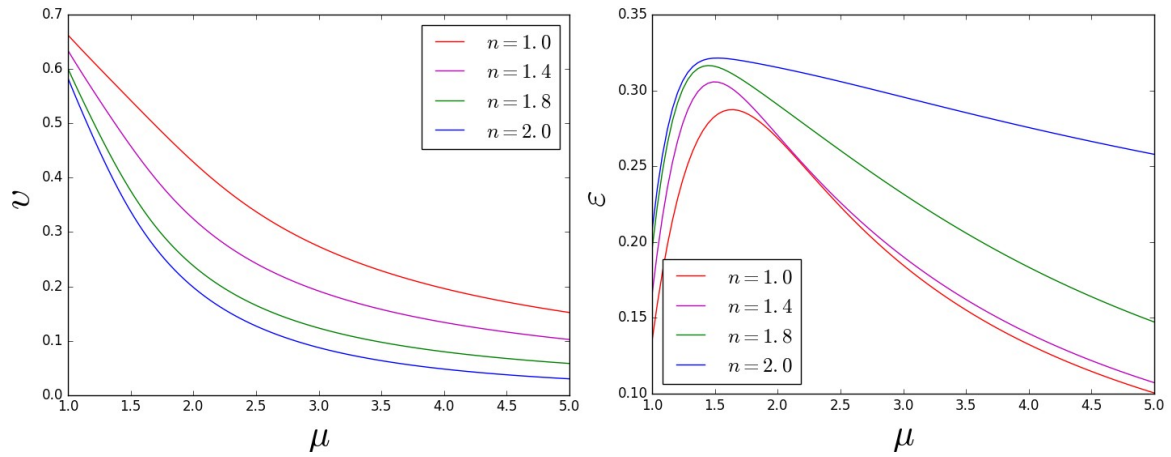

Fig. 3.6 Dependence of the scaling values of the rms velocity, v, and the comoving correlation length divided by conformal time, ϵ, on the amount of wiggles μ for different expansion rates n.

macroscopic parameters v (rms string velocities) and ϵ (comoving correlation length in units of conformal time) in the scaling regime we solve the system (3.86) numerically for different expansion rates n. The results are shown in figure 3.6. It is seen that the rms velocity v, as anticipated from the restriction (3.68), decreases with the growth of the amount of wiggles μ. This is also in agreement with our results for the rms velocity evolution (see figure 3.3) in the dynamical wiggly model for a realistic expansion history. The situation for ε is more interesting. The correlation length does not increase monotonically with the amount of wiggles but has a maximum around $\mu = 1.5 - 1.9$. This is also in agreement to our full treatment in figure 3.3 where we modelled string wiggles by varying parameter D and took a realistic expansion history.

3.6 Superconducting model (chiral case)

Another special case of current-carrying cosmic strings of notable physical interest is the case of superconducting cosmic strings. This type of strings has been studied thoroughly in the framework of field theory [45, 49, 50, 136, 137, 145, 146]. In all these cases the energy-momentum tensor on the string worldsheet has the following form:

$$T^a_b = \begin{pmatrix} A+B & -C \\ C & A-B \end{pmatrix} . \tag{3.87}$$

where A arises from the field responsible for the string core formation, while B and C represent additional contributions due to coupling with external fields (dynamics of currents). The energy-momentum tensor (3.87) is written for the worldsheet metric $\eta^{ab} = \begin{pmatrix} 1 & 0 \\ 0 & -1 \end{pmatrix}$ on a $3+1$-dimensional Minskowski spacetime background with $\varepsilon = 1$.

Consider now the two-dimensional energy-momentum tensor for the action (3.17), which reads

$$T_b^a = \begin{pmatrix} \mu_0\tilde{U} & -\mu_0\frac{\Phi}{\varepsilon} \\ \mu_0\varepsilon\Phi & \mu_0\tilde{T} \end{pmatrix}. \tag{3.88}$$

There is an obvious correspondence between the energy-momentum tensors (3.87) and (3.88); they are in agreement if we demand the chiral condition [106, 109]

$$\kappa \to 0\,, \tag{3.89}$$

which also means

$$\Delta \to 0\,; \tag{3.90}$$

here κ and Δ are defined by (3.16). These imply that $\tilde{U} = 1 + \Phi$, $\tilde{T} = 1 - \Phi$. In Minkowski space ($\epsilon = 1$) we see that $A = \mu_0$, $B = \mu_0\Phi$ and $C = \mu_0\Phi$, so we have the condition $B = C$. In order to avoid this situation and be able to reproduce a energy-momentum tensor of the form (3.87) within the Nambu-Goto approximation, we need to use at least two scalar fields. It has already been demonstrated that adding any number of additional fields (3.25) together with the definitions (3.26)-(3.28) keeps the evolution equations (3.22)-(3.23) unchanged, replacing the scalar field equation (3.24) by the set of equations (3.29). In effect, introducing additional fields makes C and B different in Minkowski space.

Indeed, when we add extra scalar fields we obtain a energy-momentum tensor in the form of (3.87) with the correspondence[4] $A = \mu_0$, $B = 2\mu_0\gamma^{00}\left(\frac{\partial f}{\partial\kappa} - \frac{\partial f}{\partial\Delta}\right)\sum_i \dot{\varphi_i}^2 = \mu_0\Psi$ and $C = \mu_0\Phi$, where Φ is given by equation (3.28) and we have assumed a Minkowski background. These correspond to

$$\hat{U} = 1 + \langle\Psi\rangle\,,\ \hat{T} = 1 - \langle\Psi\rangle\,,\ \ Q = \langle\Phi\rangle\,. \tag{3.91}$$

Thus, this multiple worldsheet field approach provides enough flexibility to reproduce the field-theoretical energy-momentum tensor variables in (3.87) within the Nambu-Goto approximation.

Let us now consider the equations of motion for chiral currents. We will apply our averaging procedure to the system of equations (3.29) for the currents, similarly to what we already did for first two equations (3.62) and (3.63) for the correlation length and string velocity. First of all, we note that in order to have the appropriate Nambu-Goto limit for the action (3.17) when $\varphi = 0$ we need to have $f(\kappa,\Delta) \xrightarrow[\kappa\to 0]{} 1$ and additionally $\frac{\partial f(\kappa,\Delta)}{\partial\kappa} \xrightarrow[\kappa\to 0]{}$ const (as well as $\frac{\partial f(\kappa,\Delta)}{\partial\Delta} \xrightarrow[\Delta\to 0]{}$ const). These conditions allow us to make simplifications, similar to what was done in reference [109], and consider the case of conserved microscopic charges for each field

$$\varepsilon\dot{\varphi}_i = \phi_i = \text{const}\,, \tag{3.92}$$

$$\varphi_i' = \psi_i = \text{const}\,, \tag{3.93}$$

[4]Here we used an assumption that all multipliers $\frac{\partial f}{\partial\Delta_i}$ are equal as well as all $\frac{\partial f}{\partial\kappa_i}$ are equal (3.89).

which leads to the additional condition $\epsilon' = 0$. Furthermore, in this case we can define Ψ and Φ as

$$\Psi = \left(\frac{\partial f}{\partial \kappa} + \frac{\partial f}{\partial \Delta}\right) \sum_i \frac{\phi_i^2}{a^2 \mathbf{x}'^2}, \tag{3.94}$$

$$\Phi = \left(\frac{\partial f}{\partial \kappa} + \frac{\partial f}{\partial \Delta}\right) \sum_i \frac{\phi_i \psi_i}{a^2 \mathbf{x}'^2}, \tag{3.95}$$

and (3.89) gives us

$$\sum_i \phi_i^2 = \sum_i \psi_i^2. \tag{3.96}$$

Expressions (3.94) and (3.95) tell us that if we use the condition of conserved microscopic charges (3.92)-(3.93) we have two variables Ψ and Φ which evolve in the same way and differ only by a multiplicative constant β:

$$\Psi\beta = \Phi, \tag{3.97}$$

where $\beta = \frac{\sum_i \phi_i \psi_i}{\sum_i \phi_i^2}$. Together with (3.96), this implies that $0 < \beta < 1$.

By direct differentiation of equation (3.94) we obtain the following evolution equations for the field Ψ (clearly, the same equations are also obeyed by Φ)

$$\dot{\Psi} + 2\frac{\dot{a}}{a}\Psi = 2\Psi \frac{\dot{\mathbf{x}} \cdot \mathbf{x}''}{\mathbf{x}'^2}, \tag{3.98}$$

$$\Psi' + 2\Psi \frac{\mathbf{x}' \cdot \mathbf{x}''}{\mathbf{x}'^2} = 0. \tag{3.99}$$

Following the approach of [109], we average the equations of motion (3.98), (3.99) and substitute the equation of state (3.91) into equations (3.62) and (3.63). This leads to the VOS model for superconducting chiral strings, taking into account energy and charge losses (for details on these loss terms see [109])

$$\frac{dL_c}{d\tau} = \frac{\dot{a}}{a} L_c \frac{v^2 + Q}{1 + Q} + v\left(\frac{Qs\beta}{(1+Q)^{3/2}} + \frac{c}{2}\right), \tag{3.100}$$

$$\frac{dv}{d\tau} = \frac{1 - v^2}{1 + Q}\left[\frac{k(v)}{L_c\sqrt{1+Q}}\left(1 - Q(1 + \frac{2s\beta}{k(v)})\right) - 2\frac{\dot{a}}{a}v\right], \tag{3.101}$$

$$\frac{dQ}{d\tau} = 2Q\left(\frac{k(v)v}{L_c\sqrt{1+Q}} - \frac{\dot{a}}{a}\right) + \frac{cv\left(1 - \sqrt{1+Q}\right)}{L_c}\sqrt{1+Q}\,. \tag{3.102}$$

We have used the assumption $\left\langle \frac{\Psi'}{\varepsilon(1+\Psi)} \right\rangle = -s\frac{v}{R_c}\frac{2Q}{1+Q}$ [109] and the fact that the correlation and characteristic lengths are related by $\xi_c = L_c\sqrt{1+Q}$.

Therefore, our general analysis of chiral current dependence in the action (3.17) including the addition of extra worldsheet fields has not introduced significant changes in the macroscopic equations describing superconducting chiral cosmic string networks, as compared to the results in [109] (the only difference is that the constant s has now been changed to βs). Note also

that the final result does not depend explicitly on the precise form of the Lagrangian; the important physics can be encoded in the equations of state of the strings, in agreement with our previous discussion.

The evolution of string networks described by equations (3.100)-(3.102) was carefully studied in [109]. It was shown that these networks have generalized scaling solutions[5] only if the following relation is satisfied

$$n = \frac{2k(\upsilon) - c\tilde{W}}{c + k(\upsilon)}, \tag{3.103}$$

where $\tilde{W} = \frac{\sqrt{1+Q_s}-1}{1+Q_s^{-1}}$, with Q_s a constant corresponding to the scaling value of the function Q. As we can see from equation (3.103), the expansion rate n for scaling solutions (with constant charge) cannot be larger than $n \leq 2$. The maximal value of n is reached when $c = 0$, while for $c = 0.23$ (which we use here) we have the condition $n \lesssim 1.6$ for scaling behaviour. For expansion rates n larger than the right hand side of (3.103) the charge Q on the string decays.

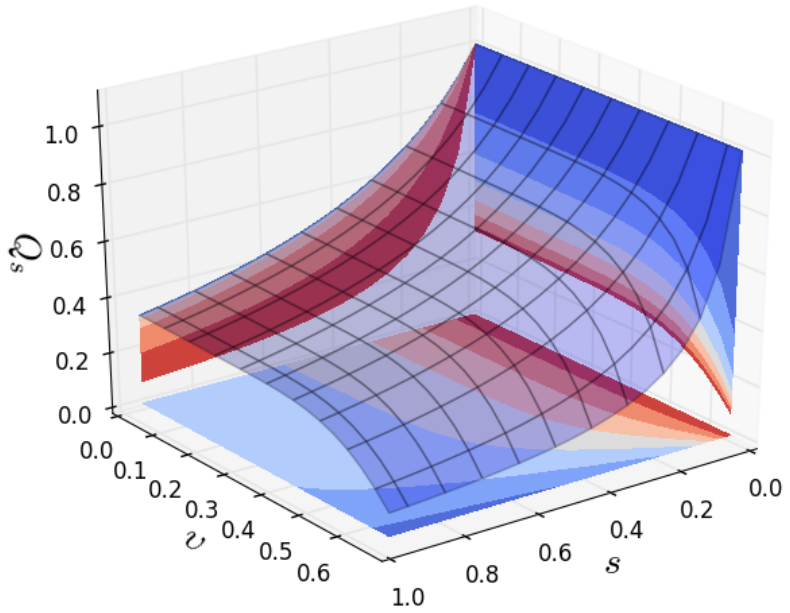

Fig. 3.7 Constraints on the possible values of the charge Q_s depending on the rms velocity υ and parameter s.

It is worth noting that at the same time the asymptotic value of the charge Q_s is limited from equation (3.101) to satisfy the following (see figure 3.7)

$$Q_s < \frac{k(\upsilon)}{2s\beta + k(\upsilon)}. \tag{3.104}$$

[5] In this context, by "generalized scaling solutions" we mean that all three quantities L_c/τ, υ and Q approach constant non-zero values (and so the strings have non-zero charge). For larger expansion rates there are also solutions with a decaying charge Q for which L_c/τ and υ are (non-zero) constants but Q approaches zero in a power-law fashion [109]. These correspond to the standard linear scaling solutions of (uncharged) Nambu-Goto strings and we do not discuss them here in detail.

For all other expansion rates that do not satisfy conditions (3.103) and (3.104), there is no scaling regime with nonzero Q. To see the evolution of the string network, we can vary Q_0 for differential equations (3.100-3.102). The result of superconducting string network evolution is presented in figure 3.8.

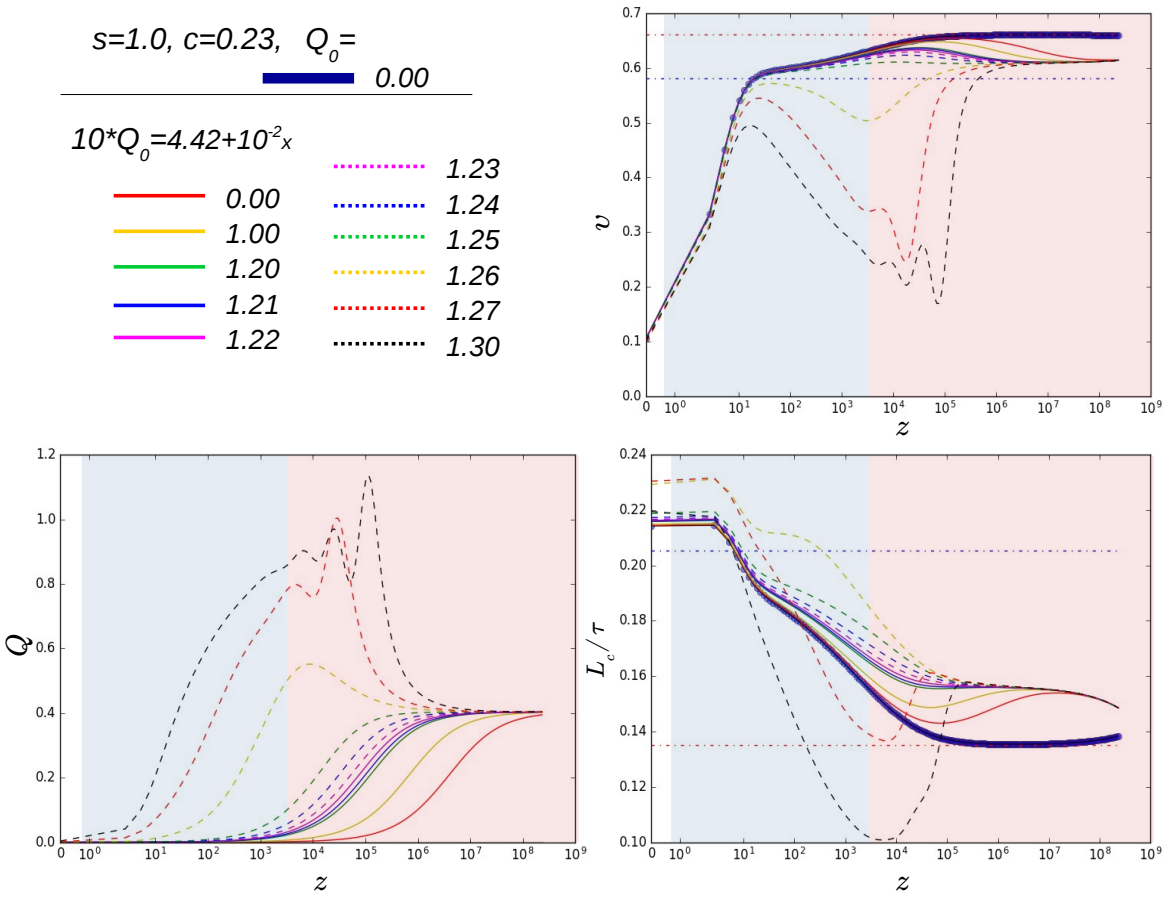

Fig. 3.8 Evolution of the rms velocity v, comoving characteristic length L_c and charge Q depending on redshift z for superconducting (chiral) cosmic string networks with different initial conditions Q_0 for the string charge, obtained by a modified version of the CMBact code [143]. The horizontal dashed red and blue lines correspond to the usual (without charge, $Q = 0$) scaling regimes for radiation (red shaded area) and matter domination (blue shaded area) eras respectively. Note that the horizontal (redshift) axis is depicted in a linear scale in the redshift range $0 < z < 1$ and in a logarithmic scale for $z > 1$.

Let us consider the network at specific values n satisfying equations (3.103), (3.104). For that we will use the typical scaling ansatz $L_c = \epsilon\tau$ with constant ϵ, v and Q in equations (3.100)-(3.101)

$$\begin{aligned} \epsilon &= n\epsilon\frac{v^2+Q}{1+Q} + v\left(\frac{Qs\alpha}{(1+Q)^{3/2}} + \frac{c}{2}\right), \\ \frac{k(v)}{\epsilon\sqrt{1+Q}}&\left[1 - Q\left(1 + \frac{2s\alpha}{k(v)}\right)\right] = 2nv. \end{aligned} \tag{3.105}$$

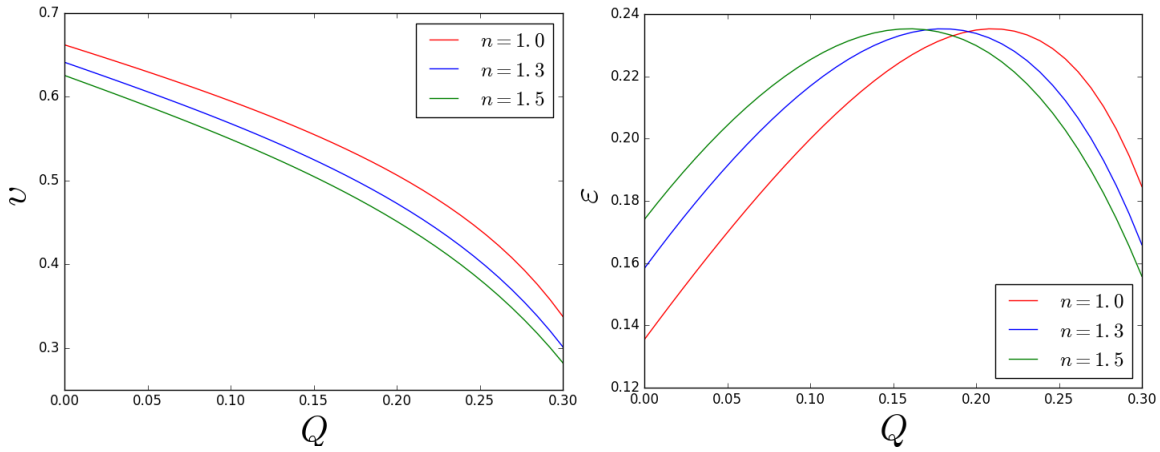

Fig. 3.9 Scaling values of rms velocity, v, and comoving correlation length divided by conformal time, ϵ, depending on the charge Q, for different expansion rates n.

The equations (3.105) describe the network evolution in the scaling regime (they will be valid only in a range of n satisfying (3.103)). We can solve these algebraic equations numerically for different values of Q. The result for ϵ and v dependence on a charge Q is shown in figure 3.9. These solutions show the connection between macroscopic parameters of a superconducting string network. It is evident that the connection for the scaling regime does not depend the dynamics of the charge Q.

3.7 Summary

In this chapter we considered strings with non-trivial structure on their worldsheets. In particular, we studied the action (3.17) describing strings with an arbitrary dependence on worldsheet currents. We obtained the set of microscopic equations for these strings (3.22), (3.34) without specifying the form of the current. Then we described how to average these equations of motion to obtain macroscopic evolution equations (without energy loss) for the string network (3.62)-(3.63). These describe the time evolution of the rms string velocity v and characteristic length L, and depend only on three parameters $\hat{U}$, $\hat{T}$ and Q defining the string equation of state. These same parameters, together with the network quantities L and v, appear directly in the string energy-momentum tensor (3.18).

We considered the case of a string with the chiral current, described by an arbitrary function in (3.17), in Minkowski space. We found the general solution for these strings, which is defined by equations (3.45), (3.52) with conditions (3.58).

For wiggly string networks we studied the specific case when the parameter κ in (3.16) only carries a time dependence, $\kappa = \kappa(\tau)$. We studied network dynamics using an effective action for wiggly cosmic strings, and introduced the averaged macroscopic equations. We evolved the macroscopic equations of wiggly string network for the "realistic" expansion scenario. Additionally, we studied the scaling regime when $a \propto t^{\lambda}$ for wiggly string network and tested the stability of these solutions.

The other type of strings that were scrutinized in this work are superconducting cosmic strings. It was shown that if we use the microscopic charge conservation (3.92) and the chiral condition ($\kappa, \Delta \to 0$, which appears in field theory studies of cosmic strings), we can obtain the averaged equations of motion (3.100)-(3.102) without specifying the precise dependence on string currents $f(\kappa_i, \Delta_i/\gamma)$ in the action (3.17). This implies that the debate on the correct form of the Lagrangian for superconducting strings [140] – while important from a fundamental physics point of view – does not have a crucial impact on phenomenological descriptions based on averaging the microscopic dynamics. By comparison to the work of [109], we notice that the introduction of additional currents for superconducting strings only led to the change $s \to \beta s$ in the macroscopic VOS model. We also evolved the superconducting string network for the "realistic" expansion and studied when the scaling solution is possible.

Chapter 4

Cosmic superstring networks

As we have seen so far, cosmic strings in general can have rather complicated properties. It is anticipated that these features bring important changes to the network evolution and should be taken into account accurately. Cosmic non-Abelian strings (see section 1.4.3) and superstrings (see section 1.7) give rise to entangled strings and junctions respectively. Such multi-tension cosmic string networks are very time-consuming for numerical simulations, and cannot be reproduced with both high-resolution and sufficiently large dynamic range. Furthermore, the superstring network evolution can be reproduced only effectively, not all properties of cosmic superstring networks can be grasped by the field theory [147–150]. As a result, due to computational limits of numerical simulations, we suggest to approach this problem by a semi-analytic method – a generalized VOS model.

In this chapter we review some important issues on cosmic strings interactions. In particular, we revisit the quantum treatment of string interactions [151–154] and kinematic constraints on junction production [85, 155–158]. We demonstrate the possible generalization of the kinematic conditions for the case of FLRW metric [159]. This generalization is probed by a straight string collision example for the FLRW background, which provides an "angle-velocity" diagram of the junction production (similar to what was done for Minkowski space in [155]).

Additionally we study the dynamics of connected strings with currents. In section 4.1.2 we discuss the influence of the presence of currents on junction dynamics. We also obtain the "angle-velocity" diagrams for collision of identical strings with currents.

To understand the evolution of junctions in the string network we review the small-scale structure description [160, 161]. This model of small-scale structure provides us with a useful tool to understand how much junctions can grow on average in a cosmic superstring network. Eventually, the introduced average growth/reduction of length at string junctions leads to a generalization of the VOS model for the case of a superstring network evolution with dynamical junctions.

4.1 Strings collisions

In section 1.7 we saw that fundamental strings (F-strings) can form a bound state with $D1$ branes (D-strings). We wish to study conditions for, and consequences of, the formation of these bound states in more detail. To do so, we start from the consideration of string collisions in Minkowski space.

4.1.1 Probability of string interactions in Minkowski space

Due to the quantum nature of F-strings, a proper treatment of their interactions should be studied in the framework of string theory. Some relevant questions of quantum strings can be grasped by the method of vertex operators in string perturbation theory [153, 154, 162]. In particular, this method allows to obtain intercommutation and reconnection probabilities, string decay rates and emission of radiation (for a detailed description see [154, 162–164]). An alternative approach to studying cosmic string interactions, which gives similar results, can be achieved by using the tools of effective field theory [165].

Let's make a concise revisit of the F and D-string interaction results based on vertex operators. The main concept of this approach is the connection of string states and vertex operators in the conformal field theory, state-operator map (details can be found in [166, 167]).

Let's use Wick rotation $\tau \to iT_E$ (Euclidean signature) to make the map between the string worldsheet and a complex z-plane

$$z = \mathrm{e}^{(T_E - i\sigma)}, \quad \bar{z} = \mathrm{e}^{(T_E + i\sigma)}. \tag{4.1}$$

In this way, the string on the complex plane is represented by a circle (for the closed string $\sigma \in [0,\, 2\pi)$) or a semicircle (for the open string $\sigma \in [0,\, \pi]$) as shown in figure 4.1. Thus, making this transformation we are led to the 2-dimensional conformal invariant theory[1] on the complex plane. Each excited state in conformal theory can be associated with a corresponding operator (*vertex* operator) acting on the origin (see figure 4.1). In this way, the lowest excited states of a string in a quantum treatment can be written as[2]

$$\begin{aligned}
&\text{tachyon}: && \int_{\partial M} :\mathrm{e}^{ip_\eta X^\eta}: ds \quad \text{(open string)},\\
&\text{tachyon}: && \int :\mathrm{e}^{ip_\eta X^\eta}: d^2z \quad \text{(closed string)},\\
&\text{photon}: && \int_{\partial M} e_\alpha :\partial_z X^\alpha \mathrm{e}^{ip_\eta X^\eta}: ds \quad \text{(open string)},\\
&\text{1-excitation}: && \int e_{\mu\nu} :\partial_z X^\mu \partial_{\bar{z}} X^\nu \mathrm{e}^{ip_\eta X^\eta}: d^2z \quad \text{(closed string)},
\end{aligned} \tag{4.2}$$

[1] Conformal invariance means that the theory is invariant under change of variables in a such way that the metric transformation corresponds to $\gamma_{ab}(\sigma,\tau) \to \omega(\sigma',\tau')\gamma_{ab}(\sigma',\tau')$, where ω is an arbitrary positive defined function.

[2] The fourth example in (4.2) represents a 2-index tensor, whose traceless symmetric part corresponds to the gravitational field, its anti-symmetric part to the Kalb–Ramond field and its trace to the scalar field (dilaton).

where p is the momentum of the string, e_a and $e_{\mu\nu}$ are polarization tensors, the index α takes as many values as the brane dimensionality to which the open string is connected and : ... : denotes normal ordering of operators.

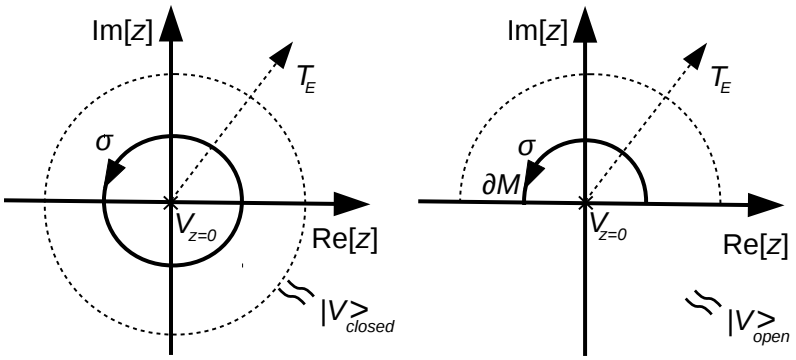

Fig. 4.1 The string worldsheet mapped on the complex plane by the relation (4.1). The origin (central point $z = 0$) of this mapping represents the far past, while the circle with infinite radius corresponds to the far future. The closed string with $\sigma \in [0, 2\pi)$ is shown on the left panel, while the open string with $\sigma \in [0, \pi]$ on the right one. To build a corresponding quantum state for the closed string $|V_{\text{closed}}>$ the vertex operator V is placed on the origin inside the circle (left panel). In the case of an open string state $|V_{\text{open}}>$ the operator V is on the boundary of the half-disk on the complex plane (right panel).

As a result, using vertex operators, it is possible to build the relevant initial and final states of the process under consideration. In this way, it is possible to represent the correlator of vertex operators

$$\mathcal{A} = \left\langle \prod_{i=1}^{N} V_i(p_i, z_i) \right\rangle, \tag{4.3}$$

where N is the number of strings in the considered process.

Calculations for the collision of macroscopic F-strings by the method of vertex operators were carried out in the work [151]. In this approach two spatial dimensions are compactified, in order to use developed string methods. Hence, the collision of strings is considered only in two noncompact $1 + 1$ dimensions, which form an angle θ, see figure 4.2. Two closed strings are placed along the compactified directions, so the angle between the strings is θ as well. The initial and final states of these closed strings are chosen to be ground states, which can be represented by four vertex operators (tachyonic states of closed strings – second line in (4.2)). This means that only the first order of string interaction is considered. The worldsheet surface for this process can be represented by a sphere, dotted with four vertex operators.

Using the general solution (3.45) it is possible to make separation in left/right-moving modes, which are holomorphic/antiholomorphic functions[3] on the complex plane z, $\tilde{z}$. We can write the momentum of strings as right and left-moving modes, where the periodicity of

[3] A holomorphic function is a function that depends only on z, while an antiholomorphic function has only $\tilde{z}$ dependence.

spatial dimensions appears with different signs [166]

$$p^{\mu}_{R,L} = p^{\mu} \pm l^{\mu}/4\pi, \tag{4.4}$$

where the vectors $p^{\mu}_{1,2}$ and $l^{\mu}_{1,2}$ are defined as

$$\begin{gathered} p^{\mu}_{1,2} = \left((\ell_{1,2}\mu_0)^2 - 4\pi\mu_0\right)^{1/2} \{1,\, \pm\tilde{v}\gamma_{\tilde{v}},\, 0,\, 0\}\,, \\ l^{\mu}_1 = \ell_1\,\{0,\, 0,\, 1,\, 0\}\,, \qquad l^{\mu}_2 = \ell_2\,\{0,\, 0,\, \cos\theta,\, \sin\theta\}\,. \end{gathered} \tag{4.5}$$

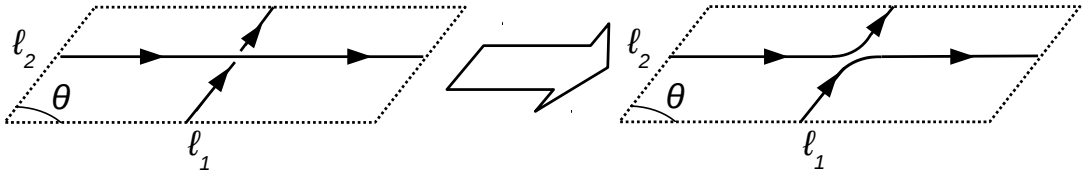

Fig. 4.2 F-strings collision. Strings are placed in the compact space: the left boundary is glied with the right one, top with bottom. Hence, these strings are closed with corresponded lengths ℓ_1 and ℓ_2. Closed strings are colliding at angle θ and reconnect.

We take into account only the leading order of non-trivial interaction, i.e. only the probability that the string ends will be exchanged, as shown in figure 4.2. All other possible scenarios of F-strings interactions (radiation/excitations) are neglected as being subdominant. By using the optical theorem, the probability of string interaction can be expressed as [151]

$$P = \frac{\mathrm{Im}(\mathcal{I}(s_R, 0))\kappa_G^2}{4\pi v\sqrt{(\ell_1\mu_0)^2 - 4\pi\mu_0)\,(\ell_2\mu_0)^2 - 4\pi\mu_0)}}, \tag{4.6}$$

where $s_R = -2p^{\mu}_{1\,R}p_{\mu\,2\,R} - 4$, κ_G is a gravitational coupling and the integral $\mathcal{I}$ comes from the scattering amplitude and will be presented below.

The optical theorem allows us to establish the connection between right/left-moving modes: $p^{\mu}_{1\,R,L} = -p^{\mu}_{4\,R,L}$, $p^{\mu}_{2\,R,L} = -p^{\mu}_{3\,R,L}$ with the condition $p^{\mu}_{i\,L}p_{\mu\,j\,L} = p^{\mu}_{i\,R}p_{\mu\,j\,R}$. Conformal symmetry on the complex plane, described by the group $SL(2,\mathbb{Z})$, gives the freedom to fix three points on the complex plane: $z_1 = \infty$, $z_2 = 0$, $z_4 = 1$, while the last one will stay as a variable $z_3 = z$. Thus, the scattering amplitude of this process can be found using equations (4.2), (4.3). These calculations give the Virasoro-Shapiro amplitude (a detailed description can be found in [167])

$$\begin{gathered} \mathcal{I}(s,t) = 2\pi\frac{\Gamma(-1 - s/16\pi\mu_0)\Gamma(-1 - b/16\pi\mu_0)\Gamma(-1 - u/16\pi\mu_0)}{\Gamma(2 + s/16\pi\mu_0)\Gamma(2 + b/16\pi\mu_0)\Gamma(2 + u/16\pi\mu_0)} \\ \xrightarrow[s\to\infty, b\to 0]{[151]} -\frac{4\pi}{b}\mathrm{e}^{-i\pi b/2}s^{2+b}, \end{gathered} \tag{4.7}$$

where $\Gamma(...)$ denotes the Gamma function and the Mandelstam variables $s = -(p^{\mu}_1 + p^{\mu}_2)^2$, $b = -(p^{\mu}_1 + p^{\mu}_3)^2$, $u = -(p^{\mu}_1 + p^{\mu}_4)^2$ satisfy the condition $s + u + b = -\mu_0\pi/8$.

The asymptotic value in the last line (4.7) is obtained in the decompactification limit $\ell_1, \ell_2 \to \infty$, i.e. compactified dimensions are sent to infinity, restoring ordinary (infinite) three spatial dimensions. As a result, using the final form of the integral (4.7) and the initial choice of the string momenta (4.5), one can rewrite the probability of F-string interaction (4.6) in the following way

$$P = \frac{\mu_0 \kappa_G^2 \left(1 + \tilde{v}^2 - (1 - \tilde{v}^2)\cos\theta\right)^2}{8\pi v (1 - \tilde{v}^2)\sin\theta}. \tag{4.8}$$

The supersymmetric extension of (4.8) was obtained in [153]. In the same manner there was considered a collision process for supersymmetric strings (not bosonic, as it was done above). Additionally, a factor that may appear due to extra dimensions was included.

In the same manner, by using the vertex operator method, one can consider the D-F strings collision process, see figure 4.3. In this case, the closed F-string transforms into an open F-string with ends on a $D0$-brane (D-string), and eventually re-connect to the closed F-string. The wordsheet surface in this case is represented by a disc with two vertex operators of closed strings inside [153].

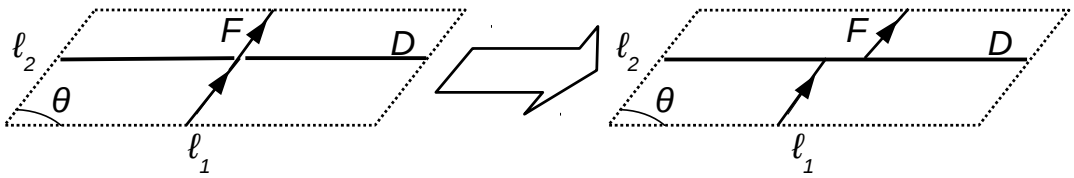

Fig. 4.3 F-D-strings collision. The closed F-string is placed in the compact space with lengths ℓ_1, ℓ_2. It meets the D-string at the angle θ. The interaction causes the connection of F-string ends with D-string, transforming the closed F-string to an open one.

The full study of these processes shows that all probabilities for F-string interactions can be written by one relation in the following convenient way

$$P_F = W_F f_F(\tilde{v}, \theta), \tag{4.9}$$

where

$$f_F = \frac{4q^2\tilde{v}^2 + g_s^2 \left(p(1 + \tilde{v}^2) - \cos\theta(1 - \tilde{v}^2)\frac{\mu_{p,q}}{\mu_F}\right)^2}{16\tilde{v}\sin\theta(1 - \tilde{v}^2)\frac{\mu_{p,q}}{\mu_F}}, \tag{4.10}$$

while the volume factor is defined as (for details see [168])

$$W_F = \min\left[\omega(\mu_{p,q}/\mu_F)^{3/4}, 8\omega, 1\right], \tag{4.11}$$

where the relation $\frac{\mu_{p,q}}{\mu_F}$ is given by (1.69) with $C_0 = 0$ and $\omega \in (0, 1]$.

The calculation for D-strings collision is more complex, due to the fact that the D-string is a composite object, i.e. it is surrounded by a "cloud" of F-strings. An estimation was obtained in [153], while a more complete treatment was provided later [165]. It is interesting

that the result of the independent computations in [165] and [153] gives a similar result

$$P_D = W_D f_D(\tilde{v}, \theta), \tag{4.12}$$

where

$$f_D = 1 - \left(1 - \min\left[\frac{\sqrt{g_s}}{2(\pi\theta)^{3/4}} \mathrm{e}^{\frac{2\sqrt{2/3}\theta\tilde{v}}{1-\sqrt{1-\tilde{v}^2}}} \exp\left[-\frac{4\sqrt{\pi}\theta^{3/2}}{g_s} \mathrm{e}^{-\frac{4\sqrt{2/3}\tilde{v}\theta}{1-\sqrt{1-\tilde{v}^2}}}\right], 1\right]\right)^{q'q}, \tag{4.13}$$

and the volume factor for this case is

$$W_D = \min\left[(\mu_{p,q}\mu_{p',q'}/\mu_F^2)^{3/4}, 1\right]. \tag{4.14}$$

As a result, in order to have the probability of interaction between a F-string and any other (p, q)-string (where simple F and D-strings are $(p = 1, q = 0)$ and $(p = 0, q - 1)$ strings correspondingly) we should use (4.9). In the case of D-string collision with some mixed strings (for $p > 1$), we should use the relation (4.12).

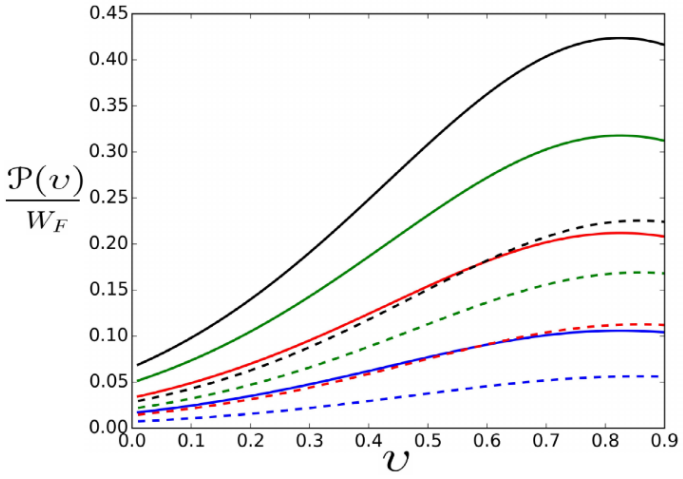

Fig. 4.4 The figure shows the result for the average probability of strings interaction as a function of the string network rms velocity. The calculations are carried out for $q = 0$, while $p = 1$ (blue), $p = 2$ (red), $p = 3$ (green), $p = 4$ (black) – dashed lines. The result for $p = 0$, while $q = 1$ (blue), $q = 2$ (red), $q = 3$ (green), $q = 4$ (black) is presented by solid lines.

Further on we will incorporate these probabilities of interaction in the string network description. In order to take into account all possible collisions between strings, we need to average probabilities (4.9), (4.12) over the angle θ and velocity υ. To do so, we need to use a distribution for the angle θ between randomly oriented strings and a proper distribution for υ. The right choice for the velocity distribution is a subtle problem. Simulations suggest to use a Gaussian distribution [105], where the "kinematic cut" (see section 4.1.4) can be added, as it was implemented in [168].

$$\mathcal{P}(\upsilon) = \frac{1}{N}\int_0^1 \int_0^{\pi/2} \mathrm{e}^{-(\upsilon-\upsilon_c)^2/\sigma_\upsilon^2} f_{distr}(\upsilon, \upsilon_c) P(\tilde{v}, \theta) \upsilon_c^2 \sin\theta d\upsilon_c d\theta, \tag{4.15}$$

where $\upsilon_c = \frac{2\tilde{\upsilon}}{1+\tilde{\upsilon}^2}$ is used to connect the central mass velocity $\tilde{\upsilon}$ in (4.5) the velocity of collision υ_c, N is a normalization factor, $\sigma_\upsilon^2 = 0.25$ is the variance of velocity [169] and f_{distr} is a distribution function defined by (4.9) or (4.12), depending on which types of strings are colliding. Figure 4.4 shows the $\mathcal{P}$ dependence on rms velocity υ.

4.1.2 Junction dynamics in Minkowski space

In the previous section we reviewed the F, D-strings interaction probabilities. Such interactions can lead to the production of junctions as it was discussed in section 1.7 (see figure 1.9). To figure out under which conditions the junction can be produced and to understand the subsequent junction dynamics, we use the approach developed in several previous papers [85, 155, 156, 159].

Let's consider junction dynamics in Minkowski space. The action for three connected strings can be defined as [170, 171][4]

$$S = -\sum_i \mu_i \int \Theta(s_i(\tau) - \sigma_i)\sqrt{-\gamma_i} d\sigma_i d\tau + \sum_i \int \mathrm{f}_{i\mu} \left(x_i^\mu(s_i(\tau), \tau) - \mathcal{X}^\mu\right) d\tau, \tag{4.16}$$

where Θ is a Heaviside function, $\mathrm{f}_{\mu\, i}$ are Lagrangian multipliers, $\mathcal{X}^\mu$ is the space-time position of the vertex (connection between strings), the index $i = 1, 2, 3$ counts the number of strings (there is no summation over these repeated indices, summation happens only if the symbol $\sum$ is written explicitly), s is a parametrisation value of σ at the vertex $\mathcal{X}^\mu$.

By making a variation of the action (4.16) with respect to $\mathbf{x}_i$ (using the parametrization (2.3)) one can obtain the standard equations of motion (2.4) for the three strings. An additional equation from the $\mathbf{x}_i$ variation appears due to the boundary term in the action (4.16) and has the form[5] [172]

$$\mu_i \left(\frac{\mathbf{x}_i'}{\varepsilon_i} + \varepsilon_i \dot{s}_i \dot{\mathbf{x}}_i \right) = \mathbf{f}_i, \tag{4.17}$$

with the condition from the $\mathcal{X}^\mu$ variation

$$\sum_i \mathbf{f}_i = 0. \tag{4.18}$$

From the variation of the Lagrange multipliers f_i we obtain the previously mentioned conditions that $\sigma = s$ at the vertex,

$$\mathbf{x}_i(s_i(\tau), \tau) = \mathbf{X}(\tau), \tag{4.19}$$

where $\mathbf{X}$ is the spatial part of $\mathcal{X}^\mu$.

[4] The action (4.16) is valid for a FLRW background as well [159, 172]. This case is considered below in section 4.1.3

[5] We obtain the equations of motion for the general FLRW metric and recover the Minkowski space by setting $\varepsilon = 1$.

The general solution of equations of motion (2.4) is (3.45). The vector **a** represents the right-moving mode, while the vector **b** is the left-moving mode, whose derivatives are normalized to unity (strings without current for comparison with (3.58))

$$|\mathbf{a}'| = |\mathbf{b}'| = 1. \tag{4.20}$$

The split into left/right-moving modes is a key point to treat junction dynamics and their production. We can chose the parametrization of strings in such way that the $\mathbf{b}_i'$ components are moving towards the string vertex (the point where all three strings connect), while modes $\mathbf{a}_i'$ are moving outwards from the connection (see figure 4.5, for $F' = 0$). The equation (4.19) allows us to express derivatives of outgoing vectors $\mathbf{a}_i'$ as a combination of the ingoing part $\mathbf{b}_i'$ and vertex motion $\dot{\mathbf{X}}$. In this sense, the ingoing set of vectors $\mathbf{b}_i'$ plays the role of initial conditions, while $\mathbf{a}_i'$ are defined by the equations.

Using the condition (4.18) with (4.17) one can express each $\dot{s}_i$ in the following way [85, 155]

$$\frac{(1-\dot{s}_i)\mu_i}{\mu} = \frac{M_i(1-c_i)}{\mathcal{M}}, \tag{4.21}$$

where $\mu = \sum\limits_i \mu_i$, $c_i = \varepsilon_{ijk}\mathbf{b}_j' \cdot \mathbf{b}_k'$, $M_i = \mu_i^2 - \frac{1}{2}|\varepsilon_{ijk}|(\mu_j - \mu_k)^2$, $\mathcal{M} = \sum\limits_j M_j(1-c_j)$.

Demanding that a "just created" string has a positive value of $\dot{s}$, we can guarantee that this string length will grow, i.e. we will have junction production.

Junctions with currents

Let's generalize the method described above for the collision of strings with currents. This problem was already studied in [173]. In this work the electric (time-like current $\kappa > 0$) and magnetic (space-like current $\kappa < 0$) regimes of currents on strings were considered (3.10). Here we present the corresponding result for the chiral current $\kappa = 0$, which has not been studied to date.

Let's start from the definition of the action for three connected strings with currents [173]

$$\begin{aligned} S = &- \sum_i \mu_i \int dt \int d\sigma_i \sqrt{-\gamma_i} f_i(\kappa_i, \Delta_i/\gamma_i)\Theta\left(s_i(t) - \sigma_i\right) + \\ &+ \sum_i \int dt\, \mathrm{f}_{\mu i}\left(x_i^\mu(s_i(t), t) - \mathcal{X}^\mu(t)\right) + \sum_i \int dt\, \mathrm{g}_i\left(\varphi_i(s_i(t), t) - \Phi(t)\right), \end{aligned} \tag{4.22}$$

where g_i is a Lagrange multiplier for the current, Φ defines the value of the current at the point where the three strings are connected and the index $i = 1, 2, 3$, as before, denotes each of three strings.

In a similar way as it was done above, varying the action (4.22) with respect to x_i^μ and φ_i, we obtain the following equations of motion

$$\begin{aligned} \partial_a \left(\mathcal{T}^{ab} x^\mu_{,b} \right) = 0, \\ \partial_a \left(\mathcal{S}^{ab} \varphi_{,b} \right) = 0. \end{aligned} \tag{4.23}$$

The boundary terms proportional to $\delta(s_i(t) - \sigma_i)$, using (3.41) and (3.50), can be expressed as

$$\begin{aligned} \mu_i \eta^{ab} x^\mu_{i,a} \lambda_b = \mathrm{f}_i^\mu, \\ \mu_i \mathcal{D}_i \eta^{ab} \varphi_{,a} \lambda_b = \mathrm{g}_i, \end{aligned} \tag{4.24}$$

where $\lambda_a = \{\dot{s}_i, \, -1\}$ and $\mathcal{D}_i = 2\left(\frac{\partial f_i}{\partial \kappa_i} - \frac{\partial f_i}{\partial \Delta_i}\right)$.

The variation of the action (4.22) with respect to $\mathcal{X}_i^\mu$ and Φ gives us

$$\begin{aligned} \sum_i \mathrm{f}_i^\mu = 0, \\ \sum_i \mathrm{g}_i = 0. \end{aligned} \tag{4.25}$$

The action (4.22) variation with respect to f_i^μ and g_i provides us the following relations

$$\begin{aligned} x_i^\mu(s_i(t), t) = X^\mu(t), \\ \varphi_i(s_i(t), t) = \Phi(t). \end{aligned} \tag{4.26}$$

As it was shown in section 3.3, the general solution of the equations of motion (4.23) for strings with a chiral current in Minkowski space has the form

$$\begin{aligned} \mathbf{x}(\tau, \sigma) = \frac{1}{2} \left(\mathbf{a}(\sigma + \tau) + \mathbf{b}(\sigma - \tau) \right), \\ \varphi(\tau, \sigma) = \frac{1}{2} F(\sigma \pm \tau), \end{aligned} \tag{4.27}$$

where we added the factor $\frac{1}{2}$ for convenience.

It is seen that for the chiral current the situation is similar to the one considered above, i.e. we can still separate the string solution in ingoing and outgoing modes. As a result, the modes that move outwards from the junction are determined by the ingoing modes. However, the situation with the current is a bit more subtle. The current on a string propagates only in one direction. Additionally, while we know the properties of the colliding strings (in particular we know $\mathcal{D}$ for both strings) it is not clear how to define the value of $\mathcal{D}$ for the junction. Should it be a free parameter, or can it somehow be restricted by other arguments as it was done for the tension (see section 1.7)? For now, we assume that $\mathcal{D}$ is a free parameter defined by kinematic constraints.

In the situation when $\mathcal{D}_3$ is a free parameter, let's consider the collision of two identical strings ($\mu_1 = \mu_2$, $F_1' = F_2'$, $\mathcal{D}_1 = \mathcal{D}_2$). We can choose the parametrization of the colliding

strings in the same way as it was done for strings without currents, i.e. all vectors $\mathbf{b}'$ represent modes that are moving towards the junction, while $\mathbf{a}'$ are outgoing modes. From (4.27) it is seen that the choice of the sign of τ for the function F defines the current direction on a string. Hence, we can chose if the current propagates toward the vertex between strings or outwards. Let's consider the collision of strings in which currents are moving towards the junction, see figure 4.5. In this situation the string solution together with the current can be written as

$$\begin{aligned} \mathbf{x}_{1,2}(t,\sigma) &= \frac{1}{2}\left(\mathbf{a}_{1,2}(\sigma+t)+\mathbf{b}_{1,2}(\sigma-t)\right), \\ \varphi_{1,2}(t,\sigma) &= \frac{1}{2}F_{1,2}(\sigma-t), \end{aligned} \tag{4.28}$$

with $|\mathbf{a}'_{1,2}|^2 = 1$, while $|\mathbf{b}'_{1,2}|^2 = 1 - \mathcal{D}_{1,2}|F'_{1,2}|^2$.

Therefore, the junction solution has to be

$$\begin{aligned} \mathbf{x}_3(t,\sigma) &= \frac{1}{2}\left(\mathbf{a}_3(\sigma+t)+\mathbf{b}_3(\sigma-t)\right), \\ \varphi_3(t,\sigma) &= \frac{1}{2}F_3(\sigma+t), \end{aligned} \tag{4.29}$$

with $|\mathbf{b}'_3|^2 = 1$, while $|\mathbf{a}'_3|^2 = 1 - \mathcal{D}_3|F'_3|^2$.

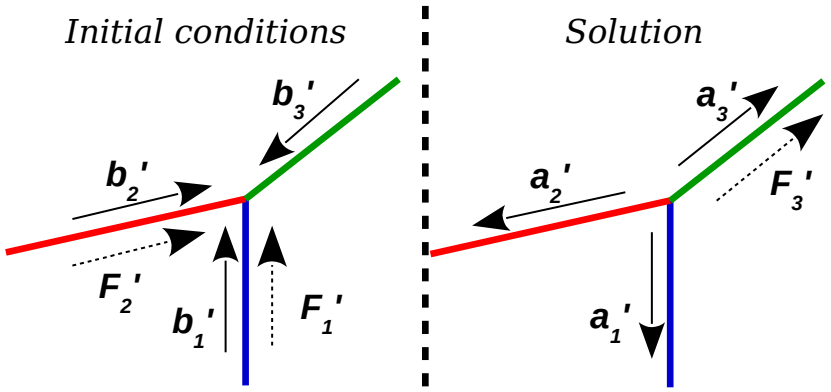

Fig. 4.5 Collision of strings with currents, whose moving modes are represented by F'_i and ingoing/outgoing modes of strings are shown by vectors $\mathbf{a}'_i$ and $\mathbf{b}'_i$ respectively.

Using solutions (4.28), (4.29) we can rewrite (4.24) with (4.25) as

$$\begin{aligned} &\sum_i \mu_i \left(\mathbf{a}'_i(1+\dot{s}_i)+\mathbf{b}'_i(1-\dot{s}_i)\right) = 0, \\ &\sum_I \mu_I \mathcal{D}_I F'_I(\dot{s}_I - 1) = \mu_3 \mathcal{D}_3 F'_3(\dot{s}_3+1). \end{aligned} \tag{4.30}$$

Differentiating (4.26) we obtain

$$\begin{aligned} &(1+\dot{s}_i)\mathbf{a}'_i - (1-\dot{s}_i)\mathbf{b}'_i = 2\dot{\mathbf{X}}(t), \\ &F'_I(\dot{s}_I - 1) = 2\dot{\Phi}(t) = F'_3(\dot{s}_3+1), \end{aligned} \tag{4.31}$$

where $X^\mu = (t,\ \mathbf{X}(t))$ and $I = 1, 2$.

As it was done above, manipulating vectors $\mathbf{a}_i$ and $\mathbf{b}_i$, it is possible to obtain equations for $\dot{s}_i$

$$\mathbf{a}'_k(1 + \dot{s}_k) = -\frac{2}{\mu}\sum_i (1 - \dot{s}_i)\mu_i \mathbf{b}'_i + (1 - \dot{s}_k)\mathbf{b}'_k. \tag{4.32}$$

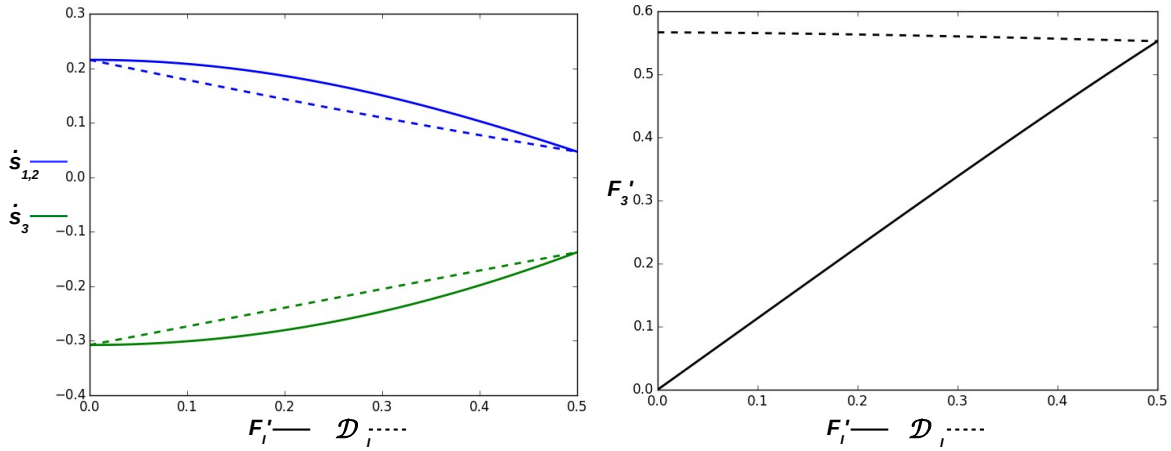

Fig. 4.6 The left panel shows how the growth/decrease rate $\dot{s}_i$ for the string configurations is changing due to variations of current properties, represented by F'_I and $\mathcal{D}_I$. The right panel shows the value of the current F'_3 generated on the junction for different values of F'_I and $\mathcal{D}_I$. All solid lines represent variation of F'_I, with fixed $\mathcal{D}_I = 0.5$, while all dashed lines represent variation of $\mathcal{D}_I$ with fixed $F'_I = 0.5$. These calculations are carried out for string tensions $\mu_1 = \mu_2 = 1$, $\mu_3 = 1.2$ when all vectors $\mathbf{b}'_i$ are orthogonal.

Squaring equations (4.32) and using the normalization conditions for $\mathbf{a}'_i$ and $\mathbf{b}'_i$ vectors, we obtain equations for $\dot{s}_i$. Since we know the values of F'_I, to solve these equations for $\dot{s}_i$ we need to define F'_3. By using the second line in (4.31) one can obtain

$$F'_3 = \frac{F'_I(\dot{s}_I - 1)}{\dot{s}_3 + 1}. \tag{4.33}$$

To define the string junction completely, we also need to find $\mathcal{D}_3$, which can be achieved by using the second line of relations (4.30). It provides the following equation

$$\mathcal{D}_3 = \frac{1}{\mu_3}\sum_I \mu_I \mathcal{D}_I. \tag{4.34}$$

We can solve numerically equations (4.32) taking into account conditions (4.33) and (4.34) for different values of the current F'_I. The result of these calculations for orthogonal vectors $\mathbf{b}'_i$ is shown in figure 4.6, where the orthogonality was chosen just for explicit demonstration of the current influence on a string growth/decrease rate.

In the situation when colliding strings are not the same, i.e. they have different values of tensions $\mu_1 \neq \mu_2$ or/and currents $F'_1 \neq F'_2$, it is seen from the second line of (4.31) that the system has an additional restriction for $\dot{s}_I$. This leads to the system of equations (4.30),

(4.31) becoming overdetermined. A similar problem appeared in the work [173], where the magnetic and electric regimes were studied.

A possible resolution for this issue is to assume that vectors $\mathbf{b}'_i$ are not completely independent. We need to fix at least one angle between the vectors $\mathbf{b}'_i$. This means that this angle should have a specific value during the whole evolution, in contrast to angles for strings without currents (see figure 1.9).

Let's assume that we have three connected strings with tensions $\mu_1 = 1$, $\mu = 1.2$, $\mu = 1.4$, while $\mathcal{D}_1 = 0.1$, $\mathcal{D}_2 = 0.2$, $F'_1 = 0.2$ and F'_2 will be varied. In this situation we can find the angle of the scalar product of vectors $c_1 = |\mathbf{b}_3| \cdot |\mathbf{b}_2| \cos\beta$. The result of such configuration is shown in figure 4.7.

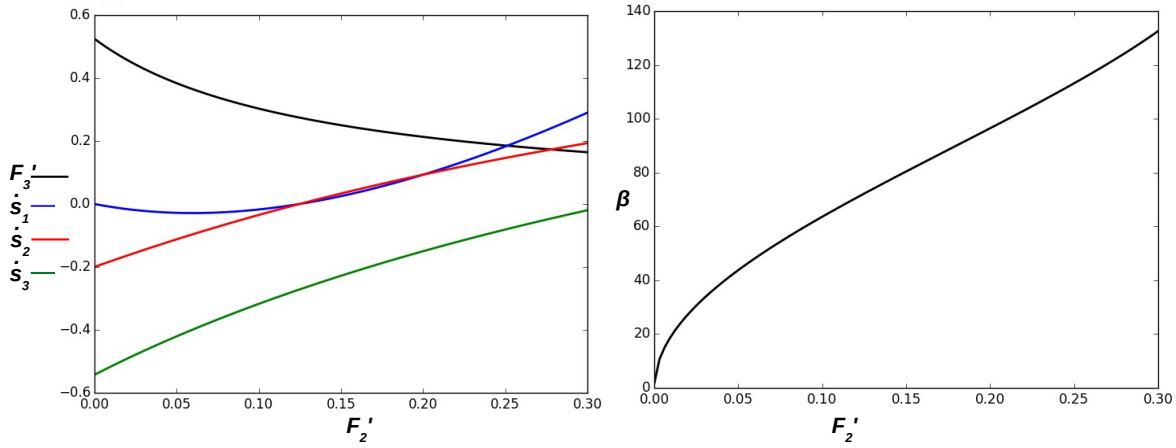

Fig. 4.7 The left panel shows how the growth/decrease rates $\dot{s}_i$ and the current F'_3 for strings depend on F'_2. The right panel shows the value of the angle β between vectors $\mathbf{b}_2$ and $\mathbf{b}_3$. Calculations are carried out for string tensions $\mu_1 = 1$, $\mu_2 = 1.2$, $\mu_3 = 1.4$, while $F'_1 = 0.2$, $\mathcal{D}_1 = 0.1$ and $\mathcal{D}_2 = 0.2$. The orientation of other vectors $\mathbf{b}_i$ is free and was chosen so that the vectors are orthogonal to each other.

In spite of the possible resolution for the overdetermined system of equations, this question needs further investigation, especially as it is not clear which angle between vectors $\mathbf{b}'_i$ should be fixed and why. In addition to that, there are still ambiguities about $\mathcal{D}$. Is it possible to implement additional constraints on the junction properties or maybe in contrast, is it possible to relax the imposed conditions by new degrees of freedom? These questions should be addressed in a field theory treatment. More numerical simulations of strings with currents collisions can shed the light on this problem [174, 175].

4.1.3 Junction dynamics in the FLRW metric

Let's consider the generalization of connected strings dynamics for the case of the FLRW metric. We can start from the action (4.16) and varying it, one can obtain the equations of string motion (2.4) and conditions from string connections (4.17-4.19), while $\varepsilon \neq 1$ and the normalization condition (4.20) is not valid anymore.

For the expanding FLRW metric there is no general solution for string equations (2.4). However it is possible to build a convenient analogue of $\mathbf{a}'$ and $\mathbf{b}'$ vectors (the same approach for the FLRW metric was used in [159] for the analysis of loops with junctions):

$$\begin{aligned} \mathbf{q} &= \mathbf{x}'/\varepsilon + \dot{\mathbf{x}}, \\ \mathbf{p} &= \mathbf{x}'/\varepsilon - \dot{\mathbf{x}}, \end{aligned} \tag{4.35}$$

where vectors (4.35) become $\mathbf{a}'$ and $\mathbf{b}'$ correspondingly for Minkowski space ($\varepsilon = 1$).

In the case of monotonic expansion of the scale factor in the FLRW metric, it is reasonable to assume that ingoing and outgoing waves are distinguishable and won't be mixed during the evolution. That is why we can assume that vectors $\mathbf{q}$ and $\mathbf{p}$ are outgoing and ingoing waves correspondingly for the vertex $\mathbf{X}$ in an expanding universe.

Taking into account the fact that $|\mathbf{q}|^2 = 1$, $|\mathbf{p}|^2 = 1$ and using equations (2.4), (4.17-4.19) one can carry out a similar analysis as it was done for Minkowski space in [155]. In this way, the final equations for junctions in an expanding universe are

$$\sum_i \mu_i \left((\mathbf{q}_i + \mathbf{p}_i) + \varepsilon_i \dot{s}_i (\mathbf{q}_i - \mathbf{p}_i)\right) = 0. \tag{4.36}$$

$$\dot{\mathbf{X}} = -\frac{1}{\mu} \sum_i \mu_i (1 - \varepsilon_i \dot{s}_i) \mathbf{p}_i, \tag{4.37}$$

$$\frac{(1 - \varepsilon_i \dot{s}_i)\mu_i}{\mu} = \frac{M_i(1 - c_i)}{\mathcal{M}}. \tag{4.38}$$

As a result, one can conclude that equations for junctions in an expanding universe can be obtained from Minkowski space just by changing $\dot{s}_i$ to $\varepsilon_i \dot{s}_i$ and changing the definitions of $\mathbf{a}'$, $\mathbf{b}'$ into the generalized parameters (4.35). The new set of equations (4.38) tells us how the growth/decrease of string happens for the FLRW metric. An important issue that stems from the above treatment is to understand under which conditions the junction will be produced. This condition just requires $\dot{s}_3 > 0$ and will be considered for straight strings below.

4.1.4 The junction production

Solution for a straight string in a FLRW background

It is always possible to chose a sufficiently small region near the collision point, where strings can be considered straight. Hence, to understand under which conditions the collision of strings leads to the junction production we can consider a straight string collision. For this purpose we need to formulate a proper straight string solution in a FLRW metric. Let's

consider the straight string ansatz, similar to the case of Minkowski space,

$$\mathbf{x} = \{C_1\sigma\cos\alpha;\, C_1\sigma\sin\alpha;\, F(\tau)\}\,, \tag{4.39}$$

where C_1 is a constant that will be defined later as well as the function $F(\tau)$.

From the ansatz (4.39) it is seen that the straight string is located on the XY-plane and moves along the Z-axis. The angle α defines the orientation of the string in the XY-plane.

It should be noted that the dependence on σ is going to be the same as in Minkowski space. However, the physical meaning of the σ parameter is not identical. Any interval of a string in Minkowski space has a fixed length and doesn't depend on time, while in a FLRW metric the length of a chosen string interval is stretching as time evolves, which implies a continuous "effective" reparametrization of the string (4.39). Meanwhile, the time component τ is substituted by the function $F(\tau)$, due to absence of the time symmetry.

Using the form (4.39) we can obtain some useful quantities

$$\mathbf{x}' = \{C_1\cos\alpha;\, C_1\sin\alpha;\, 0\}\,, \tag{4.40a}$$

$$\dot{\mathbf{x}} = \left\{0;\, 0;\, \dot{F}(\tau)\right\}, \tag{4.40b}$$

$$\varepsilon = \sqrt{\frac{\mathbf{x}'^2}{1-\dot{\mathbf{x}}^2}} = \sqrt{\frac{C_1^2}{1-\dot{F}^2}}, \tag{4.40c}$$

$$\dot{\varepsilon} = |C_1|\frac{\dot{F}\ddot{F}}{\left(1-\dot{F}^2\right)^{3/2}}. \tag{4.40d}$$

Eventually, by using expressions (4.40a)-(4.40d), one can show that equations of motion (2.4) are reduced to one equation for the function $F(\tau)$

$$\ddot{F} + 2\frac{\dot{a}}{a}\dot{F}(1-\dot{F}^2) = 0. \tag{4.41}$$

When the scale factor is $a \propto \tau^n$, the equation (4.41) has an exact solution

$$F(\tau) = \pm\tau\ {}_2F_1\left(\frac{1}{2};\, \frac{1}{4n};\, \frac{1+4n}{4n};\, -C_2\tau^{4n}\right), \tag{4.42}$$

where ${}_2F_1$ is a hypergeometric function and C_2 is a constant.

The solution (4.42) is monotonic in the argument τ for all positive n, which is anticipated from the physical interpretation of (4.42). To be able to reproduce the solution in Minkowski space, we should require that this solution goes to to $\pm v\tau$ when $n \to 0$. This condition provides $C_2 = 1/v^2 - 1 = (\gamma_v v)^{-2}$. As a result, the solution (4.42) has the form

$$\mathbf{x} = \left\{\sigma\cos\alpha;\, \sigma\sin\alpha;\, \pm\tau\ {}_2F_1\left(\frac{1}{2};\, \frac{1}{4n};\, \frac{1+4n}{4n};\, -\left(\gamma_v v\right)^{-2}\tau^{4n}\right)\right\}, \tag{4.43}$$

where we settle $C_1 = 1$ and one can check that ${}_2F_1 \xrightarrow[n\to 0]{} v$ reproduces the case for Minkowski metric.

One can notice that the constant C_1 in the solution (4.43) was chosen to be 1. It is possible to demand $C_1 = \gamma_v^{-1}$, in order to reproduce the same solution as it was used in [85]. However, when we use the generalized description with vectors (4.35), we do not need to worry about the relation $\varepsilon = 1$. Hence, we can chose another parametrization for the σ and it will not affect the final result. That is why – for convenience – we have chosen $C_1 = 1$.

Let's analyse the obtained solution (4.43). Since there is no time symmetry anymore, we should chose the "initial condition" – the moment from which the string started the evolution. The most convenient choice, which does not bring additional difficulties is $\tau = 1$ (it is possible to chose $\tau = 0$, but in that case we will be faced with the term 0^0 that can require some redefinition of C_1, C_2). At the initial moment $\tau = 1$, the velocity of the string is v. As a result, at the first moment the string solution (4.43) is identical to Minkowski space, and only further evolution brings differences in expanding space-time. The velocity $\sqrt{\dot{\mathbf{x}}^2}$ of the string starts decreasing in an expanding universe (it should be noted that the value v is a constant that just provides the initial value of velocity). Also, as it was already mentioned, it is incorrect to think that σ will be the length of the string. The length of the string should depend on time during the expansion, and σ is chosen in such way that it is the same for any time.

Collision of straight strings in expanding universe

Above we outlined the approach for description of connected strings in the FLRW metric (section 4.1.3) and demonstrated one simple straight string solution in section 4.1.4. Consequently, we can consider the collision of straight strings in a FLRW background and investigate under which conditions a junction can be produced. We are going to consider the situation only when the scale factor is $a \propto \tau^n$.

Let's now model the situation when two strings $\mathbf{x}_{1,2}$ are moving towards each other along the axis Z with initial speed v, having the angle α between them. The third string $\mathbf{x}_3$ is created in the XY-plane, and its location is defined by the angle θ and the initial velocity u

$$\begin{aligned} \mathbf{x}_{1,2} &= \left\{ -\sigma\cos\alpha;\, \mp\sigma\sin\alpha;\, \pm\tau\, {}_2F_1\left(\frac{1}{2};\, \frac{1}{4n};\, \frac{1+4n}{4n};\, -\left(\gamma_v v\right)^{-2}\tau^{4n}\right)\right\}, \\ \mathbf{x}_3 &= \left\{ \sigma\cos\theta;\, \sigma\sin\theta;\, \tau\, {}_2F_1\left(\frac{1}{2};\, \frac{1}{4n};\, \frac{1+4n}{4n};\, -\left(\gamma_u u\right)^{-2}\tau^{4n}\right)\right\}. \end{aligned} \tag{4.44}$$

In order to have a simple analytic comparison of the expanding FLRW metric and Minkowski space, let's consider the case when the tension of the first string is the same as the tension of the second one $\mu_1 = \mu_2$. In this way, $u = 0$ and $\theta = 0$. Using the equality (4.38), one can show that the solution for $\dot{s}_3$ is

$$\dot{s}_3 = \frac{2\mu_1\tilde{\gamma}(v,\tau)\cos\alpha - \mu_3}{2\mu_1 - \mu_3\tilde{\gamma}(v,\tau)\cos\alpha}, \tag{4.45}$$

where $\tilde{\gamma}(v,\tau) = \frac{\gamma_v^{-1}}{\sqrt{1+v^2(\tau^{-4n}-1)}}$.

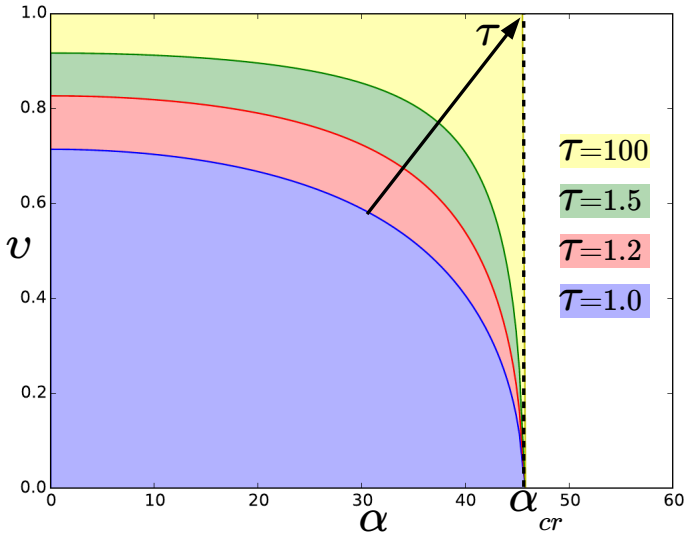

Fig. 4.8 Range of parameters: "initial velocity" v and angle α, which allow the production of the junction ($\dot{s}_3 > 0$) for the case when the heaviest string has the tension $\mu_3 = 1.4\,\mu_1 = 1.4\,\mu_2$. The evolution of strings happens in an expanding FLRW metric when $a \propto \tau^n$ with $n = 1.0$ (radiation era). The first blue area corresponds to the moment $\tau = 1.0$, later evolution is represented by other colors and the full area until $\alpha_{\rm cr}$ is reached when $\tau \to \infty$.

If we compare the equation (4.45) with the result for Minkowski space [85], it is seen that the Lorentz factor γ_v^{-1} is substituted by the function $\tilde{\gamma}$, which goes to γ_v^{-1} when $n \to 0$ or when $\tau = 1$. Let's build the velocity-angle region, when the junction can be produced ($\dot{s}_3$>0) - figure 4.8. The value $\tau = 1$ corresponds to the initial conditions of the colliding strings, which also coincide with the solution for Minkowski space. It is seen that as τ grows the region where $\dot{s}_3 > 0$ is increasing. This effect appears due to string velocity decrease in the expanding universe. Eventually the string speed tends to zero and the junction appears for all possible collisions at any smaller than critical angle $\alpha_{cr} = \arccos\left(\mu_3/(2\mu_1)\right)$.

As a result, the junction production for straight strings in the FLRW universe is different from the Minkowski case only by the change of the relative string velocity. This result suggests that we can apply the approach developed in [85, 155] to the study of junction dynamics in the FLRW metric.

Collision of straight strings with currents

Similarly as it was done above, we can consider a collision of straight strings with currents and find conditions which allow the formation of the junction in Minkowski space. In particular, we consider the collision of two equivalent strings $\mu_1 = \mu_2$, $\mathcal{D}_1 = \mathcal{D}_2$, $F_1' = F_2'$.

In the first place we need to build an appropriate solution for straight strings with a current. Following the description of strings with currents from section 3.3, we need to build new vectors $\mathbf{x}_{1,2}$ for straight strings that can satisfy the previously described properties. It can be done in the following way

$$\mathbf{y}_i = \mathbf{x}_i + \mathbf{z}_i, \tag{4.46}$$

where vectors $\mathbf{x}_i$ are defined in the same way as for ordinary straight strings in Minkowski space [155]

$$\begin{aligned} \mathbf{x}_{1,2} &= \left\{-\gamma^{-1}\sigma\cos\alpha;\, \mp\gamma^{-1}\sigma\sin\alpha;\, \pm\upsilon\tau\right\}, \\ \mathbf{x}_3 &= \{\sigma;\, 0;\, 0\}\,. \end{aligned} \tag{4.47}$$

Now we need to understand which form of vectors $\mathbf{z}_i$ should be chosen in order to be in agreement with properties (3.55), (3.57), (3.58). Using the form of the string (4.47), we can try the following ansatz

$$\begin{aligned} \mathbf{z}_{1,2} &= \left\{\gamma^{-1}f_{1,2}(\sigma-\tau)\cos\alpha;\, \pm\gamma^{-1}f_{1,2}(\sigma-\tau)\sin\alpha;\, \pm f_{1,2}(\sigma-\tau)\upsilon\tau\right\}, \\ \mathbf{z}_3 &= \{-f_3(\sigma+\tau);\, 0;\, 0\}\,, \end{aligned} \tag{4.48}$$

where f_i are arbitrary functions.

One can form ingoing and outgoing components from (3.45)

$$\begin{aligned} \mathbf{b}_i' &= \mathbf{y}_i' - \dot{\mathbf{y}}_i, \\ \mathbf{a}_i' &= \mathbf{y}_i' + \dot{\mathbf{y}}_i, \end{aligned} \tag{4.49}$$

which are normalized as

$$\begin{aligned} \mathbf{b}_{1,2}'^2 &= 1 - 4f_1'(1-f_1'), \quad \mathbf{b}_3'^2 = 1, \\ \mathbf{a}_{1,2}'^2 &= 1, \quad \mathbf{a}_3'^2 = 1 - 4f_3'(1-f_3'). \end{aligned} \tag{4.50}$$

Comparing the result for straight strings with equalities (3.55), (3.57) and (3.58), we can conclude that

$$\mathcal{D}_i F_i'^2 = f_i'(1-f_i'). \tag{4.51}$$

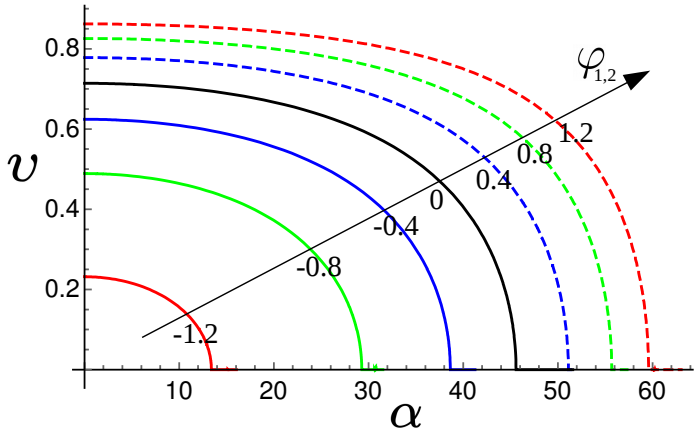

Fig. 4.9 Range of parameters: velocity υ and angle α, which allow the junction production ($\dot{s}_3 > 0$) for the case when the heaviest string has the tension $\mu_3 = 1.4\,\mu_1 = 1.4\,\mu_2$. It is seen how the region of junction production depends on the value of colliding strings currents ($\varphi_1 = \varphi_2$).

Let's consider the linearised contribution from the current

$$\begin{aligned} f'_{1,2} &= \varphi_{1,2}\,(\sigma-\tau), \\ f'_{3} &= \varphi_{3}\,(\sigma+\tau). \end{aligned} \tag{4.52}$$

where φ_i are constants.

Applying the same method as in the work [155], we can solve the kinematic equations (4.32) for straight strings with currents and find out for which range of velocities v and angles α the production of a junction is possible ($\dot{s}_3 > 0$). Solutions for different values of the current are shown in figure 4.9

4.2 Averaged junction evolution after strings collisions

In the previous section we studied the probability of cosmic (super)string interaction and possible consequence of such collisions. In order to see the effect from these results, we need to average the processes considered over the whole network and implement this to the VOS model. In particular, we need to estimate the average junction dynamics after string collisions and find out how much junctions can grow.

4.2.1 Angles between strings after collision

Let's revisit the result that all vectors of connected strings $\mathbf{x}'$ are coplanar [156] in Minkowski space. We will check that this result is valid not only in Minkowski space, but also in the FLRW background. The junction between strings is described by the vector (4.19). Hence, $\dot{\mathbf{X}}^2 = \dot{\mathbf{x}}_i^2 + \dot{s}_i^2 \mathbf{x}_i'^2$ together with the definition of ε_i it is possible to obtain

$$\begin{aligned} \dot{\mathbf{X}}^2 &= 1 - \frac{\mathbf{x}_i'^2}{\varepsilon_i^2} + \dot{s}_i^2 \mathbf{x}_i'^2 \Rightarrow \\ \Rightarrow \left(\frac{1}{\varepsilon_i^2} - \dot{s}_i^2\right) \mathbf{x}_i'^2 &= \left(\frac{1}{\varepsilon_k^2} - \dot{s}_k^2\right) \mathbf{x}_k'^2. \end{aligned} \tag{4.53}$$

Let's multiply equation (4.17) by the vector $\dot{\mathbf{X}}$, sum over the index "i" and using the relation (4.18), one can obtain

$$\sum_i \varepsilon_i \dot{s}_i \mu_i = 0. \tag{4.54}$$

Equation (4.54) is just a generalized energy conservation law for shrinking and growing junctions. Using equations (4.17), (4.18), and the definition of $\dot{\mathbf{X}}$ together with the condition (4.54), it is possible to obtain the following expression

$$\begin{aligned} \sum_i \varepsilon_i \mu_i \left(\frac{1}{\varepsilon_i^2} - \dot{s}_i^2\right) \mathbf{x}'_i &\overset{(4.53)}{=} \left(\frac{1}{\varepsilon_k^2} - \dot{s}_k^2\right) \mathbf{x}_k'^2 \sum_i \varepsilon_i \mu_i \frac{\mathbf{x}'_i}{\mathbf{x}_i'^2} = 0 \Rightarrow \\ \Rightarrow \sum_i \varepsilon_i \mu_i \frac{\mathbf{x}'_i}{\mathbf{x}_i'^2} &= 0. \end{aligned} \tag{4.55}$$

The last equation tells us that tangent vectors $\mathbf{x}_i'$ of connected strings lie in one plane, which means that three connected strings locally have to be coplanar.

To understand the string configuration right after the collision, we can use the method developed in [176]. Let's consider the string collision with the angle 2α between them, see figure 4.10. If the kinematic condition is satisfied ($\dot{s}_3 > 0$), the junction should be produced and two kinks start propagating on collided strings in opposite directions as it is shown in figure 4.10. As a result, there will be new angles between strings that we denoted as $\pi - \beta_1$, $\pi - \beta_2$ and $\beta_1 + \beta_2$.

As it was discussed above, after the collision of strings (lines JK_1, JK_2 and VJ) stay at the same plane. From the figure 4.10, following the work [176], we can obtain that

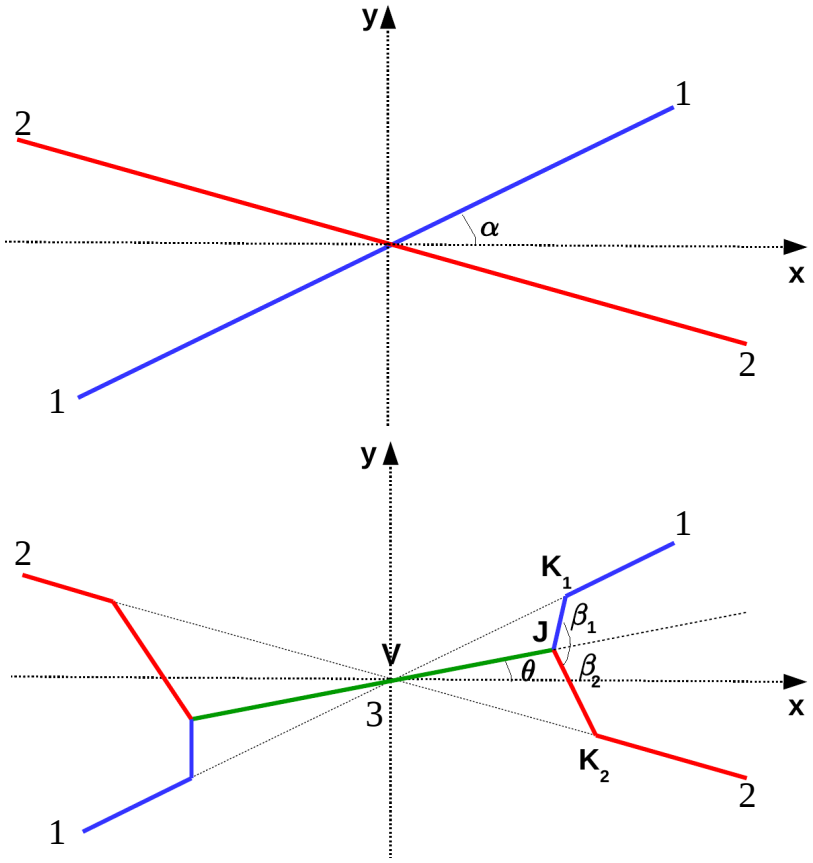

Fig. 4.10 Collision of two strings that are defined by blue and red lines. When the kinematic condition is satisfied ($\dot{s}_3 > 0$), the junction between colliding strings is produced, green line. The bottom panel shows the geometrical configuration of straight strings before collision, while the bottom panel shows the configuration right after the collision.

$$\begin{aligned} \cos\beta_1 &= \frac{VK_1\cos(\alpha-\theta) - VJ}{JK_1} = \frac{\cos(\alpha-\theta) - \dot{s}_3(0)}{\sqrt{1+\dot{s}_3(0)\left[\dot{s}_3(0) - 2\cos(\alpha-\theta)\right]}}, \\ \cos\beta_2 &= \frac{VK_2\cos(\alpha+\theta) - VJ}{JK_2} = \frac{\cos(\alpha+\theta) - \dot{s}_3(0)}{\sqrt{1+\dot{s}_3(0)\left[\dot{s}_3(0) - 2\cos(\alpha+\theta)\right]}}. \end{aligned} \tag{4.56}$$

Hence, one can obtain the expression

$$\begin{aligned}\tan\beta_1 &= \frac{\sin(\alpha-\theta)}{\cos(\alpha-\theta)-\dot{s}_3(0)},\\ \tan\beta_2 &= \frac{\sin(\alpha+\theta)}{\cos(\alpha+\theta)-\dot{s}_3(0)},\end{aligned} \tag{4.57}$$

where $\dot{s}_3(0)$ denotes the rate of junction growth at the moment of stings collision.

It should be noticed that as it was shown in [176], when $\upsilon \to 0$ we obtain $\beta_{1,2} = \pi/2$ for $\alpha = 0$. At the same time, when $\upsilon \neq 0$ for $\alpha = 0$ the angles $\beta_{1,2} = 0$.

Using the equality (4.57), it is possible to obtain angles $\beta_{1,2}$ for all possible collisions of strings. Since we are interested in the average picture, we want to know how angles $\beta_{1,2}$ depend on the rms velocity for fixed values of tensions μ_1, μ_2 and μ_3. In order to achieve this goal we need to express the angle θ and junction rate $\dot{s}_3$ as functions of α, υ and μ_i $(i = 1, 2, 3)$. For this purpose we use equations for straight strings [85]

$$\begin{aligned}[\mathcal{M}\dot{s}_3 + M_3(1-c_3)]\,\gamma_u^{-1}\cos\theta &= [M_1(1-c_1)+M_2(1-c_2)]\,\gamma_\upsilon^{-1}\cos\alpha,\\ [\mathcal{M}\dot{s}_3 + M_3(1-c_3)]\,\gamma_u^{-1}\sin\theta &= [M_1(1-c_1)-M_2(1-c_2)]\,\gamma_\upsilon^{-1}\sin\alpha,\\ [\mathcal{M} - M_3(1-c_3)]\,u &= [M_1(1-c_1)-M_2(1-c_2)]\,\upsilon\end{aligned} \tag{4.58}$$

and following from this system equations

$$\begin{gathered}\theta = \arctan\left(\frac{u}{\upsilon}\tan\alpha\right),\\ \mu_-\sin^2\alpha u^4 + \left[\mu_3^2(1-\upsilon^2) + \mu_-^2(\upsilon^2\cos^2\alpha - \sin^2\alpha)\right]u^2 - \mu_-^2\upsilon^2\cos^2\alpha = 0.\end{gathered} \tag{4.59}$$

Hence, we can numerically obtain the angles $\beta_{1,2}$ as functions of μ_i, υ and α. Taking an integration over the values of α from 0 to the maximal value of α_{cr} (the angle at which the junction still can be created) we average over all possible collisions that lead to junction production. It should be noticed that when we integrate over all possible angles, we need to take into account the multiplier in the form of $\sin\alpha$, which comes from possible string orientations (the same as it was in (4.15)). For velocity we use the distribution in the form of a delta function centred in the rms velocity value.

Carrying out numerical calculations for the average values of angles $\beta_{1,2}$, we build the plot of the angle dependence on the rms velocity. In figure 4.11 we show the averaged value of β (for $\mu_1 = \mu_2$) and β_1, β_2 (when $\mu_1 \neq \mu_2$) depending on rms velocity υ of the string network. The results for the average angles β_1 and β_2 are going to be used as initial values for the subsequent dynamics of junctions in the string network.

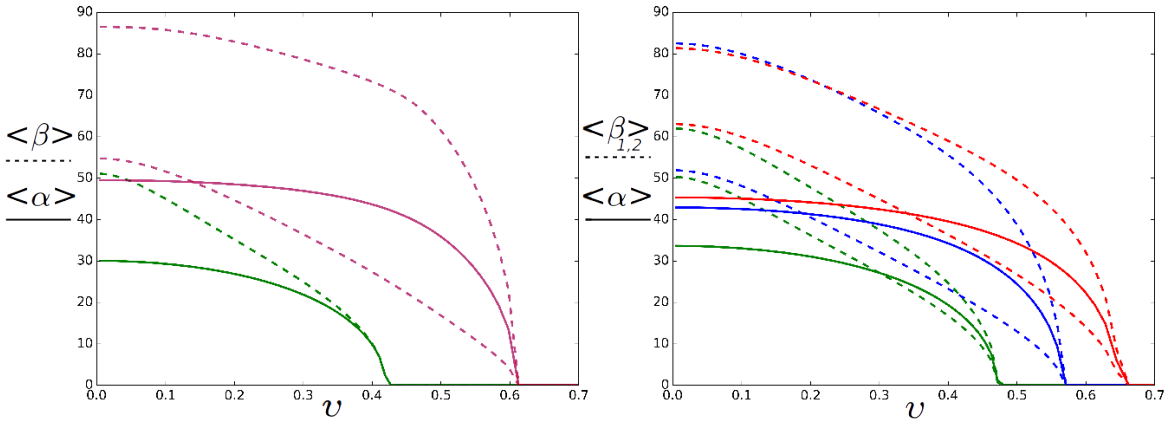

Fig. 4.11 Averaged values of angles for string configurations as shown in figure 4.10. The left panel shows calculations for $\mu_1 = \mu_2 = 1$, $\mu_3 = 1.4$, i.e. collisions of $1,2$ (green line) and $2,3 = 1,3$ (purple line) pairs of strings. The right panel demonstrates the situation for $\mu_1 = 1$, $\mu_2 = 1.2$ and $\mu_3 = 1.4$, i.e. collisions of $1,2$ (green line), $1,3$ (blue line) and $2,3$ (red line) pairs of strings. By solid lines we show average angles of string collisions that lead to junction production α. The dashed lines denote the average angles $\beta_{1,2}$.

4.2.2 Correlation function of ingoing components, small-scale structure

To understand how much junctions can grow in the string network, we need to figure out the average scalar product behaviour $h_i = 1 - \varepsilon_{ijk} < \mathbf{p}_j \cdot \mathbf{p}_k >$. In other words we need to study how these scalar products depend on junction growth in equations (4.38)

$$\langle \varepsilon_i \dot{s}_i \rangle = 1 - \frac{\mu M_i h_i}{\mu_i \mathcal{M}}, \tag{4.60}$$

where $\langle ... \rangle$ is the averaging along the string network.

To approach this problem, we can study the scalar product $< \mathbf{p}(x_1)_i \cdot \mathbf{p}(x_2)_i >$ dependence on the distance $l = x_2 - x_1$. This problem was studied numerically and analytically in a number of papers [99, 160, 161, 177–180]. Let's revisit these studies and emphasize the important points for further investigation.

Let's recall the definition of ε and notice that this variable depends on the σ parametrization. In this way, if the length of the string is reduced by a factor $p = \sigma/\tilde{\sigma}$, we have the following relation

$$\varepsilon(\tilde{\sigma}) = \sqrt{\frac{\partial_{\tilde{\sigma}} \mathbf{x}^2}{1 - \dot{\mathbf{x}}^2}} = \frac{\partial \sigma}{\partial \tilde{\sigma}} \sqrt{\frac{\partial_{\sigma} \mathbf{x}^2}{1 - \dot{\mathbf{x}}^2}} = p\, \varepsilon(\sigma). \tag{4.61}$$

We see that the equation of motion (2.4) is invariant under the transformation (4.61) if the multiplier p is a constant. However, if p is a time dependent function, there will be an additional contribution in the form

$$\dot{\varepsilon}_i + 2\frac{\dot{a}}{a}\varepsilon_i \dot{\mathbf{x}}_i^2 + \frac{\dot{p}}{p}\varepsilon_i = 0. \tag{4.62}$$

To estimate the ratio $\frac{\dot{p}}{p}$ we should remember that it is proportional to the string energy, i.e. the bigger p is, the more energy the string has. Using the effective chopping parameter to describe the average possibility for one string to lose the energy due to loops production, we can conclude that

$$\frac{\dot{p}}{p} = \frac{\dot{\rho}}{\rho}\Big|_{\text{loops}} = c\frac{|v|}{L}, \tag{4.63}$$

where in the last equality we used the usual contribution to the energy loss from the loop production mechanism.

Using the relation (4.63), we can include the phenomenological energy loss term at the microscopic level. In this case the equation (2.4) should be rewritten as

$$\dot{\varepsilon}_i + 2\frac{\dot{a}}{a}\varepsilon_i\dot{\mathbf{x}}_i^2 + \varepsilon_i|v_i|\frac{c_i}{L_{ci}} = 0, \tag{4.64}$$

where the length L_{ci} is the comoving distance that the string travels before a collision. This is similar to the mean free path and we will consider that it is equal to the correlation length.

It can be shown that with the new equation (4.64), one can rewrite the equations of motion for a string in terms of vectors $\mathbf{p}$ and $\mathbf{q}$ as [104]

$$\begin{aligned}
\dot{\mathbf{p}}_i + \frac{1}{\varepsilon_i}\mathbf{p}_i' &= \frac{\dot{a}}{a}\left(\mathbf{q}_i - (\mathbf{p}_i\cdot\mathbf{q}_i)\mathbf{p}_i\right) + \frac{\mathbf{q}_i+\mathbf{p}_i}{2}\sqrt{\frac{1-(\mathbf{p}_i\cdot\mathbf{q}_i)}{2}}\frac{c_i}{L_i},\\
\dot{\mathbf{q}}_i - \frac{1}{\varepsilon_i}\mathbf{q}_i' &= \frac{\dot{a}}{a}\left(\mathbf{p}_i - (\mathbf{p}_i\cdot\mathbf{q}_i)\mathbf{q}_i\right) + \frac{\mathbf{q}_i+\mathbf{p}_i}{2}\sqrt{\frac{1-(\mathbf{p}_i\cdot\mathbf{q}_i)}{2}}\frac{c_i}{L_i}.
\end{aligned} \tag{4.65}$$

In the same way as it was done in [160], we can chose the characteristic variable $s_\sigma(\tau)$ instead of σ, which is constant for ingoing waves ($\partial_{s_\sigma}\mathbf{p} = 0$). Using this new variable $s_\sigma(\tau)$, let's estimate how the orientation of the vector $\mathbf{p}_i$ is changing along the string (see figure 4.12). In particular we are interested in the average scalar product (correlation) between vectors of different length $h_i(l,t)$, as it was performed in [160]. For this purpose we are going to chose the $\mathbf{p}_i$ parametrization as $s_\sigma(\tau)$ and $s'_\sigma(\tau)$, which are separated by the physical length l. It should be noticed that the time dependence of parameter $s_\sigma(\tau)$ doesn't change equations (4.65). In order to understand how the average scalar product is evolving with time and depends on length, let's write the equation for the scalar product (further we will write s_σ instead of $s_\sigma(\tau)$ for compactness)

$$\begin{aligned}
&< \partial_\tau\left(\mathbf{p}_i(s_\sigma,\tau)\cdot\mathbf{p}_i(s'_\sigma,\tau)\right) >=\\
&= \frac{< \mathbf{q}_i(s_\sigma,\tau)\cdot\mathbf{p}_i(s'_\sigma,\tau) > + < \mathbf{p}_i(s_\sigma,\tau)\cdot\mathbf{p}_i(s'_\sigma,\tau) >}{2}|v_i|\frac{c_i}{L_i} +\\
&+ \frac{< \mathbf{q}_i(s'_\sigma,\tau)\cdot\mathbf{p}_i(s_\sigma,\tau) > + < \mathbf{p}_i(s_\sigma,\tau)\cdot\mathbf{p}_i(s'_\sigma,\tau) >}{2}|v_i|\frac{c_i}{L_i} +\\
&+ \frac{\dot{a}}{a}\Big(< \mathbf{q}_i(s_\sigma,\tau)\cdot\mathbf{p}_i(s'_\sigma,\tau) > + < \mathbf{p}_i(s_\sigma,\tau)\cdot\mathbf{q}_i(s'_\sigma,\tau) > -\\
&\qquad - < \mathbf{p}_i(s_\sigma,\tau)\cdot\mathbf{p}_i(s'_\sigma,\tau) > \left(\alpha_i(s_\sigma,\tau) + \alpha_i(s'_\sigma,\tau)\right)\Big),
\end{aligned} \tag{4.66}$$

where $\alpha =< \mathbf{p}\cdot\mathbf{q} >= 1 - 2v^2$ and $v^2 =< \dot{\mathbf{x}}^2 >$.

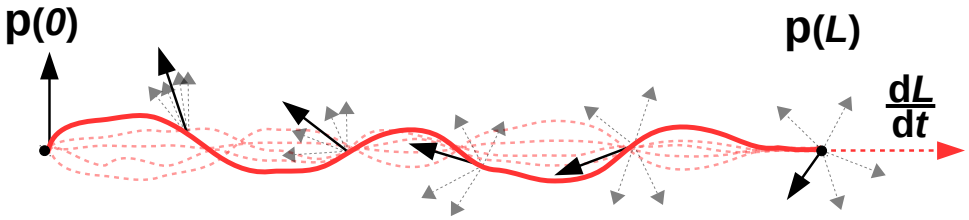

Fig. 4.12 Schematic evolution of the vector $\mathbf{p}$ along the string. Dashed lines show different possible realizations of the string and corresponding faded vectors $\mathbf{p}$. At the distance L vectors $\mathbf{p}$ in average become completely independent $< \mathbf{p}(0)\cdot\mathbf{p}(L) >= 0$. At the same time, the correlation length L is a function of time, which is anticipated to grow for expanding universe.

To treat equation (4.66) we are going to use the method from [160]. Let's consider that s_σ and s'_σ are very close to the initial $s_\sigma(0)$ and $s'_\sigma(0)$. This means that $1- < \mathbf{p}_i(s_\sigma,\tau)\cdot\mathbf{p}_i(s'_\sigma,\tau) >= O([s-s']^2)$ (we drop all terms higher than the first order $[s_\sigma - s'_\sigma]$).

The outgoing $\mathbf{q}(s_\sigma,\tau)$ and ingoing $\mathbf{p}(s'_\sigma,\tau)$ modes meet each other at the worldsheet point $(s_\sigma,\tau-\delta)$, where δ is of the order of $[s_\sigma - s'_\sigma]^3$. Hence, the product of outgoing and ingoing modes can be approximated as $< \mathbf{q}_i(s_\sigma,\tau)\cdot\mathbf{p}_i(s'_\sigma,\tau) >= \alpha_i(s'_\sigma,\tau-\delta)$. As a result, the equation (4.66) can be rewritten as

$$\partial_\tau h_i(s_\sigma,s'_\sigma,\tau) = -h_i(s_\sigma,s'_\sigma,\tau)\left(2\frac{\dot{a}}{a}\overline{\alpha}_i - \frac{|v_i|c_i}{L_i}\right) - \frac{|v_i|c_i}{L_i}(1+\overline{\alpha}_i) + O([s_\sigma - s'_\sigma]^2), \quad (4.67)$$

where $\overline{\alpha}_i = \alpha_i(s'_\sigma,\tau) + \alpha_i(s_\sigma,\tau)$.

Assuming that the scale factor is evolving according to the power law $a \propto \tau^n$, we anticipate that the correlation length is $L_i \propto \epsilon_i\tau$, where n and ϵ_i are constants. With these assumptions we can solve (4.67) and see that

$$h_i \propto \frac{g_i(s'_\sigma - s_\sigma)}{\tau^{2n\overline{\alpha}_i - |v_i|c_i/\epsilon_i}}. \quad (4.68)$$

At the same time, with established assumptions from the equation (4.64) we can notice that

$$\varepsilon_i \propto \tau^{-2nv_i^2 + |v_i|c_i/\epsilon_i} \quad (4.69)$$

and

$$\frac{s_\sigma}{\tau} = \frac{\varepsilon_i\sigma}{\tau} \propto \frac{1}{\tau^{1+2nv_i^2-|v_i|c_i/\epsilon_i}}. \quad (4.70)$$

Following [160] we can define the form of the function $g_i(s_\sigma - s'_\sigma)$ from the equation (4.69) and rewrite (4.68) as

$$h_i \propto \left(\frac{\ell_s}{t}\right)^{2\chi_i}, \quad (4.71)$$

where $\chi_i = \frac{2n\overline{\alpha}_i - \kappa_i}{1+2nv_i^2-\kappa_i}$ with $\kappa_i = \frac{|v_i|c_i}{2\epsilon_i}$, the length of a segment $\ell_s = a\int \varepsilon d\sigma$ (with the assumption that ε depends only on time).

Comparing this result (4.71) with the result from [160], we see that due to including the loop production term, we have an additional component κ_i. At first sight it seems that the χ_i can become negative due to κ_i. However, when we use data from network simulations and recall that the c_i should be length dependent ($\kappa_i \to 0$ when $l \to 0$) with a value smaller than the full chopping parameter ($c_i < 0.23$), we see that negative χ_i is not realised for the matter and radiation dominated eras.

We should remember that the treatment described is just an approximation, which is valid within a specific range of scales. If we consider the smallest scales, where loop production is insignificant, we will be faced with kink domination. In that case, as it was shown in [161], the correlator h_i has the following behaviour

$$h_{i\,kink} \propto \left(\frac{\ell_s}{t}\right). \tag{4.72}$$

The relation (4.72) can be slightly changing during the network evolution. However, we do not anticipate significant corrections when the network reaches the scaling regime.

For scales larger than the correlation length, $\ell/t > 1$, the correlation h_i reaches unity. We are interested in finding an estimate function that can mimic all ranges of ℓ/t for the correlator function h_i. Let's call the estimate function $h(\ell/t)$ (see figure 4.13).

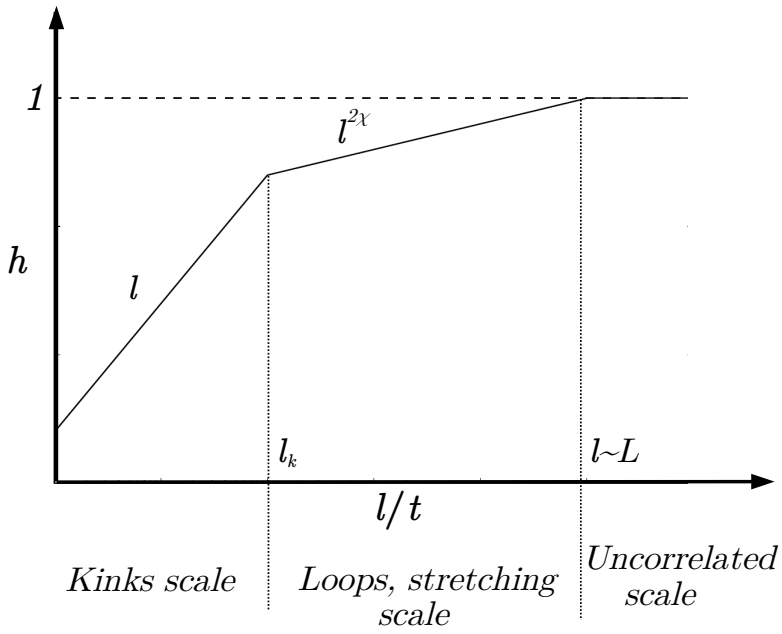

Fig. 4.13 Logarithmic scale for the function $h(\ell/t)$, which shows how the correlation between vectors decreases with distance ℓ. On small sales the function should be linear $h \propto \ell/t$. Then it becomes a power law $h \propto (\ell/t)^{2\chi}$. Eventually the function h becomes constant 1 when the distance $\ell \sim L$, where L is the correlation length.

Junction rates for the scaling string network

In the previous section we estimated the behaviour of the correlation function $h(\ell/t)$ on a string. Now, using this result, we are ready to study the junction evolution when the string network reaches the scaling regime, i.e. when the correlation length and velocity behave as $L \propto \epsilon\tau$, $\upsilon = \text{const}$. To do so, we use the average equation (4.60), where functions h_i are described by the approximated function shown in figure 4.13.

The change of conformal length for strings we define as

$$\Delta\ell_c = \dot{s} \int \varepsilon d\sigma. \tag{4.73}$$

Using the definition (4.73) one can rewrite (4.60) in the following way

$$\Delta\dot{\ell}_{i\,c} = 1 - \frac{\mu M_i h_i(\ell_{j\,c}/\tau, \ell_{k\,c}/\tau)}{\mu_i \mathcal{M}}, \tag{4.74}$$

where indices j and k are connected with index i by permutation as $|\varepsilon_{ijk}|$, which means that when $i = 1$ index $j = 2$ and $k = 3$.

We should keep in mind that we apply the dynamics of the correlation function h to the point where three strings are connected. This means that instead of focusing on the correlation function on a single string, we study the correlation between vectors on different strings. Let's assume that the decrease of the correlation function depends only on the corresponding correlation length of the string. Equivalently we are making the assumption that the small-scale structures on all strings are similar.

The important difference between correlation functions on one string and different strings is that the correlation function initially in the first case is equal to unity, while on different strings it can be smaller (which is usually the case). The initial value of the correlation function for collided strings was studied in section 4.2.1, and it depends only on the relative velocity of the colliding strings and their tensions.

Combining all results together, we can calculate how the junction will grow/decrease on average with the assumption of the scaling network regime. It is useful to rewrite equation (4.60) in the following way

$$\begin{aligned}\Delta\dot{\ell}_{i\,c} = 1 - \frac{\mu M_i}{\mu_i \mathcal{M}} h_{0\,i}(\upsilon)\Big[\eta_1 \Theta(\ell_k - \Delta\ell_{i\,c}) \left(\frac{\Delta\ell_{i\,c}}{\tau}\right) + \\ + \eta_2 \Theta(\Delta\ell_{i\,c} - \ell_k)\Theta(L - \Delta\ell_{i\,c}) \left(\frac{\Delta\ell_{i\,c}}{\tau}\right)^{2\chi_i} + \Theta(\Delta\ell_{i\,c} - L)\Big],\end{aligned} \tag{4.75}$$

where $\eta_{1,2}$ are constants that provide the continuity of the correlation function, while $h_{0\,i}(\upsilon)$ is the initial value of the function h.[6]

We chose the string tensions as $\mu_1 = 1$, $\mu_2 = 1.2$ and $\mu_3 = 1.4$. Each collision of the 1 and 2 strings leads to increase of the 3 string length. To understand how much it can grow,

[6]The initial value of h is calculated from the geometry of strings (see figure 4.10), taking into account that initial average angles are given by integration of (4.57) and demonstrated in figure 4.11

we need to use the average initial angle for such collisions, see figure 4.11 (right panel) - green line. Fixing the rms velocity and correlation length (for simplicity we have chosen to be $\upsilon = 0.5$, $L = \tau$ for all strings), we can obtain the values of s_i from the expression (4.75). Conducting calculations for this type of collisions we obtain the result shown in figure 4.14 by thin solid lines (all blue colors correspond to the first string, red to the second, green to the third).

We estimated the third string growth in the process of 1 and 2 strings collision. The same treatment can be applied for collisions of 2 and 3 strings (dash-dotted lines in figure 4.14) and for collisions of 1 and 3 strings (dashed lines in figure 4.14).

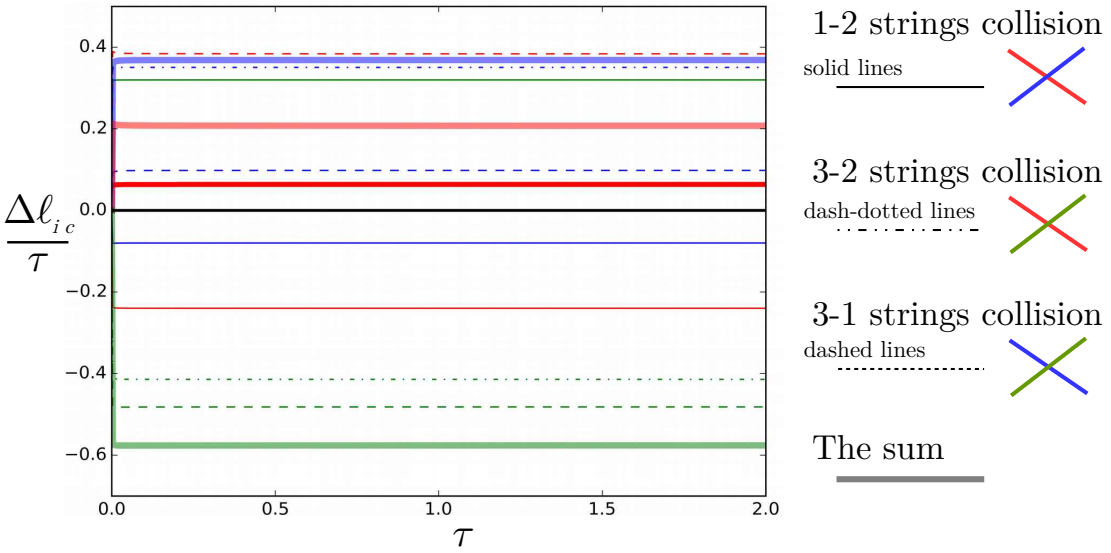

Fig. 4.14 Growth/decrease of junctions $\Delta\ell_i$ for a scaled string network $\upsilon_i = 0.5$, $L_i = \tau$, with tensions $\mu_1 = 1$, $\mu_2 = 1.2$, $\mu_3 = 1.4$. Solid lines represent the change of the length after collisions of 1-2 strings, dash-dotted of 2-3 and dashed of 1-3. Thick solid lines represent the sum of all collisions, while the black line shows the sum of all $\mu_i \Delta\ell_{i\,c}$.

4.3 VOS model for strings with dynamical junctions

As long as the preparatory work is done (sections 4.2.1 - 4.2.2), we can return to the VOS model and introduce the necessary modifications. In particular, we are aiming to obtain a model where the junction evolution is described by averaged kinematic constraints (section 4.1.3).

To achieve this goal we need to introduce energy exchange terms that correspond to dynamics of junctions. Let us calculate the probabilities of strings to meet each other and the corresponding energy densities exchange.

We can start from considering the collision of 1 and 2 strings. Let's introduce new variables Δl_i for this process, which denote changes of string length that are separated by the corresponding distances L_i. Now we can consider the probability of string j to meet a string i, which we denote as $(j \longleftrightarrow i)$ collision.

($i \longleftrightarrow i$) **probability**. In the distance L_i that is covered by the string i with velocity v_i in the time interval δt, it can meet another i string with probability $\frac{v_i}{L_i}\delta t \left(\frac{l_i}{L_i}\right)^2$, where the last multiplier appeared since the string l_i lengths are changed due to junctions and do not coincide with the correlation lengths L_i. The length l_i can be smaller or bigger than the correlation length L_i due to the junction dynamics (see figure 4.15). The change of energy density ρ_i due to loop creation is proportional to each type of energy density. Hence, taking into account the probability to create a loop of a given size by a constant parameter c, the whole term can be written as

$$c\frac{v_i}{L_i}\left(\frac{l_i}{L_i}\right)^2 \rho_i \delta t. \tag{4.76}$$

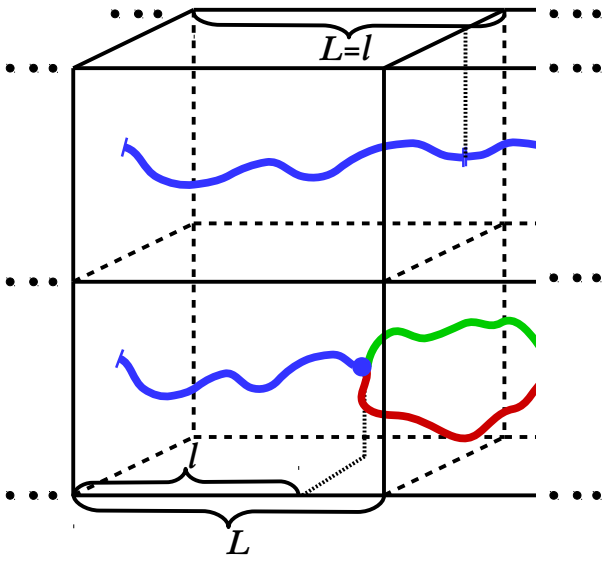

Fig. 4.15 Schematic picture of strings, where the difference between real length l and correlation length L due to the presence of a junction is demonstrated. In the top panel the usual string can be seen, with $l = L$, while on the bottom panel the junction presence is taken into account $l \neq L$.

($1 \longleftrightarrow 2$) **probability**. The probability of a string segment with length L_2, which is moving with relative velocity $v_{12} = \frac{v_1+v_2}{2}$, to collide with strings that possess lengths L_1 and are separated by distance L_1 during the time δt was calculated in [44] and has the form $\frac{v_{12}}{L_1}\frac{L_2}{L_1}\delta t$. Taking into account that in the volume $(L_1)^3$ on average there are $\left(\frac{L_1}{L_2}\right)^3$ strings of the 2nd type, the probability is then $\frac{v_{12}}{L_1}\frac{L_2}{L_1}\left(\frac{L_1}{L_2}\right)^3\delta t$. Hence, from each collision the 1st, 2nd and 3rd types of strings obtain/lose on average the following amount of energy density: $\Delta l_1/L_1^3$, $\Delta l_2/L_1^3$ and $\Delta l_3/L_1^3$ correspondingly. Until this moment we mostly repeated considerations of [44]. There should be introduced additional factors due to the fact that the real length l can be smaller/larger than the correlation length L. Taking into account the multiplier for the probability of interaction, we can conclude that the final energy exchange

in $(1 \longleftrightarrow 2)$ collision process has the form

$$\mathcal{P}_{12}(v_{12})^{1/3}\frac{v_{12}}{L_1}\frac{L_2}{L_1}\left(\frac{L_1}{L_2}\right)^3\frac{l_1}{L_1}\frac{l_2}{L_2}\frac{\Delta l_i}{L_1^3}\delta t, \tag{4.77}$$

where $\mathcal{P}_{12}$ is given by equation (4.15) for 1 and 2 strings and the index in Δl_i shows which type of string is affected by the junction energy exchange, the power 1/3 was chosen as a result of numerical simulation [181].

Similarly we can write terms for $(1 \longleftrightarrow 3)$ and $(2 \longleftrightarrow 3)$ collisions. As a result, we write the general form for the junction energy exchange for $(k \longleftrightarrow m)$ string collision:

$$\mathcal{P}_{km}(v_{km})^{1/3}v_{km}\frac{l_k}{L_k^3}\frac{l_m}{L_m^3}\Delta l_i\delta t. \tag{4.78}$$

Since the length of the string l and correlation length L are not the same, the relation between energy density and correlation length should be modified. We will hold the Brownian approximation for each string (2.12). We assume that while the length of string decreases, the string is still Brownian, but not on the whole correlation length. Hence, modifications to the energy density relations can be introduced in the form of a multiplier

$$\rho_i = \mu_i\frac{l_i}{L_i^3}. \tag{4.79}$$

Taking the time derivative we obtain the relation

$$\frac{d\rho_i}{dt} = \rho_i\left(\frac{1}{l_i}\frac{dl_i}{dt} - 3\frac{1}{L_i}\frac{dL_i}{dt}\right). \tag{4.80}$$

If there are no junctions the network evolves as standard VOS model described in chapter 2, which is why we can assume that

$$\frac{1}{l_i}\frac{dl_i}{dt} = \frac{1}{L_i}\frac{dL_i}{dt} + J_i, \tag{4.81}$$

where functions $\rho_i J_i$ represent the junction dynamics estimated above as $(k \longleftrightarrow m)$ collisions. As a result, we end up with the following terms responsible for energy loss/exchange

$$\begin{aligned}\frac{d\rho_i}{dt}\Big|_{\text{loops}} &= c\frac{v_i}{L_i}\left(\frac{l_i}{L_i}\right)^2\rho_i,\\ \frac{d\rho_i}{dt}\Big|_{\text{junctions}} &= -\mathcal{P}_{km}(v_{km})v_{km}c\frac{l_k}{L_k}\frac{l_m}{L_m}\frac{\mu_i\Delta l_i}{L_k^2L_m^2},\end{aligned} \tag{4.82}$$

where henceforth we will use $\mathcal{P}_{km}$ as $\mathcal{P}_{km}(v_{km})$ for convenience.

Collecting all factors mentioned above, we can write the equations for correlation lengths L_i, real lengths l_i, rms velocities v_i and junction dynamics Δl_i

$$\begin{aligned}
\dot{L}_{ci} &= \frac{\dot{a}}{a} v_i^2 L_{ci} + \frac{c}{2} v_i \left(\frac{l_{ci}}{L_{ci}}\right)^2 \mathcal{P}_{ii}^{1/3}, \\
\dot{l}_{ci} &= \frac{\dot{a}}{a} v_i^2 l_{ci} + \frac{c}{2} v_i \left(\frac{l_{ci}}{L_{ci}}\right)^3 \mathcal{P}_{ii}^{1/3} + \frac{c}{2} \sum_p |\varepsilon_{pkm}| \mathcal{P}_{km} v_{km} \frac{l_{ck}}{L_{ck}^3} \frac{l_{cm}}{L_{cm}^3} \Delta l_{ci} L_{ci}^3, \\
\dot{v_j} &= (1 - v_j^2) \left(\frac{k(v_j)}{L_{cj}} - 2 v_j \frac{\dot{a}}{a}\right), \\
\Delta \dot{l}_{cj} &= 1 - \frac{\mu M_i h_i (\Delta l_j / L_j, \Delta l_k / L_k)}{\mu_i \mathcal{M}}.
\end{aligned} \tag{4.83}$$

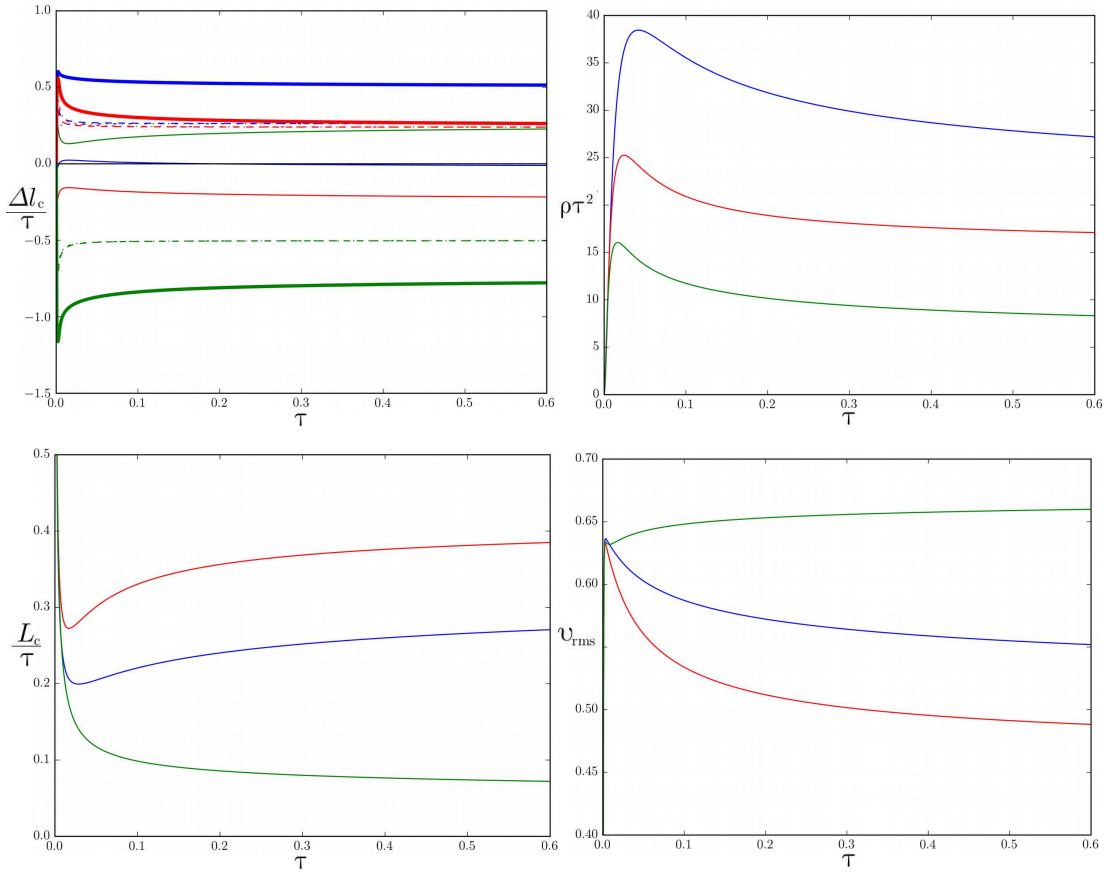

Fig. 4.16 Set of plots representing the numerical solution of equations 4.83. They represent the main macroscopic characteristics of the superstring network in the matter-dominated era, such as junction growth Δl_c (using the same notation as in figure 4.14), energy density ρ, correlation length L_c and rms velocity $v_{\rm rms}$. All green lines are related to the heaviest type of strings, red to the middle one and blue lines correspond to the lightest type of strings. It is seen that the superstring network reaches scaling behaviour.

To study the superstring network dynamics we consider three types of strings whose tensions are connected by relation (1.69) (when $C_0 = 0$) with coupling constant $g_s = 0.8$. For

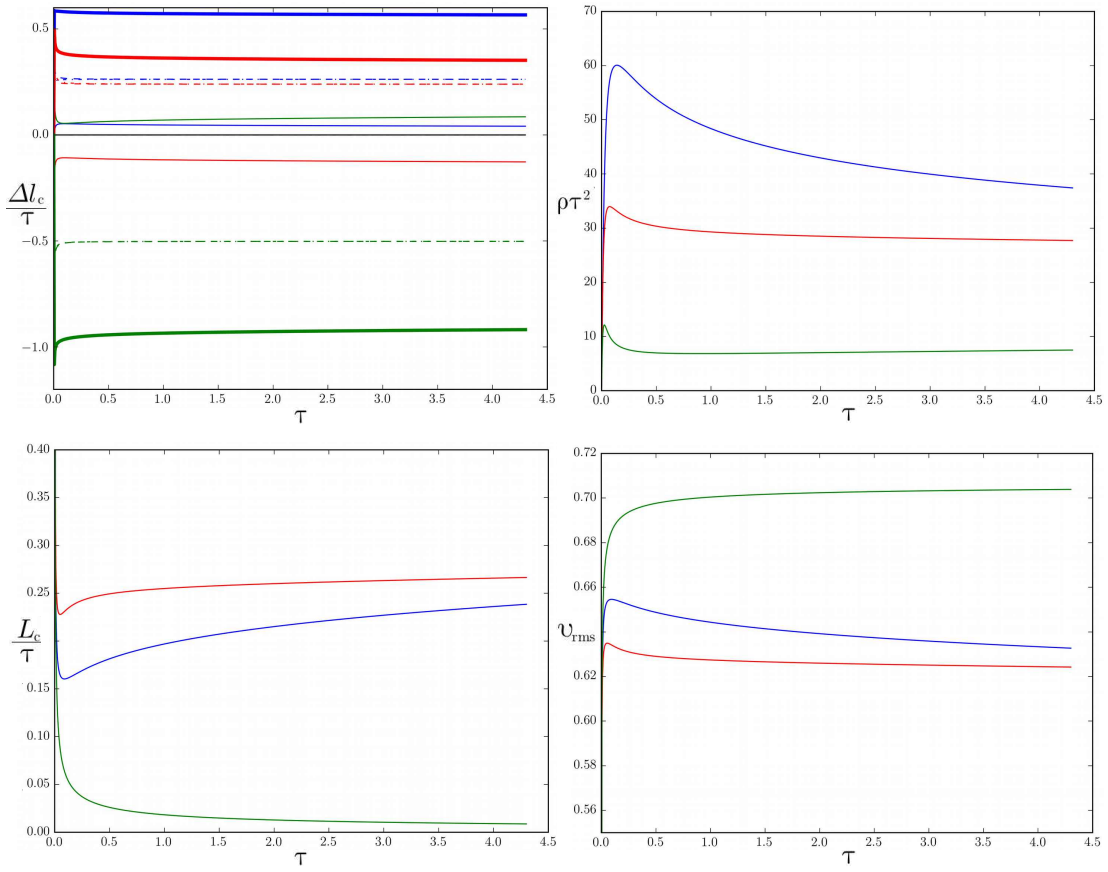

Fig. 4.17 Set of plots representing the numerical solution of equations 4.83. They represent the main macroscopic characteristics of the superstring network in the radiation-dominated era, such as junction growth Δl_c (using the same notation as in figure 4.14), energy density ρ, correlation length L_c and rms velocity v_{rms}. All green lines are related to the heaviest type of strings, red to the middle one and blue lines correspond to the lightest type of strings. It is seen that the superstring network reaches scaling behaviour.

these strings we calculate the corresponding probabilities of interactions (see section 4.1.1) and average them over all possible angles and velocities of collisions with Gaussian distribution (choosing the variance $\sigma_v^2 = 0.25$). To consider the junction dynamics we find average values of angles just after string collisions (see section 4.2.1). These angles provide initial values of the correlation function described in the section 4.2.2. All these computations produce the necessary functions for the system of differential equations (4.83). To make calculations faster we use an approximation for the correlation function h and for the probability of interaction $\mathcal{P}$. Setting the chopping parameter as $c = 0.23$ for the matter-dominated era, we find a scaling behaviour of the network, see figure 4.16. For comparison, scaling solutions for the radiation-dominated era are shown in figure 4.17.

4.4 Summary

In this section we revisited cosmic string collisions in detail. We started from a review of string interactions and kinematic constraints for junctions production. In particular, we studied the generalization of straight string collisions for the FLRW metric. As was anticipated the approach developed in [85, 155, 156] is applicable to the FLRW metric (as it was studied for loops [159]). Hence, we studied how the junction dynamics locally can be affected by the expansion of the universe. In addition we investigated the situation when strings with currents are colliding. In order to do so we estimated the solution for a straight string with a chiral current. This allowed us to apply the analyses of [85] to strings with chiral currents. We revealed the same problem for strings with currents as in the paper [173], i.e. the presence of currents can lead to overdetermined evolution equations. However, this is not the case when identical strings are colliding. This particular scenario we studied in detail and we found how the current affects the allowed region for the junction production.

The ability of strings to create junctions should influence the evolution of a string network. The second part of this chapter was devoted to the study of averaged properties of strings collisions and evolution of a superstring network. We studied the dependence of string configurations (angles between strings, see figure 4.10) on string tensions that should appear on average just after strings collisions. To understand the reason why junctions should unzip, i.e. change their dynamics, we connected the equation for the junction dynamics with the correlation function along the string. As it was seen, the junction can start unzipping due to string curvatures (for loops unzipping see [182]), wiggles that are encoded in the correlation function. Using averaged probabilities of interactions, correlation functions and velocity dependent configurations of angles, we introduced modifications that should be taken into account for superstring network consideration. As a result, we provided a full the VOS model for superstring networks that includes dynamics of junctions.

Chapter 5

Observational signals from cosmic strings

5.1 Cosmic Microwave Background

Up till now we were developing the quantitative description of the network structure and evolution of cosmic strings. These improvements are necessary to obtain more accurate predictions of the possible observational signals from string networks. The more accurate the observational signal becomes, the more clear it will be to establish scenarios of the early universe are realistic. Until today, there is no observational evidence for the presence of cosmic string networks [1]. There are different ways to testify cosmic string existence by observational signals, such as gravitational lensing [185], imprints on CMB maps [186, 187] (see [188] for a detailed description) including the CMB anisotropy [13, 189–191] and gravitational waves [192–194].

In this section we review the main observational capabilities that can indicate the existence of cosmic strings. In particular we provide a description of the CMB and stochastic gravitational background anisotropies as an outcome of cosmic string network presence.

Implementing the improvements on the cosmic string network description, given in section 3, we study possible alterations of the predictions of CMB anisotropies from cosmic strings. In particular, introducing the appropriate adjustments to the CMBact code [143][2], we investigate the influence of nontrivial internal structure of strings on CMB anisotropies.

5.1.1 Thermal History

According to the "hot big bang" scenario, the universe at the early stages of its evolution had a sufficiently high temperature to be filled with a primordial plasma, ylem [195, 196]. This period is characterized by the domination of relativistic particles (radiation-dominated era,

[1] Some excitement of possible cosmic string detection was raised in 2003 [183], which was later disproved by an independent and more accurate observation [184]

[2] The CMBact is an open access code written in Fortran.

see section 1.2) that are in thermal and chemical equilibrium (a temperature higher than few MeV provides thermal and chemical equilibrium for baryons, leptons and photons [197])[3].

To describe the primordial plasma in thermal equilibrium, one can use the phase space one-point distribution function in the following form

$$f(\mathbf{p}) = \frac{1}{\mathrm{e}^{(E(\mathbf{p})-\mu_{ch})/T_K} \pm 1}, \tag{5.1}$$

where μ_{ch} is the chemical potential, T_K is the absolute temperature, $E(\mathbf{p}) = \sqrt{\mathbf{p}^2 + m^2}$, while the " + " sign refers to Fermi-Dirac and the " − " sign to Bose-Einstein statistics.

As long as we consider particles in chemical equilibrium, the total sum of chemical potentials in (5.1) is vanishing, $\mu_{ch} = 0$. Integrating the function (5.1) one can obtain useful macroscopic quantities [198]

$$\begin{aligned} \text{number density: } n &= \frac{g}{(2\pi)^3}\int f(\mathbf{p})d^3\mathbf{p}, \\ \text{energy density: } \rho &= \frac{g}{(2\pi)^3}\int E(\mathbf{p})f(\mathbf{p})d^3\mathbf{p}, \\ \text{pressure: } P &= \frac{g}{(2\pi)^3}\int \frac{\mathbf{p}^2}{3E(\mathbf{p})}f(\mathbf{p})d^3\mathbf{p}, \end{aligned} \tag{5.2}$$

where g is the number of internal degrees of freedom.

Substituting (5.1) with $\mu_{ch} = 0$ to (5.2) it is possible to evaluate these integrals for non-relativistic ($T_K << m$) and ultrarelativistic ($T_K >> m$) limiting cases

$$\begin{array}{lll} & \textbf{non-relativistic} & \textbf{ultrarelativistic} \\ n = & g\left(\frac{mT_K}{2\pi}\right)^{3/2}\mathrm{e}^{-m/T_K}, & \begin{cases}\text{boson: } g\frac{\zeta(3)}{\pi^2}T_K^3 \\ \text{fermion: } g\left(\frac{3}{4}\right)\frac{\zeta(3)}{\pi^2}T_K^3\end{cases}, \\ \rho = & g\,m\left(\frac{mT_K}{2\pi}\right)^{3/2}\mathrm{e}^{-m/T_K}, & \begin{cases}\text{boson: } g\frac{\pi^2}{30}T_K^4 \\ \text{fermion: } g\left(\frac{7}{8}\right)\frac{\pi^2}{30}T_K^4\end{cases}, \\ P = & g\,T_K\left(\frac{mT_K}{2\pi}\right)^{3/2}\mathrm{e}^{-m/T_K}, & \begin{cases}\text{boson: } \frac{g}{3}\frac{\pi^2}{30}T_K^4 \\ \text{fermion: } \frac{g}{3}\left(\frac{7}{8}\right)\frac{\pi^2}{30}T_K^4\end{cases}, \end{array} \tag{5.3}$$

where ζ is the Riemann zeta function.

With the help of equations (5.3), one can check that the following relation holds

$$dP = \frac{\rho + P}{T_K}\,dT_K. \tag{5.4}$$

Using the second law of thermodynamics $T_K dS = dU + PdV$ (where S is the entropy, V is the volume and $U = \rho V$) together with the relation (5.4) one can show the conservation of

[3]For simplicity, the Boltzmann constant is set to unity. As a result, we directly compare the value of energy with a temperature.

the entropy

$$\frac{dS}{dt} = \frac{d}{dt}\left[V\frac{\rho+P}{T_K}\right] =$$
$$= \frac{V}{T_K}\left(\underbrace{\left[\frac{d\rho}{dt} + \frac{1}{V}\frac{dV}{dt}(\rho+P)\right]}_{(1.8)=0} + \underbrace{\left[\frac{dP}{dt} - \frac{\rho+P}{T_K}\frac{dT_K}{dt}\right]}_{(5.4)=0}\right) = 0. \tag{5.5}$$

From entropy conservation (5.5) and equations (5.3) it follows that the temperature of particles in the expanding universe falls as

$$T_K \propto a^{-1}. \tag{5.6}$$

Hence, as the universe expands the temperature of the plasma decreases. To see which particles give the largest contribution to the energy density a given time, we can notice that in (5.3) the energy density of the non-relativistic species is exponentially small. As a result, the biggest contribution to the total energy density comes from the relativistic particles, radiation. In this way, the total energy density can be approximated as the sum over all relativistic species

$$\rho_r = \sum_i \rho_i = \frac{\pi^2}{30} T_K^4 g_*(T), \tag{5.7}$$

where T_K is the temperature of the photon gas and g_* is the effective number of degrees of freedom.

The effective number of degrees of freedom consists of boson and fermion components which can have corresponding temperatures T_{Ki}[4]

$$g_* = \sum_i g_i \left(\frac{T_{Ki}}{T_K}\right)^4 + \frac{7}{8}\sum_i g_i \left(\frac{T_{Ki}}{T_K}\right)^4. \tag{5.8}$$

When the temperature drops, according to (5.6), to a value smaller than the mass of a particle species ($m < T_K$), this type of particle becomes non-relativistic. Eventually, these particles are removed from the sum (5.7) and do not contribute to the effective degree of freedom. The larger the mass of a particle, the earlier this particle becomes non-relativistic. If the equilibrium condition held at all times, the universe would be mostly filled by photons, since massive particles are exponentially suppressed. To understand why it is not the case, we need to look at the particle interaction rate

$$\Gamma_{int} = n\sigma_{int}\upsilon, \tag{5.9}$$

where σ_{int} is the cross section of particle interactions.

[4] A complete table of effective degrees of freedom depending on a temperature for different particles can be found in [198]

As long as the interaction rate Γ_{int} is bigger than the expansion rate H, particles stay in thermal equilibrium. But when the interaction rate Γ_{int} becomes smaller than H, particles decouple from thermal equilibrium. Decoupled particles *freeze-out*, which means that the following equality holds $n(T_F)a^3 = \text{const.}$, where T_F is the freezing temperature of the corresponding particle species. The value of $n(T_F)$ strongly depends on whether the particle's freezing temperature T_F is relativistic or non-relativistic.

Let's consider the moment when photons decoupled from the matter, recombination of the hydrogen atom. As it is known, the binding energy of the ground state in hydrogen atom is $E_b = 13.6eV$. In order to calculate at which temperature decoupling took place, we can use the Saha equation [199]

$$\frac{1 - X_e}{X_e^2} = \frac{2\zeta(3)}{\pi^2}\eta_{b\gamma}\left(\frac{2\pi T_K}{m_e}\right)^{3/2} \mathrm{e}^{E_b/T_K}, \tag{5.10}$$

where the baryon-to-photon ratio is given as $\eta_{b\gamma} = n_b/n_\gamma \sim 5 \cdot 10^{-10}$, the electron-baryon ratio $X_e = \frac{n_e}{n_b} = 10^{-2}$ is chosen in a such way that 99% of electrons are in the binding state[5].

From equation (5.10) one can find the temperature of hydrogen recombination, $T_{Rec} = 0.27eV \approx 3100K$. Using equations (5.6) and (1.14) together with the current value of temperature $T_0 = 2.725K$, one can see that the recombination redshift is around $z_{rec} \approx 1137$. This means that at the redshift z_{rec} photons experienced last scattering and started to travel freely in space. This photon radiation, emitted from the hot universe due to stretching of the wavelength (1.14) is detected today in the microwave range, and is called as the cosmic microwave background.

5.1.2 CMB anisotropies

As it was described in the previous section, decoupled photons after the recombination moment travel through the universe and are observed as a CMB. The result of observations reveal that the CMB radiation is highly isotropic (temperature for any direction in the sky map is almost the same $T_0 \approx 2.7K$) with an almost perfect black body spectrum. Small inhomogeneities, as it was predicted by [201–203], appear in the CMB map only on the level 10^{-5}. Measurements of such small temperature fluctuations were accomplished by a range of missions, such as COBE [204], WMAP [205] and Planck [206]. The study of the CMB anisotropies provide a precise method to constraint cosmological scenarios [2].

Let's review the basic phenomena that cause CMB anisotropies. To do so, we start from the consideration of metric perturbations on a flat FLRW background. As it was shown, it is possible to decompose perturbations for scalar, vector and tensor modes and treat them separately [207]. The vector perturbations rapidly decay in the expanding universe[6]. Let's consider scalar perturbations encoded in the line element. In the Newtonian gauge we can

[5] For more detailed and accurate description see [200]

[6] A comprehensive description of perturbations evolution is given in [208]

write the metric as

$$ds^2 = a(\tau)^2 \left[(1+2\Psi)d\tau^2 - (1-2\Phi)\delta_{ik}dx^i dx^k\right], \tag{5.11}$$

where Ψ is a Newtonian gravitational potential and Φ represents scalar density perturbations. In the case when the energy-momentum tensor is isotropic, the following relation takes place $\Psi = \Phi$.

Substituting the perturbed metric (5.11) with a perturbed energy-momentum tensor (1.4)

$$\delta T^\mu_\nu = (\delta P + \delta\rho)\, U^\mu U_\nu + (P+\rho)\,(\delta U^\mu U_\nu + U^\mu \delta U_\nu) - \delta P \delta^\mu_\nu - \Pi^\mu_\nu, \tag{5.12}$$

where Π^μ_ν is the anisotropic tensor (with traceless spatial part).

Substituting (5.11) and (5.12) into Einstein equations (1.3) one obtains the evolution of small scalar fluctuations. In this way, one can obtain the equation for the overdensity parameter $\delta = \frac{\delta\rho}{\rho}$ and the equation for the peculiar velocity divergence θ in Fourier space [209]

$$\begin{aligned} \dot\delta &= -(1+\omega)\left(\theta - 3\dot\Phi\right), \\ \dot\theta &= -\frac{\dot a}{a}(1-3\omega)\theta - \frac{\dot\omega}{1+\omega}\theta + \frac{\omega}{1+\omega}k^2\delta - k^2\sigma_\gamma - k^2\Psi, \end{aligned} \tag{5.13}$$

where $(\rho+P)k^2\sigma_\gamma = (k^i k_j - \frac{1}{3}\delta^i_j)\Pi^j_i$ and k^i are wave vectors of the corresponding Fourier space. The equations (5.13) were obtained under the assumption that perturbations are isentropic (adiabatic and reversible).

To study the temperature fluctuation ΔT_K, whose direction on the CMB map is given by a unit vector $\mathbf{n}$, it is useful to make a spherical harmonics expansion

$$\Delta T_K(\mathbf{n}) = \sum_{lm} a_{lm} Y_l^m(\mathbf{n}), \tag{5.14}$$

where $Y_l^m(\mathbf{n})$ are spherical harmonic functions with l running over positive integers (the bigger is l the smaller the size of anisotropies) while m runs over integers from $-l$ to l.

Let's consider the simplest non-trivial average characteristic for the temperature fluctuations, whose relation to the angular power spectrum C_l can be written as

$$\langle a_{lm} a_{l'm'}\rangle = \delta_{ll'}\delta_{mm'} C_l. \tag{5.15}$$

As a result, using the relation (5.15), one can obtain the average product of separated ΔT_K in the form

$$\langle \Delta T_K(\mathbf{n}) \Delta T_K(\mathbf{n}')\rangle = \sum_l C_l \left(\frac{2l+1}{4\pi}\right) P_l(\mathbf{n},\mathbf{n}'), \tag{5.16}$$

where P_l denotes Legendre polynomials.

Since we observe the CMB anisotropies only from one location it is not possible to make an average over different positions of view. Hence, the observed $C_l^{\rm obs}$ is actually an average over the values m, which means that

$$C_l^{\rm obs} = \frac{1}{2l+1}\sum_m |a_{lm}|^2. \tag{5.17}$$

The difference between the observed (5.17) and theoretical (5.15) values, called *cosmic variance*, determines the limit of accuracy with which it is possible to measure C_l [200]

$$\left\langle \frac{C_l - C_l^{\rm obs}}{C_l} \right\rangle^2 = \frac{2}{2l+1}. \tag{5.18}$$

To describe photon fluctuations one can use the kinetic equations for the distribution of photons f_γ. Since the photon energy is smaller than the mass of the electron around the time of recombination, the collision term is described by the Thomson scattering. Hence, the Boltzmann equation for the photon temperature fluctuations $\Theta_\gamma = \frac{\Delta T_K}{T_K}$ can be written as [210]

$$\begin{aligned}\frac{d}{d\tau}\left(\mathrm{e}^{-\tau_\gamma}(\Theta_\gamma+\Psi)\right) = -\dot\tau_\gamma \mathrm{e}^{-\tau_\gamma}\left(\Psi - \mathbf{n}\cdot\mathbf{v}_b + \frac{3}{16\pi}\int d\mathbf{n}'\Theta_\gamma(\mathbf{n}')\left[1+(\mathbf{n}\cdot\mathbf{n}')\right]\right) + \\ + \mathrm{e}^{-\tau_\gamma}\left(\dot\Phi+\dot\Psi\right),\end{aligned} \tag{5.19}$$

where the optical depth is $\tau_\gamma = \int_{\tau_R}^{\tau} a n_e \sigma_T d\tau'$, τ_R is the (conformal) time of the recombination, σ_T is the Thomson cross-section and $\mathbf{v}_b$ is the peculiar velocity of electrons.

Numerical treatment of the equation (5.19) together with the perturbation equations (5.13) for the tightly coupled system of baryons and photons reveals good agreement between observational data and the theoretical description of the CMB anisotropies, see figure 5.1.

5.2 CMB anisotropies from cosmic strings

Among different methods for detecting observational signals from cosmic string networks, CMB anisotropies offer one of the most sensitive and robust probes [13]. Current results obtained using cosmic string network simulations [212, 213] and calibrated semi-analytic models [191] yield very similar constraints for simple global cosmic strings, the current limit on the string tension being at the level of $G\mu \lesssim 10^{-7}$. However, as discussed above, it is the latter approach that allows us to go beyond these vanilla strings and quantitatively study the observational effects of additional properties on cosmic strings.

To study the CMB signal we pay particular attention to the special cases of wiggly strings and superconducting strings. In the case of wiggly strings this generalises and extends the work of [143], where string wiggles were taken into account through a constant free parameter α. In our approach we can construct the most general model for wiggly strings, leading to a full description of wiggles, including their evolution and their effect on the string equations of motion. For superconducting strings, some of the relevant model parameters are less well

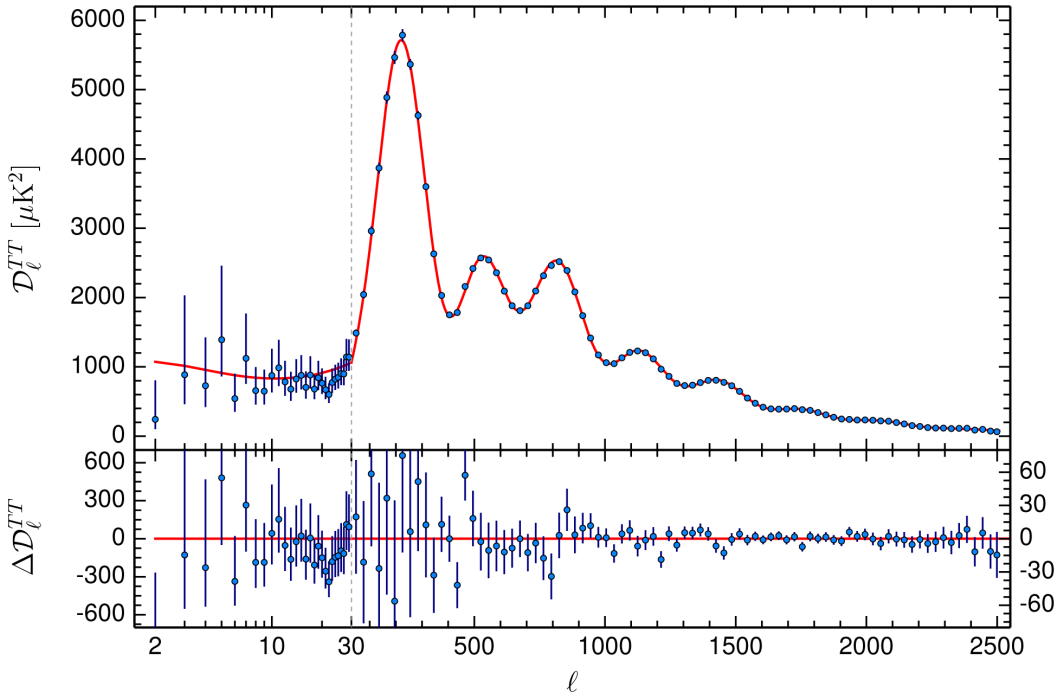

Fig. 5.1 The observational result of temperature fluctuations by Planck mission compared with the best fit ΛCDM model, where $\mathcal{D}_l = C_l(l(l+1))/(2\pi)$ [211].

known (due to the lack of numerical simulations of these models) but we are also able to provide a full description. In both cases, our results will enable a more detailed and robust comparison to observations, which we leave for future work.

We now concentrate on how modifications of cosmic string properties can influence the predictions for the CMB anisotropy. We follow the approach of [143, 214, 215]. Rather than working with the full network of cosmic strings, we consider a number of straight string segments in Minkowski space that decay according to the evolution of strings in an expanding FLRW metric, and have velocities and lengths determined by the VOS model [143, 215].

5.2.1 General approach

To consider the CMB temperature anisotropies caused by cosmic strings, we start from the Fourier transform of the energy-momentum tensor (3.18). We apply the Fourier transform to a single straight string segment on which the contribution from string currents has been averaged as above

$$\Theta^{\mu\nu} = \mu_0 \int_{-\xi_0\tau/2}^{\xi_0\tau/2} \left[\hat{U}\epsilon\dot{X}^\mu\dot{X}^\nu - \hat{T}\frac{X'^\mu X'^\nu}{\epsilon} - Q\left(\dot{X}^\mu X'^\nu + \dot{X}^\nu X'^\mu\right)\right] \mathrm{e}^{i\mathbf{k}\cdot\mathbf{X}} d\sigma, \tag{5.20}$$

where the vector $X^\mu = x_0^\mu + \sigma X'^\mu + \tau\dot{X}^\mu$ represents the straight, stick-like solution for a string moving with velocity υ (so that $\dot{X}^\mu\dot{X}_\mu = 1 - \upsilon^2$) and with worldsheet coordinates σ and τ in the transverse temporal gauge. The comoving length of a string segment at conformal time τ is $\xi_0\tau$, where ξ_0 will be determined from the macroscopic evolution equations

(3.62-3.63). Variables $\hat{U}$, $\hat{T}$ and Q are constants for the straight string, as follows from the equations of motion (3.22-3.24). The four-vector $x_0^\mu = (1, \mathbf{x_0})$ is the random location for a single string segment, while X'^μ and $\dot{X}^\mu$ are randomly oriented and satisfy the transverse condition $X'_\mu \dot{X}^\mu = 0$. We can choose these vectors[7] as

$$\dot{X}^\mu = \begin{pmatrix} 1 \\ \upsilon(\cos\theta\cos\phi\cos\psi - \sin\phi\sin\psi) \\ \upsilon(\cos\theta\sin\phi\cos\psi + \cos\phi\sin\psi) \\ -\upsilon\sin\theta\cos\psi \end{pmatrix},$$
$$X'^\mu = \begin{pmatrix} 0 \\ \sin\theta\cos\phi \\ \sin\theta\sin\phi \\ \cos\theta \end{pmatrix}. \tag{5.21}$$

Without loss of generality we can choose the wave vector along the third axis $\mathbf{k} = k\hat{k}_3$ and integrating over σ we obtain the following expressions

$$\Theta_{00} = \frac{\mu_0 \hat{U}}{\sqrt{1-v^2}} \frac{\sin(kX_3\xi_0\tau/2)}{kX_3/2} \cos(\mathbf{k}\cdot\mathbf{x}_0 + kX_3 v\tau), \tag{5.22}$$

$$\Theta_{ij} = \Theta_{00}\Big[v^2\dot{X}_i\dot{X}_j - \hat{T}/\hat{U}(1-v^2)X'_iX'_j - vQ/\hat{U}\left(\dot{X}_iX'_j + \dot{X}_jX'_i\right)\Big], \tag{5.23}$$

where the indices i, j run over the 3-dimensional spatial coordinates.

The scalar, vector and tensor components can be defined as

$$\Theta^S = (2\Theta_{33} - \Theta_{11} - \Theta_{22})/2, \tag{5.24}$$

$$\Theta^V = \Theta_{13}, \tag{5.25}$$

$$\Theta^T = \Theta_{12}. \tag{5.26}$$

Substituting (5.22) and (5.23) in (5.24)-(5.26), we obtain the scalar, vector and tensor contributions for a straight string segment with energy-momentum tensor (3.18), (5.20)

$$\frac{2\Theta^S}{\Theta_{00}} = \Big[v^2(3\dot{X}_3\dot{X}_3 - 1) - 6vQ/\hat{U}X'_3\dot{X}_3 - (1-v^2)\hat{T}/\hat{U}(3X'_3X'_3 - 1)\Big], \tag{5.27}$$

[7]Note that although we work in the transverse temporal gauge we have chosen the normalization $\mathbf{X}'^2 = 1$. This may seem to be inconsistent as $\mathbf{X}'^2 = \epsilon^2(1-\dot{\mathbf{X}}^2)$ and ϵ is evolving according to equation (3.22). However, we are implicitly taking this effect into account by having the limits of the integral (5.20) be time-dependent through the time evolution of ξ_0. This evolves according to the macroscopic equation (3.62), which has been derived by averaging equations (3.34) and (3.22).

$$\frac{\Theta^V}{\Theta_{00}} = \left[v^2 \dot{X}_1 \dot{X}_3 - \hat{T}/\hat{U}(1-v^2) X_1' X_3' - vQ/\hat{U} \left(X_1' \dot{X}_3 + \dot{X}_1 X_3' \right) \right], \tag{5.28}$$

$$\frac{\Theta^T}{\Theta_{00}} = \left[v^2 \dot{X}_1 \dot{X}_2 - \hat{T}/\hat{U}(1-v^2) X_1' X_2' - vQ/\hat{U} \left(X_1' \dot{X}_2 + \dot{X}_1 X_2' \right) \right]. \tag{5.29}$$

Following the prescription of reference [216], we can then calculate the unequal time two-point correlators by averaging over locations, string orientations and velocity orientations of the string segment

$$\begin{aligned} &\left\langle \Theta^I(k,\tau_1)\Theta^J(k,\tau_2) \right\rangle = \\ &= \frac{2\mu_0^2 \mathcal{F}(\tau_1,\tau_2,\xi_0)}{16\pi^3} \int_0^{2\pi} d\phi \int_0^{\pi} \sin\theta d\theta \int_0^{2\pi} d\psi \int_0^{2\pi} d\chi \, \Theta^I(k,\tau_1)\Theta^J(k,\tau_2) \, . \end{aligned} \tag{5.30}$$

Here, the indices I and J correspond to the scalar, vector, tensor and "00" components. The function $\mathcal{F}(\tau_1,\tau_2,\xi_0)$ describes the string decay rate. It is chosen to have the same form as for ordinary (without currents) cosmic strings [143]

$$\mathcal{F}(\tau_1,\tau_2,\xi_0) = \frac{1}{\left(\xi_0 \mathrm{Max}(\tau_1,\tau_2)\right)^3}, \tag{5.31}$$

but here ξ_0 is determined by the modified VOS equations (3.60-3.61). The phase $\chi = \mathbf{k}\cdot\mathbf{x}_0$ arises from varying over string locations $\mathbf{x}_0$ (refer to equation (5.22)), which we integrate over.

We can write the general form of the correlators as

$$\left\langle \Theta^I(k,\tau_1)\Theta^J(k,\tau_2) \right\rangle = \frac{\mu_0^2 \mathcal{F}(\tau_1,\tau_2,\xi_0)}{k^2(1-v^2)} B^{I-J}(\tau_1,\tau_2). \tag{5.32}$$

If we are only interested in the approximation $k\tau < 1$ (superhorizon scales), we can expand B^{I-J} keeping only terms that are up to quadratic in k. In this case the non-zero correlators are the following

$$B^{00-00} \approx \hat{U}^2 \xi_0^2 k^2 \tau_1 \tau_2, \tag{5.33}$$

$$B^{S-S} \approx \frac{1}{5} \frac{B^{00-00}}{\hat{U}^2} \left(\hat{U}^2 v^4 + \hat{T}\hat{U} v^2 (1-v^2) + \hat{T}^2 (1-v^2)^2 + 3v^2 Q^2 \right), \tag{5.34}$$

$$B^{V-V} \approx \frac{1}{3} B^{S-S}, \tag{5.35}$$

$$B^{T-T} \approx \frac{1}{3} B^{S-S}. \tag{5.36}$$

In the Appendix A we give exact expressions for the equal time two-point correlators $B^{I-J}(\tau)$ and provide semi-analytic expressions for the unequal time two-point correlators, valid for all modes k (i.e. from sub-Hubble through to super-Hubble).

Having computed the correlators (5.32), let us now assume that the cosmic string network under consideration has reached a scaling regime. We can then assume that ξ_0, υ together with $\hat{U}$, $\hat{T}$ and Q do not depend on τ and σ. To obtain an analytic estimate of the string-induced CMB anisotropy, let us consider the string network evolving in the matter domination epoch ($n = 2$). For this case we can use the following solution of the linearised Einstein-Boltzmann equations [214, 217]

$$\begin{aligned} \frac{\Delta T}{T} &= -\frac{1}{2}\int_{\tau_i}^{\tau_f} d\tau \dot{h}_{ij} n^i n^j, \\ \dot{h}_{ij} &= \dot{h}^S_{ij} + \dot{h}^V_{ij} + \dot{h}^T_{ij}, \end{aligned} \tag{5.37}$$

$$\dot{h}^S_{ij} = -\rho \sum_k \mathrm{e}^{i\mathbf{k}\cdot\mathbf{x}} \int_0^\tau d\tau' \left(\frac{1}{3}\delta_{ij} \left(\frac{\tau'}{\tau}\right)^6 (\Theta^{Tr} + 2\Theta^S) - k_i k_j \left(\frac{\tau'}{\tau}\right)^4 \Theta^S \right), \tag{5.38}$$

$$\begin{aligned} \dot{h}^V_{ij} &= \sum_k \mathrm{e}^{i\mathbf{k}\cdot\mathbf{x}} \left(\dot{V}_i k_j + \dot{V}_j k_i \right), \\ \dot{V}_i &= \rho \int_0^\tau d\tau' \left(\frac{\tau'}{\tau}\right) \Theta^V_i, \end{aligned} \tag{5.39}$$

$$\begin{aligned} \dot{h}^T_{ij} &= \rho \int_0^\tau d\tau' k^3 \tau'^4 F(k\tau', k\tau) \Theta^T_{ij}, \\ F(k\tau', k\tau) &= G_1(k\tau')\dot{G}_2(k\tau) - G_2(k\tau')\dot{G}_1(k\tau), \end{aligned} \tag{5.40}$$

where $\rho = 16\pi G$, $G_1(k\tau) = \frac{\cos(k\tau)}{(k\tau)^2} + \frac{\cos(k\tau)}{(k\tau)^3}$, $G_2(k\tau) = \frac{\cos(k\tau)}{(k\tau)^3} + \frac{\sin(k\tau)}{(k\tau)^2}$, $\frac{\Delta T}{T}$ are the CMB temperature fluctuations, n^i is a unit vector defining the direction of CMB photons, and Θ^{Tr} is the trace of the Fourier transformed energy-momentum tensor.

We can now compute the angular power spectrum C_l of the CMB anisotropy using the expressions [214]:

$$C^S_l = \frac{1}{2\pi}\int_0^\infty k^2 dk \left\langle \int_0^{\tau_0} d\tau \left(\frac{1}{3}\dot{h}_1 + \dot{h}_2 \frac{d^2}{d(k\Delta\tau)^2} \right) j_l(k\Delta\tau) \right\rangle^2, \tag{5.41}$$

$$C^V_l = \frac{2}{\pi}\int_0^\infty k^2 dk l(l+1) \left\langle \int_0^{\tau 0} d\tau \dot{h}^V \frac{d}{d(k\Delta\tau)} \left(j_l(k\Delta\tau)/(k\Delta\tau) \right) \right\rangle^2, \tag{5.42}$$

$$C^T_l = \frac{1}{2\pi}\int_0^\infty k^2 dk \frac{(l+2)!}{(l-2)!} \left\langle \int_0^{\tau 0} \frac{d\tau}{(k\Delta\tau)^2} \dot{h}^T j_l(k\Delta\tau) \right\rangle^2, \tag{5.43}$$

where $\Delta\tau = \tau_0 - \tau$ (with τ_0 the value of conformal time today), $j_l(k\Delta\tau)$ are spherical Bessel functions, and $\dot{h}_1$, $\dot{h}_2$ are defined as

$$\dot{h}_1(\tau) = -\rho \int d\tau' \left(\frac{\tau'}{\tau}\right)^6 (\Theta^{Tr}(\tau') + 2\Theta^S(\tau')), \tag{5.44}$$

$$\dot{h}_2(\tau) = -\rho \int d\tau' \left(\frac{\tau'}{\tau}\right)^4 \Theta^S(\tau'). \tag{5.45}$$

We proceed by making a further approximation on the correlators (5.32). The dominant contribution to the two-point correlator is when $\tau_1 \to \tau_2$ (see for example [216]), which allows us to approximate (5.32) as

$$\left\langle \Theta^I(k,\tau_1)\Theta^J(k,\tau_2)\right\rangle = \frac{\mu_0^2 \mathcal{F}(\tau_1,\tau_2,\xi_0)}{k^2(1-v^2)} B^{I-J}(\tau_1)\delta(\tau_1-\tau_2), \tag{5.46}$$

where $\delta(\tau_1-\tau_2)$ is the Dirac delta function and $B^{I-J}(\tau_1) = B^{I-J}(\tau_1,\tau_1)$.

By using this form of the correlators (5.46) one can rewrite equations (5.41), (5.42) and (5.43) as

$$C_l^S = \frac{\kappa^2}{2\pi}\int_0^\infty k^2 dk \int_0^{\tau 0} d\tau_1 \int_0^{\tau 0} d\tau_2 \int_0^{\tau_1} d\tau_1' \frac{f(\tau_1',\xi_0)}{k^2(1-v^2)} \frac{\tau_1'^8}{\tau_1^4\tau_2^4} F_{sc}(\tau_1'), \tag{5.47}$$

$$\begin{aligned} C_l^V = \frac{2\kappa^2}{\pi}\int_0^\infty k^2 dk l(l+1) \int_0^{\tau 0} d\tau_1 \int_0^{\tau 0} d\tau_2 \frac{j_l'(k\tau_1)}{k\tau_1}\frac{j_l'(k\tau_2)}{k\tau_2} \\ \int_0^{\tau_1} d\tau_1' \frac{\tau_1'^8 f(\tau_1',\xi_0)}{k^2(1-v^2)} B^{V-V}(\tau_1'), \end{aligned} \tag{5.48}$$

$$\begin{aligned} C_l^T = \frac{\kappa^2}{2\pi}\int_0^\infty k^2 dk \frac{(l+2)!}{(l-2)!} \int_0^{\tau 0} d\tau_1 \int_0^{\tau 0} d\tau_2 \frac{j_l(k\tau_1)}{(k\tau_1)^2}\frac{j_l(k\tau_2)}{(k\tau_2)^2} \\ \int_0^{\tau 1} d\tau_1' k^6 \tau_1'^8 F(\tau_1',\tau_1) F(\tau_2',\tau_2) \frac{f(\tau_1',\xi_0)}{k^2(1-v^2)} B^{T-T}(\tau_1'), \end{aligned} \tag{5.49}$$

where $f(\tau_1',\xi_0) = \mathcal{F}(\tau_1',\tau_1',\xi_0)$ and

$$\begin{aligned} F_{sc} = \frac{1}{9} j_l(k\tau_1) j_l(k\tau_2) \frac{\tau_1'^4}{\tau_1^2\tau_2^2}\Big(B^{Tr-Tr}(\tau_1') + 4B^{Tr-S}(\tau_1') + 4B^{S-S}(\tau_1')\Big) + \\ + \frac{1}{3}\left(j_l''(k\tau_1) j_l(k\tau_2)\frac{\tau'^{\,2}}{\tau_2^2} + j_l''(k\tau_2) j_l(k\tau_1)\frac{\tau'^{\,2}}{\tau_1^2}\right)\Big(B^{Tr-S}(\tau_1') + 2B^{S-S}(\tau_1')\Big) + \\ + j_l''(k\tau_1) j_l''(k\tau_2) B^{S-S}(\tau_1'), \end{aligned} \tag{5.50}$$

with trace components:

$$B^{Tr-Tr}(\tau_1') = \left[1 + v^2 - \tilde{T}/\tilde{U}(1-v^2)\right]^2 B^{00-00}(\tau_1'), \tag{5.51}$$

$$B^{Tr-S}(\tau_1') = \left[1 + v^2 - \tilde{T}/\tilde{U}(1-v^2)\right] B^{00-S}(\tau_1'). \tag{5.52}$$

In the final form of equations (5.47) and (5.50) we have expressed the contribution from the "00" component in terms of the trace component "Tr" using the relations (5.51) and (5.52), which can be derived from (5.22) and (5.23). It should be stressed that in obtaining equations (5.47), (5.48) and (5.49) we have only used the approximation (5.46). We have thus succeeded to derive full semi-analytic expressions for the scalar, vector and tensor contributions to the angular powerspectrum from cosmic strings with arbitrary currents, valid in matter domination and under the approximation (5.46).

In the superhorizon limit $k\tau < 1$ considered above, the two-point correlators have the simple form (5.33)-(5.36) and we can factor out from the integrals (5.47)-(5.49) the key

quantities characterising the cosmic string network: v, ξ_0, $\hat{U}$, $\hat{T}$ and Q. This allows us to establish a direct connection between cosmic string network parameters and the string contribution to CMB anisotropies, valid on superhorizon scales. For the vector (5.48) and tensor (5.49) contributions it is easy to see that

$$C_l^{V,T} \sim (G\mu_0)^2 \frac{\hat{U}^2 v^4 + \hat{T}\hat{U} v^2(1-v^2) + \hat{T}^2(1-v^2)^2 + 3v^2 Q^2}{\xi_0(1-v^2)}\,, \tag{5.53}$$

which agrees with the result of [216] in the limit $Q = 0$, $U = \alpha\mu_0$ and $T = \mu_0/\alpha$.

The treatment of the scalar mode (5.47) is more subtle. We will estimate it to leading order, using the following asymptotic form of the spherical Bessel function $j_l(x) \sim x^l$, valid when $0 < x << \sqrt{l+1}$. This approximation is justified when we consider the scalar contribution at large multipole moments l. Since the angular power spectrum C_l for cosmic string networks typically peaks at $l > 500$ we can take the leading term of (5.50) as $j_l''(k\tau_1) j_l''(k\tau_2) B^{S-S}(\tau_1')$. It follows that, in this approximation, the scalar contribution will be the same as the above approximate expressions for the vector and tensor components

$$C_{1<<l}^{S} \sim (G\mu_0)^2 \frac{\hat{U}^2 v^4 + \hat{T}\hat{U} v^2(1-v^2) + \hat{T}^2(1-v^2)^2 + 3v^2 Q^2}{\xi_0(1-v^2)}. \tag{5.54}$$

5.2.2 The CMB for a wiggly string network

In order to investigate in detail the effects of string wiggles on the predicted CMB anisotropies from cosmic string networks, we implement the wiggly VOS model (3.71)-(3.73) into the CMBact code [143]. The original code was developed so as to take into account the presence of string wiggles in the computation of the string-induced CMB anisotropy. However, in the original CMBact package, wiggles were modelled by a single (constant) phenomenological parameter $\alpha = \mu$ modifying the effective mass per unit length and string tension at the level of the energy-momentum tensor (5.55). In other words, within the approximations of the original CMBact code, the amount of wiggles was not a dynamical parameter and did not influence the equations of motion, while from the wiggly VOS model we have just discussed it is clear that these effects must, in general, be present. Here, we implement the full description of wiggly strings in CMBact. Using the equation of state for wiggly strings (3.13) we first rewrite the energy-momentum tensor (3.18) as

$$T^{\mu\nu}(y) = \frac{\mu_0}{\sqrt{-g}} \int d^2\sigma \left(\epsilon\mu \dot{\mathbf{x}}^\mu \dot{\mathbf{x}}^\nu - \frac{\mathbf{x}'^\mu \mathbf{x}'^\nu}{\epsilon\mu} \right) \delta^{(4)}(y - x(\sigma))\,, \tag{5.55}$$

where μ is the amount of wiggles, which is now dynamical, satisfying equation (3.73) (compare to the work [143], the parameter $\mu = 1/\alpha$). The size of string segments is set to be equal[8] to the correlation length $\xi_0\tau$. We also change the VOS equations of motion in CMBact to the full system (3.71)-(3.73) and implement the energy-momentum components (5.27)-(5.29).

[8]For an even more realistic model we could consider the strings segments to have a range of sizes and speeds picked from appropriate distributions as in [191], but here we want to focus on the effects of string wiggles only and compare to the results of the original CMBact code, which also takes all segments to have the same size and speed.

With these modifications, we achieve a full treatment of wiggly cosmic string networks in CMBact.

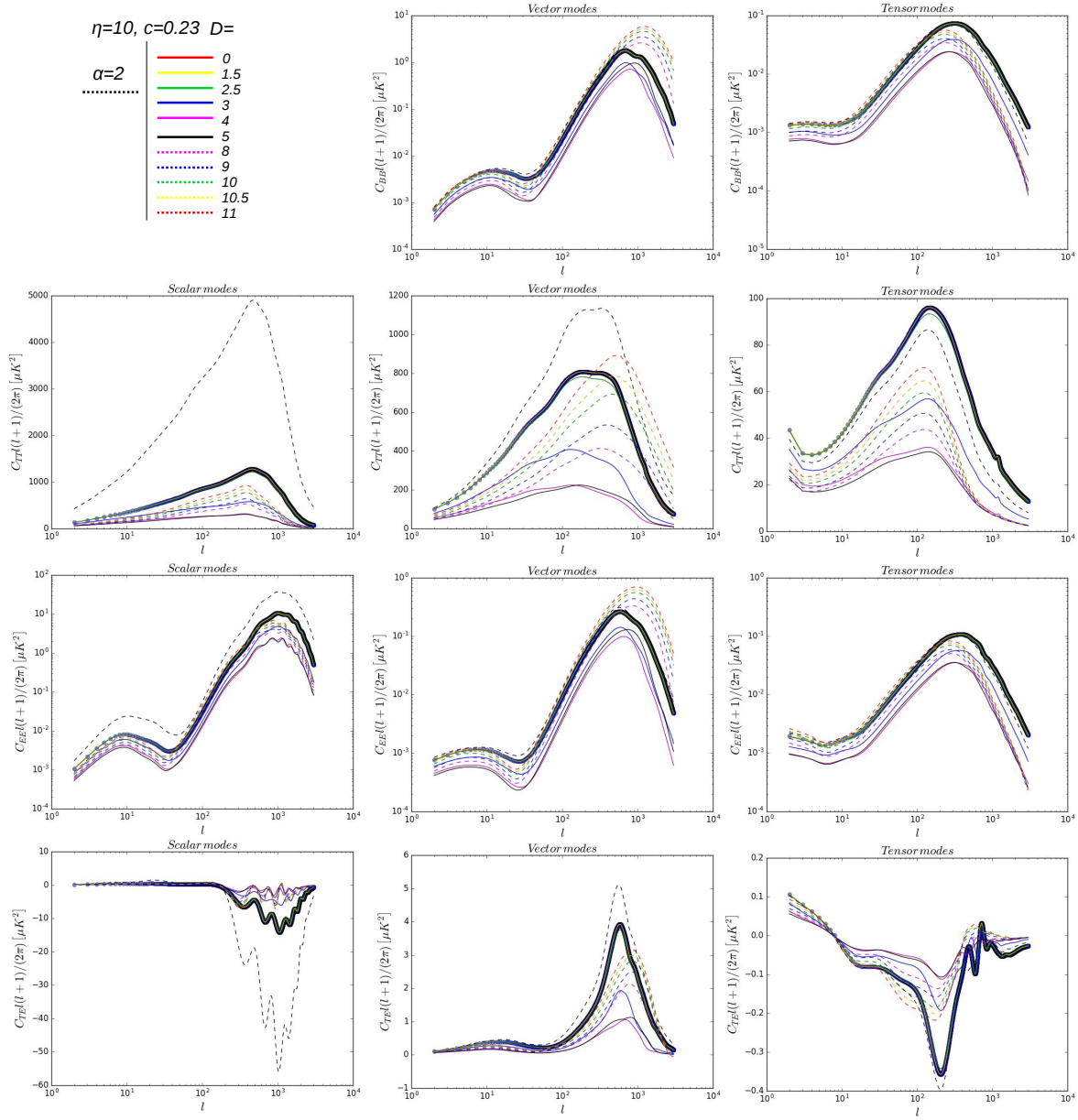

Fig. 5.2 CMB anisotropy for wiggly cosmic string networks obtained by a modified version of the CMBact code [143]. The panels show scalar, vector and tensor contributions (top to bottom) of the BB, TT, TE and EE modes (left to right). (Note there is no BB contribution from scalar modes.) These have been computed for different values of D with fixed η. The CMBact result from [143] with $\alpha = 2$ is shown by the black dashed line for comparison.

In section 3.5 we already studied the network evolution of wiggly strings, see figure 3.3, and in figure 5.2 the corresponding CMB anisotropies computed in our modified version of CMBact are shown. In both figures we show the corresponding results of the original CMBact code [143] for comparison. Regarding figure 3.3, we note that the accuracy of

CMBact is comparatively worse at low redshifts; this explains why the effects of the matter to acceleration transition seemingly become visible around redshifts of a few, while the onset of acceleration occurs below $z = 1$. This point is not crucial for our analysis, since our goal is to make a comparative study of the effects of the additional degrees of freedom on the strings. Moreover, these low redshifts have a relatively small effect on the overall CMB signal. Nevertheless, this is an issue which should be addressed if this code is to be used for quantitative comparisons with current or forthcoming CMB data.

Figure 5.2 shows how the full treatment of wiggly cosmic string networks affects the prediction for the string-induced CMB anisotropy. Note that the CMB contribution is generally smaller than for ordinary cosmic strings (i.e. without wiggles, $\mu = 1$). This is mainly due to a reduction in the rms string velocity v (see figure 3.3) when the amount of wiggles μ increases. In view of the observed changes to the usual CMB predictions for cosmic strings, we argue that to achieve accurate results for wiggly cosmic strings, one should study them in the framework of the complete wiggly model (3.71)-(3.73) and the modified version of CMBact developed here. This generally leads to a weakening of the CMB-derived constraint on the string tension μ_0 (but note that there is also a region in parameter space – for large D – where the correlation length can actually become smaller than for ordinary strings, see figure 3.3).

Note that both the evolution and CMB results from our wiggly VOS model are somewhat closer in comparison to results from Abelian-Higgs simulations (and similarly ordinary VOS results are closer to Nambu-Goto simulations). It is then tempting to speculate that wiggles play a dynamical role analogous to that of the averaged field fluctuations that appear in Abelian-Higgs field theory simulations (as opposed to effective Nambu-Goto simulations). This hypothesis may be investigated by direct comparisons of Abelian-Higgs and Goto-Nambu simulations with suitably high resolutions and dynamic ranges.

Since we have computed the velocity v and correlation length $\xi_0\tau = \sqrt{\mu}\varepsilon\tau$ in the scaling regime, we can use equations (5.53) and (5.54) to estimate how the contribution to the CMB anisotropy from cosmic strings depends on the amount of string wiggles. For wiggly cosmic strings the angular power spectrum C_l has the following dependence (which coincides with the result in [216])

$$C_l \sim (G\mu_0)^2 \frac{\mu^4 v^4 + \mu^2 v^2(1-v^2) + (1-v^2)^2}{\mu^2 \xi_0 (1-v^2)}, \tag{5.56}$$

where scalar, vector and tensor components depend on string parameters in the same way.

We can now compare the dependence in equation (5.56) with our numerical results using our modified CMBact code. By choosing the μ value for the matter domination era and looking at the peak ($l \approx 700$) of the sum of the scalar, vector and tensor contributions we plot them in comparison to the analytic estimate from (5.53) and (5.54). This comparison is shown in figure 5.3. For our approximate estimate it is seen that after a fast decrease of C_l's with growing amount of wiggles μ, the value of C_l reaches a plateau. A similar behaviour is seen for vector, tensor and scalar components obtained from the full treatment using our modified CMBact code, even though the agreement is somewhat weaker for the scalar contribution.

These results reaffirm the approximations used to estimate the analytic dependence of C_l on the string network characteristics.

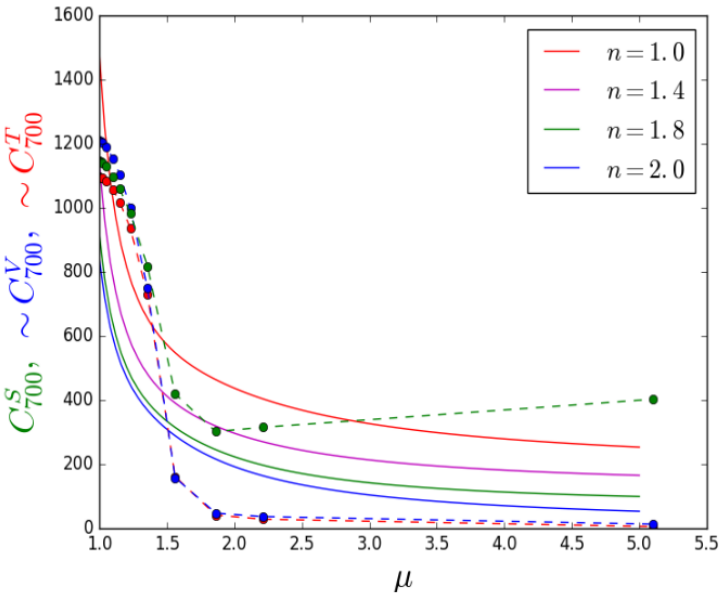

Fig. 5.3 Comparison between the behaviour of the string-induced angular power spectrum C_l for different amounts of wiggles in our analytic approximation (solid lines) and the numerical computation using our modified CMBact code (circles). The dependence on μ has been estimated analytically using equations (5.54), (5.53) together with the equations for the scaling regime of the network (3.86). Using the value of μ in the matter domination era and C_l's for scalar (green), vector (blue) and tensor (red) components at $l = 700$ (where the sum peaks), we have obtained the $C_l - \mu$ dependence from the CMBact code.

5.2.3 The CMB for a superconducting chiral string network

Similar analyses can be accomplished for the CMB anisotropies from a superconducting chiral cosmic string network. In section 3.6 we already studied the evolution of such networks. We saw that there are no general scaling solutions for all ranges of expansion rates of the superconducting chiral string network. However, in all cases (even in the absence of scaling solutions) we can still evolve the network with our modified VOS model and use equations (5.27)-(5.29) with the energy-momentum tensor

$$T^{\mu\nu}(y) = \frac{\mu_0}{\sqrt{-g}} \int \sqrt{-\gamma} \left((1+\Psi) u^\mu u^\nu - (1-\Psi) v^\mu v^\nu - \beta\Psi (u^\mu v^\nu + v^\mu u^\nu) \right) \delta^{(4)}(y - x(\sigma)) d^2\sigma \tag{5.57}$$

to modify the CMBact code for a superconducting chiral cosmic string network. In the absence of scaling the charge Q for the cosmic string network evolution is controlled mainly by the initial condition Q_0. Note that, unlike the wiggly case, there are currently no numerical simulations which can provide us with benchmarks for the value of this charge. Thus, by

varying Q_0 we obtain different evolutions for cosmic superconducting string networks (see figure 3.8) and their corresponding contributions to the CMB anisotropy (see figure 5.4).

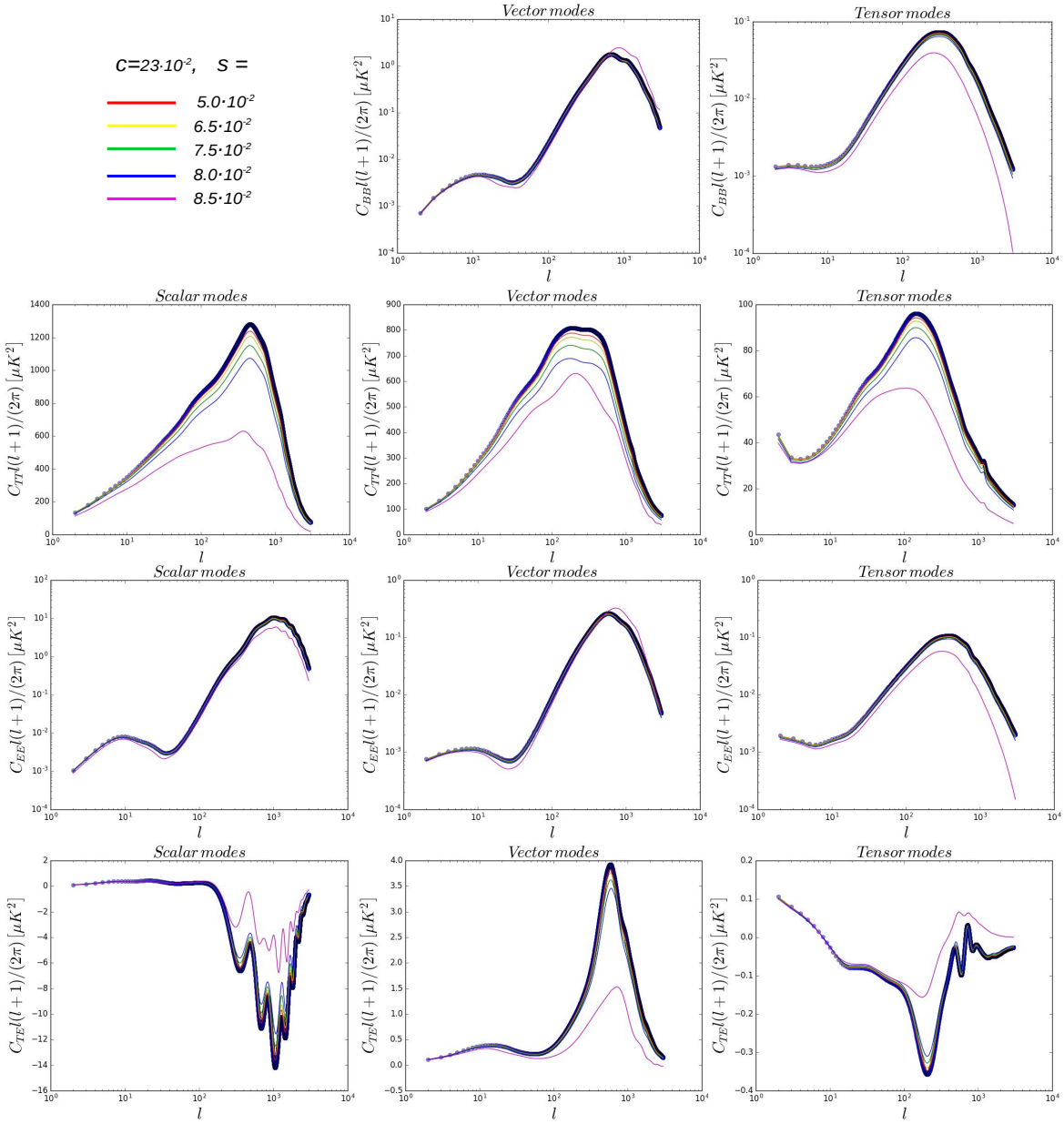

Fig. 5.4 CMB anisotropy results for superconducting (chiral) cosmic sting networks obtained by our modified version of CMBact [143]. The panels show the scalar, vector and tensor contributions (top to bottom) to the BB, TT, TE and EE power spectra (left to right). The calculations are done for different initial conditions of the charge Q_0.

We can also check the analytic estimate for C_l in (5.54). In the case of superconducting chiral strings the value of C_l can be represented as

$$C_l \sim (G\mu_0)^2 \, \frac{v^4(1+3\beta^2Q^2)+v^2(3Q^2(1-\beta^2)+4\beta Q-1)+(1-\beta Q)^2}{\varepsilon(1-v^2)}, \tag{5.58}$$

where scalar, vector and tensor components depend on string parameters in the same way.

We use the solution of algebraic equations (3.105) for different values of Q (some solutions are shown in 3.9) to estimate the C_l dependence on the charge Q (5.58). The result of these calculations is presented in figure 5.5.

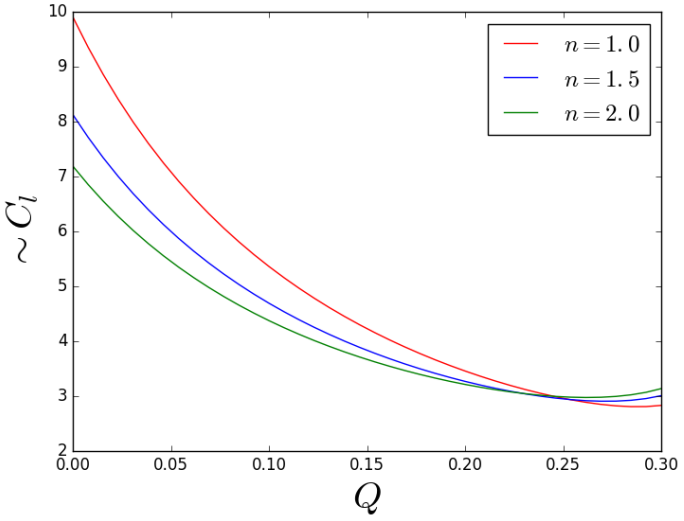

Fig. 5.5 The behaviour of C_l for different values of a string charge Q, obtained from the analytical approximation.

Concerning the angular power spectra C_l, it should be noted that it is difficult to make extensive comparisons in the case of superconducting strings, as there is no scaling behaviour in the full range of expansion rates n and we do not know which Q values we should choose from our numerical results in figure 5.4. However, it is clear that the analytic approach and numerical computation are in qualitative agreement. In particular the angular power spectrum C_l in both our numerical calculations using the modified CMBact code (figure 5.4) and the analytic estimate (figure 5.5) we observe that the string rms velocity v tends to decrease as we increase the charge Q. The comoving correlation length in units of the conformal time ϵ increases for small values of the charge, but then reaches a maximum and eventually decreases for higher values of the charge Q.

5.3 Other observational constraints on cosmic strings

In the previous section we gave a description of the cosmic string influence on CMB anisotropies. In addition to the CMB study, there are many other tools that can allow to detect/restrict existence of cosmic strings. Below we mention main approaches to search for the cosmic string signal and corresponding limits that were imposed.

5.3.1 Gravitational lensing and the Kaiser-Stebbins effect

If one consider the standard straight static string oriented along the axis Z in Minkowski space, the energy-momentum tensor has the form [218]

$$T^{\mu\nu} = \mu_0 \delta(x)\delta(y)\mathrm{diag}(1,0,0,1). \tag{5.59}$$

Using the expression for the linearised Einstein equations

$$\partial^\rho \partial_\rho h_{\mu\nu} = -16\pi G \left(T_{\mu\nu} - \frac{1}{2}\eta_{\mu\nu} T^\sigma_\sigma \right), \tag{5.60}$$

where the metric perturbation $h_{\mu\nu} = \eta_{\mu\nu} - g_{\mu\nu}$ is $|h_{\mu\nu}| << 1$, one can find that

$$\begin{aligned} h_{00} = h_{33} &= 4(U-T)G\mu_0 \log(r/r_0), \\ h_{11} = h_{22} &= 4(U+T)G\mu_0 \log(r/r_0). \end{aligned} \tag{5.61}$$

For the standard string $U = T = \mu_0$ the following line element in the cylindrical coordinates system corresponds to (5.61)

$$ds^2 = dt^2 - dz^2 - (1 - h(r)) \left(dr^2 + r^2 d\theta^2 \right), \tag{5.62}$$

where $h(r) = 8G\mu_0 \log(r/r_0)$ (for details see [35]).

The following coordinate transformation

$$\begin{aligned} r'^2 &= (1 - h(r))r^2/(1 - 8G\mu_0), \\ \theta' &= (1 - 4G\mu_0)\theta \end{aligned} \tag{5.63}$$

provides a new form of the line element (up to linear order in $G\mu$)

$$ds^2 = dt^2 - dz^2 - dr'^2 - r'^2 d\theta'^2, \tag{5.64}$$

which is locally the same as usual Minkowski space.

The difference between the metric (5.64) and the Minkowski line element in the possible range of values for the new angle θ': $0 < \theta' < 2\pi(1 - 4G\mu)$. The fact that θ' doesn't reach 2π implies the presence of an angle deficit

$$\delta_\theta = 8\pi G\mu. \tag{5.65}$$

It should be noted that there is a generalization for the angle deficit (5.65) [219], which states that for the metric

$$ds^2 = \mathrm{e}^{A(r)} \left(dt^2 - dz^2 \right) - dr^2 - \mathrm{e}^{B(r)} d\theta^2 \tag{5.66}$$

the angle deficit is

$$\delta'_\theta = 8\pi G\mu + \frac{\pi}{2} \int_0^\infty \left(\frac{\partial A(r)}{\partial r} \right)^2 \mathrm{e}^{B(r)/2} dr. \tag{5.67}$$

As it is seen, the generalized angle deficit can be only bigger $\delta'_\theta > \delta_\theta$. Using the general expression for the mass per unit length and tension (3.30), we can see from (5.61) that h_{00} and h_{33} are not zero anymore. Their presence leads to the metric form (5.66) and an additional contribution to the angle deficit from non-trivial string structure in the form (5.67). The bigger the presence of current/wiggles, the bigger the angle deficit.

The effect of the angle deficit allows us to look for the presence of cosmic strings through gravitational lensing. A cosmic string plays the role of a cylindrical lens, as shown in figure 5.6. It was shown that by using the reasonable assumption $G\mu << 1$, that it is possible to find the angular separation between lensed images [220]

$$\delta\varphi = \frac{L_{QS}}{L_{QS} + L_{OS}} \delta_\theta \sin\beta, \tag{5.68}$$

where L_{QS} (L_{OS}) is the length between the object Q (observer O) and the string S, while β is the angle between plane of the "sight" and the cosmic string (for clarity see figure 5.6).

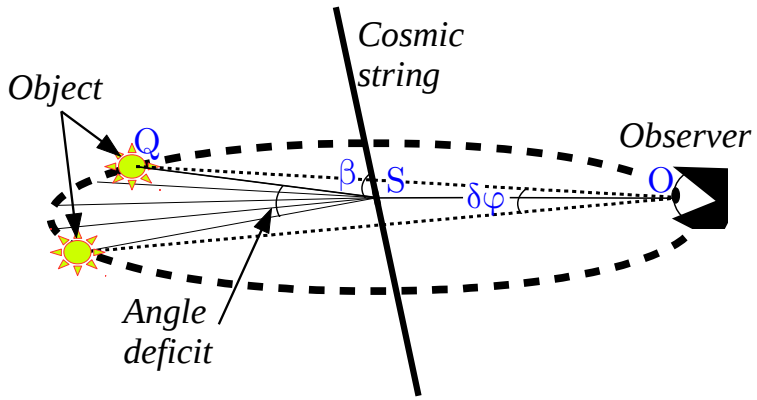

Fig. 5.6 Due to angle deficit associated with the metric (5.64) the presence of a cosmic string can be tested by its gravitational lensing. In this schematic picture, the object behind the string can be seen by an observer as two separated images.

The gravitational lensing of astrophysical objects caused by cosmic strings didn't reveal any signs of strings so far [221] and established the limit on their tensions $G\mu < 2.3 \cdot 10^{-6}$ [222]. The lensing analysis was also extended to a CMB study. Specifically, the Kaiser-Stebbins effect [223] states that the moving string should give rise to a temperature discontinuity in the CMB map. If the string moves with velocity transverse to the sky map, the radiation ahead the motion will be red-shifted, while the radiation behind will be blue-shifted. The temperature anisotropy of the Kaiser-Stebbins effect is given by the following relation [223]

$$\frac{\Delta T_K}{T_K} = G\mu\upsilon\gamma_\upsilon, \tag{5.69}$$

where υ is the transverse velocity of the string (γ_υ is the corresponding Lorentz factor).

The study of the Kaiser-Stebbins effect together with lensing led to the constraint $G\mu < 7.36 \cdot 10^{-7}$ on the string tension [187], while corresponding constraint on superstrings with junctions were found to be around $G\mu < 10^{-7}$ [224, 225].

Concerning the Kaiser-Stebbins effect for strings with non-trivial structure, it should be noted that while the effective tension (with current) should increase, thus enhancing the signal, the string deceleration due to the current will counteract this effect. Thus, using our results for scaling networks with wiggles and strings with a current from sections 3.5.1 and 3.6, we can give a simple estimation of the Kaiser-Stebbins effect variation due to non-trivial structure. In figure 5.7 we compare the result for usual strings with wiggly and charged strings[9].

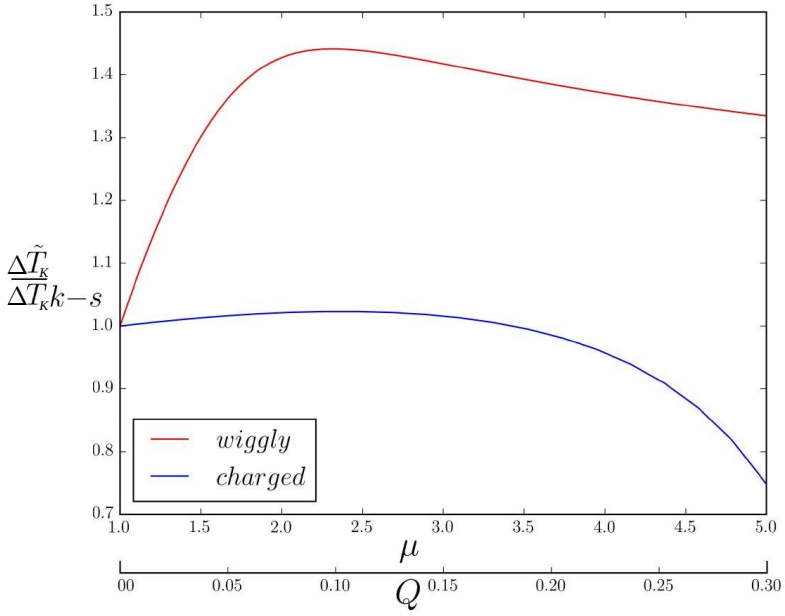

Fig. 5.7 Effect on the Kaiser-Stebbins anisotropy (5.69) of non-trivial structures on strings, i.e. wiggly strings and strings with a current. $\Delta\tilde{T}_K$ denotes the temperature variation of non-trivial strings, while ΔT_K corresponds to the standard one.

5.3.2 Gravitational radiation

One of the most promising signals which allows to scrutinize the presence of cosmic strings is gravitational radiation. The emission of gravitational waves by cosmic strings was at first pointed out in [226]. Later investigation showed that there is a characteristic emission of gravitational waves caused by by kinks and cusps [227, 228] (for more details see [229, 230] and for cosmic superstrings [231–233]).

If we consider a string network, we anticipate the presence of many gravitational bursts due to kinks and cusps, which in turn produce anisotropies in a gravitational background radiation. Looking ahead, especially in the light of direct detection of gravitational waves [234] and future missions (for instance the LISA mission [235]), the detailed study of the cosmic string gravitational background can raise the level of a sensitivity of a cosmic string probe.

[9]It should be noted that since the Kaiser-Stebbins effect depends on transverse velocity v_T, we use the relation between the absolute mean square velocity and transverse mean square velocity $v_T = \frac{\pi}{4}v$.

Let's follow the recent development [236–242] to review the basic steps of stochastic gravitational background studies. We start from the consideration of the perturbed metric in the Newtonian gauge (5.11), where we denote

$$\begin{aligned} \Psi &= \tilde{\Psi} + \Pi, \\ \Phi &= \tilde{\Psi} - \Pi, \end{aligned} \tag{5.70}$$

with a parameter Π that represents the contribution from the anisotropy part in the energy-momentum tensor.

For the metric (5.11) with (5.70), working to linear order, it is possible to show that the density parameter of gravitational waves Ω_{gw} can be written as [242, 243]

$$\begin{aligned} \Omega_{gw}(\nu_o, \mathbf{e}_o) = \frac{\pi \nu_o^3}{3H_o^2} \int_0^{\tau_*} d\tau a^2 \int d\theta_G \overline{n} R \times \\ \left[1 + \delta_n - \tilde{\Psi}_o - \Pi_o + 2\left(\tilde{\Psi} + \Pi\right) + \mathbf{e} \cdot \mathbf{v}_o + 2\int_\tau^{\tau_o} d\tau' \frac{\partial \tilde{\Psi}}{\partial \tau'}\right] \int_{S^2} d^2\sigma_s r_s^2 \tilde{h}^2, \end{aligned} \tag{5.71}$$

where ν_o is frequency in the observer rest frame (hereinafter all indices "o" refer to variables in the observer's rest frame), θ_G is a source parameter of gravitational waves (for details see [243]), $\delta_n = \frac{n-\overline{n}}{\overline{n}}$ is the number density inhomogeneity ($\overline{n}$ is the background value of the number density), R is the burst rate per system, the unit vector $\mathbf{e}$ defines the direction of observation, the vector $\mathbf{v}$ defines the peculiar velocity of the cosmic fluid ($\mathbf{v}_o$ for the observer), $\tilde{h}$ is the Fourier transform of the total gravitational wave strain magnitude, the last integration is taken over the spherical surface with solid angle $d^2\sigma_s$ and a radius r_s centred on the source.

The time τ_* in (5.71) is connected with the rate of arrival of observable signals emitted at the time scale $\tau \geq \tau_*$ inside the proper volume element dV multiplied by the signal duration Δt [242, 244]. Consequently, the time τ_* should be defined from the integral equation

$$\Lambda = \Delta t \int d\theta_G \int_{\tau_*}^{\tau_o} f_o \overline{n} R dV, \tag{5.72}$$

where f_o is the number of emitted signals that can be observed at the frequency ν_o (the following values with $_*$ are related to the time τ_*).

To study fluctuations from astrophysical sources we need to get rid of the Doppler shift contribution caused by the peculiar motion of the observer. To do so, we should introduce the quantity

$$\delta_{gw} = \frac{\Omega_{gw}\big|_{\mathbf{v}_0=0} - \overline{\Omega}_{gw}}{\overline{\Omega}_{gw}}, \tag{5.73}$$

where the background density parameter of gravitational waves is $\overline{\Omega}_{gw} = \Omega_{gw}\big|_{\mathbf{v}_0=0,\delta_n=0}$.

To use the standard statistical analysis of a sky map, similarly to the CMB case, one can consider the multipole expansion in the form

$$C_l = 2\pi \int_{-1}^{1} d(\cos\theta_o) \left\langle \delta_{gw}(\mathbf{e}_o)\delta_{gw}(\mathbf{e}_0')\right\rangle P_l(\cos\theta_o), \tag{5.74}$$

where θ_o is the angle between $\mathbf{e}_o$ and $\mathbf{e}_o'$.

To apply the above analysis for gravitational waves from cosmic strings, we need to find the form of $\tilde{h}$ in the equation (5.71). As it was already mentioned, the main contribution to $\tilde{h}$ is coming from cusps and kinks of cosmic strings. The form of the function $\tilde{h}$ was obtained in the work [229]. Let's review the treatment of gravitational radiation form cosmic loops. The Fourier transformed energy-momentum tensor (5.20) can be rewritten as [229]

$$\Theta^{\mu\nu} = -\frac{\mu_0}{\ell_o} I_+^{(\mu} I_-^{\nu)}, \tag{5.75}$$

where

$$I_\pm^\mu = \int_0^{\ell_o} d\sigma_+ X_\pm'^\mu \mathrm{e}^{-\frac{1}{2}kX_\pm}, \tag{5.76}$$

with $\sigma_\pm = \sigma \pm \tau$, $X_\pm^{\mu\prime} = X^{\mu\prime} \pm \dot{X}^\mu$ and $0 < \sigma < \ell_o$.

For string loops it is possible to have the situation when $X_\pm^\mu$ coincide with each other. This situation leads to the cusp formation. At the cusp point $X'^\mu = 0$, i.e. the string has a sharp form, while $\dot{X}^\mu = 1$ shows that this point moves with the speed of light. To study the region near the cusp we should make a Taylor expansion around this point

$$X_\pm^\mu(\sigma_\pm) = \ell_o^\mu \sigma_\pm + \frac{1}{2}\ddot{x}_\pm^\mu \sigma_\pm^2 + \frac{1}{6}\dddot{x}_\pm^{(3)\,\mu} \sigma_\pm^3 + \dots, \tag{5.77}$$

where $x_\pm^\mu = X_\pm^\mu(\sigma_c)$ is calculated at the cusp point σ_c.

Using the Taylor expansion (5.77) with the condition $\dot{X}^\mu X_\mu' = 0$, one can find out that $kX_\pm = \omega \ell_{o\,\mu} X_\pm^\mu \approx -\frac{1}{6}\omega(\ddot{x}_\pm^\mu)^2\sigma_\pm^3$ which helps to estimate the integral (5.78) [229, 245]

$$I_\pm^\mu = \frac{2(12)^{2/3}\pi i}{3\Gamma(1/3)} \frac{\ddot{x}_\pm^\mu}{|\ddot{x}_\pm|^{4/3}} \frac{1}{\omega^{2/3}}, \tag{5.78}$$

where we used the fact that $k^\mu = \omega \ell_o^\mu$

At the same time, small perturbations on the metric $h_{\mu\nu}$ caused by cosmic strings can be linearly approximated as [229]

$$h_{\mu\nu} \approx \frac{\kappa_{\mu\nu}}{r} \approx \frac{2G\ell_o|\nu|\Theta_{\mu\nu}}{r}, \tag{5.79}$$

where $\omega = 2\pi\nu$.

As a result, substituting (5.78) and (5.75) into the expression for $\kappa_{\mu\nu}$ one can obtain the gravitational waveform from cusps on cosmic strings

$$\kappa_c^{\mu\nu}(\nu, \mathbf{n}) = \frac{8}{\Gamma(1/3)^2}\left(\frac{2}{3}\right)^{2/3} \frac{G\mu_0\ell_o^{2/3}}{\nu^{1/3}} \Theta\left(\nu - 2/\ell_o\right) \Theta\left(\theta_c - \arccos(\mathbf{n}_c, \mathbf{n})\right), \tag{5.80}$$

where we used that $|\ddot{x}^{\mu}_{\pm}| \approx 2\pi/\ell_o$ and the angle for the cusp $\theta_c \approx \left(\frac{4}{\sqrt{3}\nu\ell_o}\right)$, $\mathbf{n}_c$ is a unit vector that shows the direction of radiation of gravitational waves from the cusp.

A quite similar treatment can be applied to obtain the waveform from kinks on cosmic strings. The final result gives the following relation

$$\kappa^{\mu\nu}_k(\nu, \mathbf{n}) = \frac{2\sqrt{2}}{\pi\Gamma(1/3)}\left(\frac{2}{3}\right)^{1/3}\frac{G\mu_0\ell_o^{1/3}}{\nu^{2/3}}\Theta\left(\nu - 2/\ell_o\right)\Theta\left(\theta_b - \arccos(\mathbf{n}_k, \mathbf{n})\right), \tag{5.81}$$

where $\mathbf{n}_k$ is a unit vector responsible for the gravitational radiation direction form the kink.

In order to use the equation (5.71) to treat gravitational waves from cosmic strings, we need to introduce the main characteristics of a string network. In particular, considering kinks and cusps on cosmic string loops, we can introduce the number density of loops n_s with characteristic size ℓ_o. Numerical simulations suggest a scaling behaviour for this parameters as follows

$$\begin{aligned} \ell_o &= \epsilon_o t, \\ \mathcal{F}_o &= t^4 n_s, \end{aligned} \tag{5.82}$$

where $\mathcal{F}_o$ and ϵ_o are constants that can be determined from numerical simulations (for details see [115, 246–249]).

In this way, it was shown that using the relation (5.71) with (5.73), it is possible to estimate the gravitational radiation from cosmic loops as [242]

$$\begin{aligned} \delta_{gw} = \frac{2(G\mu_0)^2}{3\pi^2 H_o^2 \nu_o \overline{\Omega_{gw}}}\int_0^{t_*}\frac{dt}{t^4}a^5\int_0^{\epsilon_{o*}}(\mathcal{F} - \overline{\mathcal{F}})\Theta(\epsilon_o t - 2a/\nu_o) \\ \left[N_k^2 + 4AN_k\left(\frac{\nu_o\epsilon_o t}{a}\right)^{1/3} + A^2 N_c\left(\frac{\nu_o\epsilon_o t}{a}\right)^{2/3}\right], \end{aligned} \tag{5.83}$$

where $\overline{\mathcal{F}}_o = t^4\overline{n}$, $N_k = N_c = RT_p$ is the number of bursts per oscillation period $T_p = \frac{\ell_o}{2}$ from kinks and cusps and the constant $A = \frac{2^{13/3}\pi^2}{3^{5/6}\Gamma(1/3)^2}$.

At the same time the contribution from infinite strings with kinks should be taken into account as well. Calculations of the contribution from infinite strings were carried out in [250]. All in all, it is seen that for standard strings in a scaling regime (see for the case of the VOS model [251]) the gravitational radiation has a solid description. A forecast for the gravitational radiation allows us to make a comparison with observational data and put constraints on cosmic strings. Such constraints were imposed by the work [252], where the strongest limit is coming from the pulsar timing array (see [192] for details), see figure 5.8.

While the description of gravitational radiation from standard cosmic strings is accomplished, the same treatment for strings with non-trivial structure is not completely applicable. First of all, it is seen that there are no cusps in the case when chiral currents are present (see 3.3). As a result, the above treatment is not valid and should be substituted by the study of pseudo cusps [245] (some progress for the chiral strings was achieved in the paper [253]) and the corresponding contribution from the current should be added to the study of gravitational radiation from kinks.

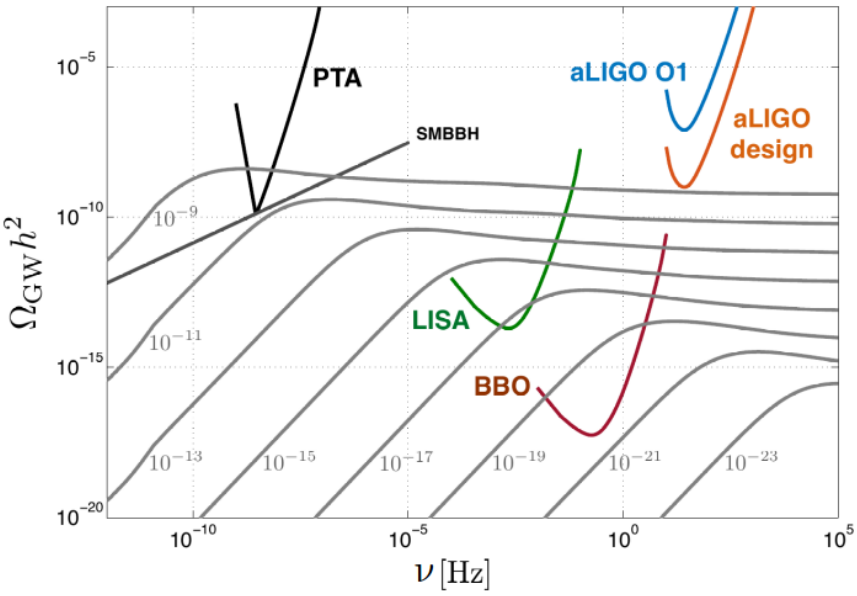

Fig. 5.8 The gravitational radiation prediction for strings with different tensions and corresponding constraints from the observational data [252].

For cosmic superstring networks we anticipate a contribution from strings with different tensions and different scaling characteristics (see for example [254]). Additionally, such cosmic string networks should have fewer loops, due to junction production, and as a result we can anticipate fewer cusps from loops. At the same time, as it was shown in [255] there are cusps on strings with junctions. Moreover for superstrings one should include possible gravitational radiation from junctions [256] and from subsequent kinks [257]. This can have especially significant contribution in the case of multiple reconnections [258, 259]. As a result, for the non-vanilla strings the treatment for gravitational radiation should be studied in more detail.

5.4 Summary

In this chapter we briefly reviewed one of the main observational tools for precision cosmology - anisotropies of the CMB. Since the presence of cosmic strings should leave a fingerprint in the CMB maps and power spectrum, the proper study of this observable is a good test to restrict/detect cosmic strings. We used the formalism developed in chapter 3 for cosmic string networks with non-trivial structure evolution to estimate the CMB anisotropies caused by such strings. In particular, we studied wiggly and chiral superconducting cosmic string networks. We saw that the contribution to the CMB can decrease when the deviation from standard strings increases. This important issue should be taken into account when trying to impose restrictions on early universe models by checking the absence of a signal from cosmic strings. The comparison was done with a modification of the CMBact code. We also obtained analytic integrals for fast CMB calculation. They allow to apply Markov chain methods to constrain the presence of non-trivial cosmic strings. Additionally we found simple estimations of anisotropy magnitudes caused by cosmic strings with currents.

Another estimation of the current influence on a CMB prediction from cosmic strings was done in the framework of the Kaiser-Stebbins effect. We saw that the decrease of the string network rms velocity doesn't allow the Kaiser-Stebbins effect to increase the CMB anisotropies significantly due to the presence of currents.

In the last part of this section we reviewed the main developments for the gravitational radiation from cosmic strings. We pointed out the most important issues where strings with non-trivial structure can affect this observational signal. Moreover, we reviewed the main changes that should be implemented in order to study gravitational radiation from a cosmic superstring network.

Chapter 6

Conclusions

Let's summarize the result of the cosmic string exploration presented in this thesis. We started from the study of domain wall networks evolution in expanding FLRW universes. We have simulated the wall network evolution in expanding universes with different fixed expansion rates, as well as sets of simulations which span the entire radiation-matter transition. In addition to the study of the Kibble scaling regime we found the conformally stretched regime, which is caused by the Hubble damping due to fast expansion rate of simulations (until $1 - \lambda = 10^{-7}$). Two regimes of simulations allowed us to improve the calibration of the VOS model and confirm the validity of the utilized approach for the broad range of regimes. Additionally we need to emphasize that the radiation-matter transition doesn't have scaling behaviour. As a result, it is interesting to conduct the detailed comparison of the VOS model (for analytic description see [260]) and simulations as a supplementary test of the semi-analytic approach.

It is worth recalling the main characteristics of the wall simulations that were studied. By fitting the phenomenological parameters to the simulations, we found that the energy loss term that should be responsible for the sphere-like objects production is typically subdominant in comparison with the term which is responsible for the scalar radiation. We also revisited the role of damping mechanisms in the cosmological evolution of topological defect networks. In particular we have explicitly demonstrated that a sufficiently large Hubble damping (that is a sufficiently fast expansion rate) eventually leads to a linear scaling regime where the network is non-relativistic, but this is typically preceded by a stretching regime counterpart which we characterized for the first time.

In the future it will be interesting to provide a similar analysis for cosmic strings. In this case we anticipate that the contribution from the loop chopping parameter is going to be more important, but significant differences remain between the results of field theory and Goto-Nambu simulations. Although they may partially be explained by the different spatial resolution and dynamical range of both types of simulations, it is not clear that numerical differences provide a satisfactory explanation. A fully calibrated VOS model will allow a direct comparison between both types of simulations, enabling a test of their consistency.

In chapter 3 we investigated cosmic strings with nontrivial structure. In particular, we obtained general microscopic equations that describe the non-trivial string evolution in section

3.2. For the specific case of strings with chiral currents, we found an exact solution for a string defined by the general Lagrangian of section 3.3. Applying the averaging procedure in section 3.4 we formulated the general macroscopic description for the string network with non-trivial internal structure. In particular we obtained equations that describe time evolution of the rms string velocity v and characteristic length L of a string network. These equations depend only on three parameters $\hat{U}$, $\hat{T}$ and Q defining the string equation of state. These parameters, together with the network quantities L and v, appear directly in the string energy-momentum tensor (3.18) which seeds the string-induced CMB anisotropy. This provided a direct connection between modelling string evolution and computing CMB anisotropies from cosmic string networks, which has allowed us to obtain simple analytic estimates for the dependence of the string angular power spectrum C_l on macroscopic network parameters (5.53)-(5.54) in chapter 5. For a more complete semi-analytic treatment of the CMB anisotropy for strings with currents, we have adapted the methodology of [216] and have provided coefficients for the relevant integrals in the Appendix A.

In sections 5.2.2 and 5.2.3 we considered two specific cases of strings with currents: wiggly and superconducting cosmic strings respectively. In each case we computed the CMB signal numerically using appropriately modified versions of CMBact.

For wiggly string networks (section 5.2.2) we studied the specific case when the parameter κ in (3.16) only carries a time dependence, $\kappa = \kappa(\tau)$. Using the equation of state (3.65) for wiggly strings we obtained a relation between wiggles and velocities that puts limitations on a wiggly string network evolution. Also we explored the scaling solution and stability condition of differential equations for a wiggly string network in section 3.5.1. We studied the network dynamics using an effective action and introduced the averaged macroscopic equations into CMBact, allowing us to compute CMB anisotropies from these strings in the section 5.2.2. CMBact has already built in the option to study wiggly strings, but this was done through a single constant parameter. Here, for the first time, we were able to take into account the time evolution of wiggles and their influence on the macroscopic equations of motion for the string network. This full treatment brought important changes in modelling wiggly cosmic string networks. From figure 5.2 we see that wiggly strings can produce a lower signal in CMB anisotropy than ordinary strings (when the other parameters are fixed), which had not been appreciated before our work. We have also compared our analytic estimation (5.56) to our numerical results from the CMBact code. The comparison shows that the main trend for C_l (decreasing of C_l as μ increases, for multiple moments $l >> 1$) is captured correctly. We argue that for reliable constraints on wiggly string networks through the CMB signal, the evolution of string currents and its effect on string dynamics – as captured by our wiggly model – should be taken into account.

We point out that comparing results from our analytic wiggly string network evolution and the standard VOS model for ordinary cosmic strings, has a broad resemblance to the differences that appear between Abelian-Higgs and Nambu-Goto numerical simulations for strings. In particular, increasing the amount of wiggles μ leads to slower rms velocities and a lower contribution to the string-induced CMB anisotropy decreases. This is similar to the difference between Abelian-Higgs and Nambu-Goto string networks, where the Abelian-Higgs

strings tend to be slower and produce a lower CMB signal. This is, at present, a speculative observation requiring further investigation to see if a more firm analogy may be established.

Another type of strings that were considered in the section 3.6 are superconducting cosmic strings. We demonstrated that the condition of the microscopic charge conservation (3.92) and the chiral condition ($\kappa, \Delta \to 0$) allow us to obtain the averaged equations of motion (3.100)-(3.102) without specifying the Lagrangian dependence on string currents $f(\kappa_i, \Delta_i/\gamma)$. This implies that the debate on the correct form of the Lagrangian for superconducting strings [140] – while important from a fundamental physics point of view – does not have a crucial impact on phenomenological VOS descriptions. Introducing the appropriate modifications to CMBact in the section 5.2.3, we have found that the string-induced CMB anisotropies tend to decrease with increasing the charge Q of superconducting stings. Since the charge Q does not have a scaling behaviour in the full range of physically relevant expansion rates (3.103), but generally decreases with evolution, the main effect on the CMB anisotropy comes from the initial charge Q_0 at the moment of string formation. We varied the initial charge to obtain a range of network dynamics histories and computed the corresponding CMB signal predictions. Numerical simulations are needed to further quantify the relevant model parameters.

The approach developed in section 5.2.1 can be useful in Markov chain Monte Carlo analysis of cosmological models with cosmic strings [191]. It allows to obtain more accurate constraints on string networks with non-trivial structure parameters directly from CMB observations.

Chapter 4 presented studies of superstring interactions. In section 4.1 we briefly reviewed the main approach towards the study of cosmic string interactions. It should be underlined that this scheme provides a powerful and fundamentally grounded method for a proper superstring treatment and should be taken into account in radiation processes [163]. In section 4.1.2 we revisited the kinematic constraint for junction production and junction dynamics in Minkowski space. This study was generalized for the case when strings posses chiral currents. In particular, we explored the allowed region in angle-velocity space for forming junctions in the case of colliding strings with chiral currents. For the general case we were faced with a similar problem that appeared in [173]; the system of equations is overdetermined. We suggested possible resolutions, but further research, especially numerical simulations, are required to make this situation more clear. We want to mention an additional relevant issue that maybe related to similar problem – the degrees of freedom of colliding strings and a junction that can be fixed by some fundamental principles. How justified is the tension condition (1.69) for the bound-state of a junction in a cosmological framework since it was calculated only for unbroken supersymmetry? This question was already raised in [261], but no answer is given yet.

In sections 4.2.1 and 4.2.2 we revised studies of average string configurations just after the collision and average correlation functions. These results lead us to the development of the VOS model with dynamical junctions in the section 4.3. Specifically we gave an explanation of the reason why junctions should stop growing and how we can track their dynamics on a macroscopic level.

Finally, it is worth noting that our studies show that possible additional effects of cosmic (super)strings have a non-trivial impact on observational signatures (only some were considered for the CMB in chapter 5). The greatest observational opportunity to see these outcomes seems to be the stochastic gravitational wave background generated by string networks. Our results on string evolution and the methodology developed here will be useful for further studies in this direction.

Appendix A

Analytic expressions for equal-time correlators

As shown in [216] the integral (5.30) can be expanded in the following way

$$\left\langle \Theta^I(k,\tau_1)\Theta^J(k,\tau_2)\right\rangle = \frac{f(\tau_1,\tau_2,\xi_0)\mu_0^2}{k^2(1-\upsilon^2)}\sum_{i=1}^{6} A_i^{IJ}\left[I_i(x_-,\rho)-I_i(x_+,\rho)\right], \tag{A.1}$$

where I, J correspond to the "00", scalar, vector and tensor components of the energy-momentum tensor and the form of the six integrals I_i are as given in [216].

The coefficients A_i^{IJ}, together with the full expressions for the analytic equal time correlators B^{IJ}, are listed below (where, in this Appendix, we use the definitions $\rho = k|\tau_1-\tau_2|\upsilon$, $x_{1,2} = k\xi_0\tau_{1,2}$, $x_\pm = (x_1 \pm x_2)/2$):

$$\begin{aligned}
A_1^{00-00} &= 2\hat{U}^2 \\
A_i^{00-00} &= 0 \\
&\quad (i=2,..,6) \\
A_1^{00-S} &= \hat{U}(\hat{T}+(2\hat{U}-\hat{T})v^2) \\
A_2^{00-S} &= -3\hat{U}\left(\hat{T}(1-v^2)+\hat{U}v^2\right) \\
A_3^{00-S} &= 0 \\
A_4^{00-S} &= -3\hat{U}^2v^2 \\
A_5^{00-S} &= 3\hat{U}^2v^2 \\
A_6^{00-S} &= 0 \\
A_1^{S-S} &= \frac{-27\hat{U}^2v^4+\rho^2(\hat{T}+(2\hat{U}-\hat{T})v^2)^2}{2\rho^2} \\
A_2^{S-S} &= \frac{3\left(9\hat{U}^2v^4+\rho^2\left(\hat{T}^2(1-v^2)^2-\hat{U}^2v^4\right)\right)}{2\rho^2} \\
A_3^{S-S} &= -\frac{9}{2}\left(\left(\hat{U}v^2+\hat{T}(1-v^2)\right)^2-4v^2Q^2\right)
\end{aligned}$$

$$
\begin{aligned}
A_4^{S-S} &= \frac{3\hat{U}v^2\left(9\hat{U}v^2-\rho^2(\hat{T}(1-v^2)+2\hat{U}v^2)\right)}{\rho^2}\\
A_5^{S-S} &= -\frac{3\hat{U}v^2\left(9\hat{U}v^2-\rho^2(\hat{T}(1-v^2)+2\hat{U}v^2)\right)}{\rho^2}\\
A_6^{S-S} &= 9v^2\left(\hat{U}^2v^2+\hat{T}\hat{U}(1-v^2)-2Q^2)\right)\\
A_1^{V-V} &= \frac{3\hat{U}^2v^4+\rho^2v^2Q^2}{\rho^2}\\
A_2^{V-V} &= -\frac{3\hat{U}^2v^4}{\rho^2}\\
A_3^{V-V} &= \left(\hat{U}v^2+\hat{T}(1-v^2)\right)^2-4v^2Q^2\\
A_4^{V-V} &= -\left(6/\rho^2-1\right)\hat{U}^2v^4-v^2Q^2\\
A_5^{V-V} &= \left(6/\rho^2-1\right)\hat{U}^2v^4+v^2Q^2\\
A_6^{V-V} &= -2v^2\left(\hat{U}^2v^2+\hat{T}\hat{U}(1-v^2)-2Q^2\right)\\
A_1^{T-T} &= \frac{\rho^2\hat{T}^2\left(1-v^2\right)^2-3\hat{U}^2v^4}{4\rho^2}\\
A_2^{T-T} &= \frac{3\hat{U}^2v^4-\rho^2\left(\hat{T}^2\left(1-v^2\right)^2-\hat{U}^2v^4\right)}{4\rho^2}\\
A_3^{T-T} &= -\frac{1}{4}\left(\hat{U}v^2+\hat{T}(1-v^2)\right)^2+v^2Q^2\\
A_4^{T-T} &= \frac{v^2\left(3\hat{U}^2v^2+\rho^2\left(\hat{T}\hat{U}(1-v^2)+2Q^2\right)\right)}{2\rho^2}\\
A_5^{T-T} &= -\frac{v^2\left(3\hat{U}^2v^2+\rho^2\left(\hat{T}\hat{U}(1-v^2)+2Q^2\right)\right)}{2\rho^2}\\
A_6^{T-T} &= \frac{v^2}{2}\left(\hat{U}^2v^2+\hat{T}\hat{U}(1-v^2)-2Q^2\right)
\end{aligned}
$$

$$B^{00-00}(\tau)=2\hat{U}^2(\cos(x)-1+xSi(x)),$$

$$B^{00-S}=\frac{1}{2x}\left(\hat{U}(2\hat{T}+v^2(\hat{U}-2\hat{T}))(x\cos(x)+3\sin(x)+x(xSi(x)-4))\right),$$

$$
\begin{aligned}
B^{S-S}=\frac{x\cos(x)}{16x^3}\Bigg(\Bigg[8\hat{T}\hat{U}v^2(1-v^2)(x^2-18)+8\hat{T}^2(1-v^2)^2(x^2-18)+\\
+\hat{U}^2v^4(11x^2-54)+288v^2Q^2\Bigg]+x^3\Bigg[32\Big(3v^2Q^2-\hat{U}^2v^4-\hat{T}\hat{U}v^2(1-v^2)-\\
-\hat{T}^2(1-v^2)^2)\Big)+\left(11\hat{U}^2v^4+8\hat{T}\hat{U}v^2(1-v^2)+8\hat{T}^2(1-v^2)^2\right)xSi(x)\Bigg]-\\
-3\sin(x)\Bigg[8\hat{T}\hat{U}v^2(1-v^2)(x^2-6)+8\hat{T}^2(1-v^2)^2(x^2-6)-\hat{U}^2v^4(18+z^2)+96v^2Q^2\Bigg],
\end{aligned}
$$

$$B^{V-V} = \frac{1}{24x^3}\Big(3x\cos(x)\left[16\hat{T}(1-v^2)(\hat{T}-(\hat{T}-\hat{U})v^2)+\hat{U}^2v^4(6+z^2)+4v^2(x^2-8)Q^2\right]+$$
$$x^3\left[16\hat{T}(1-v^2)(\hat{T}-(\hat{T}-\hat{U})v^2)-32v^2Q^2+3v^2x(\hat{U}^2v^2+4Q^2)Si(x)\right]-$$
$$3\sin(x)\left[16\hat{T}(1-v^2)(\hat{T}-(\hat{T}-\hat{U})v^2)+\hat{U}^2v^4(6-x^2)+4v^2(x^2-8)Q^2\right]\Big),$$

$$B^{T-T} = \frac{1}{96x^3}\Big(3x\cos(x)\Big[(3\hat{U}^2v^4+8\hat{T}\hat{U}v^2(1-v^2)+8\hat{T}^2(1-v^2)^2)(x^2-2)+$$
$$+16v^2(2+x^2)Q^2\Big]+x^3\Big[64\hat{T}(1-v^2)(v^2(\hat{T}-\hat{U})-\hat{T})-64v^2Q^2+3x(3\hat{U}^2v^4+$$
$$+8\hat{T}\hat{U}v^2(1-v^2)+8\hat{T}^2(1-v^2)^2+16v^2Q^2)Si(x)\Big]+3\sin(x)\Big[\hat{U}^2v^4(6-5x^2)$$
$$+8\hat{T}\hat{U}v^2(1-v^2)(2+x^2)+8\hat{T}^2(1-v^2)^2(2+x^2)+16v^2(x^2-2)Q^2\Big]\Big).$$

List of figures

List of tables

References

[1] T. Kibble, "Cosmic strings reborn?," *COSLAB*, 2004, arXiv:astro-ph/0410073v2.

[2] Planck Collaboration XIII, "Planck 2015 results XIII cosmological parameters," *Astron.Astrophys.*, vol. 594, no. A13, p. 63, 2016, arXiv:1502.01589.

[3] B. D. Fields, "The Primordial Lithium Problem," *Annual Review of Nuclear and Particle Science*, vol. 61, no. 1, pp. 47–68, 2011, arXiv:1203.3551v1.

[4] A. J. Krasznahorkay and et al., "Observation of Anomalous Internal Pair Creation in ^{8}Be: A Possible Indication of a Light, Neutral Boson," *Phys. Rev. Lett.*, vol. 116, p. 042501, Jan 2016, arXiv:1504.01527v1.

[5] A. G. Riess and et al., "A 2.4% Determination of the Local Value of the Hubble Constant," *The Astrophysical Journal*, vol. 826, no. 1, p. 56, 2016, arXiv:1604.01424v3.

[6] J.-P. Uzan, "The big-bang theory: construction, evolution and status," *Introductory lecture notes from the Poincaré seminar XX (2015) and Les Houches school "Cosmology after Planck: what is next¿'*, p. 69, 2016, arXiv:1606.06112v1.

[7] A. Linde, "Particle physics and inflationary cosmology," *Contemp. Concepts Phys., 5:1-362*, 2005, arXiv:hep-th/0503203.

[8] J. Martin, C. Ringeval, and V. Vennin, "Encyclopædia inflationaris," *Physics of the Dark Universe*, vol. 5-6, no. Supplement C, pp. 75 – 235, 2014, arXiv:1303.3787v3. Hunt for Dark Matter.

[9] D. Baumann and L. McAllister, *Inflation and String Theory*. Cambridge University Press, Cambridge, 2015, arXiv:1404.2601v1.

[10] T. W. B. Kibble, "Topology of cosmic domains and strings," *J.Phys. A*, vol. 9, no. 8, pp. 1387–1398, 1976.

[11] Y. Zeldovich, I. Kobzarev, and L. Okun, "Cosmological consequences of the spontaneous breakdown of discrete symmetry," *Zh.Eksp.Teor.Fiz.*, vol. 67, pp. 3 – 11, 1974.

[12] P. Salomonson, B.-S. Skagerstam, and A. Stern, "On the primordial monopole problem in grand unified theories," *Physics Letters B*, vol. 151, no. 3, pp. 243 – 246, 1985.

[13] Planck Collaboration XXV, "Planck 2013 results. XXV. Searches for cosmic strings and other topological defects," *Astron. Astrophys.*, vol. 571, p. A25, 2014, arXiv:1303.5085v1.

[14] I. B. Zeldovich, "Cosmological fluctuations produced near a singularity," *MNRAS*, vol. 192, pp. 663–667, Sept. 1980.

[15] G. Dvali, R. Kallosh, and A. V. Proeyen, "D-term strings," *JHEP*, vol. 2004, no. 01, p. 035, 2004, arXiv:hep-th/0312005v3.

[16] G. Dvali and A. Vilenkin, "Formation and evolution of cosmic D-strings," *JCAP*, vol. 2004, no. 03, p. 010, 2004, arXiv:hep-th/0312007v2.

[17] E. J. Copeland, R. C. Myers, and J. Polchinski, "Cosmic F- and D-strings," *JHEP*, vol. 2004, no. 06, p. 013, 2004, arXiv:hep-th/0312067v5.

[18] S. Sarangi and S.-H. H. Tye, "Cosmic string production towards the end of brane inflation," *Phys.Lett.B*, vol. 536, no. 3-4, p. 185, 2002, arXiv:hep-th/0204074v1.

[19] H. Firouzjahi and S.-H. H. Tye, "Brane inflation and cosmic string tension in superstring theory," *JCAP*, vol. 0503, p. 009, 2005, arXiv:hep-th/0501099v3.

[20] N. T. Jones, H. Stoica, and S.-H. H. Tye, "The production, spectrum and evolution of cosmic strings in brane inflation," *Phys.Lett.*, vol. B, no. 563, pp. 6–14, 2003, arXiv:hep-th/0303269v1.

[21] R. Jeannerot, J. Rocher, and M. Sakellariadou, "How generic is cosmic string formation in SUSY GUTs," *Phys.Rev.D*, vol. 68, p. 103514, 2003, arXiv:hep-ph/0308134v1.

[22] Y. Cui, S. Martin, D. E. Morrissey, and J. Wells, "Cosmic strings from supersymmetric flat directions," *Phys.Rev.D*, vol. 77, p. 043528, 2008, arXiv:0709.0950v2.

[23] R. Jeannerot and M. Postma, "Chiral cosmic strings in supergravity," *JHEP*, vol. 0412, p. 043, 2004, arXiv:hep-ph/0411260.

[24] A. Achúcarro, A. Celi, M. Esole, J. Van den Bergh, and V. P. A., "D-term cosmic strings from N=2 supergravity," *JHEP*, vol. 0601, p. 102, 2006, arXiv:hep-th/0511001v2.

[25] M. Majumdar and A. C. Davis, "Cosmological creation of D-branes and anti-D-branes," *JHEP*, vol. 2002, no. 03, p. 056, 2002, arXiv:hep-th/0202148v3.

[26] E. Allys, "Bosonic condensates in realistic supersymmetric GUT cosmic strings," *JCAP*, vol. 1604, no. 04, p. 009, 2016, arXiv:1505.07888v3.

[27] M. Koehn and M. Trodden, "Supersymmetric k-defects," *Phys.Lett.*, vol. B, no. 755, pp. 498–503, 2016, arXiv:1512.09138v1.

[28] G. Ballesteros, R. J., A. Ringwald, and C. Tamarit, "Standard Model-Axion-Seesaw-Higgs Portal Inflation. Five problems of particle physics and cosmology solved in one stroke," *JCAP*, vol. 1708, no. 08, p. 001, 2017, arXiv:1610.01639v2.

[29] G. Lazarides, I. N. R. Peddie, and A. Vamvasakis, "Semi-shifted hybrid inflation with B-L cosmic strings," *Phys.Rev.*, vol. D, no. 78, p. 043518, 2008, arXiv:0804.3661v2.

[30] D. F. Chernoff and S.-H. H. Tye, "Inflation, string theory and cosmic strings," *Int.J.Mod.Phys.*, vol. D24, no. 3, p. 1530010, 2015, arXiv:1412.0579v2.

[31] R. H. Brandenberger, "Searching for cosmic strings in new observational windows," *Nuclear Physics B - Proceedings Supplements*, vol. 246-247, no. Supplement C, pp. 45 – 57, 2014, arXiv:1301.2856v1. Proceedings of the 9th International Symposium on Cosmology and Particle Astrophysics.

[32] R. H. Brandenberger, "Probing Particle Physics from Top Down with Cosmic Strings," *The Universe*, vol. 1, no. 4, pp. 6 – 23, 2013, arXiv:1401.4619v1.

[33] M. Kawasaki, K. Saikawa, and T. Sekiguchi, "Axion dark matter from topological defects," *Phys. Rev. D*, vol. 91, p. 065014, Mar 2015, arXiv:1412.0789v3.

[34] B. Gripaios and O. Randal-Williams, "Topology of electroweak vacua," *Physics Letters B*, vol. 782, pp. 94 – 98, 2018, arXiv:1610.05623v2.

[35] A. Vilenkin and E. P. S. Shellard, *Cosmic Strings and Other Topological Defects*. Cambridge University Press, Cambridge, 2000.

[36] M. B. Hindmarsh and T. W. B. Kibble, "Cosmic strings," *Rept.Prog.Phys.*, vol. 58, pp. 477–562, 1995, arXiv:hep-ph/9411342v1.

[37] A. Vilenkin and A. E. Everett, "Cosmic Strings and Domain Walls in Models with Goldstone and Pseudo-Goldstone Bosons," *Phys. Rev. Lett.*, vol. 48, pp. 1867–1870, Jun 1982.

[38] H. Nielsen and P. Olesen, "Vortex-line models for dual strings," *Nuclear Physics B*, vol. 61, pp. 45 – 61, 1973.

[39] M. Bucher, "The Aharonov-Bohm effect and exotic statistics for non-Abelian vortices," *Nuclear Physics B*, vol. 350, no. 1, pp. 163 – 178, 1991.

[40] M. G. Alford, K.-M. Lee, J. March-Russell, and J. Preskill, "Quantum field theory of non-Abelian strings and vortices," *Nuclear Physics B*, vol. 384, no. 1, pp. 251 – 317, 1992, arXiv:hep-th/9112038v1.

[41] H. J. de Vega and F. A. Schaposnik, "Vortices and electrically charged vortices in non-Abelian gauge theories," *Phys. Rev. D*, vol. 34, pp. 3206–3213, Nov 1986.

[42] N. D. Mermin, "The topological theory of defects in ordered media," *Rev. Mod. Phys.*, vol. 51, pp. 591–648, Jul 1979.

[43] K. Hashimoto and D. Tong, "Reconnection of non-Abelian cosmic strings," *JCAP*, vol. 2005, no. 09, p. 004, 2005, arXiv:hep-th/0506022v2.

[44] A. Avgoustidis and E. P. S. Shellard, "Velocity-Dependent Models for Non-Abelian/Entangled String Networks," *Phys.Rev.*, vol. D78, p. 103510, 2008, arXiv:0705.3395v3.

[45] E. Witten, "Superconducting strings," *Nuclear Physics B*, vol. 249, no. 4, pp. 557 – 592, 1985.

[46] E. Copeland, D. Haws, M. Hindmarsh, and N. Turok, "Dynamics of and radiation from superconducting strings and springs," *Nuclear Physics B*, vol. 306, no. 4, pp. 908 – 930, 1988.

[47] D. Haws, M. Hindmarsh, and N. Turok, "Superconducting strings or springs?," *Physics Letters B*, vol. 209, no. 2, pp. 255 – 261, 1988.

[48] B. Hartmann, F. Michel, and P. Peter, "Radial excitations of current-carrying vortices," *Physics Letters B*, vol. 767, pp. 354 – 359, 2017, arXiv:1608.02986v3.

[49] M. Lilley, P. Peter, and X. Martin, "Coupled currents in cosmic strings," *Phys. Rev.*, vol. D79, p. 103514, 2009, arXiv:0903.4328v1.

[50] M. Lilley, F. Di Marco, J. Martin, and P. Peter, "Nonabelian Bosonic Currents in Cosmic Strings," *Phys. Rev.*, vol. D82, p. 023510, 2010, arXiv:1003.4601v1.

[51] B. Hartmann, F. Michel, and P. Peter, "Excited cosmic strings with superconducting currents," *Phys. Rev. D*, vol. 96, p. 123531, Dec 2017, arXiv:1710.00738v2.

[52] D. Förster, "Dynamics of relativistic vortex lines and their relation to dual theory," *Nuclear Physics B*, vol. 81, no. 1, pp. 84 – 92, 1974.

[53] M. Anderson, F. Bonjour, R. Gregory, and J. Stewart, "Effective action and motion of a cosmic string," *Phys. Rev. D*, vol. 56, pp. 8014–8028, Dec 1997, arXiv:hep-ph/9707324v1.

[54] P. Coles and F. Lucchin, *Cosmology The Origin and Evolution of Cosmic Structure.* Chichester, UK: Wiley, 2002.

[55] S. Dodelson, *Modern Cosmology.* Amsterdam, Netherlands: Academic Press„ 2003.

[56] G. 't Hooft, "Magnetic monopoles in unified gauge theories," *Nuclear Physics B*, vol. 79, no. 2, pp. 276 – 284, 1974.

[57] A. Polyakov, "Particle spectrum in the quantum field theory," *JETP Lett.*, vol. 20, pp. 194–195, 1974.

[58] MoEDAL Collaboration, "Search for magnetic monopoles with the MoEDAL forward trapping detector in 13 TeV proton-proton collisions at the LHC," *Phys. Rev. Lett.*, vol. 118, p. 061801, Feb 2017, arXiv:1611.06817v2.

[59] Y. Zeldovich and M. Khlopov, "On the Concentration of Relic Magnetic Monopoles in the Universe," *Phys.Lett.*, vol. 79B, pp. 239–241, 1978.

[60] D. Baumann, "Inflation," *TASI 2009*, pp. 523–686, 2012, arXiv:0907.5424v2.

[61] A. Linde, "Hybrid inflation," *Phys. Rev. D*, vol. 49, pp. 748–754, Jan 1994, arXiv:astro-ph/9307002v3.

[62] F. Quevedo, S. Krippendorf, and O. Schlotterer, "Cambridge Lectures on Supersymmetry and Extra Dimensions," *DAMTP, lectures*, arXiv:1011.1491v1.

[63] P. Binetruy, *Supersymmetry: Theory, experiment and cosmology.* Oxford Univ. Pr., 2006.

[64] E. D. Stewart, "Inflation, supergravity, and superstrings," *Phys. Rev. D*, vol. 51, pp. 6847–6853, Jun 1995, arXiv:hep-ph/9405389v2.

[65] M. K. Gaillard, H. Murayama, and K. A. Olive, "Preserving flat directions during inflation," *Physics Letters B*, vol. 355, no. 1, pp. 71 – 77, 1995, arXiv:hep-ph/9504307v1.

[66] J. McDonald, "F term Hybrid Inflation, the η-problem and Extra Dimensions," *JHEP*, vol. 2002, no. 12, p. 029, 2002, arXiv:hep-ph/0201016v6.

[67] S. C. Davis, A. C. Davis, and M. Trodden, "N=1 supersymmetric cosmic strings," *Phys.Lett.*, vol. B, no. 405, pp. 257–264, 1997, arXiv:hep-ph/9702360v1.

[68] J. Rocher and M. Sakellariadou, "Constraints on supersymmetric grand unified theories from cosmology," *JCAP*, vol. 2005, no. 03, p. 004, 2005, arXiv:hep-ph/0406120v2.

[69] J. Rocher and M. Sakellariadou, "D-term inflation in non-minimal supergravity," *JCAP*, vol. 2006, no. 11, p. 001, 2006, arXiv:hep-th/0607226v2.

[70] R. Battye, B. Garbrecht, and A. Moss, "Tight constraints on F- and D-term hybrid inflation scenarios," *Phys. Rev. D*, vol. 81, p. 123512, Jun 2010, arXiv:1001.0769v1.

[71] C. Pallis and Q. Shafi, "Update on minimal supersymmetric hybrid inflation in light of PLANCK," *Physics Letters B*, vol. 725, no. 4, pp. 327 – 333, 2013, arXiv:1304.5202v3.

[72] J. Urrestilla, A. Achúcarro, and A. C. Davis, "D-Term Inflation without Cosmic Strings," *Phys. Rev. Lett.*, vol. 92, p. 251302, Jun 2004, arXiv:hep-th/0402032v2.

[73] C. P. Burgess, M. Majumdar, D. Nolte, F. Quevedo, G. Rajesh, and R.-J. Zhang, "The inflationary brane-antibrane universe," *Journal of High Energy Physics*, vol. 2001, no. 07, p. 047, 2001, arXiv:hep-th/0105204v3.

[74] M. Majumdar, "A tutorial on links between cosmic string theory and superstring theory," *COSLAB 2004*, 2005, arXiv:hep-th/0512062v2.

[75] G. Dvali and S.-H. Tye, "Brane inflation," *Physics Letters B*, vol. 450, no. 1, pp. 72 – 82, 1999, arXiv:hep-ph/9812483v1.

[76] S. Kachru, R. Kallosh, A. Linde, J. Maldacena, L. McAllister, and S. P. Trivedi, "Towards inflation in string theory," *Journal of Cosmology and Astroparticle Physics*, vol. 2003, no. 10, p. 013, 2003, arXiv:hep-th/0308055v2.

[77] S. Kachru, R. Kallosh, A. Linde, and S. P. Trivedi, "de Sitter vacua in string theory," *Phys. Rev. D*, vol. 68, no. 4, p. 046005, 2003, arXiv:hep-th/0301240v2.

[78] I. R. Klebanov and M. J. Strassler, "Supergravity and a confining gauge theory: duality cascades and chi SB-resolution of naked singularities," *Journal of High Energy Physics*, vol. 2000, no. 08, p. 052, 2000, arXiv:hep-th/0007191v4.

[79] N. Barnaby, C. Burgess, and J. Cline, "Warped reheating in brane–antibrane inflation," *JCAP*, vol. 2005, no. 04, p. 007, 2005, arXiv:hep-th/0412040v3.

[80] J. H. Schwarz, "An SL(2, Z) multiplet of type IIB superstrings," *Physics Letters B*, vol. 360, no. 1, pp. 13 – 18, 1995, arXiv:hep-th/9508143v5.

[81] K. Becker, M. Becker, and J. Schwarz, *String Theory and M-Theory: A Modern Introduction*. Cambridge University Press, 2007.

[82] J. Polchinski, *String theory. Vol. 2: Superstring theory and beyond*. Cambridge University Press, 1998.

[83] E. Witten, "Bound states of strings and p-branes," *Nuclear Physics B*, vol. 460, no. 2, pp. 335 – 350, 1996, arXiv:hep-th/9510135v2.

[84] K. Dasgupta and S. Mukhi, "BPS nature of 3-string junctions," *Physics Letters B*, vol. 423, no. 3, pp. 261 – 264, 1998, arXiv:hep-th/9711094v1.

[85] E. J. Copeland, T. W. B. Kibble, and D. A. Steer, "Collisions of Strings with Y junctions," *Phys. Rev. Lett.*, vol. 97, p. 021602, Jul 2006, arXiv:hep-th/0601153v3.

[86] R. Battye, B. Garbrecht, A. Moss, and H. Stoica, "Constraints on brane inflation and cosmic strings," *JCAP*, vol. 2008, no. 01, p. 020, 2008, arXiv:0710.1541v3.

[87] R. Gwyn, M. Sakellariadou, and S. Sypsas, "Theoretical constraints on brane inflation and cosmic superstring radiation," *JHEP*, vol. 2011, no. 9, p. 75, 2011, arXiv:1105.1784v3.

[88] C. J. A. P. Martins and E. P. S. Shellard, "Quantitative string evolution," *Phys. Rev.*, vol. D54, pp. 2535–2556, 1996, arXiv:hep-ph/9602271v2.

[89] C. J. A. P. Martins and E. P. S. Shellard, "Extending the velocity dependent one scale string evolution model," *Phys. Rev.*, vol. D65, p. 043514, 2002, arXiv:hep-ph/0003298v1.

[90] C. J. A. P. Martins and A. Achúcarro, "Evolution of local and global monopole networks," *Phys. Rev. D*, vol. 78, p. 083541, Oct 2008, arXiv:0806.2671v1.

[91] P. P. Avelino, C. J. A. P. Martins, and J. C. R. E. Oliveira, "One-scale model for domain wall network evolution," *Phys. Rev. D*, vol. 72, p. 083506, Oct 2005, arXiv:hep-ph/0507272v1.

[92] A. Avgoustidis and E. P. S. Shellard, "Cosmic string evolution in higher dimensions," *Phys. Rev. D*, vol. 71, p. 123513, Jun 2005, arXiv:hep-ph/0410349v2.

[93] L. Sousa and P. P. Avelino, "Cosmological evolution of p-brane networks," *Phys. Rev. D*, vol. 84, p. 063502, Sep 2011, arXiv:1107.4582v1.

[94] L. Sousa and P. P. Avelino, "p-brane dynamics in (N+1)-dimensional FRW universes: A unified framework," *Phys. Rev. D*, vol. 83, p. 103507, May 2011, arXiv:1103.1381v1.

[95] A. M. M. Leite and C. J. A. P. Martins, "Scaling Properties of Domain Wall Networks," *Phys. Rev.*, vol. D84, p. 103523, 2011, arXiv:1110.3486v1.

[96] A. M. M. Leite, C. J. A. P. Martins, and E. P. S. Shellard, "Accurate Calibration of the Velocity-dependent One-scale Model for Domain Walls," *Phys. Lett.*, vol. B718, pp. 740–744, 2013, arXiv:1206.6043v2.

[97] W. H. Press, B. S. Ryden, and D. N. Spergel, "Dynamical evolution of domain walls in an expanding universe," *Astrophys.J.*, vol. 347, p. 590, 1989.

[98] C. J. A. P. Martins, J. N. Moore, and E. P. Shellard, "A Unified model for vortex string network evolution," *Phys. Rev. Lett.*, vol. 92, p. 251601, 2004, arXiv:hep-ph/0310255v2.

[99] C. J. A. P. Martins and E. P. S. Shellard, "Fractal properties and small-scale structure of cosmic string networks," *Phys. Rev.*, vol. D73, p. 043515, 2006, arXiv:astro-ph/0511792v1.

[100] T. Kibble, "Some implications of a cosmological phase transition," *Physics Reports*, vol. 67, no. 1, pp. 183 – 199, 1980.

[101] T. Kibble, "Evolution of a system of cosmic strings," *Nuclear Physics B*, vol. 252, pp. 227 – 244, 1985.

[102] D. P. Bennett, "Evolution of cosmic strings," *Phys. Rev. D*, vol. 33, pp. 872–888, Feb 1986.

[103] D. P. Bennett, "Evolution of cosmic strings. II," *Phys. Rev. D*, vol. 34, pp. 3592–3607, Dec 1986.

[104] A. Albrecht and N. Turok, "Evolution of cosmic string networks," *Phys. Rev. D*, vol. 40, pp. 973–1001, Aug 1989.

[105] D. Austin, E. J. Copeland, and T. W. B. Kibble, "Evolution of cosmic string configurations," *Phys. Rev. D*, vol. 48, pp. 5594–5627, Dec 1993, arXiv:hep-ph/9307325v1.

[106] C. Martins and E. Shellard, "Vorton formation," *Phys.Rev.*, vol. D, no. 57, pp. 7155–7176, 1998, arXiv:hep-ph/9804378v1.

[107] C. Martins, E. Shellard, and J. Vieira, "Models for Small-Scale Structure on Cosmic Strings: Mathematical Formalism," *Phys.Rev.*, vol. D90, no. 4, p. 043518, 2014, arXiv:1405.7722v1.

[108] A. S. Nunes, A. Avgoustidis, C. J. A. P. Martins, and J. Urrestilla, "Analytic models for the evolution of semilocal string networks," *Phys. Rev. D*, vol. 84, p. 063504, Sep 2011, arXiv:1107.2008v2.

[109] M. F. Oliveira, A. Avgoustidis, and C. J. A. P. Martins, "Cosmic string evolution with a conserved charge," *Phys.Rev.*, vol. D85, p. 083515, 2012, arXiv:1201.5064v1.

[110] A. Vilenkin, "Effect of Small Scale Structure on the Dynamics of Cosmic Strings," *Phys. Rev.*, vol. D41, p. 3038, 1990.

[111] C. J. A. P. Martins and E. P. S. Shellard, "Scale-invariant string evolution with friction," *Phys. Rev. D*, vol. 53, pp. R575–R579, Jan 1996, arXiv:hep-ph/9507335v1.

[112] C. Martins, *Defect Evolution in Cosmology and Condensed Matter*. SpringerBriefs in Physics. Springer, Cham, 2016.

[113] T. Vachaspati, A. E. Everett, and A. Vilenkin, "Radiation from vacuum strings and domain walls," *Phys. Rev. D*, vol. 30, pp. 2046–2053, Nov 1984.

[114] C. J. A. P. Martins, I. Y. Rybak, A. Avgoustidis, and E. P. S. Shellard, "Stretching and kibble scaling regimes for hubble-damped defect networks," *Phys. Rev. D*, vol. 94, p. 116017, Dec 2016, arXiv:1612.08863v1.

[115] J. J. Blanco-Pillado, K. D. Olum, and B. Shlaer, "Large parallel cosmic string simulations: New results on loop production," *Phys.Rev.*, vol. D, no. 83, p. 083514, 2011, arXiv:1101.5173v2.

[116] M. Hindmarsh, J. Lizarraga, J. Urrestilla, D. Daverio, and M. Kunz, "Scaling from gauge and scalar radiation in Abelian Higgs string networks," *Phys.Rev.*, vol. D96, no. 2, p. 023525, 2017, arXiv:1703.06696v3.

[117] C. Martins, "Wiggly Cosmic Strings," *Astrophys.Space Sci.*, vol. 261, no. 1, pp. 311–314, 1998.

[118] E. J. Copeland and P. M. Saffin, "On the evolution of cosmic-superstring networks," *JHEP*, vol. 11, p. 023, 2005, arXiv:hep-th/0505110v2.

[119] S. H. H. Tye, I. Wasserman, and M. Wyman, "Scaling of multi-tension cosmic superstring networks," *Phys. Rev.*, vol. D71, p. 103508, 2005, arXiv:astro-ph/0503506v3. [Erratum: Phys. Rev.D71,129906(2005)].

[120] A.-N. Davis and P. Peter, "Cosmic strings are current-carrying," *Physics Letters B*, vol. 358, no. 3, pp. 197 – 202, 1995, arXiv:hep-ph/9506433v1.

[121] R. Brandenberger, B. Carter, A.-C. Davis, and M. Trodden, "Cosmic vortons and particle physics constraints," *Phys. Rev. D*, vol. 54, pp. 6059–6071, Nov 1996, arXiv:hep-ph/9605382v1.

[122] S. C. Davis, A. C. Davis, and M. Trodden, "Cosmic strings, zero modes and SUSY breaking in non Abelian N=1 gauge theories," *Phys.Rev.*, vol. D, no. 57, pp. 5184–5188, 1998, arXiv:hep-ph/9711313v1.

[123] A. Everett, "New mechanism for superconductivity in cosmic strings," *Phys.Rev.Lett.*, vol. 61, pp. 1807–1810, 1988.

[124] M. Hindmarsh, K. Rummukainen, and D. J. Weir, "New solutions for non-Abelian cosmic strings," *Phys.Rev.Lett.*, vol. 117, no. 25, p. 251601, 2016, arXiv:1607.00764v2.

[125] B. Carter, "Integrable equation of state for noisy cosmic string," *Phys.Rev.*, vol. D41, pp. 3869–3872, 1990.

[126] B. Carter, "Transonic elastic model for wiggly Goto-Nambu string," *Phys.Rev.Lett.*, vol. 74, pp. 3098–3101, 1995, arXiv:hep-th/9411231v1.

[127] B. Carter, "Basic brane theory," *Classical and Quantum Gravity*, vol. 9, no. S, p. S19, 1992.

[128] B. Carter, "Brane dynamics for treatment of cosmic strings and vortons," *2nd Mexican School on Gravitation and Mathematical Physics*, 1997, arXiv:hep-th/9705172v1.

[129] B. Carter, "Stability and characteristic propagation speeds in superconducting cosmic and other string models," *Physics Letters B*, vol. 228, no. 4, pp. 466 – 470, 1989.

[130] P. Peter, "Superconducting cosmic string: Equation of state for spacelike and timelike current in the neutral limit," *Phys. Rev. D*, vol. 45, pp. 1091–1102, Feb 1992.

[131] B. Carter and P. Peter, "Supersonic string models for Witten vortices," *Phys.Rev.*, vol. D, no. 52, pp. 1744–1748, 1995, arXiv:hep-ph/9411425v1.

[132] B. Carter, "Dilatonic formulation for conducting cosmic string models," *Ann. Phys.*, vol. 9, no. 3-5, pp. 247–257, 2000, arXiv:hep-th/0002162v1.

[133] X. Martin, "Cancellation of longitudinal contribution in wiggly string equation of state," *Phys. Rev. Lett.*, vol. 74, pp. 3102–3104, Apr 1995.

[134] N. Nielsen, "Dimensional reduction and classical strings," *Nucl.Phys.*, vol. B167, pp. 249–260, 1980.

[135] E. Babichev, P. Brax, C. Caprini, J. Martin, and D. Steer, "Dirac Born Infeld (DBI) cosmic strings," *JHEP*, vol. 2009, no. 03, p. 091, 2009, arXiv:0809.2013v1.

[136] C. Ringeval, "Fermionic massive modes along cosmic strings," *Phys. Rev.*, vol. D64, p. 123505, 2001, arXiv:hep-ph/0106179v2.

[137] C. Ringeval, "Equation of state of cosmic strings with fermionic current carriers," *Phys. Rev.*, vol. D63, p. 063508, 2001, arXiv:hep-ph/0007015v2.

[138] E. Allys, "Bosonic structure of realistic SO(10) supersymmetric cosmic strings," *Phys.Rev.*, vol. D93, no. 10, p. 105021, 2016, arXiv:1512.02029v3.

[139] J. J. Blanco-Pillado, K. D. Olum, and A. Vilenkin, "Dynamics of superconducting strings with chiral currents," *Phys. Rev. D*, vol. 63, p. 103513, Apr 2001, arXiv:astro-ph/0004410v3.

[140] B. Carter and P. Peter, "Dynamics and integrability property of the chiral string model," *Phys.Lett.*, vol. B, no. 466, pp. 41–49, 1999, arXiv:hep-th/9905025v1.

[141] A. C. Davis, T. W. B. Kibble, M. Pickles, and D. A. Steer, "Dynamics and properties of chiral cosmic strings in Minkowski space," *Phys. Rev. D*, vol. 62, p. 083516, Sep 2000, arXiv:astro-ph/0005514v1.

[142] J. Vieira, C. Martins, and E. Shellard, "Models for small-scale structure on cosmic strings. II. Scaling and its stability," *Phys.Rev.*, vol. D94, no. 9, p. 099907, 2016, arXiv:1611.06103v1.

[143] L. Pogosian and T. Vachaspati, "Cosmic microwave background anisotropy from wiggly strings," *Phys.Rev.*, vol. D60, no. 8, p. 083504, 1999, arXiv:astro-ph/9903361v4.

[144] J. N. Moore, E. P. S. Shellard, and C. J. A. P. Martins, "On the evolution of Abelian-Higgs string networks," *Phys. Rev.*, vol. D65, p. 023503, 2002, arXiv:hep-ph/0107171v3.

[145] C. T. Hill and L. M. Widrow, "Superconducting Cosmic Strings with Massive Fermions," *Phys. Lett.*, vol. B189, pp. 17–22, 1987.

[146] M. Hindmarsh, "Superconducting Cosmic Strings With Coupled Zero Modes," *Phys. Lett.*, vol. B200, pp. 429–433, 1988.

[147] P. Saffin, "A practical model for cosmic (p,q) superstrings," *JHEP*, vol. 2005, no. 09, p. 011, 2005, arXiv:hep-th/0506138v1.

[148] A. Rajantie, M. Sakellariadou, and H. Stoica, "Numerical experiments with p F-and q D-strings: the formation of (p, q) bound states," *JCAP*, vol. 2007, no. 11, p. 021, 2007, arXiv:0706.3662v3.

[149] J. Urrestilla and A. Vilenkin, "Evolution of cosmic superstring networks: a numerical simulation," *JHEP*, vol. 2008, no. 02, p. 037, 2008, arXiv:0712.1146v2.

[150] J. Lizarraga and J. Urrestilla, "Survival of pq-superstrings in field theory simulations," *JCAP*, vol. 1604, no. 04, p. 053, 2016, arXiv:1602.08014v2.

[151] J. Polchinski, "Collision of macroscopic fundamental strings," *Physics Letters B*, vol. 209, no. 2, pp. 252 – 254, 1988.

[152] J. Dai and J. Polchinski, "The decay of macroscopic fundamental strings," *Physics Letters B*, vol. 220, no. 3, pp. 387 – 390, 1989.

[153] M. G. Jackson, N. T. Jones, and J. Polchinski, "Collisions of cosmic F- and D-strings," *JHEP*, vol. 2005, no. 10, p. 013, 2005, arXiv:hep-th/0405229v2.

[154] M. G. Jackson, "Interactions of cosmic superstrings," *JHEP*, vol. 2007, no. 09, p. 035, 2007, arXiv:0706.1264v2.

[155] E. J. Copeland, T. W. B. Kibble, and D. A. Steer, "Constraints on string networks with junctions," *Phys. Rev. D*, vol. 75, p. 065024, Mar 2007, arXiv:hep-th/0611243v2.

[156] E. J. Copeland, H. Firouzjahi, T. W. B. Kibble, and D. A. Steer, "Collision of cosmic superstrings," *Phys. Rev. D*, vol. 77, p. 063521, Mar 2008, arXiv:0712.0808v1.

[157] P. Salmi, A. Achúcarro, E. J. Copeland, T. W. B. Kibble, R. de Putter, and D. A. Steer, "Kinematic constraints on formation of bound states of cosmic strings: Field theoretical approach," *Phys. Rev. D*, vol. 77, p. 041701, Feb 2008, arXiv:0712.1204v2.

[158] N. Bevis and P. M. Saffin, "Cosmic string Y-junctions: A comparison between field theoretic and Nambu-Goto dynamics," *Phys. Rev. D*, vol. 78, p. 023503, Jul 2008, arXiv:0804.0200v2.

[159] H. Firouzjahi, S. Khoeini-Moghaddam, and S. Khosravi, "Cosmic string collision in cosmological backgrounds," *Phys. Rev. D*, vol. 81, p. 123506, Jun 2010, arXiv:1004.0068v1.

[160] J. Polchinski and J. V. Rocha, "Analytic study of small scale structure on cosmic strings," *Phys. Rev. D*, vol. 74, p. 083504, Oct 2006, arXiv:hep-ph/0606205v4.

[161] E. J. Copeland and T. W. B. Kibble, "Kinks and small-scale structure on cosmic strings," *Phys. Rev. D*, vol. 80, p. 123523, Dec 2009, arXiv:0909.1960v2.

[162] D. Skliros and M. Hindmarsh, "String vertex operators and cosmic strings," *Phys. Rev. D*, vol. 84, p. 126001, Dec 2011, arXiv:1107.0730v1.

[163] M. G. Jackson and X. Siemens, "Gravitational wave bursts from cosmic superstring reconnections," *Journal of High Energy Physics*, vol. 2009, no. 06, p. 089, 2009, arXiv:0901.0867v2.

[164] D. P. Skliros, *Vertex Operators for Cosmic Strings*. PhD thesis, the University of Sussex, 2010.

[165] A. Hanany and K. Hashimoto, "Reconnection of colliding cosmic strings," *Journal of High Energy Physics*, vol. 2005, no. 06, p. 021, 2005, .

[166] J. Polchinski, *String theory. Vol. 1: An introduction to the bosonic string*. Cambridge University Press, 1998.

[167] D. Tong, "Lectures on String Theory," arXiv:0908.0333v3.

[168] A. Pourtsidou, A. Avgoustidis, E. J. Copeland, L. Pogosian, and D. A. Steer, "Scaling configurations of cosmic superstring networks and their cosmological implications," *Phys. Rev. D*, vol. 83, p. 063525, Mar 2011, arXiv:1012.5014v2.

[169] A. Avgoustidis and E. J. Copeland, "Effect of kinematic constraints on multitension string network evolution," *Phys. Rev. D*, vol. 81, p. 063517, Mar 2010.

[170] G. S. Sharov, "String baryon model "triangle"," *Theoretical and Mathematical Physics*, vol. 113, pp. 1263–1276, Oct 1997, arXiv:hep-th/9808099v1.

[171] G. 't Hooft, "Minimal strings for baryons," in *C04-07-12.5, ITP-UU-04-17, SPIN-04-10*, vol. 5805 of *Hadrons and Strings Workshop: A Trento ECT Workshop*, (Trento, Italy), 2004, arXiv:hep-th/0408148v1.

[172] A. Pourtsidou, *Cosmic Strings with Junctions: Dynamics and Cosmological Implications*. PhD thesis, the University of Nottingham, 2010.

[173] D. A. Steer, M. Lilley, D. Yamauchi, and T. Hiramatsu, "Y-junction intercommutations of current carrying strings," *Phys. Rev. D*, vol. 97, p. 023507, Jan 2018, arXiv:1710.07475v1.

[174] K. Moriarty, E. Myers, and C. Rebbi, "The dynamical interactions of cosmic strings," *Journal of Computational Physics*, vol. 88, no. 2, pp. 467 – 476, 1990.

[175] P. Laguna and R. A. Matzner, "Numerical simulation of bosonic-superconducting-string interactions," *Phys. Rev. D*, vol. 41, pp. 1751–1763, Mar 1990.

[176] A. Avgoustidis, A. Pourtsidou, and M. Sakellariadou, "Zipping and unzipping in string networks: Dynamics of Y-junctions," *Phys. Rev. D*, vol. 91, p. 025022, Jan 2015, arXiv:1411.7959v1.

[177] T. W. B. Kibble and E. Copeland, "Evolution of small-scale structure on cosmic strings," *Physica Scripta*, vol. 1991, no. T36, p. 153, 1991.

[178] G. R. Vincent, M. Hindmarsh, and M. Sakellariadou, "Scaling and small-scale structure in cosmic string networks," *Phys. Rev. D*, vol. 56, pp. 637–646, Jul 1997, arXiv:astro-ph/9612135v1.

[179] V. Vanchurin, K. Olum, and A. Vilenkin, "Cosmic string scaling in flat space," *Phys. Rev. D*, vol. 72, p. 063514, Sep 2005, arXiv:gr-qc/0501040v3.

[180] M. Hindmarsh, S. Stuckey, and N. Bevis, "Abelian higgs cosmic strings: Small-scale structure and loops," *Phys. Rev. D*, vol. 79, p. 123504, Jun 2009, arXiv:0812.1929v2.

[181] A. Avgoustidis and E. P. S. Shellard, "Effect of reconnection probability on cosmic (super)string network density," *Phys. Rev. D*, vol. 73, p. 041301, Feb 2006, arXiv:astro-ph/0512582v1.

[182] H. Firouzjahi, J. Karouby, S. Khosravi, and R. Brandenberger, "Zipping and unzipping of cosmic string loops in collision," *Phys. Rev. D*, vol. 80, p. 083508, Oct 2009, arXiv:0907.4986v2.

[183] M. Sazhin and et al., "CSL-1: chance projection effect or serendipitous discovery of a gravitational lens induced by a cosmic string?," *Monthly Notices of the Royal Astronomical Society*, vol. 343, no. 2, pp. 353–359, 2003, arXiv:astro-ph/0302547v1.

[184] E. Agol, C. J. Hogan, and R. M. Plotkin, "Hubble imaging excludes cosmic string lens," *Phys. Rev. D*, vol. 73, p. 087302, Apr 2006, arXiv:astro-ph/0603838v3.

[185] E. Morganson, P. Marshall, T. Treu, T. Schrabback, and R. D. Blandford, "Direct observation of cosmic strings via their strong gravitational lensing effect - II. Results from the HST/ACS image archive," *Monthly Notices of the Royal Astronomical Society*, vol. 406, no. 4, pp. 2452–2472, 2010, arXiv:0908.0602v1.

[186] R. J. Danos, R. H. Brandenberger, and G. Holder, "Signature of cosmic string wakes in the CMB polarization," *Phys. Rev. D*, vol. 82, p. 023513, Jul 2010, arXiv:1003.0905v1.

[187] O. S. Sazhina and M. V. Scognamiglio, D.and Sazhin, "Observational constraints on the types of cosmic strings," *The European Physical Journal C*, vol. 74, p. 2972, Aug 2014, arXiv:1312.6106v2.

[188] G. Riccio, *The Observational Signatures of Cosmic Strings*. PhD thesis, University of Naples Federico II, 2009.

[189] A. Lopez-Eiguren, J. Lizarraga, M. Hindmarsh, and J. Urrestilla, "Cosmic microwave background constraints for global strings and global monopoles," *JCAP*, vol. 2017, no. 07, p. 026, 2017, arXiv:1705.04154v2.

[190] A. Lazanu, E. P. S. Shellard, and M. Landriau, "CMB power spectrum of Nambu-Goto cosmic strings," *Phys. Rev. D*, vol. 91, p. 083519, Apr 2015, arXiv:1410.4860v3.

[191] T. Charnock, A. Avgoustidis, E. Copeland, and M. A., "CMB constraints on cosmic strings and superstrings," *Phys.Rev.*, vol. D93, no. 12, p. 123503, 2016, arXiv:1603.01275v2.

[192] L. Lentati and et al., "European Pulsar Timing Array limits on an isotropic stochastic gravitational-wave background," *MNRAS*, vol. 453, no. 3, pp. 2576–2598, 2015, arXiv:1504.03692v3.

[193] C. Caprini and et al., "Science with the space-based interferometer eLISA. II: gravitational waves from cosmological phase transitions," *JCAP*, vol. 2016, no. 04, p. 001, 2016, arXiv:1512.06239v2.

[194] B. P. Abbott and L. et al., "Constraints on cosmic strings using data from the first Advanced LIGO observing run," *Phys. Rev. D*, vol. 97, p. 102002, May 2018, arXiv:1712.01168v2.

[195] R. A. Alpher, H. Bethe, and G. Gamow, "The origin of chemical elements," *Phys. Rev.*, vol. 73, pp. 803–804, Apr 1948.

[196] R. A. Alpher and R. C. Herman, "Theory of the origin and relative abundance distribution of the elements," *Rev. Mod. Phys.*, vol. 22, pp. 153–212, Apr 1950.

[197] V. Mukhanov, *Physical Foundations of Cosmology*. Cambridge University Press, 2005.

[198] L. Husdal, "On Effective Degrees of Freedom in the Early Universe," *Galaxies*, vol. 4, no. 4, 2016.

[199] M. Saha, "LIII. Ionization in the solar chromosphere," *The London, Edinburgh, and Dublin Philosophical Magazine and Journal of Science*, vol. 40, no. 238, pp. 472–488, 1920.

[200] S. Weinberg, *Cosmology*. Oxford University Press, 2008.

[201] E. R. Harrison, "Fluctuations at the threshold of classical cosmology," *Phys. Rev. D*, vol. 1, pp. 2726–2730, May 1970.

[202] P. J. E. Peebles and J. T. Yu, "Primeval Adiabatic Perturbation in an Expanding Universe," *ApJ*, vol. 162, p. 815, Dec. 1970.

[203] Y. B. Zeldovich, "A hypothesis, unifying the structure and the entropy of the Universe," *MNRAS*, vol. 160, p. 1P, 1972.

[204] G. F. Smoot and et al., "Structure in the COBE differential microwave radiometer first-year maps," *ApJ*, vol. 396, pp. L1–L5, Sept. 1992.

[205] E. Komatsu and et al., "Seven-year Wilkinson Microwave Anisotropy Probe (WMAP) Observations: Cosmological Interpretation," *The Astrophysical Journal Supplement Series*, vol. 192, no. 2, p. 18, 2011, arXiv:1001.4538v3.

[206] Planck Collaboration, "Planck 2015 results - I. Overview of products and scientific results," *A&A*, vol. 594, p. A1, 2016, arXiv:1502.01582v2.

[207] E. Lifshitz, "Republication of: On the gravitational stability of the expanding universe," *General Relativity and Gravitation*, vol. 49, p. 18, Jan 2017.

[208] V. Mukhanov, H. Feldman, and R. Brandenberger, "Theory of cosmological perturbations," *Physics Reports*, vol. 215, no. 5, pp. 203 – 333, 1992.

[209] C.-P. Ma and E. Bertschinger, "Cosmological Perturbation Theory in the Synchronous and Conformal Newtonian Gauges," *"ApJ"*, vol. 455, p. 7, Dec. 1995, arXiv:astro-ph/9506072v1.

[210] A. Challinor and H. Peiris, "Lecture notes on the physics of cosmic microwave background anisotropies," *AIP Conference Proceedings*, vol. 1132, no. 1, pp. 86–140, 2009, arXiv:0903.5158v1.

[211] Planck Collaboration, "Planck 2015 results - XI. CMB power spectra, likelihoods, and robustness of parameters," *A&A*, vol. 594, p. A11, 2016, arXiv:1507.02704v3.

[212] A. Lazanu and E. P. S. Shellard, "Constraints on the Nambu-Goto cosmic string contribution to the CMB power spectrum in light of new temperature and polarisation data," *JCAP*, vol. 2015, no. 02, p. 024, 2015, arXiv:1410.5046v3.

[213] J. Lizarraga, J. Urrestilla, D. Daverio, M. Hindmarsh, and M. Kunz, "New CMB constraints for Abelian Higgs cosmic strings," *JCAP*, vol. 1610, no. 10, p. 042, 2016, arXiv:1609.03386v3.

[214] N. Turok, U. Pen, and U. Seljak, "The Scalar, vector and tensor contributions to CMB anisotropies from cosmic defects," *Phys.Rev.*, vol. D, no. 58, p. 023506, 1998, arXiv:astro-ph/9706250v2.

[215] A. Albrecht, R. A. Battye, and J. Robinson, "Detailed study of defect models for cosmic structure formation," *Phys.Rev.*, vol. D, no. 59, p. 023508, 1999, arXiv:astro-ph/9711121v2.

[216] A. Avgoustidis, E. Copeland, A. Moss, and D. Skliros, "Fast Analytic Computation of Cosmic String Power Spectra," *Phys.Rev.*, vol. D, no. 86, p. 123513, 2012, arXiv:1209.2461v2.

[217] U. Pen, D. Spergel, and N. Turok, "Cosmic structure formation and microwave anisotropies from global field ordering," *Phys.Rev.*, vol. D, no. 49, pp. 692–729, 1994.

[218] A. Vilenkin, "Gravitational field of vacuum domain walls and strings," *Phys. Rev. D*, vol. 23, pp. 852–857, Feb 1981.

[219] D. Garfinkle, "General relativistic strings," *Phys. Rev. D*, vol. 32, pp. 1323–1329, Sep 1985.

[220] A. Vilenkin, "Cosmic strings as gravitational lenses," *APJL*, vol. 282, pp. L51–L53, July 1984.

[221] M. V. Sazhin and et al., "Gravitational lensing by cosmic strings: what we learn from the CSL-1 case," *Monthly Notices of the Royal Astronomical Society*, vol. 376, no. 4, pp. 1731–1739, 2007, arXiv:astro-ph/0611744v2.

[222] E. Morganson, P. Marshall, T. Treu, T. Schrabback, and R. D. Blandford, "Direct observation of cosmic strings via their strong gravitational lensing effect – ii. results from the hst/acs image archive," *Monthly Notices of the Royal Astronomical Society*, vol. 406, no. 4, pp. 2452–2472, 2010.

[223] N. Kaiser and A. Stebbins, "Microwave anisotropy due to cosmic strings," *Nature*, vol. 310, pp. 391–393, 1984.

[224] R. Brandenberger, H. Firouzjahi, and J. Karouby, "Lensing and CMB anisotropies by cosmic strings at a junction," *Phys. Rev. D*, vol. 77, p. 083502, Apr 2008, arXiv:0710.1636v1.

[225] R. H. Danos, R. J.and Brandenberger, "Searching for signatures of cosmic superstrings in the CMB," *JCAP*, vol. 2010, no. 02, p. 033, 2010, arXiv:0910.5722v1.

[226] A. Vilenkin, "Gravitational radiation from cosmic strings," *Physics Letters B*, vol. 107, no. 1, pp. 47 – 50, 1981.

[227] D. Garfinkle and T. Vachaspati, "Radiation from kinky, cuspless cosmic loops," *Phys. Rev. D*, vol. 36, pp. 2229–2241, Oct 1987.

[228] T. Damour and A. Vilenkin, "Gravitational wave bursts from cosmic strings," *Phys. Rev. Lett.*, vol. 85, pp. 3761–3764, 2000, arXiv:gr-qc/0004075v1.

[229] T. Damour and A. Vilenkin, "Gravitational wave bursts from cusps and kinks on cosmic strings," *Phys. Rev.*, vol. D64, p. 064008, 2001, arXiv:gr-qc/0104026v1.

[230] J. Polchinski and J. V. Rocha, "Cosmic string structure at the gravitational radiation scale," *Phys. Rev. D*, vol. 75, p. 123503, Jun 2007, arXiv:gr-qc/0702055v2.

[231] T. Damour and A. Vilenkin, "Gravitational radiation from cosmic (super)strings: Bursts, stochastic background, and observational windows," *Phys. Rev.*, vol. D71, p. 063510, 2005, arXiv:hep-th/0410222v2.

[232] X. Siemens, J. Creighton, I. Maor, S. R. Majumder, K. Cannon, and J. Read, "Gravitational wave bursts from cosmic (super)strings: Quantitative analysis and constraints," *Phys. Rev. D*, vol. 73, p. 105001, May 2006, arXiv:gr-qc/0603115v2.

[233] P. Binetruy, A. Bohe, T. Hertog, and D. A. Steer, "Gravitational wave signatures from kink proliferation on cosmic (super-)strings," *Phys. Rev.*, vol. D82, p. 126007, 2010, arXiv:1009.2484v1.

[234] B. P. Abbott and et al. LIGO Scientific Collaboration and Virgo Collaboration, "Observation of Gravitational Waves from a Binary Black Hole Merger," *Phys. Rev. Lett.*, vol. 116, p. 061102, Feb 2016, arXiv:1602.03837v1.

[235] P. Binétruy, A. Bohé, C. Caprini, and J.-F. Dufaux, "Cosmological backgrounds of gravitational waves and eLISA/NGO: phase transitions, cosmic strings and other sources," *JCAP*, vol. 2012, no. 06, p. 027, 2012, arXiv:1201.0983v3.

[236] D. G. Figueroa, M. Hindmarsh, and J. Urrestilla, "Exact Scale-Invariant Background of Gravitational Waves from Cosmic Defects," *Phys.Rev.Lett.*, vol. 110, no. 10, p. 101302, 2013, arXiv:1212.5458v2.

[237] S. Kuroyanagi, K. Takahashi, N. Yonemaru, and H. Kumamoto, "Anisotropies in the gravitational wave background as a probe of the cosmic string network," *Phys.Rev.*, vol. D95, no. 4, p. 043531, 2017, arXiv:1604.00332v2.

[238] X. Siemens, V. Mandic, and J. Creighton, "Gravitational-Wave Stochastic Background from Cosmic Strings," *Phys. Rev. Lett.*, vol. 98, p. 111101, Mar 2007, arXiv:astro-ph/0610920v2.

[239] J. J. Blanco-Pillado and K. D. Olum, "Stochastic gravitational wave background from smoothed cosmic string loops," *Phys. Rev. D*, vol. 96, p. 104046, Nov 2017, arXiv:1709.02693v2.

[240] C. Ringeval and T. Suyama, "Stochastic gravitational waves from cosmic string loops in scaling," *JCAP*, vol. 2017, no. 12, p. 027, 2017, arXiv:1709.03845v2.

[241] C. Caprini and D. G. Figueroa, "Cosmological Backgrounds of Gravitational Waves," arXiv:1801.04268v2.

[242] A. Jenkins and M. Sakellariadou, "Anisotropies in the stochastic gravitational wave background: formalism and the cosmic string case," arXiv:1802.06046v3.

[243] G. Cusin, C. Pitrou, and J.-P. Uzan, "Anisotropy of the astrophysical gravitational wave background: Analytic expression of the angular power spectrum and correlation with cosmological observations," *Phys. Rev. D*, vol. 96, p. 103019, Nov 2017, arXiv:1704.06184v2.

[244] T. Regimbau, S. Giampanis, X. Siemens, and V. Mandic, "Stochastic background from cosmic (super)strings: Popcorn-like and (Gaussian) continuous regimes," *Phys. Rev. D*, vol. 85, p. 066001, Mar 2012, arXiv:1111.6638v3.

[245] M. J. Stott, T. Elghozi, and M. Sakellariadou, "Gravitational wave bursts from cosmic string cusps and pseudocusps," *Phys. Rev. D*, vol. 96, p. 023533, Jul 2017, arXiv:1612.07599v2.

[246] V. Vanchurin, K. D. Olum, and A. Vilenkin, "Scaling of cosmic string loops," *Phys. Rev. D*, vol. 74, p. 063527, Sep 2006, arXiv:gr-qc/0511159v4.

[247] K. D. Olum and V. Vanchurin, "Cosmic string loops in the expanding universe," *Phys. Rev. D*, vol. 75, p. 063521, Mar 2007, arXiv:astro-ph/0610419v3.

[248] V. Vanchurin, "Cosmic string loops: Large and small, but not tiny," *Phys. Rev. D*, vol. 77, p. 063532, Mar 2008.

[249] L. Lorenz, C. Ringeval, and M. Sakellariadou, "Cosmic string loop distribution on all length scales and at any redshift," *JCAP*, vol. 2010, no. 10, p. 003, 2010, arXiv:1006.0931v2.

[250] M. Kawasaki, K. Miyamoto, and K. Nakayama, "Gravitational waves from kinks on infinite cosmic strings," *Phys. Rev. D*, vol. 81, p. 103523, May 2010, arXiv:1002.0652v2.

[251] L. Sousa and P. P. Avelino, "Stochastic Gravitational Wave Background generated by Cosmic String Networks: Velocity-Dependent One-Scale model versus Scale-Invariant Evolution," *Phys.Rev.*, vol. D88, no. 2, p. 023516, 2013, arXiv:1304.2445v1.

[252] J. J. Blanco-Pillado, K. Olum, and X. Siemens, "New limits on cosmic strings from gravitational wave observation," *Physics Letters B*, vol. 778, pp. 392 – 396, 2018, arXiv:1709.02434v2.

[253] E. Babichev and V. Dokuchaev, "Gravitational radiation from chiral string cusps," *Phys. Rev. D*, vol. 67, p. 125016, Jun 2003, arXiv:astro-ph/0303659v1.

[254] L. Sousa and P. P. Avelino, "Probing cosmic superstrings with gravitational waves," *Phys. Rev. D*, vol. 94, p. 063529, Sep 2016, arXiv:1606.05585v1.

[255] T. Elghozi, W. Nelson, and M. Sakellariadou, "Cusps and pseudocusps in strings with Y-junctions," *Phys. Rev. D*, vol. 90, p. 123517, Dec 2014, arXiv:1403.3225v2.

[256] R. Brandenberger, H. Firouzjahi, J. Karouby, and S. Khosravi, "Gravitational radiation by cosmic strings in a junction," *JCAP*, vol. 2009, no. 01, p. 008, 2009, arXiv:0810.4521v2.

[257] P. Binetruy, A. Bohe, T. Hertog, and D. A. Steer, "Gravitational Wave Bursts from Cosmic Superstrings with Y-junctions," *Phys. Rev.*, vol. D80, p. 123510, 2009, arXiv:0907.4522v1.

[258] A. Achúcarro and G. J. Verbiest, "Higher Order Intercommutations in Cosmic String Collisions," *Phys. Rev. Lett.*, vol. 105, p. 021601, Jul 2010, arXiv:1006.0979v1.

[259] G. J. Verbiest and A. Achúcarro, "High speed collision and reconnection of Abelian Higgs strings in the deep type-II regime," *Phys. Rev. D*, vol. 84, p. 105036, Nov 2011, arXiv:1106.4666v1.

[260] R. P. L. Azevedo and C. J. A. P. Martins, "Cosmic strings and other topological defects in nonscaling regimes," *Phys. Rev. D*, vol. 95, p. 043537, Feb 2017, arXiv:1702.08453v1.

[261] E. J. Copeland, R. C. Myers, and J. Polchinski, "Cosmic superstrings II," *Comptes Rendus Physique*, vol. 5, no. 9, pp. 1021 – 1029, 2004. String theory and fundamental forces - Strings 04, part I.